Modelling the retreat of the Uummannaq ice stream system, central west Greenland.

JOHNSON, CHARLOTTE,ELIZABETH

Modelling the retreat of the Uummannaq ice stream, central west Greenland.

A thesis submitted for the degree of Master of Science

Department of Geography

Durham University 2019

Charlotte Elizabeth Johnson

Declaration

I confirm that no part of the material presented in this thesis has previously been submitted for a degree in this or any other university. In all cases the words of others, where relevant, have been fully acknowledged.

Charlotte Johnson
Durham University
May 2019

Abstract

I aim to understand what controlled the retreat pattern of the Uummannaq ice stream (UISS) during the last deglaciation. Evidence for the pattern of retreat is recorded in marine bathymetric and sedimentological data in the central trough (Ó Cofaigh *et al.,* 2013). On land, on the islands that sit within the fjord (Ubekendt and Karrat) and on the fjord margins, geomorphological evidence records the thinning of the ice surface through time (Roberts *et al.,* 2013; Lane *et al.,* 2014). These records are set within a chronological framework of radiocarbon and cosmogenic dates, which suggest that the ice stream was grounded close to the continental shelf edge at the Last Glacial Maximum, and had begun rapid retreat by 17ka BP. However, it is unclear what controlled the retreat pattern identified in the Uummannaq system.

Modelling the UISS using a 1-D numerical model provides the opportunity to combine the chronology and geometries inferred from the landforms and to test the influence of various controls upon the retreat of the ice stream. The model has the capability to dynamically and robustly simulate grounding line retreat behaviour over millennial timescales (Jamieson *et al.,* 2014). Marine geophysical data and dates from islands are used to constrain the numerical model and sensitivity tests are conducted to explore its response to a range of forcing patterns. The model retreat is simulated from a steady-state LGM configuration and was subjected to a series of retreat perturbations forced independently or simultaneously by either rising sea level, sub marine melting, ice temperature and surface melt. Comparing the simulated behaviour of the UISS against the geomorphological and cosmogenic exposure evidence for ice surface thinning onshore confirms that the UISS responds non-linearly to the applied forcings. This is likely to be because of the influence of topographic controls in the system, which appears to be the key modulator of retreat. Ice temperature and climate also have an impact on retreat and thinning of the UISS, but ultimately, a combination of sea level rise, submarine melt, increasing atmospheric temperatures are needed to reconstruct the retreat of the UISS that fits with the geomorphic evidence presented.

Acknowledgements

I would like to thank my supervisor, Stewart Jamieson, for his endless support when building the flowline model and sourcing necessary data. His patience and determination were vital this past year. I am also grateful to Dave Roberts for providing field evidence and insight into the geomorphology of the Uummannaq system and without whom, validating the final model output would have been difficult.

Special thanks to my parents and friends who have been a constant source of support and encouragement during my research and time at Durham University.

Table of Contents

List of Figures

List of Tables

1. Introduction and rationale

The Greenland Ice Sheet (GrIS) is the only remaining ice sheet in the northern hemisphere. Containing over 7 m of sea level equivalent, it is the second largest potential contributor to global mean sea-level (GMSL) rise. The ice sheet presently adds 0.5 mma^{-1} to GMSL rise (Shepherd & Wingham, 2007) and under future climate scenarios this figure is expected to rise (Rignot *et al.,* 2011). The melt-water produced by the GrIS, through surface melting, submarine melting and iceberg calving, is likely impacting on the Atlantic Meridional Overturning Circulation (Bamber *et al.,* 2009). Recent mass balance observations of the GrIS show a marked increase in mass loss over the past decade (Shepherd *et al.,* 2012- Fig. 1a). This rapid change has predominately occurred due to short-term increases in; surface melting (Mote, 2007; Fettweis *et al.,* 2011; Box, 2006; Ettema, 2009), dynamic thinning channeled through fast flowing corridors of ice (Fig. 1b, Rignot & Kanagaratnam, 2006; Howat *et al.,* 2008; Krabill *et al.,* 2004, Pritchard *et al.,* 2009) and enhanced rates of calving (Banver *et al.,* 2000; Bennett, 2003). Marine terminating outlet glaciers in Greenland are particularly susceptible to dynamic changes in a warming climate as they are affected by not only atmospheric warming but also oceanic warming and relative sea level rise (Nick *et al.,* 2009). These outlet glaciers move at velocities of up to 12, 000 m/yr^{-1} (Fig. 1b).

Despite observations of ocean forcing on grounding line retreat in some of the fastest flowing of Greenland's outlet glaciers (Hill *et al.,* 2018; Straneo *et al.,* 2012), a number of issues continue to restrict our understanding of the longer-term dynamics of the GrIS. For example, contemporary observations demonstrate that marine-based outlet glaciers and ice streams are responding asynchronously to variable ocean and climate forcing, and at a different rate to the terrestrial terminating ice sheet margins (Rignot and Kanagaratnam, 2006; Holland *et al.,* 2008; Joughin *et al.,* 2010). However, these observations cover only decadal timescales, and it is unclear if this behavior can be upscaled in order to forecast GrIS response to warming scenarios over the next century to millennial timescales. Understanding the longer-term (centennial to millennial) response of ice steams to climatic and oceanic change is therefore essential as they are responsible for the bulk loss of ice to the oceans and their dynamics are largely unknown beyond very short timescales.

A.

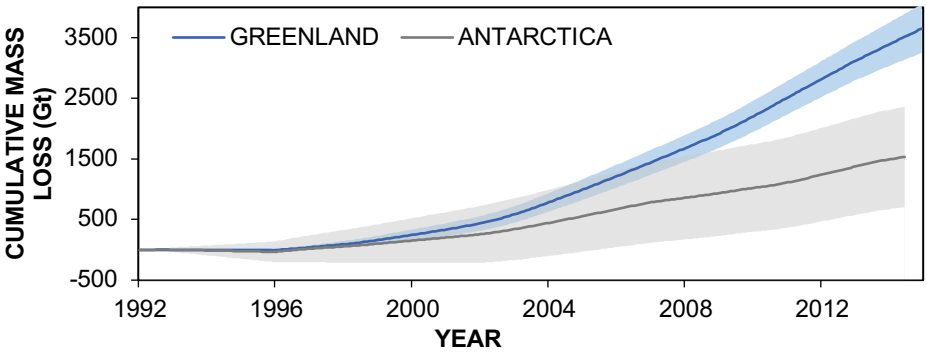

B.

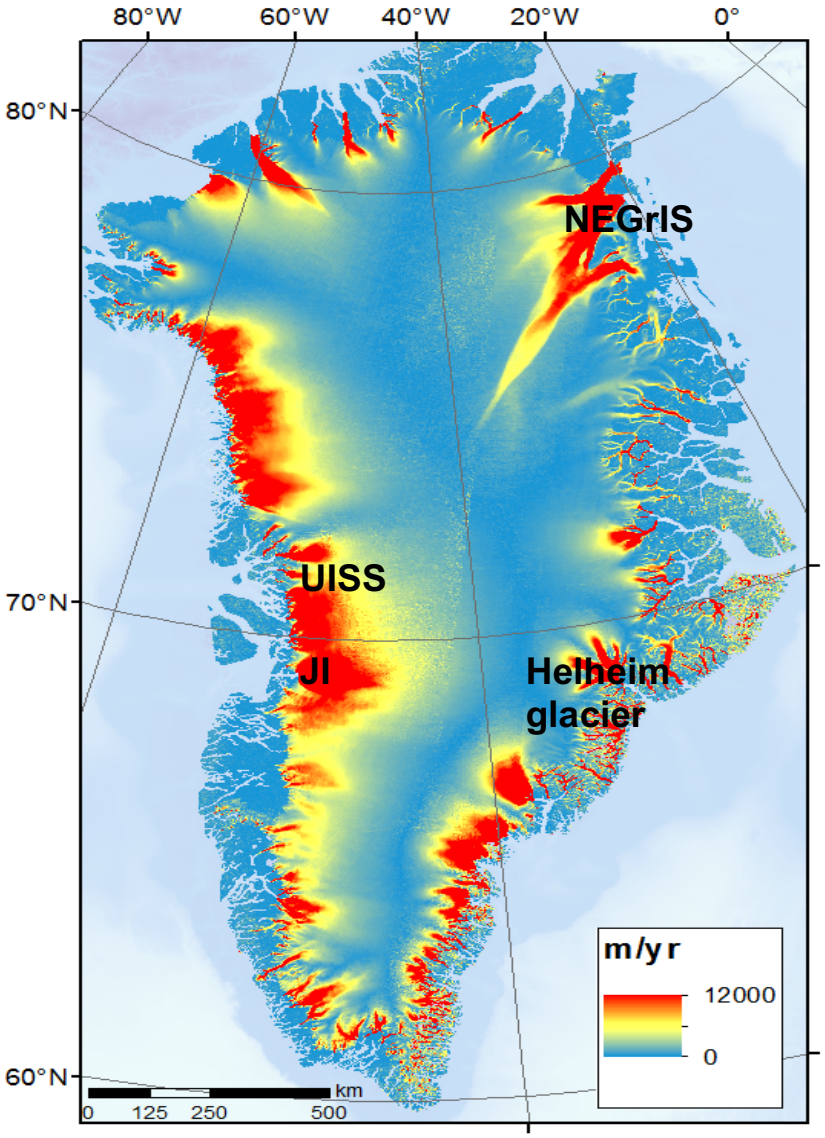

Figure 1. A) Cumulative mass loss (Gt) between 1992-2014 for the Greenland Ice sheet and the Antarctic Ice sheet created using gravity measuring satellite data from Shepherd *et al.,* 2012 updated in 2014 at the AGU. B) GrIS ice velocities sampled at 250 m resolution derived from InSAR, SAR and Landsat 8 optical imagery data (Joughin *et al.,* 2017).

The Uummannaq ice stream system (UISS) drained ~6% of the GrIS at the LGM exerting a significant control on ice and water flux to the West Greenland shelf edge and into Baffin Bay (Roberts *et al.,* 2013). It, therefore, would have played a major role in regulating GrIS internal dynamics and mass balance (Roberts *et al.,* 2013) and would have influenced North Atlantic thermohaline circulation. As the UISS is one of the best constrained ice streams in terms of its palaeo behavior (O'Cofaigh *et al.,* 2013), it offers the opportunity to provide insight into understanding the longer-term responses of glaciers and ice streams (Dowdeswell *et al.,* 2016). This study first considers the geological, geomorphological, and geochronological evidence relating to UISS in order to reconstruct the deglacial retreat of the West GrIS. Secondly, in combination with the geomorphological data, ice surface profiles for the flowline are used to provide constraints on the configuration of a large Greenland cross-shelf ice stream system. Finally, the forcing mechanisms driving UISS deglaciation are discussed with reference to regional changes in topography as well as atmospheric, oceanic, and sea-level forcing mechanisms.

1.1. Controls on ice stream retreat

Ice streams are spatially restricted fast flowing corridors of ice surrounded by slower moving ice (often by several orders of magnitude) (Paterson, 1984). They can potentially be disproportionately influential in regulating ice sheet mass balance at the beginning of deglaciations even though they occupy a small area of the ice sheet perimeter (Stokes & Clark 2016). Owing to their ability to rapidly drain large portions of ice sheets from the draw-down of ice from the ice sheets' interior, they play a critical role in controlling overall ice sheet mass balance. Subsequently, ice streams are an intrinsic part of the cryospheric system and accurate model reconstructions of ice sheets and dynamics should mirror their ability to contribute to mass loss.

However, the sub-decadal record of glacier change is not necessarily a representative analogue with which to make confident predictions of ice stream response and sensitivity to climate forcing on centennial scales (Joughin & Alley, 2011). Therefore, improved understanding of their short and long-term variability, their relationship to the ice sheets they drain, and their impact upon ice sheet stability in the past is instrumental in predicting ice stream response to current and future climate change (Bennett, 2003; Rignot & Kanagaratnam, 2006; Moon *et al.,* 2008; Khan *et al.,* 2010; Velicogna, 2009; Nick *et al.,* 2013). This can be done by reconstructing the retreat patterns of major marine terminating outlet glaciers since the LGM.

1.2. History of West Greenland ice sheet retreat patterns

The interest in resolving the history of the GrIS is two-fold. Firstly, the GrIS is the only northern hemisphere ice sheet to have survived the Last Glacial-Interglacial Transition, despite being in a region of vigorous climatic change (Funder *et al.,* 1989) suggesting that the ice sheet is relatively resilient to external forcings. This makes the GrIS landscape suitable for identifying a suite of geomorphic features. Secondly, as previously eluded to, the GrIS contains around 7 m water-equivalent of ice and is therefore an important factor when considering contemporary GMSL change (Oerelmans, 1993; Krabill *et al.,* 2004).

Thus far, the body of literature on LGM ice streams in West Greenland has focused on areas around Disko Bugt, Sissimuit and Jakobshavn Isbrae (Roberts & Long, 2005; O Cofaigh *et al.,* 2013; Hogan *et al.,* 2016). Here, evidence depicts an advance of topographically routed outlet glaciers, which converged on the continental shelf during the LGM (e.g. UISS; Jakobshavn; Hotsteinborg; Melville Bugt). The onset of deglaciation from the continental shelf is relatively late compared to deglaciation in other areas of Greenland (Roberts *et al.,* 2010). For example, retreat in East Greenland was well under way by 18.0 ka BP (Jennings *et al.,* 2006; Evans *et al.,* 2002; Hakansson *et al.,* 2007), leading retreat in West Greenland by 1 thousand years (kyr) (Jennings *et al.,* 2017). The influence of warm ocean water impinging on the shelf has been proposed as the driver for retreat in the East (Jennings *et al.,* 2006; Knutz *et al.,* 2011) but the controls on the initial retreat in the West are less clear owing to the timing, and asynchronicity of the response within major neighbouring ice streams at the LGM (Weidick & Bennike, 2007; O Cofaigh *et al.,* 2013a; Roberts *et al.,* 2013; Rignot & Kanagaratnam, 2006; Sheldon *et al.,* 2016). Evidence from coastal landform features and marine geophysical datasets indicate that the LGM GrIS was drained at its periphery by a number of confluent ice streams and outlet glaciers (Evans *et al.,* 2002; 2009; Roberts & Long, 2005; Roberts *et al.,* 2009; 2010; 2013; Dowdeswell *et al.,* 2010; 2014; O Cofaigh *et al.,* 2013a). The behaviour of these outlets was moderated by changing air and ocean temperatures (Velicogna & Wahr, 2006; *et al.,* 2010; Andresen *et al.,* 2011; Bjork *et al.,* 2012).

1.3. Study Area: The Uummannaq Region

Central west Greenland currently has the highest concentration of outlet glaciers in Greenland (Reeh, 1985; Velicogna & Wahr, 2006) and 11 of these major outlet glaciers are located in the Uummannaq catchment.

The Uummannaq region is a mountainous area that lies between 70.33°N and 72.00°N and covers approximately 40,000 km^2, with peaks reaching over 2000 m above sea level (asl). The area (Fig. 2) comprises a convergent network of 11 fjords through which outlet glaciers advanced and coalesced

during the LGM, forming the UISS (O Cofaigh *et al.,* 2013b; Roberts *et al.,* 2013). The trough was approximately 50 km wide, up to 600 - 1000 m deep and extended across the adjacent continental shelf, flowing into the deep waters of Baffin Bay. This trough is one of several large cross shelf troughs that dissect the modern west Greenland continental shelf (Batchelor & Dowdeswell 2013; O Cofaigh *et al.,* 2013a) and formed due to erosion from repeated advance and retreat of the GrIS during the Quaternary (Dowdeswell *et al.,* 2014). Several geological and topographical factors have also been important in influencing trough evolution. In the onset zone, the UISS is bounded to the north and south by large peninsulas which form topographic barriers confining the flux of ice from the local outlet glaciers. A shallow submarine sill, located at the boundary between the Cretaceous and Tertiary bedrock at Qeqertat Imat (Fig. 3) is thought to have partially deflected active ice from the northern Uummannaq fjords south into Igdlorssuit Sund which then coalesced with southern outlet glaciers (Roberts *et al.,* 2013; Lane *et al.,* 2014). The north–south trending trough marks a transition from multiple small fjords into Iglorssuit Sund, a single trough, and is coincident with a Cretaceous basin filled with marine mudstones and sandstones (Fig. 3) (Pedersen & Pulvertaft, 1992; Dam *et al.,* 2000; Henriksen *et al.,* 2000). These softer lithologies are more susceptible to both basal and lateral erosion than Archean basement rocks and Tertiary basalt, thus the decrease in the number of fjords into a single broad trough is partially geologically controlled with less resistant lithologies, and thus increasing erosional efficiency, allowing a single glacial channel to develop (Roberts *et al.,* 2013; Jess *et al.,* 2019)

The development of a single channel allowed the establishment of a fast-flowing, efficient glacial drainage system, (Swift *et al.,* 2008; Roberts *et al.,* 2013). This focussing of ice into a single channel results in glacial valley widening and over-deepening, increasing driving stresses and the areal extent of basal melting (Paterson, 1994; Kleman *et al.,* 1997). In turn, this increases basal melt-water flux facilitating enhanced basal lubrication and fast ice flow (Swift *et al.,* 2008). Furthermore, the subsequent decrease in lateral confinement and increase in ice-flow efficiency within Igdlorssuit Sund would have encouraged the draw-down of ice from the inner fjord system and promoted the establishment of the UISS trunk zone. This situation is not unique to the Uummannaq region: Scoresby Sund, East Greenland evolved due to feedbacks operating between fjord morphometry, basement geology and ice-flow behaviour (Swift *et al.,* 2008).

The largest outlet glaciers in the UISS are the Rink-Isbrae in the north and Store Gletscher in the south. Respectively these calve up to 10.5 - 16.7 km^3 a^{-1} and 13.2 - 17.5 km^3 a^{-1} of ice into the ocean (Rignot & Kanagaratnam, 2006). Rink-Isbrae, the fastest-flowing and highest discharging outlet glacier in the northern Uummannaq region drains into the head of Rink-Karrat fjord and is joined by Umiamako Fjord becoming Karrat fjord (Rignot & Kanagaratnam, 2006). Rink-Karrat fjord is a 6-10 km wide, over-deepened, glacial trough with depths reaching 1200 m close to the present ice margin. For the purpose of this study, two islands, Karrat (Fig. 2a) and Ubekendt Ejland (Fig. 2b), are identified as critical pinning points for the UISS during retreat. Karrat Ejland bifurcates Rink-Karrat fjord with

<300 m deep water to the north and 600-700 m deep water to the south (approximately 28 km^2) whilst Ubekendt (approximately 468 km^2) sits along the northern edge of the main trunk zone.

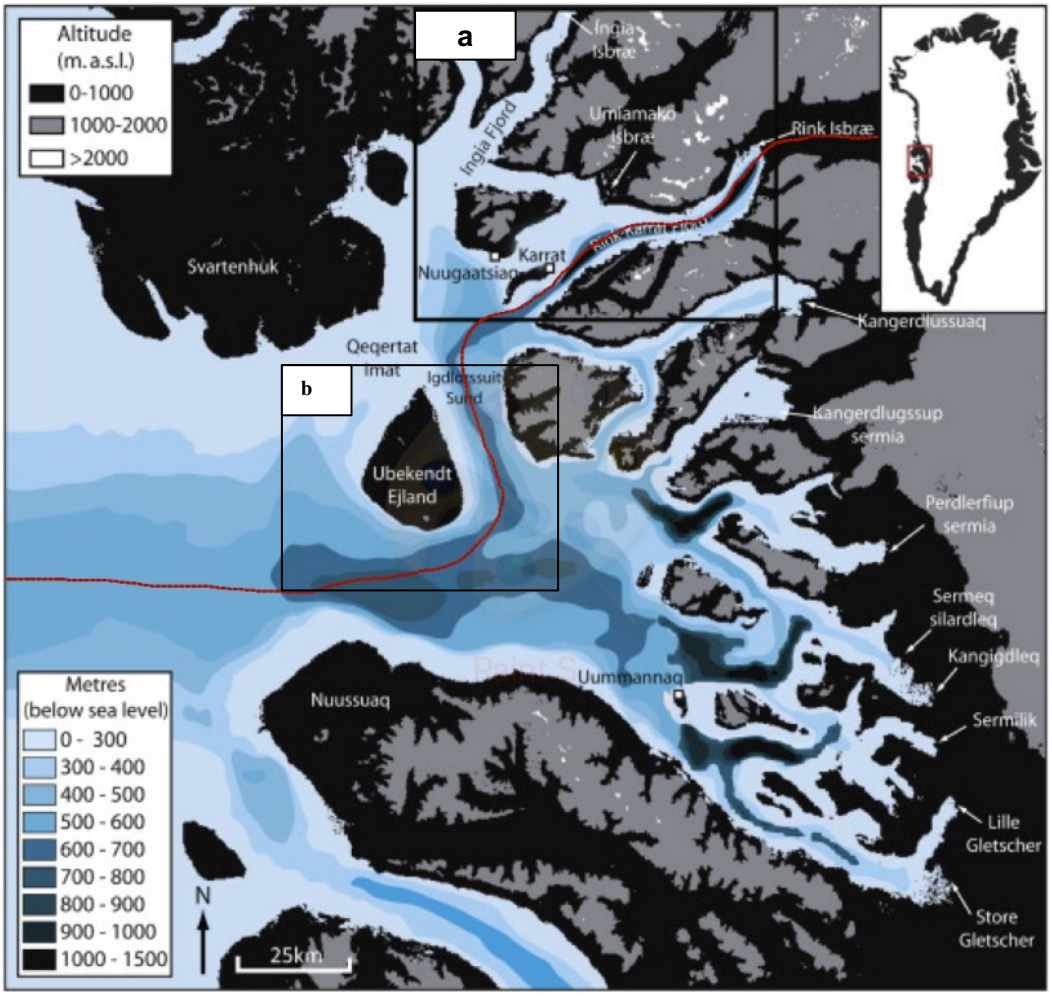

Figure 2. Geographical location map of the Uummannaq catchment and its fjords in central West Greenland (Lane *et al.,* 2016). A) Karrat Ejland, Umiamako, Rink-Karrat fjord is discussed in section 2. B) Ubekendt Ejland – discussed in section 2. Flowline illustrated by red line.

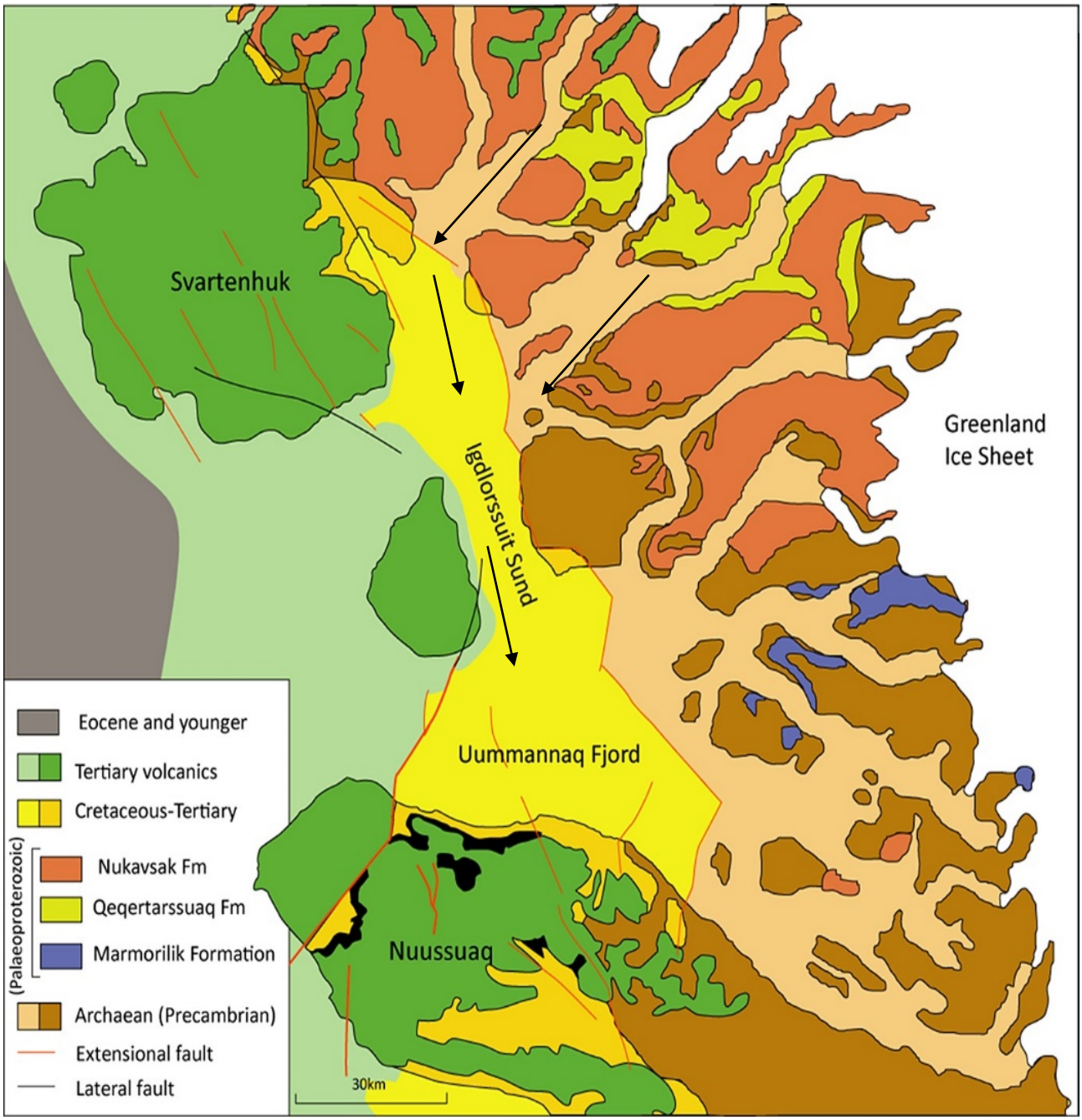

Figure 3. Geology of the Uummannaq catchment (adapted from Roberts *et al.,* 2013). Black arrows illustrate the deflection of ice from the fjord heads entering Igdlorssuit Sund due to the underlying geology.

1.4. Aims

The aim of this project is to understand the controls on the retreat of the UISS following the LGM.

The retreat of the UISS is recorded in marine bathymetric and sedimentological data in the central trough (Ó Cofaigh *et al.,* 2013, *see section 2*). On land, on the islands that sit within the fjord (Ubekendt, Karrat, Ikersak), and on the fjord margins, geomorphological evidence records the thinning of the ice surface and ice margin retreat through time (Roberts *et al.,* 2013; Lane *et al.,* 2014). These records are set within a chronological framework of radiocarbon and cosmogenic dates, which suggest that the retreat began around 17 ka BP and reached the present day margin at 10 ka BP. Thus, the UISS is one of a few in the world where onshore and offshore ice histories can be combined to understand the geometry and timing of long-term retreat. Modelling the UISS using a numerical model provides the opportunity to combine the chronology data and reconstructed ice stream geometries (inferred from the landforms) to test the influence of various controls upon the retreat of the ice stream. Experiments can be applied to a suite of forcing scenarios either independently or simultaneously and in stepped or linear manner. The purpose of this holistic approach is to gain a clearer understanding of the sensitivity of the UISS and its feeder glaciers to a range of external and internal driving mechanisms. Furthermore, reconstructing the UISS retreat during the LGM and exploring the link between the offshore grounding line position and onshore ice surface evolution can then be used to explore the behaviour of other ice streams in Greenland and to elucidate dynamic feedback mechanisms.

1.4.1. Objectives

These aims will be investigated using the following objectives:

1. To review the key evidence that constrains the timing and pattern of UISS retreat in order to understand the key constraints for a numerical ice stream model.

2. To build the model and set up a stable LGM configuration for the field area – model spin up. This forms the basis of the retreat experiments.

3. To test the sensitivity of the model to various forcings applied in isolation or combination.

4. To produce a final evaluation of the paleoenvironmental variables that controlled the UISS decay.

2. Geomorphological and Chronological Constraints on UISS history

Palaeo ice streams are extremely powerful erosional agents that leave behind a geomorphological signature providing information on the thermal conditions of the ice sheet, the basal topography, and the bed roughness. The UISS exhibits regional flow convergence, an onset zone and a trunk zone (Fig. 4). In the Uummannaq catchment there is now a 400 km distance between the terminus of Rink Glacier, and the continental shelf edge. The sea floor of the cross-shelf trough is characterised by landforms produced by past UISS activity such as erosion and deposition.

Mapping and dating these glacial landforms and the glacimarine sediments that drape them have revealed the long-term glacial evolution of the ice stream (O Cofaigh *et al.*, 2013; Dowdeswell *et al.,* 2014; Lane *et al.,* 2014). The inherent spatial variability of these landforms is a product of subglacial ice stream conditions and bedrock lithology and structure. For example, the onset zone has a hard bed signal formed through selective linear erosion and areal scour (Fig. 4 - Roberts *et al.,* 2013) whilst the trunk has a soft bed signal with evidence of ice streaming across the mid to outer shelf (O Cofaigh *et al.,* 2013). These landforms can be separated into onshore and offshore features that provide information on the past ice sheet extent and deglacial retreat when used in combination with cosmogenic and radiocarbon dating techniques to provide a chronology of the UISS.

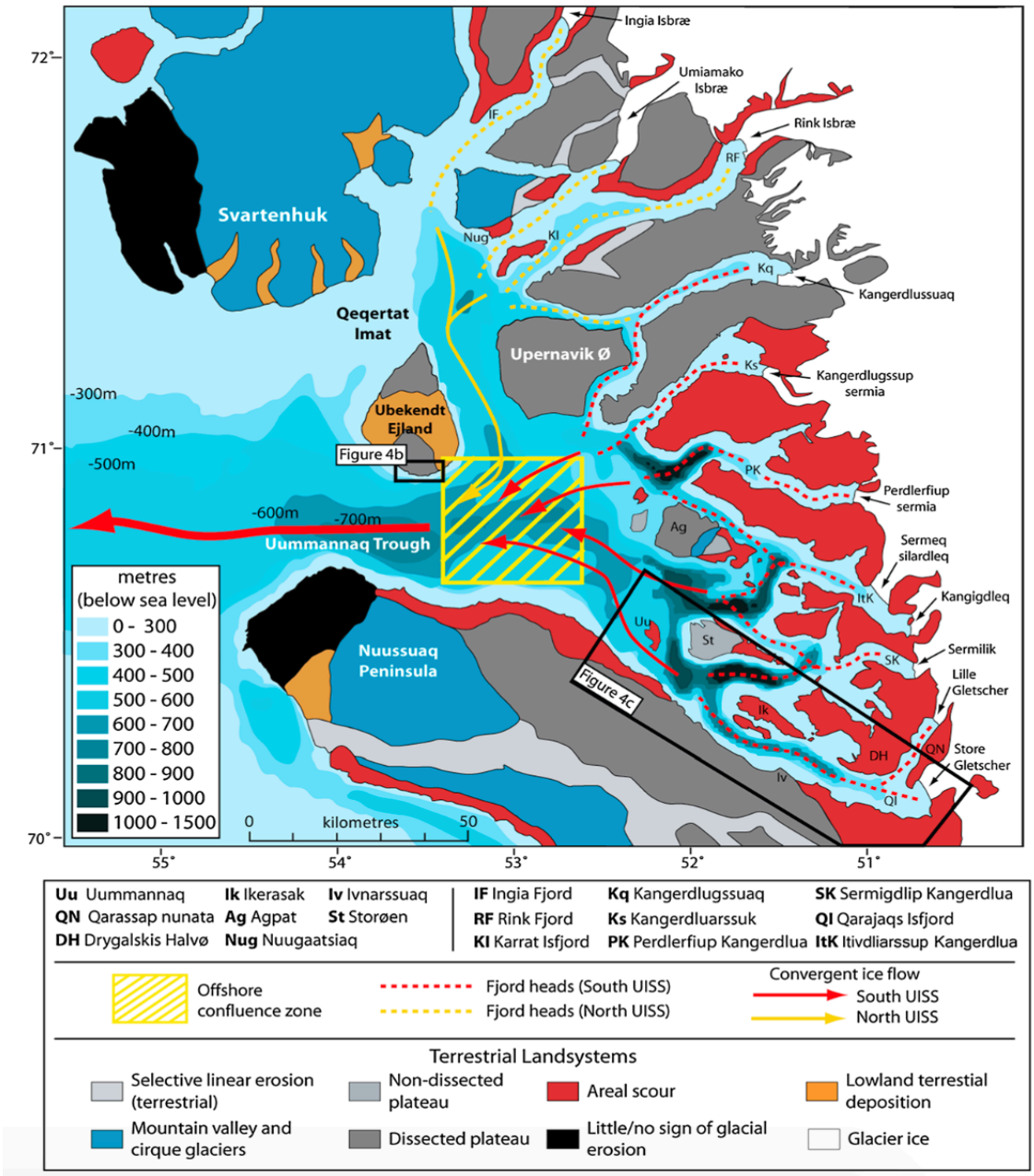

Figure 4. Landscape overview of the Uummannaq region. The terrain between Store Gletscher and Ingia Isbrae is 1500–2000 m asl and forms a dissected plateau. Regional scale flow convergence is caused by a combination of fjord head alignment and the confluence of Iglorssuit Sund and the Uummannaq trough to the SE of Ubekendt Ejland. The sea floor to the north Ubekendt is shallow (<200 m below sea level) compared to the area to the east and south, where the floors of Igdlorssuit Sund and Uummannaq trough are > 800 m below sea level (Roberts et al., 2013).

2.1. Offshore

The continental shelf of West Greenland harbours the imprint of at least six large, cross-shelf ice streams that reached the shelf edge at the LGM (Roberts *et al.,* 2013). The Uummannaq Trough contained one of these ice streams, approximately 200 km long and 20–25 km wide (Dowdeswell *et al.,* 2014). The over-deepening in the Uummannaq channel is indicative of long-term subglacial erosion by an ice stream that flowed via basal sliding and bed deformation (Hogan *et al.,* 2016). The outer Uummannaq Fjord has the widest variety of submarine landforms anywhere within the Uummannaq system (Dowdeswell *et al.,* 2014). The well-developed streamlined landforms, orientated parallel to trough long axes, are interpreted by Dowdeswell et al., (2014) as a product of deformational and depositional processes at the bed of the UISS during both advance and retreat.

The western end of the Uummannaq Trough is marked by a large trough mouth fan (O´Cofaigh *et al.,* 2013b – Fig. 5). This provides compelling evidence for extensive cross-shelf glaciation at the LGM (O'Cofaigh *et al.,* 2013b). Offshore of Greenland, large fans have been mapped at the Disko shelf-edge in West Greenland and at the edges of the Scoresby Sund and Kangerlussuaq Troughs in East Greenland (Dowdeswell *et al.,* 1997, 2010; O´Cofaigh *et al.,* 2013a). Such high-latitude, glacier-influenced fans are built-up predominantly from the delivery of diamictic debris to the shelf edge and upper slope when ice sheets advanced to the shelf break during Quaternary full-glacial conditions (Vorren *et al.,* 1998). The debris flows are stacked on the slope and contribute to the formation of the Uummannaq trough mouth fan (O´Cofaigh *et al.,* 2013b).

East of the fan edge, the local bathymetry shallows to 400-500 m deep across a distinct bank inferred to be a terminal moraine ridge (McCarthy, 2011; O'Cofaigh *et al.,* 2013). The core JR175-VC45 (VC45 – Table 1, Fig. 5) from the 10 m high moraine ridge at the mouth of the Uummannaq trough yields a radiocarbon date of 14.8 ka BP from benthic foraminifera that constrains the timing of deglacial retreat from the shelf edge (O'Cofaigh *et al.,* 2013). The absence of multiple recessional moraines suggests that UISS retreat was so rapid through the outer trough that there was insufficient time for recessional moraines to form, or that the ice margin retreated as a floating ice shelf (Streuff *et al*., 2017; Dowdeswell *et al.,* 2014). However, in core VC46 (Table 1), the cessation of GDF deposition infers ice stream retreat started at 17.1 ka BP (Jennings *et al.* 2017). This date is earlier than that measured on the nearby moraine ridge on the outer shelf at core JR175-VC45 which yields a date from glacimarine sediments only 5 cm above a basal till (O'Cofaigh *et al.,* 2013b).

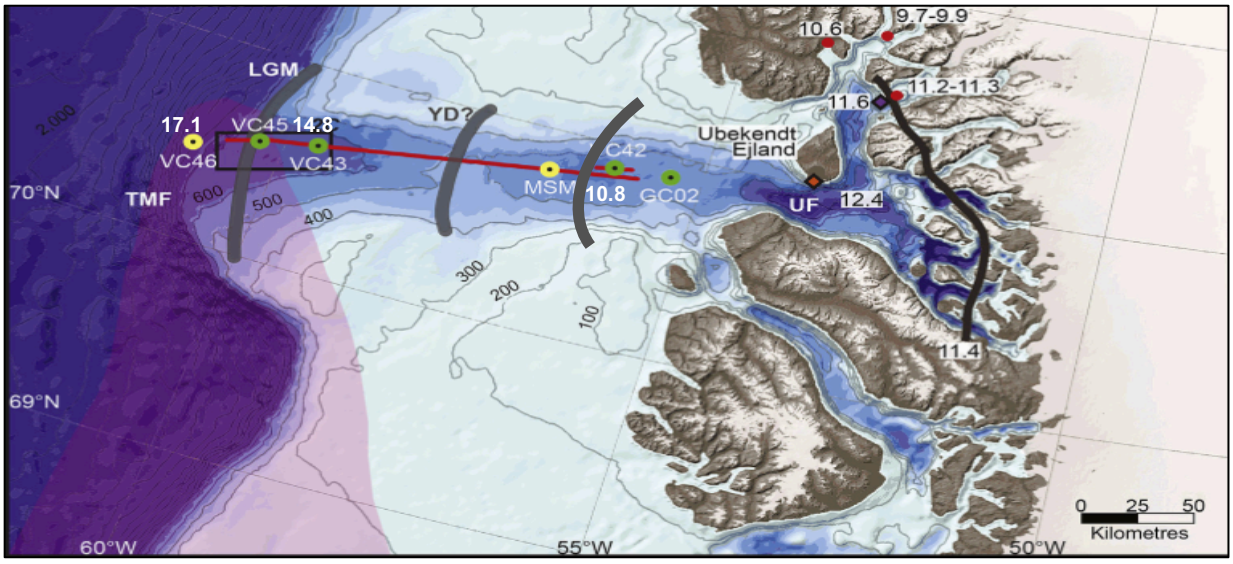

Figure 5. Map of the Uummannaq trough, bathymetry, core sites and deglacial dates. The grey lines on the outer shelf and mid-shelf represent the ice extent at the LGM and the possible YD still stand. The translucent pink outline represents the "pinch-- out" of the IRD belt. TMF = trough mouth fan. The grey lines represent the GZWs. The extent of the GrIS is shown in white. Adapted from Roberts et al., 2013.

Table 1. Sediment core ages from the Uummannaq trough.

Core	Age	Comment	Reference
VC46	17.1 ka BP	deglacial retreat from the shelf edge	Jennings et al., 2017
VC45	14.8 ka BP	deglacial retreat from the shelf edge	O'Cofaigh et al., 2013
MSM343520	10.8 ka BP	minimum deglacial age of the UISS from the mid-shelf GZW	McCarthy 2011

2.1.1. Uummannaq Trough

The presence of mega scale glacial lineations, drumlins, crags and tails, demonstrate that the GrIS advanced through the fjord system to fill the whole of Uummannaq Trough and reached the shelf edge (Fig. 6, Jennings *et al.,* 2014; O Cofaigh *et al.,* 2013a).

Sedimentary streamlined landforms, typically with an elongation ratio of 20:1, are interpreted as MSGLs and are typically associated with ice streams operating over a soft bed (Clark, 1994; Canals *et al.,* 2000; O´Cofaigh *et al.,* 2002; Ottesen *et al.,* 2005). Several sets of streamlined features are orientated approximately along fjord long axes, although there is a clear curvilinear trend in the orientation of the landforms. In the inner 20 km of the Uummannaq trough these features are intensely streamlined in the direction of ice flow (east to west).

Further offshore, between 30-60 km from the fjord mouth, south of Ubekendt, the seafloor of the Uummannaq Trough is entirely sedimentary and dominated by linear to curvilinear streamlined features (Dowdeswell *et al.,* 2014; O Cofaigh *et al.,* 2013). These landforms have a drumlin-like character with blunt nosed landward faces and streamlined tails that narrow seaward. Their location

at about 55°W (Fig. 7) is a little unusual because drumlins are usually found in the onset zones of former ice streams (cf. Wellner *et al.,* 2001; Lowe and Anderson, 2002). In this case, they are located in the Uummannaq trough, down-flow of well-developed MSGL's and crag-and-tail landforms. They are accompanied on their upstream side by cresentic depressions which may develop through erosional scour by meltwater, and limited development of subglacial channels nearby likely indicates water at the bed (Streuff *et al.,* 2017). The presence of many of these streamlined sedimentary landforms over the region suggest the Uummannaq Fjord hosted a former ice stream (Dowdeswell *et al.,* 2014).

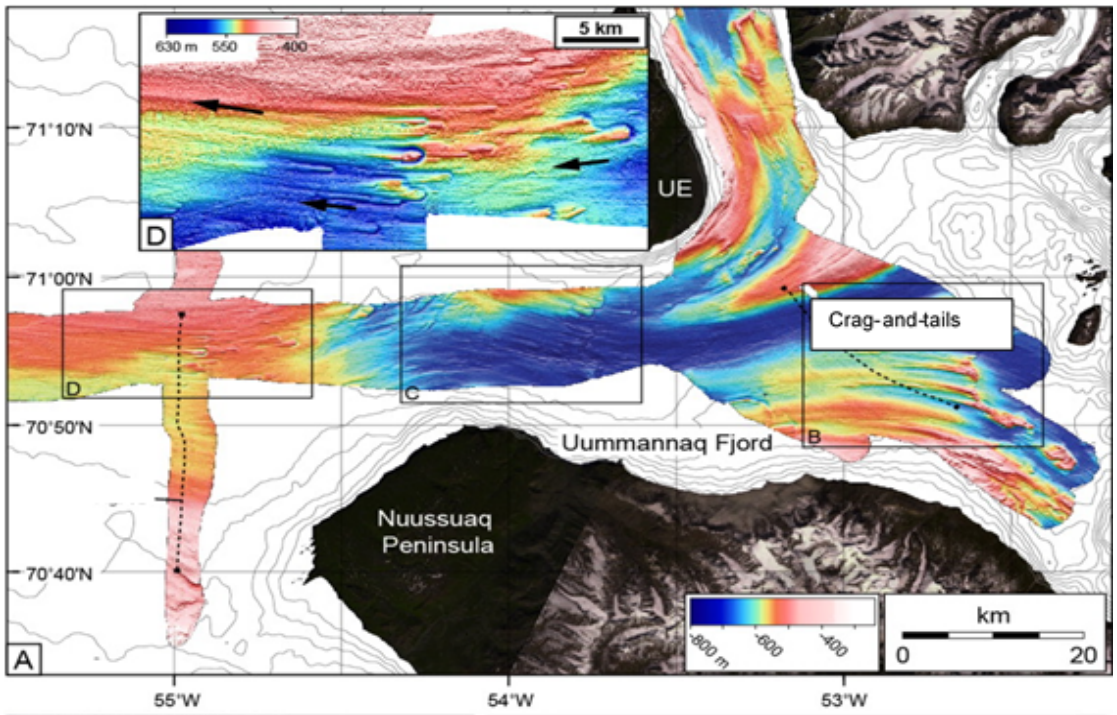

Figure 6. Swath-bathymetric imagery of the outer fjord and inner shelf of the UIS (Dowdeswell et al., 2014). (A) Shaded-relief image of the geomorphology of outer Uummannaq Fjord (located in Fig. 1) with the positions of subsequent figures shown. (B) crag-and-tail features. (C) streamlined features and possible channels. (D) streamlined sediments and cresentic landforms. Black arrows in panels B, C and D indicate inferred directions of former ice flow.

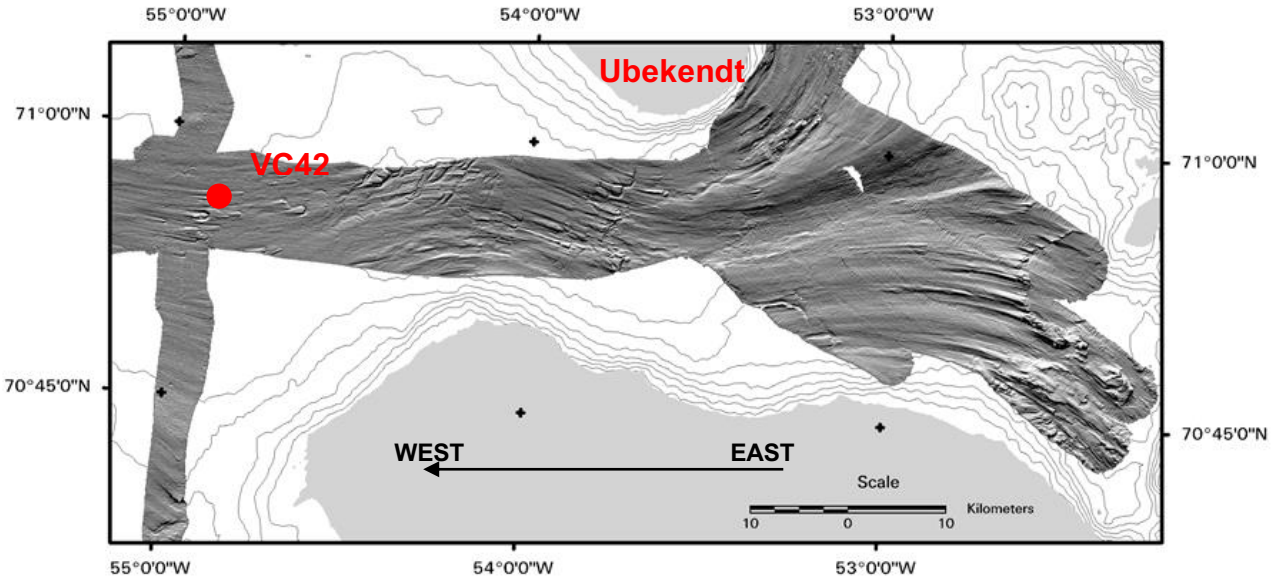

Figure 7. Mega scale glacial lineations in the Uummannaq Trough (Dowdeswell et al., 2014).

As the trough sides shallow towards the west, sedimentary lineations are replaced by series of irregular furrows that are closely-spaced and typically a few meters deep: these irregular features dominate the sea-floor morphology of the outermost shelf at about 56.5°W and at water depths of less than 570 m (Dowdeswell *et al.,* 2014). Furrows occur where semi-buoyant icebergs impinge on the sea floor (Syvitski *et al.,* 2001). The record of LGM and deglacial landforms is heavily reworked at water depths shallower than about 500 m by the ploughing action of deep-keeled icebergs. Below this depth very little ploughing occurs as a result of the thickness of the terminal ice cliffs from which icebergs drifting through the Uummannaq fjord shelf system are calved (Dowdeswell *et al.,* 2016). This is typical of many high-latitude shelves where high fluxes of large icebergs (104–105 km^2) occurred during deglaciation (Dowdeswell *et al.,* 2016). Ploughmarks at the mouth of Uummannaq Trough down to about 850 m are present only where iceberg fragmentation and the overturning of icebergs have taken place, resulting in particularly deep keels (Dowdeswell *et al.,* 2016). Isolated slope parallel depressions up to about 40 m deep in water depths of 850–1085 m on the West Greenland upper slope have also been ascribed to ploughing by huge icebergs, probably produced during break-up of the last full-glacial ice sheet (Kuijpers *et al.,* 2007).

Within the Uummannaq trough three grounding zone wedges (GZW) are present (Fig. 5 & 8; Dowdeswell *et al.,* 2014). They occur at 55°, 56° and 58°W, and indicate that the ice margin may have stabilized for decades or centuries during retreat (Mosola and Anderson, 2006; Dowdeswell and Fugelli, 2012). Consequently, the ice margin likely retreated episodically, punctuated by at least three still stands (Dowdeswell *et al.,* 2014). The outer GZW is 40 m thick, whereas the inner GZWs are 10-20 m thick and this implies that the retreating ice margin may have been stable for only half the time of the still stand on the outer shelf (assuming a constant rate of delivery of basal debris to the ice front). The GZW at 55° coincides with a narrowing and shallowing trough (Fig. 2) which is likely to have increased lateral drag and resistive stresses, thickening the ice and increasing basal drag. This would have reduced ice flux between Karrat and Ubekendt (Roberts *et al.,* 2013) and may have temporarily stabilized the ice margin (Hogan *et al.,* 2016) sufficient to override and reduce calving rates and retreat rates. The age of the GZW at 55° is unknown, but, based on the two constraining ages on the outer and mid shelf, it must have formed during a still stand that occurred between 14.9 and 10.8 cal kyrs BP (MSM323520 – Table 1, O'Cofaigh *et al.,* 2013; Dowdeswell *et al.,* 2014). Formation during a possible re-advance during this period cannot be ruled out, but there is no data to corroborate this. The lack of large numbers of small transverse-to flow sediment ridges in the trough suggests that retreat between GZW may have been relatively rapid (Dowdeswell *et al.,* 2014).

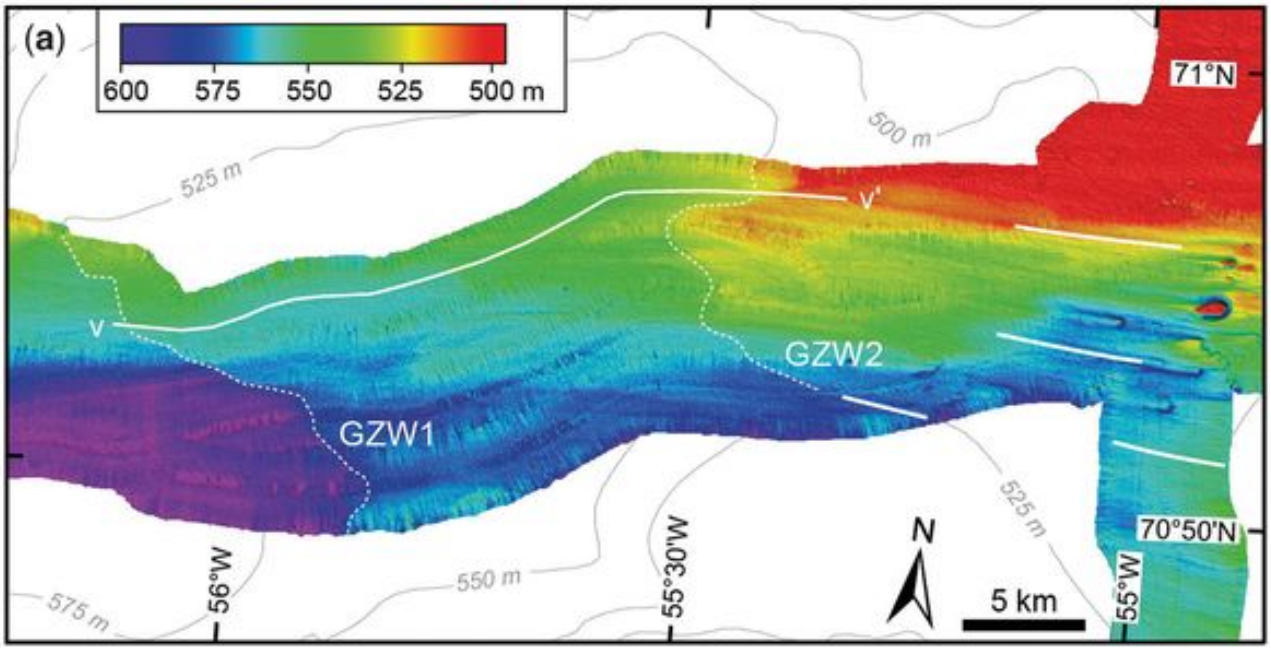

Figure 8. Two of the grounding zone wedges (GZW1 & GZW2) approximately 10-20 m thick in the Uummannaq trough (Dowdeswell et al., 2014).

2.1.2. South Uummannaq trough west of Sermigdlip Kangerdlua and Qarajaqs Isfjord

Where streamlined subglacial landforms have an up-ice rock core and a down-ice sedimentary tail, they are interpreted as crag-and-tail features (Benn & Evans, 2010). The 15 km long convex bedrock ridges in the inner 20 km or so of Uummannaq Fjord 52.5°W are consistent with this (Fig. 6B). These landforms are buried under a drape of fine-grained glacimarine sediment indicating that they are relict features of the former ice stream (Dowdeswell *et al.,* 2014).

At and beyond the location where Uummannaq fjord narrows to about 25 km wide, between Ubekendt Ejland and Nuussuaq Peninsula (Fig. 6) the landform suite becomes more complex, although still streamlined in a generally east-west direction. In the Uummannaq fjord and adjoining shelf trough, streamlined subglacial bedforms up to 16 km long, 0.6 km wide, and with elongation rations of 1:40 are present on the seafloor (Dowdeswell *et al.,* 2014). The occurrence of these subglacially produced landforms demonstrates unequivocally that the GrIS advanced to fill the whole of Uummannaq trough and reached the shelf edge. Radiocarbon dates from the Uummannaq shelf and upper slope confirm that the MSGLs are linked to the presence of ice during the last full glacial period (Jennings *et al.,* 2014; 2017; O Cofaigh *et al.,* 2013a).

2.1.3. Inner Rinks system & Fjord heads

The seafloor of Rink Fjord and Karrat Fjord is relatively flat for the most part, with protruding bedrock pinnacles and ridges (Dowdeswell *et al.,* 2014). Within a few kilometres of the modern marine terminus of Rink Glacier there are two basins over 1000 m deep, separated by a large transverse ridge (100 m asl) that stretches across the fjord in about 650 m of water (Dowdeswell *et al.,* 2014). In the relatively deep basin inshore of the moraine ridge, two streamlined landforms are interpreted as mega-scale glacial lineations (MSGLs), formed subglacially before the retreat of Rink Glacier from this area over the past century. The submarine ridge is interpreted to mark the position of Rink Isbrae during the Little Ice Age (LIA) (Dowdeswell *et al.,* 2014). Similar transverse ridges, for example in Svalbard and Chilean fjords, are also linked to LIA glacier growth (e.g. Ottesen & Dowdeswell, 2009). The relatively large size of the submarine moraine ridge implies that the ice stream stabilized in this position for sufficient time for the ridge to accumulate. Consequently, it is likely that the ice stream may have been in this position for the majority of the Holocene (Lane *et al.,* 2016).

2.2. Onshore

A suite of onshore geomorphic features are present in the UISS, including ice depositional and erosional landforms. There are three key locations, Ubekendt, Karrat, and the spur of Rink-Karrat fjord, relevant to constraining the LGM minimum ice surface elevation, ice extent, and thinning. The following section outlines the main elements of this evidence and reflects on what these can be used to infer about the ice stream.

During glacial periods the UISS was sufficiently thick and flowing fast enough to cause widespread glacial erosion across the Uummannaq region (Roberts *et al.,* 2013). This is evident in the inner fjord areas where glacial abrasion and widespread areal scour is common below 1000 m asl (Fig. 4).

Adjacent to the fjords, across the whole area, high altitude terrain comprise dissected plateaux ranging in elevation between 1000 – 2000 m asl. These are characterised by autochthonous blockfield and protected by local cold-based ice caps. Only in the south of the region close to Store Gletscher, where the mountains drop to around 1000 m asl, has the landscape been completely overrun by warm-based ice. This focussed glacial erosion of low-altitude areas and troughs, and the development of relict high altitude plateaux is the result of long-term selective erosion. In the Uummannaq region the contrast in the physical relief becomes progressively more dominant to north of the catchment. In addition, selective linear erosion has caused the large- scale abandonment of peripheral areas due to UISS onset and trunk zone development (Roberts *et al.,* 2013; Lane *et al.,* 2014). Once the Uummannaq Trough had developed as a significant topographical feature it would have been able to control regional ice flux during full glacial conditions, causing draw-down of ice from individual outlet glaciers and a switch to a single, large trunk zone. As a result, Svartenhuk and Nuussuaq became

starved of regional ice flux and only developed local ice caps (Roberts et al. 2013).

Cosmogenic radionuclide dating (CRN) has been employed extensively in the Uummannaq region to establish exposure and burial history. It is clear that many of the troughs were heavily eroded during the last glacial cycle and ^{10}Be ages provide a simple exposure history bracketing ice margin retreat between 12.5 and 6.0 ka (Roberts *et al.,* 2013). A number of radiocarbon dates from lake sediments have also been used to support the deglacial chronology onshore (Lane *et al.,* 2014). However, it is also clear that above 800 m asl in the landscape many bedrock surfaces and erratics harbour a degree of isotope inheritance, as a result of either limited erosion, long term exposure or burial by cold-based ice across high plateaux (Roberts *et al.,* 2013; Briner *et al.,* 2013; Strunk *et al.,* 2017). Periglacial slope processes have also caused the reworking of erratics in some areas (Roberts *et al.,* 2013).

The transition from areally scoured terrain to blockfield across the region can be used as a crude gauge on the vertical limit of warm-based ice; though the upper surface of many local fjord glaciers, (and the UISS as it formed) may have been coalescent with local ice caps during the LGM (Roberts *et al.,* 2013; Lane *et al.,* 2016; Briner *et al.,* 2013). Such 'trimlines' may also represent englacial thermal boundaries within the ice (Fig. 9 - Ballantyne, 1997). A better set of controls on ice thickness is provided by lateral moraine staircases which are common on steeper terrain adjacent to fjord walls and which mark the sequential, top down thinning of the ice stream from the outer to inner coast (Roberts *et al.,* 2013; Lane *et al.,* 2016).

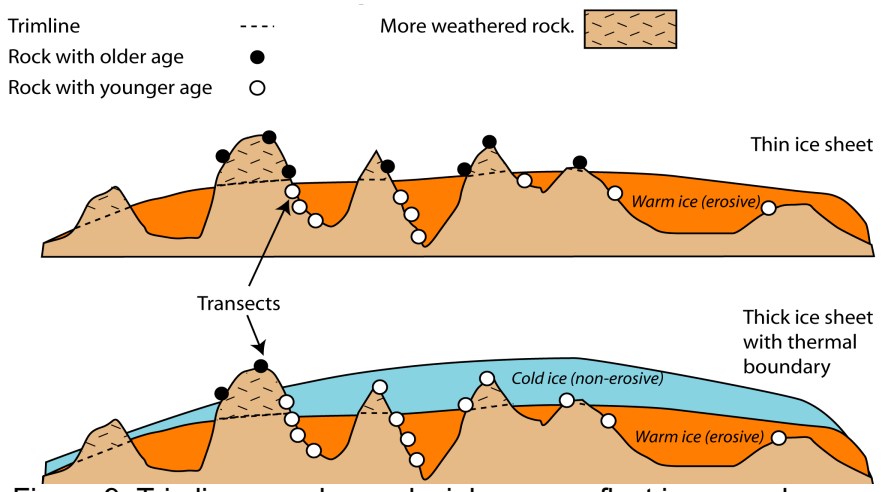

Figure 9. Trimlines can be englacial or can reflect increased exposure/weathering during an ice age. CRN dating helps estimate ice sheet thickness (Makintosh et al., 2007).

2.2.1 Key sites

This study focuses on the fastest discharging ice stream in the UISS, the Rink-Isbrae (10.5-16.7 km^3 yr^{-1}), which is an order of magnitude greater than Ingia-Isbrae (1.1 km^3 yr^{-1}) (Rignot and Kanagaratnam, 2006). Several key sites along our chosen flowline (section 4) aid in constraining ice

thickness, ice margin position and thinning rates along the UISS during deglaciation. They include Ubekendt Ejland, Karrat Ejland and the Rinks/Umiamako spur. Also detailed is the area around Ikerasak and Store Gletscher which helps to build a regional picture of ice thickness and deglaciation, though these sites sit to the south of our chosen model flowline. Using the field evidence and CRN ages, it is possible to reconstruct the extent of warm and cold-based ice, minimum ice stream surface elevation, and a retreat chronology for the UISS.

2.2.2 Ubekendt

Ice thickness: The limit of upper warm-based ice on Ubekendt Ejland is likely to be below 1090 m asl (Fig. 10). Above this elevation, the landscape is covered in autochthonous blockfields and local cold-based ice with exposure ages varying from 86.9 ka BP (^{10}Be), 68.7 ka BP (^{36}Cl) and 31.3 ka BP (^{10}Be) suggesting that this area has a complex exposure and burial history (Table 1). It may even have been ice free for a long period of time (pre-LGM) (Lane *et al.,* 2014). The terrain on Ubekendt below 750 m asl bedrock becomes markedly smooth and abraded, inferring former active warm-based ice below that altitude.

Moraines: A lateral moraine staircase along the south side of Ubekendt marks thinning of the ice stream as it sat in the Uummannaq trough. The highest lateral moraine reported by Roberts *et al.,* (2013) is at 682 m asl with a clear staircase marking thinning down to 122 m asl (Fig. 11). The low-lying saddle across the centre of the island (200–350 m asl – Fig. 10) also displays a distinct suite of overrun moraines that record ice-margin recession and re-advance (Lane *et al.,* 2016). Associated with them is a series of ice-marginal deltas that mark the final retreat of ice across Ubekendt and into Igdlorssuit Sund.

Deglacial chronology: The scatter of CRN exposure ages below 770 m asl on the southern side of Ubekendt do not show a uniform pattern of ice thinning and exposure with ages varying between 12.3 and 63.7 ka (Table 1). There is clearly a problem with inheritance within this mixed assemblage of erratic and bedrock samples (Roberts *et al.,* 2013). The two youngest cosmogenic radionuclide ages (12.5 & 12.3 ka) could, theoretically, point to almost instantaneous thinning of the UISS between 770 m and 122m asl, but this seems highly unlikely given the lateral moraine staircase points to sequential thinning. Another problem with low elevation deglaciation by 12.5 ka is the assertion by Sheldon et al., (2016) that the UISS grounding line was fixed at a GZW to the west of Ubekendt during the Younger Dryas (Fig. 5). This would imply that the CRN dates from Ubekendt Ejland are too old on account of either incomplete resetting of the cosmogenic isotope clock by glacial erosion, or ice thinning or marginal retreat.

Table 2. Cosmogenic nuclide ages from Ubekendt and Karrat Ejland. Adapted using data from Lane et al., 2014 and Roberts et al., 2013.

No.	m asl	Age	Geomorphology	Comment	Reference
Ubekendt					
UBE2	233	12.5 (36Cl)	Upper limit of till and erratics	Constraint on deglacial thinning	Roberts et al., 2013
UBE1	125	17.2 (36Cl)	Base of lateral moraine	Elevation of features	Roberts et al., 2013
UBE10	682	63.7 (36Cl)	Upper limit of lateral moraine	Elevation of features	Roberts et al., 2013
UBE14	770	12.3 (10Be)	Erratic on frost reworked till	Constraint on deglacial thinning	Roberts et al., 2013
UBE7	485	25.3 (10Be)	Erratic	Ice free during LGM	Roberts et al., 2013
UBE11	688	43.7 (10Be)	Erratic on frost reworked till	Ice free during LGM	Roberts et al., 2013
UBE18	975	31.3 (10Be)	Erratic on frost reworked till	Ice free during LGM	Roberts et al., 2013
UBE22	1142	86.9 (10Be)	Erratic on frost reworked till	Ice free during LGM	Roberts et al., 2013
UBE20	1012	68.8 (36Cl)	Erratic on frost reworked till	Ice free during LGM	Roberts et al., 2013
UBE13	756	23.8	Quartzite boulder	Minimum LGM surface elevation	Roberts et al., 2013
Karrat					
KA2	720	11.6	Glacially abraded bedrock	LGM ice covered this point	Lane et al., 2014
KA9	482	12.14(10Be)	Glacially abraded bedrock	Constraint on deglacial chronology	Lane et al., 2014
Lake	270	11.4 (14C)	bedrock from lake	Constraint on deglacial chronology	Lane et al., 2014
KA6	276	11.9 (10Be)	Glacially abraded bedrock	Constraint on deglacial chronology	Lane et al., 2014
KA17	69	6.9 (10Be)	Glacially abraded bedrock	Constraint on deglacial chronology	Lane et al., 2014
KA24	1019	18.9 (10Be)	Partially abraded bedrock	LGM ice covered this point	Lane et al., 2014
KA10	380	7.2(10Be)	Glacially abraded bedrock	Constraint on deglacial chronology	Lane et al., 2014
KA19	148	6.5 (10Be)	Glacially abraded bedrock	Constraint on deglacial chronology	Lane et al., 2014
K1	210	11.1(10Be)	Upper of set of 3 moraines	Constraint on retreat behaviour	Lane et al., 2014
K3	49	11.1(10Be)	Lowest of set of 3moraines	Constraint on retreat behaviour	Lane et al., 2014
KA11	286	9.0 (10Be)	Glacially abraded bedrock	Constraint on deglacial chronology	Lane et al., 2014
25	1075	80(10Be)	Erratics	Ice free at all times	Lane et al., 2014
Rink-Karrat spur					
KA3	1402	18.9	Bedrock	LGM ice covered this area	Lane et al., 2014
KA5	1964	92 (10Be)	Shattered bedrock	Ice free at all times	Lane et al., 2014
KA23	110	5.2	Glacially abraded bedrock	LGM ice covered this point	Lane et al., 2014
KA27	162	6.6 (10Be)	Glacially abraded bedrock	Constraint on deglacial chronology	Lane et al., 2014
KA20	400	5.5 (10Be)	Glacially abraded bedrock	Constraint on deglacial chronology	Lane et al., 2014
KA21	411	5.3 (10Be)	Glacially abraded bedrock	Constraint on deglacial chronology	Lane et al., 2014
Ikersak					
IKE1	956	11.4 (10Be)	Glacially abraded bedrock	Constraint on deglacial chronology	Roberts et al., 2013
IKE6	129	11.4 (10Be)	Glacially abraded bedrock	Constraint on deglacial chronology	Roberts et al., 2013
IKE8	810	88.8 (10Be)	Glacially abraded bedrock	Ice free at all times	Roberts et al., 2013
IKE9	807	37.1 (10Be)	Glacially abraded bedrock	Ice free at all times	Roberts et al., 2013
IKE10	642	11.3 (10Be)	Glacially abraded bedrock	Constraint on deglacial chronology	Roberts et al., 2013
IKE11	497	11.6 (10Be)	Glacially abraded bedrock	Constraint on deglacial chronology	Roberts et al., 2013
IKE13	163	9.3 (10Be)	Glacially abraded bedrock	Constraint on deglacial chronology	Roberts et al., 2013
IKE17	1170	120 (10Be)	Erratic	Ice free at all times	Roberts et al., 2013
IKE18	1182	121 (10Be)	Erratic	Ice free at all times	Roberts et al., 2013
IKE22	39	8.7 (10Be)	Glacially abraded bedrock	Constraint on deglacial chronology	Roberts et al., 2013
IKE24	120	11 (10Be)	Glacially abraded bedrock	Constraint on deglacial chronology	Roberts et al., 2013

Figure 10. Cross sectional profile of Ubekendt Ejland with the proposed ice surface elevation and geomorphic features.

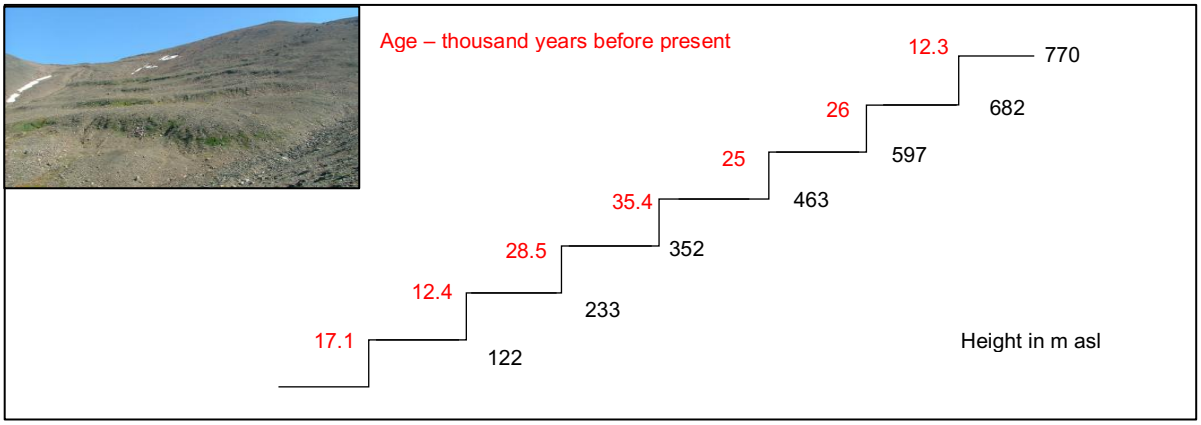

Figure 11. Lateral moraine staircase in the south of Ubekendt Ejland. The exposure ages indicate that inheritance has impacted the ages of the lateral moraines.

2.2.3. Karrat Ejland

Ice thickness: Around Karrat, ridge summits above 800 m asl mark a transition between areally scoured terrain to heavily weathered and frost shattered bedrock, and once over 1000 m asl the terrain is dominated by autochthonous blockfield. The low elevation areas on Karrat are characterised by areally scoured terrain with roches moutonnées indicative of warm-based ice (Lane *et al.,* 2015). Striations record two clear phases of ice flow, with an initial ice flow of 32°-212° overprinted as later ice shifted to a trajectory of 88°-268° as it became topographically constrained during deglaciation (Fig. 12). The highest terrestrial cosmogenic nuclide date on Karrat Ejland was from KA2 (724 m asl) (an in-situ bedrock slab) that yielded ages of 11.7 and 13.5 ka BP for ^{10}Be and ^{26}Al respectively. These are robust exposure ages and suggest that warm-based ice operated up to at least 724 m asl during the last glacial cycle. The highest occurrence of abraded, striated bedrock observed on

Qerqertarssuaq just to the north was 1040 m asl, bracketing the upper limit of warm-based ice to 724 – 1040 m asl (Lane *et al.,* 2015).

Moraines: A lateral moraine staircase on western Qerqertarssuaq points to sequential thinning between 786 – 340 m asl as the UISS thinned, but the moraines lack a robust chronology. In contrast, a series of low elevation moraines that follow the coast between Karrat (K1-K3) and Qerqertarssuaq (N1 – N3) are well constrained chronologically and clearly relate to ice margin pinning across the outer Karrat fjord between 210 and 49 m asl (Lane *et al.,* 2016)

Deglacial Chronology: Cosmogenic samples KA6 and KA11 on Karrat provide maximum ages for deglaciation prior to moraine formation (K1-K3) between 11.9 – 9.1ka BP and these agree with a radiocarbon date from Karrat Lake (~11.2 ka BP). These dates support the theory proposed by Philipps et al., (2018) whereby retreat in to the inner fjords occurred by 11.0 ka BP. The moraines are bracketed by several CRN ages which suggest they formed between 9.1 and 6.5 ka BP. The young ages given by KA18 and KA15 (3.4 and 2.2 ka BP respectively) are anomalous, and do not fit with exposure ages further east which suggest the UISS retreated into the inner fjord between 6.6 and 5.0 ka (Lane *et al.,* 2016; Table 1).

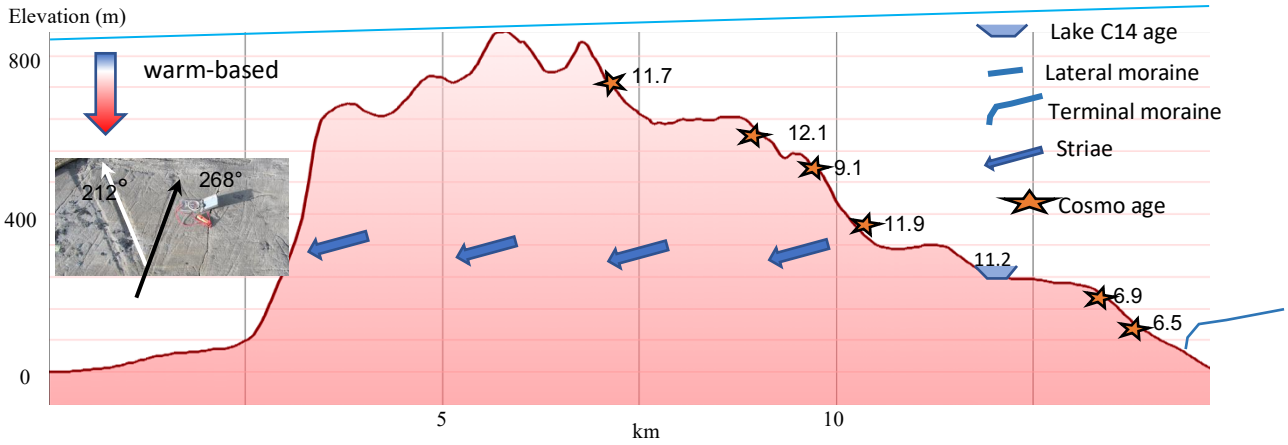

Figure 12. Cross sectional profile of Karrat Ejland. Blue line is the upper limit of warm based ice at around 820 m asl and the orange line represents the maximum elevation for striations at around 400 m asl.

2.2.4. Rink-Umiamako spur to inner Rink-karrat fjord

Ice thickness: In the inner Rink area high level terrain above 1400 m asl is mantled by extensive autochthonous blockfield. A CRN age from in situ bedrock at 1964 m asl gave ages of 92.0 ka BP (Fig. 14) ^{10}Be and 96.1 ka BP ^{26}Al respectively, suggesting that this surface had experienced minimal erosion during MIS4-2 and was either protected by cold based ice or completely ice free (*See Strunk et al., 2017 for discussion of complex exposure/burial histories*). The possible upper limit of warm-based ice is constrained by KA3, a sample from a glacially smoothed bedrock dated to 18.9 ka BP ^{10}Be and 22.5 ka BP ^{26}Al; which would infer warm-based ice operating up to ~ 1400m asl (Fig. 14).

Moraines: Two sets of small, poorly developed, lateral moraines were mapped on the spur between Rink and Umiamako fjords (Lane *et al.,* 2016). The first, R1-R3 records ice activity within Rink fjord with the moraines running sub-parallel to each other at 365-235 m asl (Fig. 13) (Lane *et al.,* 2016). The second set, UM1-UM3, lie on the spur between two fjords running further downhill at 192-37 m (Lane *et al.,* 2016). These features provide constraints on the vertical upper limit of warm-based ice and ice margin retreat through the mid to inner Rink fjord during the Holocene.

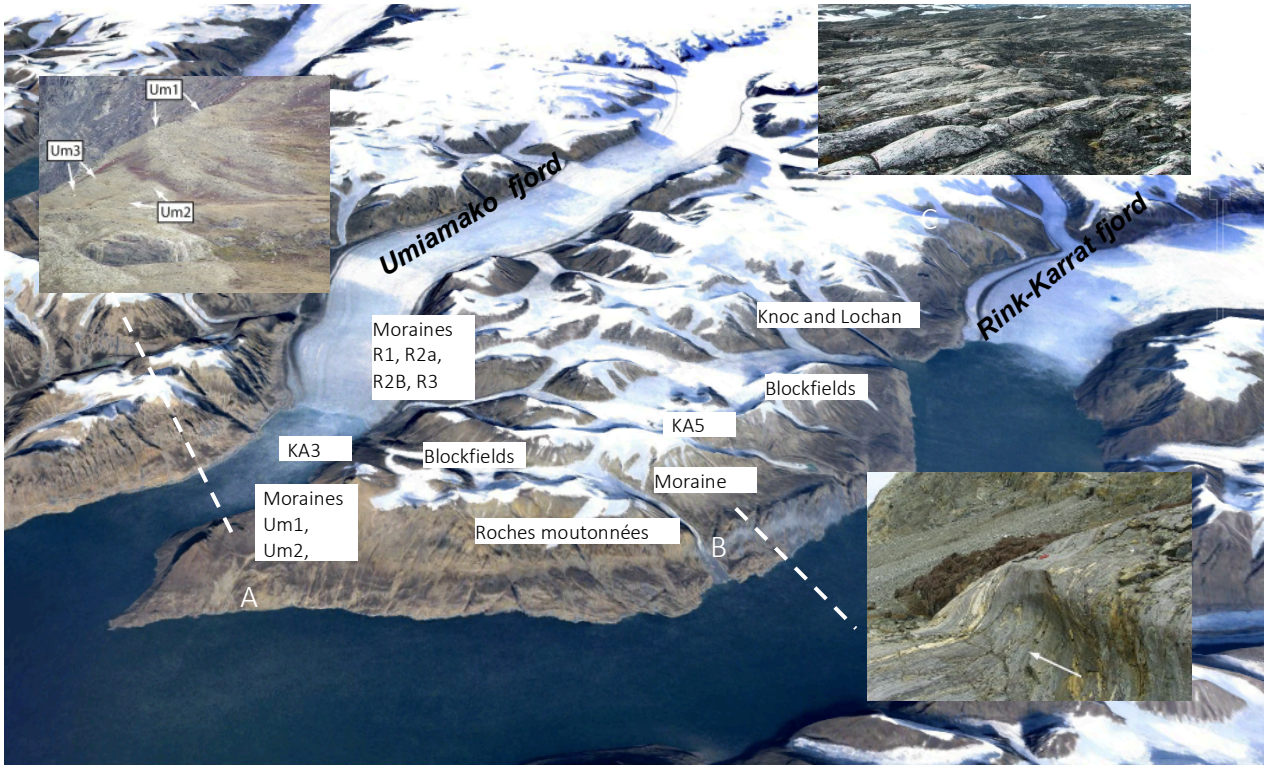

Figure 13. Evidence of striated, ice moulded roche moutonnee with lateral p-forms in the Karrat and Umiamako confluence. A fragmentary lateral moraine at 740 m asl in inner Rink Fjord and moraines Um1-3 and R3 (all arrowed) at the Rink–Umiámáko confluence. Autochonous blockfields are present at 1400 m asl in inner Rink Fjord and at 1900 m asl on Pyramid Stubben (Lane et al. 2015)

Deglacial chronology: Lane *et al.,* (2016) clearly show that the ice margin had reached the Rink-Umiamako spur by 6.6 ka (KA27) and retreated into inner Rink by 5.0 ka BP (KA21, KA23, KA20). CRN ages KA20 and KA21 are ~ 400 m asl inferring relatively late thinning of the ice into the Holocene, but the higher ages from ~1400 m asl of deglaciation at 18.9 ka (KA3) suggest that ice thinning had been on going throughout deglaciation and into the Holocene. This points to upstream thinning of the UISS system as ice withdrew from the outer continental shelf.

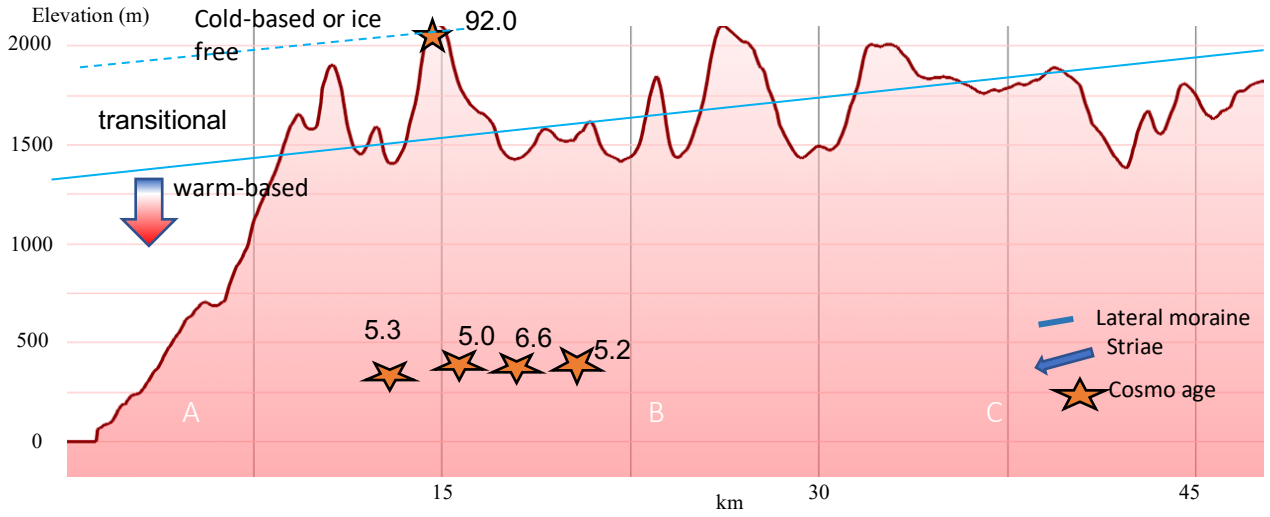

Figure 14. Cross sectional Profile of the Inner Rink-Karrat fjord with associated ice surface profile and geomorphic features.

2.2.5 South UISS – Storoen/Ikersak/Nuussuaq

Ice thickness: On Nuussuaq trimlines (Fig. 15B) were identified as limits separating glacially eroded terrain from shattered periglacial blockfield at around 1200 m asl (Kelly, 1985; Roberts *et al.,* 2013). Above this, local ice caps cover much of the region. In-situ bedrock from sites within blockfields on top of the Nuussuaq Peninsula (Fig. 15A) (1200 m asl) have cosmogenic ages over 100 ka BP (pre-MIS4). These either point to local cold-based ice caps above 1200 m asl, or prolonged periods of ice free conditions as the concordant $^{26}Al/^{10}Be$ ages on Nuussuaq do not support an excessively long burial periods. Hence, these high elevation blockfield terrains have not been affected by glacial abrasion and erosion by the main UISS (Roberts *et al.,* 2013). Opposite Ikerask on the northern edge of the Nuussuaq Peninsula, areally scoured terrain extends up to 966 m asl indicating the UISS overtopped the trough at some point (Roberts *et al.,* 2013). However, the summit of Ikersak Ejland (~825 m asl) is not heavily abraded suggesting it was close to the upper limit of warm-based ice. Two samples CRN (IKE8 and IKE9) from in situ bedrock samples (Table 1) close to the Ikerask summit yielded contrasting exposure ages of 88.8 and 37.1 (^{10}Be) suggesting inheritance and only partial erosion of the bedrock at this elevation (Roberts *et al.,* 2013). Based on LIA trimline zones it is likely that the ice margin advanced up to 300 m outboard of its present margin and this would explain why Marble Lake Lobe, Erratic Lake and Bedrock Lake are still presently proglacial lakes (Phillips *et al.,* 2018).

Moraines: Roberts *et al.,* (2013) note several high elevation lateral moraines that point to the UISS overtopping the Nuussuaq fjord walls up to ~ 800 m (Fig. 15B). These can be traced along the northern edge of the Nuussuaq Peninsula to the west past Uummannaq and they constrain the upper

surface of the ice stream. Ice marginal positions are difficult to constrain but the Drygalksi moraine complex clearly marks the ice margin retreating close to Store Gletscher around ~9.9 ka (Cronauer *et al.,* 2016).

Deglacial chronology: CRN ages from Uummannaq Ejland suggest the UISS margin had retreated east of the island by 11.0 ka BP. This is supported by a range of bedrock and erratic CRN ages that point to both rapid thinning (from 642 m asl) and ice margin retreat at lower elevation (129 m asl) on Ikerasak by 11.6 to 11.4 ka. Ice retreat east of Ikerasak to the Store Gletscher margin was complete by 8.7 ka (IKE 22).

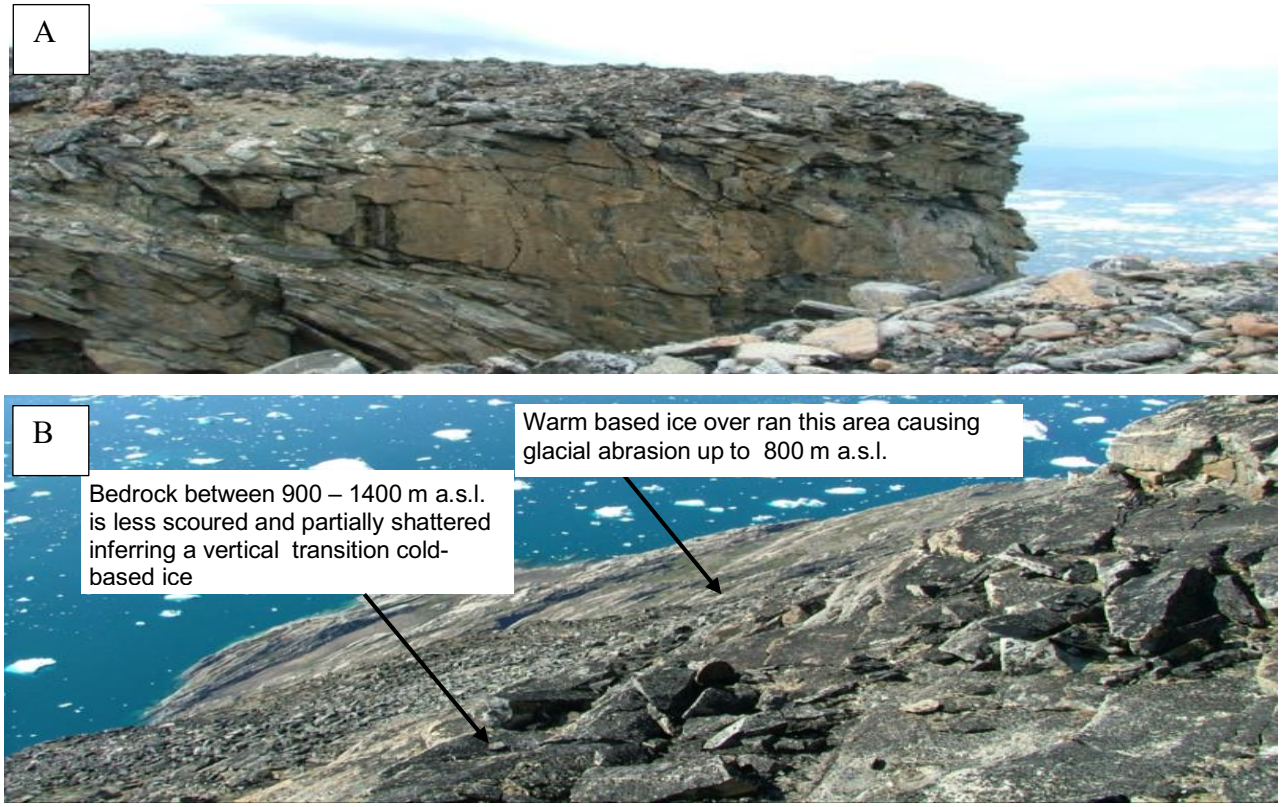

Figure 15. A-B) Blockfields on the northern side of Nuussuaq Peninsula. Photo from Roberts et al., 2013.

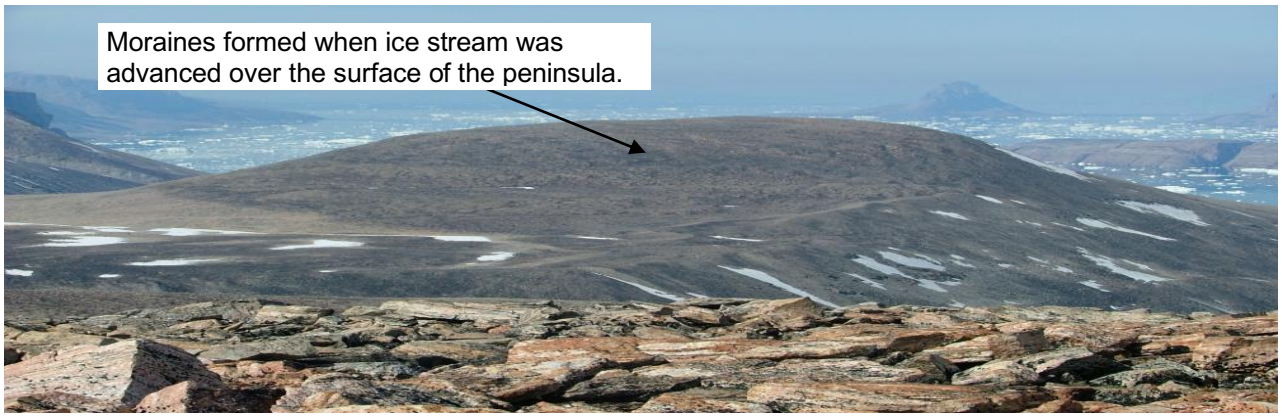

Figure 16. Lateral push moraine on the Nuussuaq Peninsula and erratics deposited by warm-based ice. Photo from Roberts et al., 2013.

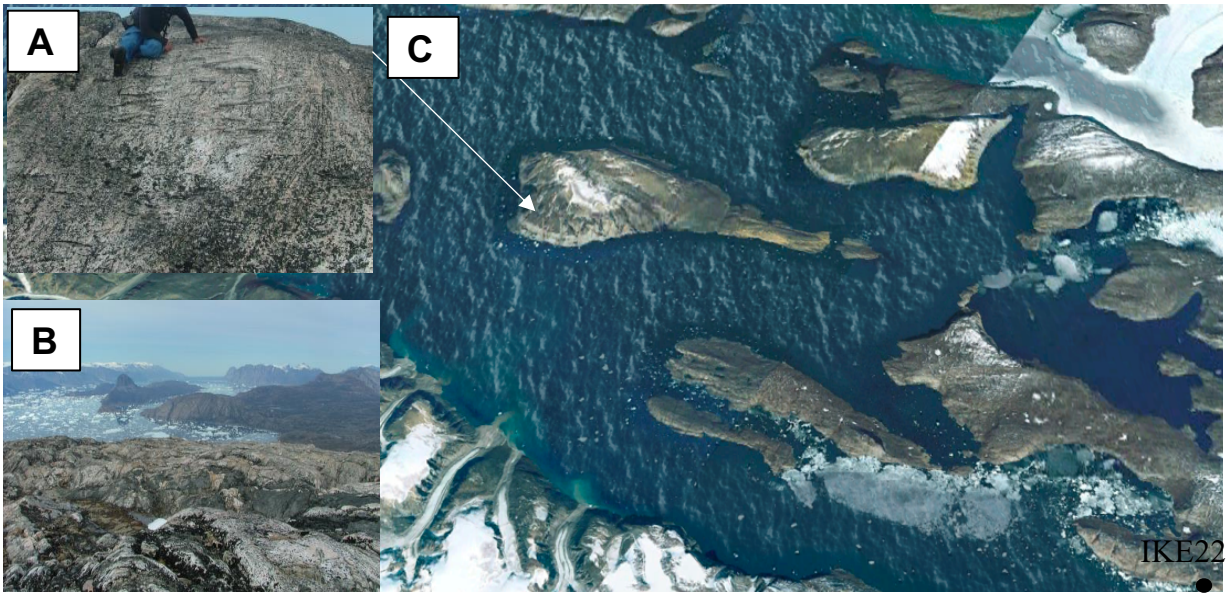

Figure 17. A) Striations on storoen, B) Knoch and Lochan features. Photos from Roberts et al., 2013. C) Cross sectional profiles of Storeon and Ikerasak from Google Earth.

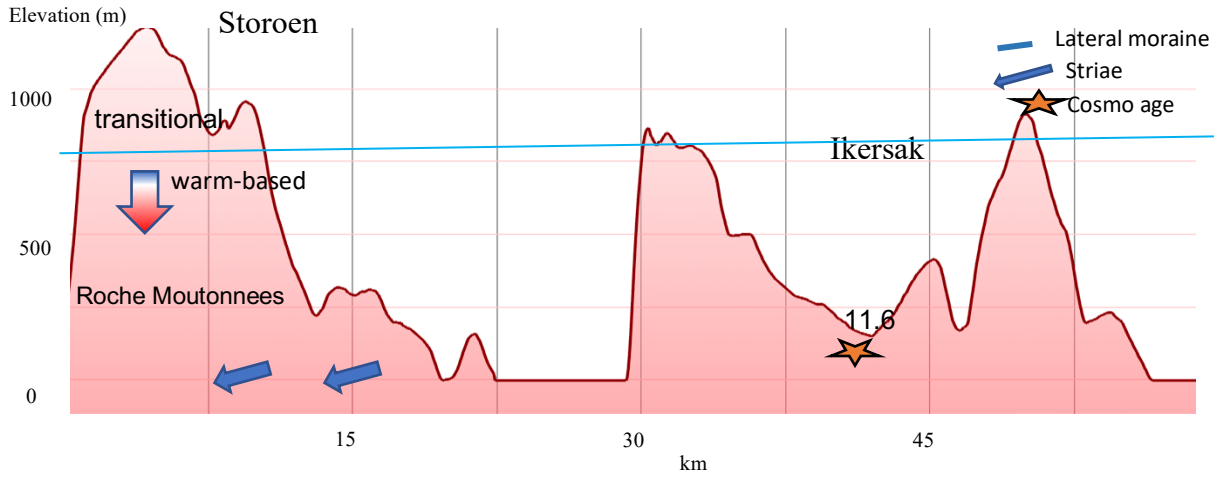

Figure 18. Cross sectional profile of Storoen and Ikersak (see Fig 17 for cross-sectional location) with the upper limit of warm based ice in the blue line.

2.3. Summary of the key geomorphology and deglaciation history

Combining ice thickness and the deglacial chronologies of the geomorphic evidence from the three key sites it is likely that the UISS overtopped Ubekendt Ejland which became ice free around 12.5 ka BP. In the north, ice thickness in the vicinity of Karrat Ejland reached up to 1000 m asl during the LGM and became ice free around 11.0 ka BP. The UISS stabilized on the east of Karrat Ejland between 11.0 – 6.5 ka BP before retreating into the fjord heads. In the south, around Ikersak, warm-based ice reached up to 800 m asl during the LGM and became ice free around 11.0 ka BP.

3. Timing and rate of the UISS retreat

Evidence presented in the literature is reviewed in the following sections in order to discuss (i) When the ice margin retreated from the shelf edge; (ii) whether it retreated episodically, gradually or rapidly; (iii) What the potential forcings were that initiated and drove retreat. This information will be used to control and constrain the numerical modelling aspect of this project.

3.1. When did the ice margin retreat from the shelf edge?

The timeline of the UISS retreat is constrained by three radiocarbon dates from the offshore region of the ice stream and a suite of cosmogenic nuclide dates from islands in the inner fjords. In core VC46 (*see table 1 for core dates*), the end of glacigenic debris flows deposition and onset of hemipelagic sedimentation at 17.1 ka BP marks the initial grounding-line retreat of the UISS (Jennings *et al.* 2017). This date is earlier than that measured on the nearby moraine ridge on the outer shelf at core JR175-VC45 which yields a date of 14.8 ka BP from glacimarine sediments only 5 cm above a basal till (O'Cofaigh *et al.,* 2013b). However, the lithological sequence suggests that the full deglaciation sequence was not captured in that core (Sheldon *et al.,* 2016) so the mismatch between dates may be less significant than the dates suggest. In the mid-trough region, core VC42 did not contain sufficient carbonate material for radiocarbon dating, however, Core MSM343520 dated retreat to 10.8 ka BP from a sample that lies 1.5 m above the till within distal glacimarine, massive pebbly muds that contain a strong melt-water faunal signal (O'Cofaigh *et al.,* 2013b). This date indicates a minimum deglacial age for the landward retreat of the UISS from the mid-shelf GZW. This phase of retreat is suggested to correspond to the last IRD event recorded in the outer shelf cores, beginning at the end of the Younger Dryas, ca. 11.5 cal kyr BP (Jennings *et al.,* 2017).

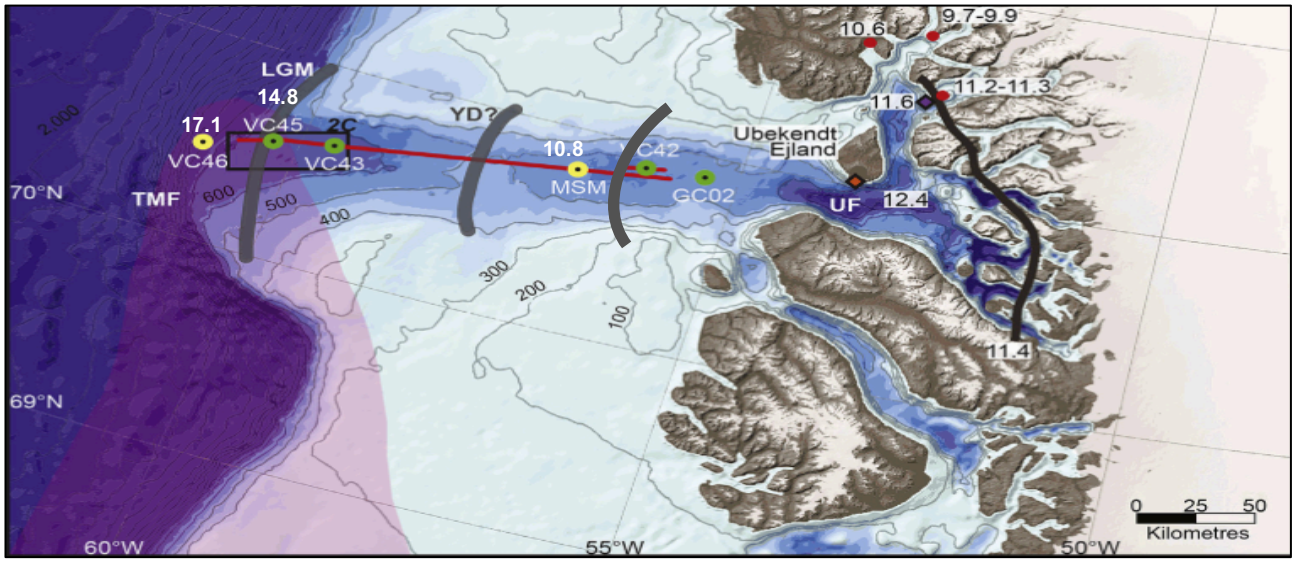

Figure 19. Map of the Uummannaq trough, bathymetry, core sites and deglacial dates. The grey lines on the outer shelf and mid-shelf represent the ice extent at the LGM and the possible YD still stand. The translucent pink outline represents the "pinch- out" of the IRD belt. TMF = trough mouth fan. The grey lines represent the GZWs and the extent of the GrIS is shown in white. Adapted from Roberts et al., 2013.

3.2. Did the UISS retreat episodically, gradually or rapidly?

The rate of retreat of the UISS could have been fast and relatively continuous or stepwise/episodic. In the former, the ice stream is assumed to have retreated rapidly from the continental shelf similar to the Jakobshav Isbrae (Long & Roberts 2002; Lloyd *et al.,* 2005; Hogan *et al.,* 2011; Kelly *et al.,* 2013) whilst, in a stepwise retreat the ice stream would have experienced short periods of still stands at bedrock highs or fjord width constrictions (Weidick, 1996; Rasch, 2000; Hogan *et al.,* 2016).

Following the retreat of the grounded ice, core VC46 shows the deposition of a fine grained sediment barren of ice rafted debris (IRD) and the deposition of this layer is thought to have continued until 15.3 ka BP (Jennings *et al.,* 2017). Had the ice margins and grounding line retreated landward rapidly by calving this unit would have contained IRD clasts >2 mm instead, this lack of IRD is attributed to signify the retention of a buttressing ice shelf, pervasive sea ice, and the landward shallowing bathymetry of the outer shelf as the grounding line retreated slowly across the outer shelf. In the presence of an ice shelf, coarser-grained material would have been preferentially deposited proximal to the grounding line, leaving icebergs calved from the ice-shelf front relatively clean of debris (Jennings et *al.,* 2017).

The timing of GZW formation on the mid-shelf is unresolved, but, based on the two constraining ages on the outer and mid shelf, it must have formed during a still stand that occurred between 14.8 and 10.8 cal kyr BP, hence it could represent a YD ice margin position (Sheldon *et al.,* 2016; Dowdeswell *et al.,* 2014). This contradicts the retreat model proposed by Roberts et al. (2013) who suggested that surface exposure ages on Ubekendt point to deglacial of Ubekendt by 12.4 ka BP (Roberts *et al.,* 2013). This retreat from Ubekendt at ~ 12.4 ka may be manifested in the long glaciomarine record below the dated horizon (10.8ka) in core VC 42 but this requires further research.

The UISS was grounded close to the present coast by the early Holocene, following retreat by calving and strong melting under the influence of atmosphere and ocean warming and a reverse bed slope into the adjoining deep fjords (Roberts *et al.,* 2013). Cosmogenic isotope ages from the adjacent coastal area suggest that UISS was thinning dramatically by the end of the YD and that the ice margin had retreated into the fjords by 11.4 ka BP, implying rapid ice retreat from the deep trough on the inner shelf (Lane *et al.,* 2014; Roberts *et al.,* 2013). The ensuing rapid mass loss by calving produced pulses of IRD and intervals of high IRD concentration in VC42 indicate the loss of the fringing ice shelf and retreat of a predominantly grounded ice front by calving of debris laden icebergs between the LGM and the early Holocene (Knutz *et al.,* 2013; Jennings *et al.,* 2017).

3.3. Which forcings may have initiated and driven retreat?

The retreat of the UISS was likely governed by a range of factors, such as, increasing solar insolation, increasing air/ocean temperatures and sea level rise. In addition, topographic controls evolved from long term glacial erosion and the area's uplift history, were also influential on grounding line stability (Roberts *et al.,* 2013; Lane *et al.,* 2014). It is likely that the deglaciation following the LGM began on the outer shelf by 17.1 ka BP, with increased air temperature, rising relative sea level and bathymetric over-deepening driving the UISS back to the fjord mouths by 11.4-11.0 ka BP. In the south, topographic constrictions stabilized the ice from 11.0-9.3 ka BP (Lane *et al.,* 2014). Nevertheless, it remains unclear whether any of these were dominant drivers, or if they simultaneously controlled retreat.

3.3.1. Topographic controls

It has been proposed that marine-based ice sheets resting on retrograde beds are inherently unstable and subject to possible large-scale disintegration: the Marine Ice Sheet Instability or MISI (Weertman, 1974; Mercer, 1961; Schoof, 2007a). Once perturbed from a steady state position, an unstable marine ice sheet will continue to either advance or retreat, without the need of any additional forcing until a new stable state is found. Nevertheless, Gudmundsson *et al.,* (2012) demonstrates that retrograde slopes at the grounding lines of marine ice sheets do not per se imply instability if grounded pinning points between the ice and bedrock interface can increase the buttressing force exerted on the ice shelf. Jamieson et al (2012) identified that grounding line retreat on a retrograde slope could be significantly slowed down and that such slowdowns in their particular example of Marguerite Bay in Antarctica, occurred in the same locations as GZWs were found on the trough floor. In the case of Rink-Karrat fjord, ice margin stagnation occurred during the Holocene Thermal Maximum (HTM) despite warmer temperatures. Therefore, ice stream marginal stability was likely controlled by non-climatic factors, such as the lateral drag exerted by the sides of the trough in the offshore region and by the valley sides inland (*Section 2*) (Lane *et al.,* 2014). This slowed retreat, as ice in the north became pinned at the mouth of Rink-Karrat fjord between 11.6 - 6.9 ka BP (Lane *et al.,* 2014): confirming the ability of topography and fjord width to override climate and sea-level drivers. This concept, questions those estimates of the rate of potential near-future contribution of glaciers to GMSL change based solely on the notion that those resting on a retrograde slope are inherently unstable.

Furthermore, the onset of hemiplegic sedimentation at 17.1 ka BP (Jennings *et al.,* 2017) marks grounding line retreat of the UISS from the continental shelf edge. The deep trough of the UISS may have allowed earlier access of warm intermediate water to the grounding line, thereby assisting earlier retreat (Sheldon *et al.,* 2016; Jennings *et al.,* 2017). Thus, the topography of the region is important because deeper fjords permit the intrusion of Atlantic waters (AW) toward the glaciers, whilst shallow sills created by former glacier advances, fjord narrowing or shoaling may limit the access of

subsurface AW to the glacier grounding lines (Christoffersen *et al.,* 2011; Mortensen *et al.,* 2011; Chauche *et al.,* 2014; Gladish *et al.,* 2015). Bed topography and fjord width is therefore cited as a crucial control on ice stream retreat rate (Schoof, 2007; Jamieson *et al.,* 2012).

Along the southern arm of the UISS the grounding line retreated towards Store Gletscher becoming topographically pinned at ~11.4 – 11.0 ka BP, but from 9.3 ka BP onwards retreat rates increased with the ice reaching the present Store Gletscher margin by 8.7 ka BP. This coincided with increased air temperatures and peak summer insolation at the start of the Holocene (Roberts *et al.,* 2013).

The northern arm of the UISS also deglaciated quickly from Ubekendt, calving into Karrat/Rinks and Ingia Fjords. Lateral moraines north of Karrat again point to stepwise thinning of the UISS as ice retreated. At ~11.3 ka BP the ice front in Karrat/Rinks fjord stabilised until ~6.5 ka BP and seemingly became unresponsive to both climate and marine forcing for 5 kyrs due to topographic pinning (Roberts *et al.,* 2013)

The pattern of ice residing on Karrat Ejland during the middle of the Holocene is anomalous when compared to the deglaciation pattern within the Uummannaq fjord system and elsewhere in Greenland (Bennike, 2000; Funder *et al.,* 2011; Briner *et al.,* 2013; Roberts *et al.,* 2013). The reason for this anomalous pattern is unknown, but it may relate to topographical/bathymetric controls and the fjord geometry (Lane *et al.,* 2014) (e.g. fjords are narrower). In addition, the fjord inland from Karrat widens, and also deepens (from 400 m to 1000m; Rignot *et al.,* 2016). Thus, once ice retreated from Karrat it probably would have receded quickly via rapid calving through its major over-deepening until reaching shallow waters, which exist near and behind the present position of Rinks Isbrae (Morlighem *et al.,* 2014; Rignot *et al.,* 2015, 2016).

3.4. External controls

There are a range of external controls such as, ocean warming, increasing atmospheric temperatures and rising sea level, that could have potentially influenced the retreat of the UISS.

3.4.1. Ocean warming

Analyses of benthic and planktonic foraminiferal assemblages, sea ice biomarkers IP_{25} and $\delta^{18}O$ of planktonic foraminifera (*neogloboquadrina pachyderma sinistral)* in the interval 17.5-10.8 ka BP indicate that the UISS retreat was followed quickly by incursion of the WGC, suggesting that the warm water may have enhanced ice retreat (Sheldon *et al.,* 2016; Jennings *et al.,* 2017). The warm subsurface Atlantic water forms the West Greenland Current (WGC) at the confluence of the East Greenland Current (EGC) and the Irminger Current (IC) (Fig. 20) and was limited to depths below the ice stream grounding lines during the LGM. The deeper UISS (>600 m) retreated first (17.1 ka BP –

VC46) marked by the onset of hemipelagic sedimentation, while to the south, the shallower Disko ice stream began retreating at ca. 16.2 ka BP (Jennings *et al.,* 2017). In cores VC46 and VC42 a fine-grained interval barren of IRD occurs after ice retreat and this suggests that the grounding lines were protected from accelerating mass loss (calving) by a buttressing ice shelves and by landward shallowing bathymetry on the outer shelf (Jennings *et al.,* 2017). Two ocean warming events have been identified during the retreat of the UISS and these occurred during 16.8 ka BP and 15.8-14.9 ka BP (Jennings *et al.,* 2017).

The timing of this first ocean warming event coincides with, or slightly lags, Heinrich event 1 (16.8 ka BP) from Hudson Strait (Hemming, 2004) and this reflects the IC advection that could have supplied the warm subsurface water farther north along the central west Greenland margin. The second interval of subsurface ocean warming occurred between 15.8 and 14.9 ka BP (Knutz *et al.,* 2011). The instability of outlet glaciers draining the Laurentide, Innuitian and GrIS into northern Baffin Bay periodically released cold, fresh water that would have enhanced sea ice formation and slowed GrIS melt.

During the YD, offshore sedimentary records in central West Greenland document strong cooling and a lack of GrIS melt-water in the West Greenland Current, and an increase in iceberg rafted material from northern Baffin Bay (Jennings *et al.,* 2017). The hypothetical formation of a large grounding zone wedge west of Ubekendt Ejland in the Uummannaq Trough prior to, and during, the Younger Dryas (12.8–11.6 ka BP) occurs during this ocean cooling period (Sheldon *et al.,* 2016; Dowdeswell *et al.,* 2014). A final phase of IRD deposition signifies retreat from this mid-shelf grounding zone wedge (Sheldon *et al.,* 2016) and foraminifera in this unit indicate warmer Atlantic-sourced water was present and possibly helped to drive the ice retreat to the inner shelf (cf. Bindschadler, 2006).

Today the influx of warm water to the base of an West Greenland glaciers has been shown to accelerate grounding line retreat (Holland *et al.,* 2008; Mouginot *et al.,* 2017). While it is likely that the WGC played an important role in sustaining ice retreat after the Younger Dryas and through the early Holocene (Andresen *et al., 2011*; Gramling, 2015), the palaeo environments represented in the outermost shelf core (VC45) at this site suggest that the sedimentary record did not include the most ice-proximal conditions and the data thus does not allow tracking of the initial retreat of the LGM ice or the first onset of the WGC (O'Cofaigh *et al.,* 2013a). Although there are insufficient data to conclude that the WGC played a strong role in initiating the ice stream retreat (Knutz *et al.,* 2011), it is likely that the warm current helped to sustain the ice retreat, as has been observed along modern marine Greenland ice sheet margins (Holland *et al.,* 2008; Straneo *et al.,* 2010; 2012). This demonstrates that the initial UISS retreat from the shelf edge was closer in timing to that of ice retreat in East Greenland of 18–17 cal ka BP (Jennings *et al.,* 2017), contrary to what was previously thought (Vaskogg *et al.,* 2015; Ó Cofaigh *et al.,* 2013b; Jennings *et al.,* 2006; Evans *et al.,* 2002). Dominant

Atlantic water fauna suggest that the WGC was established on the outer shelf in East Greenland by 13.9 ka BP, which is earlier than reconstructions of ocean temperature on the West Greenland shelf by McCarthy (2011).

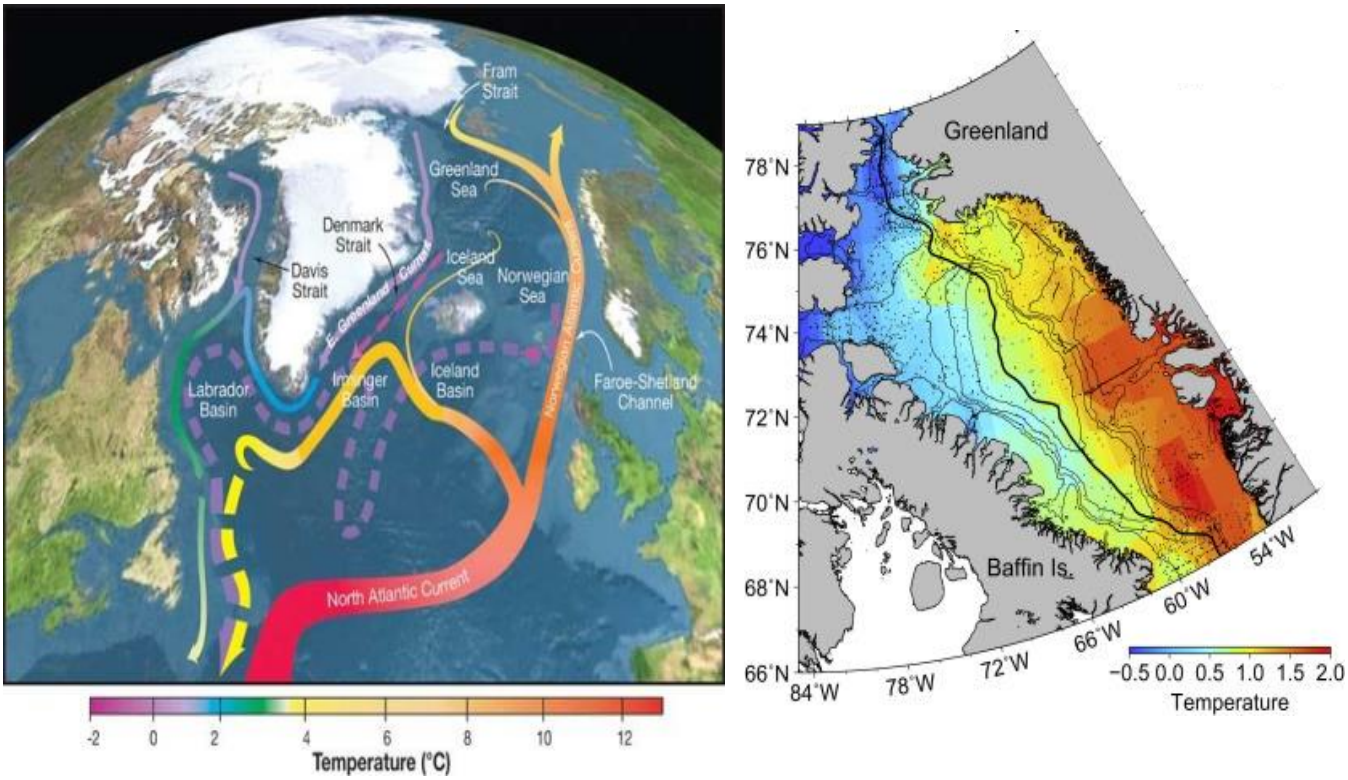

Figure 20. a) The WGC begins at the confluence of the EGC and the IC as they round the southern tip of Greenland and flow north along the shelf of West Greenland (Ribergaard et al. 2008) and the warmer and saltier Irminger current flows below the EGC (Buch 2000a,b) B) The SST in the West of Greenland exceeds 1°C, compared with the cold north-west waters (Straneo & Heimback, 2013).

3.4.2. Sea Level rise

The retreat at 17.0 ka BP coincides with a period of increasing solar insolation (Huybers, 2006) and gradual eustatic sea level rise in west Greenland (Lambeck *et al.,* 2014; Long *et al.,* 1999; Simpson *et al.,* 2009) (Fig. 21). However, it is difficult to differentiate between the driving force of this signal (did rising sea level precede ocean warming or did falling sea level help stabilize the retreat.) Lane *et al.,* (2014) indicate that the UISS had retreated to the inner fjords by 11.6 ka BP under the influence of rising sea level and deepening bathymetry. A parallel scenario is presented by Roberts *et al.,* (2013) from the southern sector of the Uummannaq fjords, with rapid ice retreat into the fjords by 11.4 ka BP.

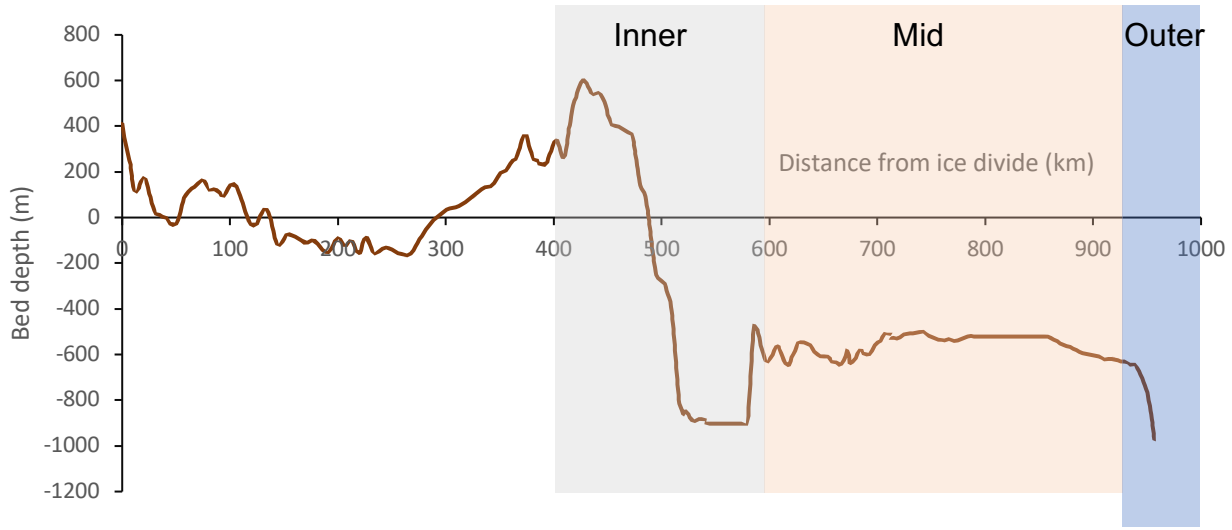

Figure 21. Relative sea level was increasing from 20 – 13 ka BP during the time of deglaciation and was highest during the HTM. Created using model output data from Simpson et al. 2009. 'Outer' refers to sea level at the shelf edge, 'mid' refers to sea level on the middle shelf and 'inner' refers to sea level in the fjords.

3.4.3. Air temperature increase

Temperature records from the Greenland Ice Core Project (GRIP) illustrate fluctuations in regional temperature (Fig. 22). In a scenario where retreat began at 15.0 ka BP (O'Cofaigh *et al.,* 2013a; Jennings *et al.,* 2014), then the timing of the retreat of the UISS from the outer shelf would correspond with the onset of the warmer Bølling- Allerød interstadial (Grootes *et al.,* 1993) or the Greenland interstadial 1e (14.7 - 14.1 ka BP) (Lowe *et al.,* 2008) a period of increasing solar insolation (Huyers, 2006). This suggests that the UISS was responsive to the climatic signals of the Bølling-Allerød and Younger Dryas, similar to findings from southern and northern Greenland (Knutz *et al.,* 2011; Larsen *et al.,* 2018).

Geophysical data indicate that the retreating ice stream stabilised on the mid-shelf sometime around 10.8 cal kyr BP, and likely remained there until the end of the Younger Dryas event, forming a large grounding-zone wedge (Dowdeswell *et al.,* 2014). When compared with the GRIP $\delta^{18}O$ climate record (Grootes *et al.,* 1993), stabilisation of the ice stream margin on the mid-shelf coincides with cooling from the Bølling interstadial into the Allerød period.

Dates suggest that ice in the north became pinned at the mouth of Rink-Karrat Fjord between 11.6 - 6.9 ka BP, remaining stable through the Holocene Thermal Maximum, demonstrating the ability of topography to override climate and sea-level drivers (Lane *et al.* 2015).

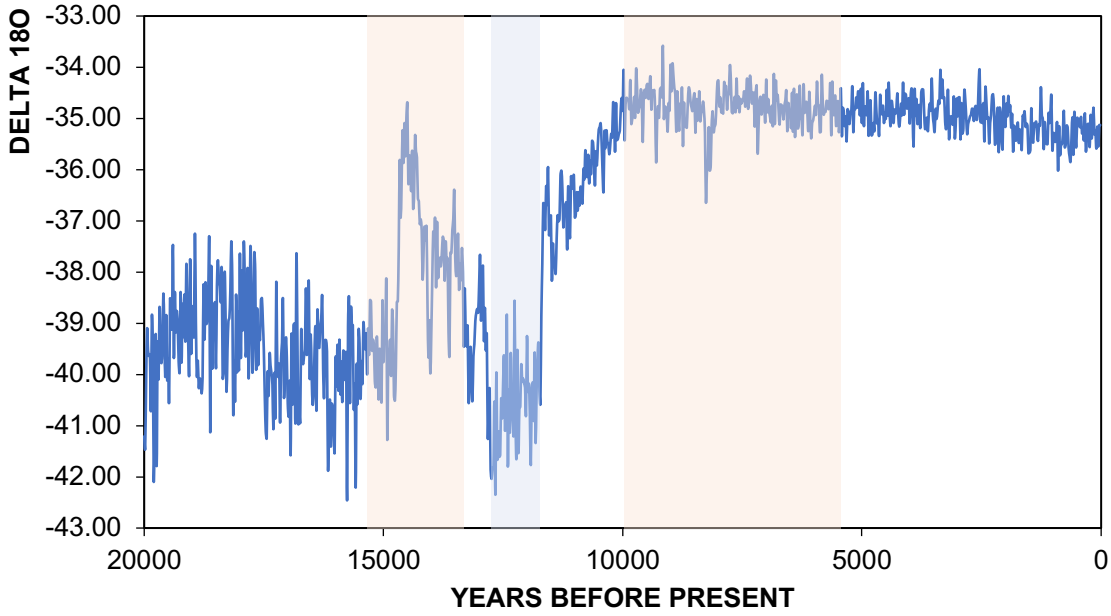

Figure 22. The HTM was characterised by temperature 2-3°C warmer than present, (Axford et al. 2013) a peak in summer insolation a drop in sea level (Simpson et al. 2009).The shaded bands highlight periods of sustained warmer (red) and cooler (blue) temperatures.

3.5. Summary of retreat

In summary, from the above it would suggest that retreat from the outer shelf at 17.1 ka BP (Fig. 24a) began following an ocean warming event and rising sea level (Fig. 23). This supports Jennings et al., (2017) who proposed that retreat was underway by 17.1 ka BP rather than by 14.8 ka BP in response to atmospheric temperature increase (O'Cofaigh *et al.,* 2013a; Jennings *et al.,* 2014).

Retreat from Ubekendt Ejland at 12.4 ka BP to Karrat Ejland at 11.7 ka BP was rapid and 65 km occurred within 0.7 kyrs as the northern UISS progressively 'unzipped' as individual outlet glaciers retreated into fjords (Lane *et al.,* 2014). This occurs during the latter part of the Greenland stadial 1 (12.9 - 11.7 ka BP) and an increase in air temperatures (GRIP) and a peak in relative sea level at 12.0 ka, support this (Roberts *et al.,* 2013; Lane *et al.,* 2014). During this time evidence from GZWs on the mid shelf suggest that the UISS underwent a YD advance (Jennings *et al.,* 2017; Sheldon *et al.,* 2016).

Final stages of retreat into the inner fjords by 11.4 -11.0 ka BP is likely to have been driven by increased air temperatures prior to the HTM and bathymetric over-deepening. Adopting the theoretical analysis of Schoof (2007) it is probable that once retreat was underway an increase in water depths of over 600 m in the Uummannaq trough would have led to an increase in ice discharge and rapid

thinning and retreat (Fig 24). Slow down of retreat may have occurred due to shallowing and narrowing as the grounding line entered the fjord heads.

At Karrat Ejland there was a period of ice margin stabilization around ~11.2 - 6.9 ka BP (Roberts *et al*. 2013; Lane *et al.,* 2014). The formation of moraines K1-K3 on eastern Karrat support this and the closely nested patterns of the moraines suggests that were not formed by a series of separate re-advances. These moraines have been cited as a response to the Greenland 9.3 and 8.2 climatic events (Long and Roberts, 2002; Briner *et al.,* 2005; Young *et al.,* 2011a; 2013). This marginal still stand in Rink-Karrat fjord from the early Holocene through to the HTM (11 – 5 ka BP) was characterised by a warm climate (Kaufmann *et al.,* 2004; Jansen, 2007; Wariner, 2008; Renssen *et al.,* 2009) with temperatures 2-3°C warmer than present and suppressed precipitation levels causing moisture starvation (Bennike, 2010; Axford, 2013). Therefore, this still stand was controlled by non-climatic factors such as channel width around Karrat narrowing to 5 km and depth shallowing to ~400 m (Lane *et al.,* 2014) The shallowing of the bed would have decreased the relative magnitude of ice flux necessary to maintain a stable grounding line (Mercer, 1961; Schoof, 2007; Jamieson *et al.,* 2012). Equally, the narrowing of the channel would have decreased the flux though increased lateral resistance (Mercer, 1961; Whillans and Van der Veen, 1997) and up ice surface profile steepening (Jamieson *et al.,* 2012).

Retreat resumed at 6.9 ka BP reaching the spur between Rink and Umiamako fjord by 6.5 ka BP and to the current margin by 5.0 ka BP (Lane *et al.,* 2014 - Fig. 23A & B for grounding line positions and corresponding climate).

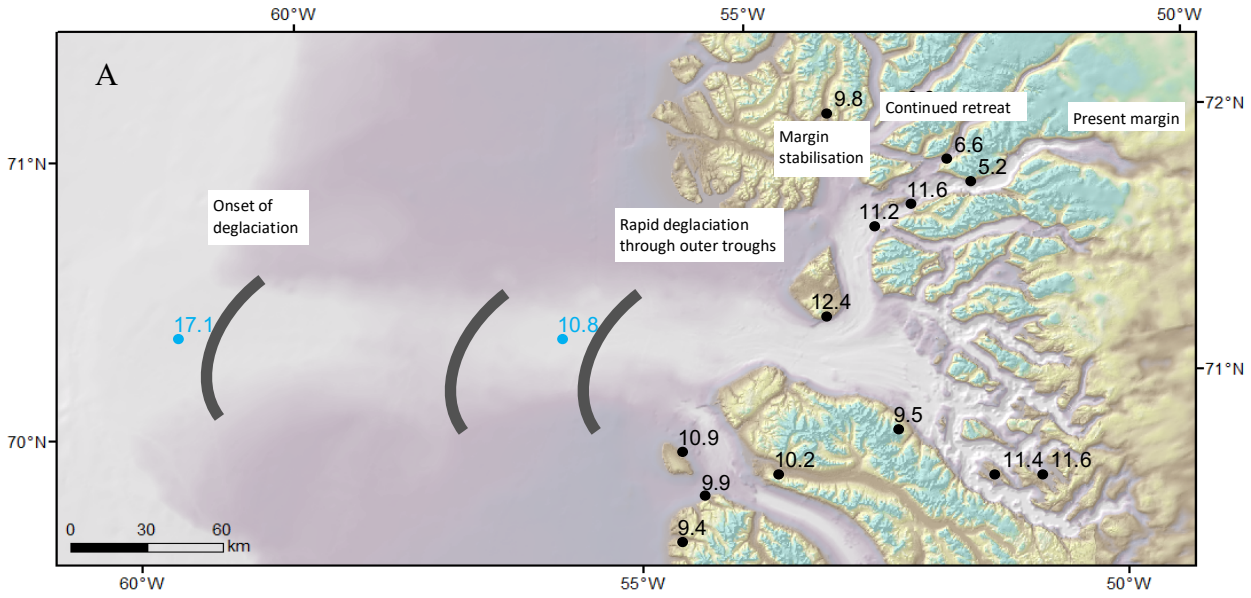

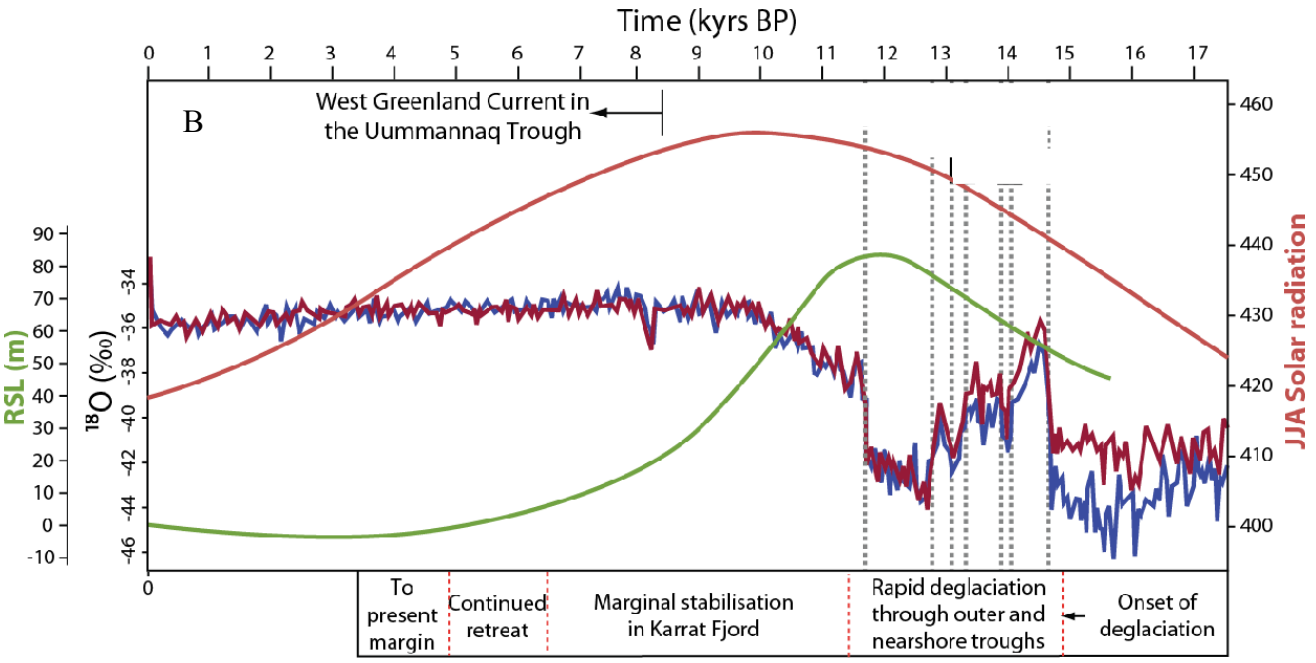

Figure 23. A) Geochronology of the Uummannaq catchment including deglacial dates (see Table 1 for complete data set). All ages are in ka BP with blue dates = deglacial dates and black dates = exposure ages. The grey lines represent the position of the GZWs. B) Retreat of the UISS (Lane *et al.,* 2014), NGRIP (blue) and GRIP (red) δ18O record for the past 17 kyr (Lowe *et al.,* 2008), relative sea level curve from Arveprinsens Ejland (Long *et al.,* 1999, Simpson *et al.,* 2009), and JJA radiation for 70N.

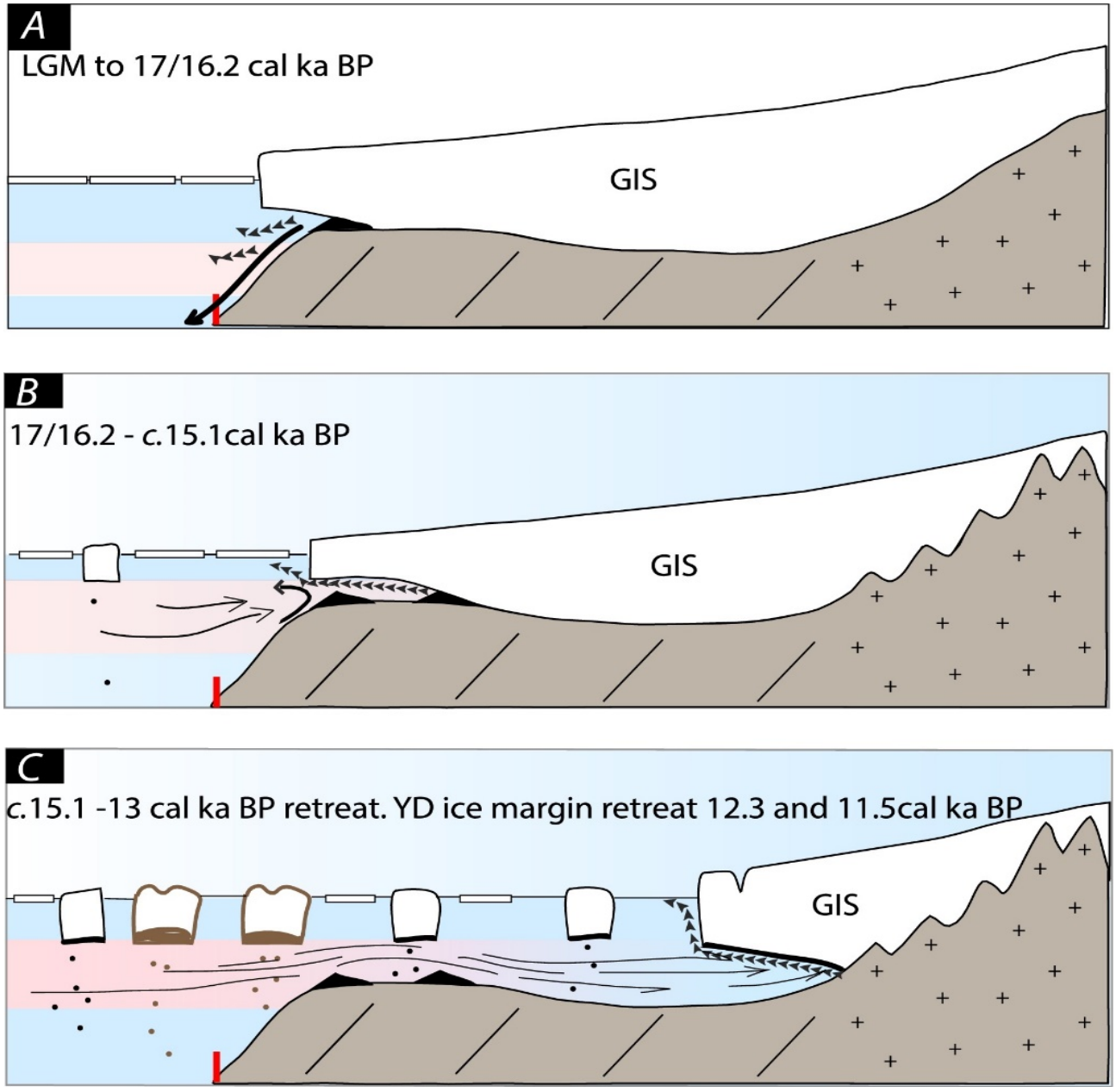

Figure 24. Schematic illustrations summarizing the ice sheet ocean interactions in central west Greenland (modified from Knutz et al., 2011). A) illustrates the LGM position of the GIS outlets at the shelf edge with the ice margin feeding the trough mouth fans and heavy sea ice in Baffin Bay. B) illustrates the initial retreat of the ice from the shelf edge and retention of a buttressing ice shelf that filtered out coarse material at the grounding line, released fines to the slope, and produced small grounding zone wedges on the outer Uummannaq Trough. A slight reduction in buttressing sea ice is depicted. C) illustrates the calving retreat of the ice sheet as the grounding line retreat toward a reverse slope under the influence of warm ocean water. Brown-based icebergs and IRD denote a northern Baffin Bay (NBB) source whereas black-based icebergs denote a central West Greenland (CWG) source. (Jennings *et al.,* 2017).

4. Methodology

Our approach is to use a 1-dimensional flow line model to explore the sensitivity of the model to a range of forcing mechanisms to determine the governing controls of grounding line retreat. The approach consists of three parts:

(i) to simulate a steady state ice stream that reaches the continental shelf edge, corresponding to the LGM ice stream extent (section 3 above),

(ii) to study the post-LGM retreat response and sensitivity of the ice stream to varying magnitudes of individual and combined forcings (sea level, ice temperature, ELA and ocean melt) applied as perturbations.

(iii) to investigate the post-LGM retreat behavior of the ice stream to non-linear forcings (GRIP data for ice temperature and Simpson *et al.,* 2009 for sea-level curves).

First, the numerical model will be outlined, followed by the experimental design (the set of experiments).

4.1. Numerical Model

The simulation of dynamic grounding-line evolution and response is not well-suited to low-resolution fixed-grid models that are commonly used to simulate long-term ice- sheet evolution (Vieli & Payne, 2005; Pattyn *et al.,* 2012). Therefore, this study uses a one-dimensional numerical flowline model that is specifically designed for tracking grounding-line motion by using a robust treatment of dynamic grounding-line behaviour that relies on a moving spatial grid to accurately evolve to changes at the ice-ocean boundary (Vieli & Payne, 2005; Nick *et al.,* 2009; Jamieson *et al.,* 2012). The grounding line is tracked continuously using a moving grid which avoids grid size dependency typically found in fixed resolution models because the resolution reduces as the grounding line retreats towards the ice divide (Vieli & Payne, 2005).

The model considers variations in both along-flow bed geometry and ice stream width and this ensures an accurate representation of the resistive stresses from the bed and lateral margins and the transfer of stresses in upstream and downstream directions. Despite their simplicity, numerical flowband models have been successfully applied to a range of locations and agree well with observations (Nick *et al.,* 2009; Vieli & Nick, 2011; Jamieson *et al.,* 2012; Whitehouse *et al.,* 2017). For example, Whitehouse et al., (2017) found a good agreement between field data relating to past ice extent in the Weddell Sea when using a numerical flowline model to investigate the controls on grounding line motion. Specifically, they demonstrated that ice shelf basal melt plays an important role in controlling grounding line advance, while a reduction in ice shelf buttressing is found to be necessary for grounding line retreat. Likewise, reconstructing the deglacial retreat of the Marguerite Bay palaeo-ice stream consistently reproduces rapid retreat punctuated by a series of slowdowns that

correspond to retreat on a bed that deepens inland, with retreat rate slowdowns controlled by narrowings in the topography (Jamieson *et al.,* 2012).

The flowline model can be run at high spatial resolution (e.g. sub km) and the resolution constantly evolves in response to grounding line position such that there are always the same number of grid cells within the ice stream. This means that as the grounding line retreats the resolution effectively increases. As a result, the grounding line positions can be simulated accurately and are not preconditioned by the location of a grid cell boundary like simpler models. Equally, the models fast run time (relative to 3D models) makes it possible to explore the ice stream's behaviour in response to a large suite of forcing parameters over multi-millennial time scales.

The model was incapable of running with a prescribed ice shelf in place, despite the fact that it has been applied successfully to other ice streams (e.g Weddell sea, Whitehouse *et al.,* 2017). The reasons for this are unclear and were unsurmountable for this case study. It is assumed it is a numerical issue related to the geometric set up of the model, but this cannot be confirmed. As a consequence, this version of the model does not include an ice shelf and therefore the impacts of potential ice shelf debuttressing could not be investigated. Additionally, the impact of ocean melting could not be tested in an ideal manner because in the absence of an ice shelf, melt can only be applied to the end cell of the ice stream. Therefore, to test the response of the ice stream to changes in ocean-driven melt rates, a particularly high melt rate was applied to the final cell of the grounded ice as a proxy for a lower melt rate being applied to a larger area under an ice shelf. This allows us to investigate how the velocity of the ice stream responds under changing melt conditions in the absence of an ice shelf in this instance of the model.

The time dependent evolution of ice flow, ice surface, and internal stress is calculated along a 1000 km flowline derived by tracing lineated landforms in the offshore region West of the modern GrIS and up onto the ice sheet following the path of modern ice flow. The flowline extends from the modern ice divide where the ice stream width is determined by the topographic ridgeline (Fig. 25). As the flowline moves into the fjord heads the orientations of MSGLs define the central flow. The lateral extents of the MSGL often correspond to a topographic break in slope, which represents the shoulder of the trough. Therefore, where the swath-bathymetric data are laterally limited, it is assumed that most of the ice-stream flow took place within the bounds of the trough shoulders, using them to define the ice-stream width. Beyond the continental shelf break, the width is rapidly increased to simulate a shear margin of a laterally unconfined system where surrounding fast ice on the shallower continental shelf would not have buttressed the ice stream. Ice velocities provided by the MEaSUREs Greenland Ice Sheet Velocity Map at 250 m resolution were used to identify the central flowline (Joughin *et al.,* 2010a, b).

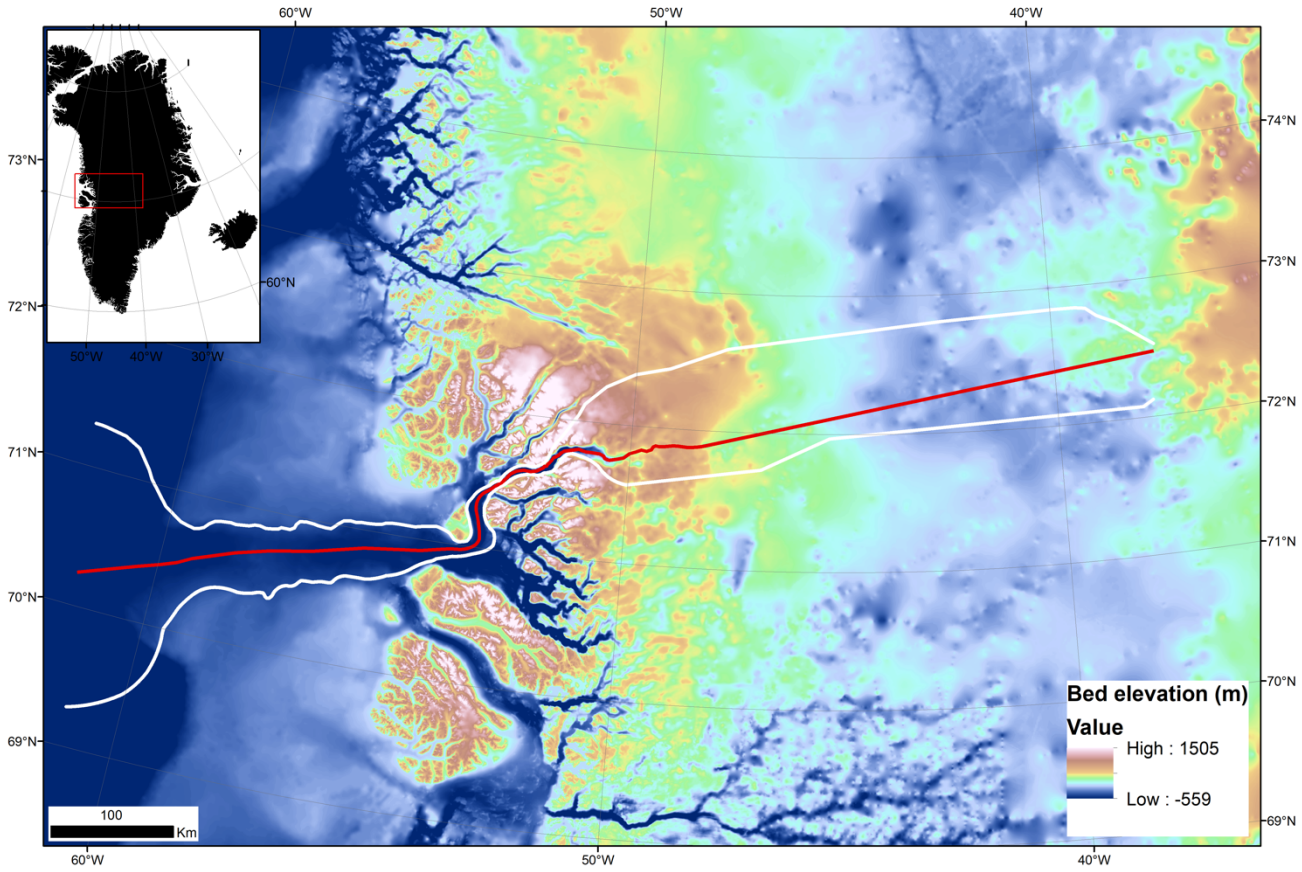

Figure 25. The flowline geometry applied in our numerical model designed to capture flow through the Rinks Isbrae and out onto the continental shelf edge. Red= central flowline used in the model, white = northern and southern boundaries of the UISS as defined by the trough shoulder and fjord walls (see text).

Below I outline how the model calculates ice flow. The constants and parameters used in the equations can be found in Table 1 of the Appendix.

Assuming no sliding at the bed the vertically averaged horizontal velocity (u) is given by Eq (2) where s is the surface elevation, n the flow law exponent in Glen's flow law and the constant C is given by Eq (1).

$$C = \frac{2A(\rho_i g)^n}{n+2} \quad (1)$$

$$C\left(\frac{\partial s}{\partial x}\right)^n + h^{n+1} + \tau_{lat} = u \quad (2)$$

The stress balance is depth- and width-averaged and driving stress, τ_d, is balanced by basal, τ_b, and lateral shear stress, τ_{lat}, together with longitudinal stress gradients, $\partial \tau_{xx}/\partial x$, in the direction of ice flow, x:

$$\frac{\partial \tau_{xx}}{\partial X} + \tau_b + \tau_{lat} = \tau_d \quad (3)$$

By iterating for the effective viscosity, *v*, using equation 2 is solved.

$$v = A^{-1/n} \left|\frac{\partial u}{\partial x}\right|^{(1-n)/n} \quad (4)$$

The along-flow variation in ice-stream width and surface accumulation, *a*, is accounted for by ice surface evolution, given by

$$\frac{\partial H}{\partial t} = a - \frac{1}{W}\frac{\partial (uHW)}{\partial x} \quad (5)$$

For an ice stream the resistance from the bed is assumed to be linearly related to the velocity u at the bed (a viscous till is assumed). The equation determining the vertically averaged ice stream velocity u is (Eq x) where β^2 is the friction coefficient to be specified.

$$2\frac{\partial}{\partial x}\left(Hv\frac{\partial u}{\partial x}\right) - \beta^2 u = \rho_i g H \frac{\partial S}{\partial x} \quad (6)$$

Following van der Veen and Whillans, (1996) by assuming zero flow at the ice margin lateral drag was calculated. The basal boundary condition is defined by a Weertman-type nonlinear sliding relation (Weertman, 1974) that is a function of effective pressure, *N*, at the bed. For an ice-stream thickness, *H*, and half width, *W*, the stress-balance equation (Equation 1) results in an expression for depth- and width-averaged ice flow, *u*, produced by

$$2\frac{\partial}{\partial x}\left(Hv\frac{\partial u}{\partial x}\right) - \beta\left(\frac{u}{N}\right)^{\frac{1}{m}} + \frac{H}{W}\left(\frac{5u}{2AWf_{lat}}\right)^{\frac{1}{n}} = \rho_i g H \frac{\partial S}{\partial x} \quad (7)$$

This method is consistent with a boundary layer theory, which is important for avoiding errors imposed by model numeric. Consequently, the model performs well in inter-comparison tests against grounding line behaviour (Pattyn *et al.,* 2012).

Fsoft is the lateral softness scaling factor used to soften lateral drag i.e margins are fractured. A value of 1 means basal and lateral stress factors are equal, above 1 means fractured sides. The lateral resistance factor is calculated in equation 8, where gga is the gravitational acceleration.

$$Factlat = \left(\frac{5}{(gga(i)fsoft)(width(i+1)+width(i))}\right)^{\frac{1}{n}} \quad (8)$$

4.2. Model and boundary conditions

The complex structural features in bed elevation, such as valleys, ridges, bumps and hollows have vital implications for both channeling ice flow toward the continental margin, and for controlling the amount of warm, Atlantic Water that reaches the glaciers. The ice stream bed profile was extracted along the flow line at 400 m horizontal intervals, with present day bathymetric and topographic values obtained from bedmachine3 (Morlighem *et al.,* 2014, 2015).

4.2.1. Basal conditions

A user defined basal traction parameter is defined for each point along a flowline such that larger values result in higher shear stresses at the bed. Within the flowline model this basal traction parameter is multiplied by the ice overburden pressure with the result that basal shear stress evolves as the ice stream evolves, increasing as the ice gets thicker or faster, or as the ice surface gets steeper. Where the bed lies below sea level a low value of basal slip is assigned (eq. 9a), and this assumes that these regions contain soft deformable marine sediments. Internal deformation of cold ice is well understood but this is not the case for basal sliding, for which many parameters are poorly constrained therefore the model is left to readjust these values as a function of effective pressure to calculate β at every time step:

$$\beta_{belowsealevel} = \frac{\beta_{mask}(\rho_i H + \rho_w z_{bed})}{5e^5} \quad (9a)$$

$$\beta_{abovesealevel} = \frac{\beta_{mask}\rho_i H}{5e^5} \quad (9b)$$

4.2.2. Mass balance forcing

We control mass balance by applying an ELA to the model and then adjusting accumulation at different rates above and below the ELA. The elevation of the ELA itself can be fluctuated up or down as a function of air temperature such that the ELA is related to temperature through an adiabatic lapse rate of 5.1°C km^{-1} (Fortuin & Oerlemans, 1990). Thus, a temperature depression of 1°C moves the ELA downward by 190 m. Flemming *et al.,* (1997), through surface energy balance modeling of north-west Spisbergen glaciers with a modern ELA of about 400 m, show that a 3°C temperature change would shift the ELA below sea level, providing support for the simple approach adopted here whereby a maximum ELA increase of 800 m corresponds to a temperature change of 6°C. The long term ELA for the West GrIS is currently situated below 1200 m (Zwally *et al.,* 2005). However, in the last decade the ELA shifted upward significantly; in the warm summer of 2012 it was above 1850 m asl (Van der Wal *et al.,* 2012). Therefore, through adjustments to the air temperature, the surface mass balance of the ice sheet can be modified. The LGM current position is 600 m asl. This simple palaeoclimate is comparable in terms of precipitation and mean –annual surface temperature to that derived from

unpublished GCM simulations of the LGM climate in the Eurasian Arctic using the Hadley centre model.

The ELA function applies a mass balance equation depending on if the surface is above or below the ELA. If the ice surface is below the ELA then a linear equation is applied:

$$Mass\ balance\ below\ ELA = 0.0003(y(i) - ELA + 0.1)$$

Poinar did a statistical comparison of RACMO data vs ELA and developed a polynomial expression that relates mass balance to ELA (Poinar *et al.,* 2015). This was applied in model simulations where a climate forcing was used to adjust the volume of surface melting.

$$Mass\ balance\ above\ ELA = \frac{3(5e^{-10}(2400 + (y(i) - ELA)^3 + 2.1e^{-6}(2400 + \big(y(i) - ELA)\big)^2 - 0.0005\big(2400 + (y(i) - ELA)\big) - 3.6357\big))}{4}$$

4.3. Experiment Design

The overall approach is to first develop an initial experiment that involved simulating a stable LGM configuration. Thereafter, the various retreat experiments were initiated from that stable LGM condition. I outline the spin-up and retreat experiment design below.

4.3.1. LGM spin up

The accumulation values were scaled in the model for the advance experiments to 75% of modern in order to represent accumulation during the LGM as inferred from the GISP2 ice core accumulation record (Cuffey & Clow, 1997) (Fig. 26).

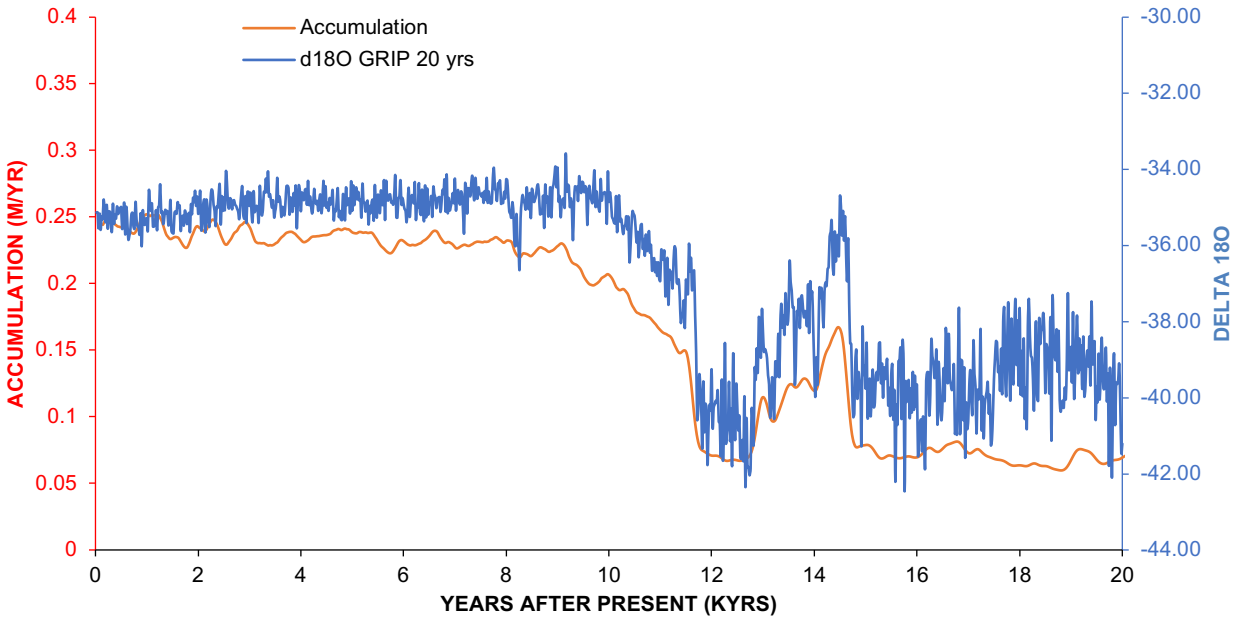

Figure 26. Accumulation data from the GISP2 ice core infers that during the LGM accumulation was 75% lower than present day conditions (Alley, 2000); the average accumulation rate during the LGM (between 15-30 kyr BP) was 5.5 to 7 cm yr-1, approximately 25% of the modern accumulation rate.

4.3.2. LGM ice stream configuration

Geophysical evidence (*Section 2*) has demonstrated that ice expanded through the main fjord to reach the shelf edge during the LGM (Funder & Hansen, 1996; Roberts *et al.,* 2013; Evans *et al.,* 2002, 2009; O Cofaigh *et al.,* 2004; Dowdeswell *et al.,* 2010; Funder *et al*., 2011). We therefore assume that prior to developing a number of retreat experiments, we need to simulate a UISS with a grounding line that is stable at the continental shelf edge.

For the LGM simulation we provide the model with an initial ice surface and bed topography with the bed topography being provided by bedmachine3 (Fig . 27 - Morlighem *et al.,* 2017). We used the geomorphological data (section 2; Roberts et al., 2013) that provides information about LGM ice surface to define an 'idealised' LGM ice surface profile for the LGM simulation. It is likely that the UISS overtopped Ubekendt Ejland (700 m asl) and reached up to 1000 m asl in the vicinity of Karrat Ejland and 1964 m near the Rink-Karrat fjord head. This ice surface was extended out to the continental shelf edge following the geophysical evidence for ice extent. The calving face of the marine terminating glacier was assumed to be stable at a maximum of 100 m height (Bassis and Walker, 2012; Hughes and Nakagawa, 1989).

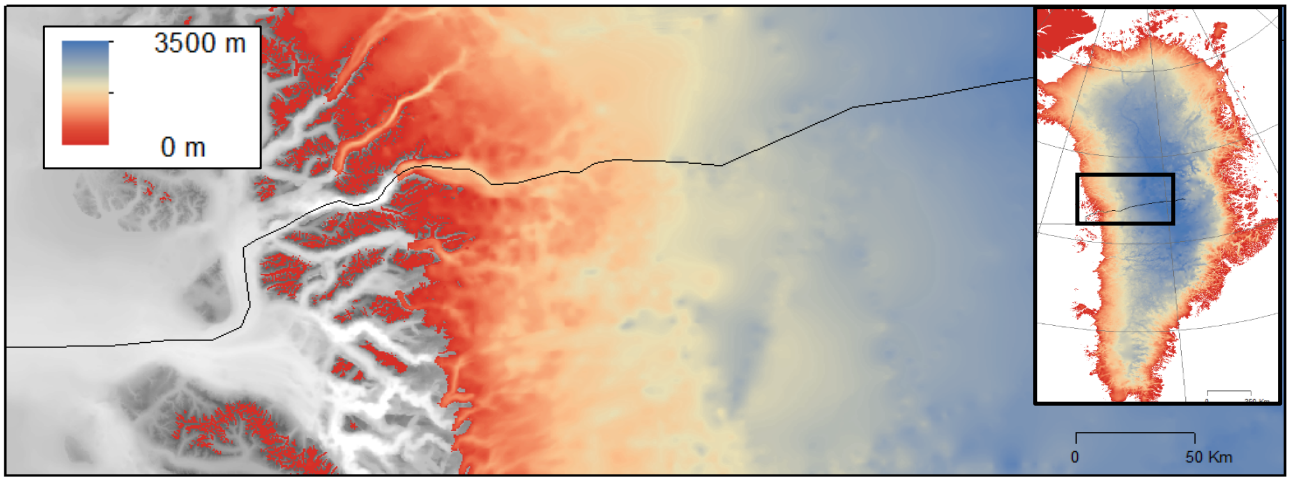

Figure 27. Map of central west Greenland showing current GrIS ice thickness data (Morlighem et al., 2017) and the flowline used in the model (black line).

The experiment sets are all initiated from a geophysically consistent steady-state LGM ice-stream configuration (Fig. 28) with the grounding line stable at the continental shelf break in order to avoid initial adjustment effects that are unrelated to effects from imposed perturbations. This steady-state initiation is generated by keeping the maximum melt rate (M_{max}) at -0.5 m a^{-1}. Sea level is held static at 60 m below present-day levels, the ELA at 600 m above present-day sea level and ice temperature at -30 °C. The model is then run for 1000 years, to let the ice surface reach equilibrium. This closest model output to the LGM configuration constrained by the geomorphic evidence uses an average bed topography in the Uummannaq trough, enhanced lateral drag, accumulation from multiple feeder catchments and a narrow ice stream width in the marine portion. In terms of LGM configuration the upper points of Ubekendt and Karrat both fit the ice surface profile assumed for the LGM.

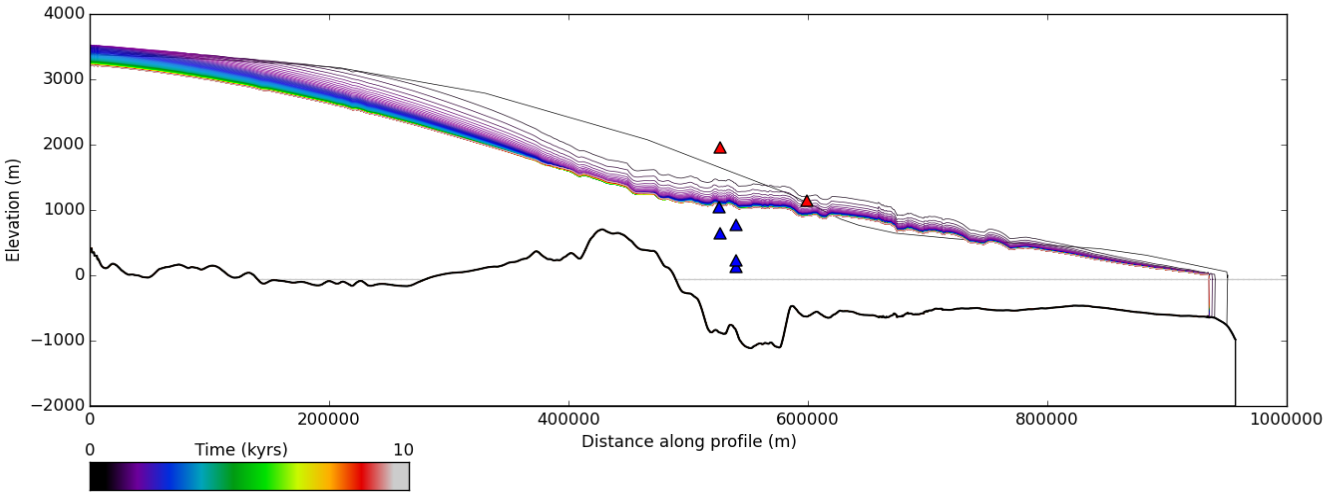

Figure 28. Stable LGM configuration of the UISS. The blue triangles = areas that are proven to be covered by ice as constrained by the geomorphic field data, whilst red triangles = regions that were ice free.

4.4. Retreat experiments

The retreat experiments are driven by applying time-dependent variations in relative sea level, ice temperature (which acts as proxy for air temperature), maximum ocean-driven melt (M_{max}) and ELA. Three sets of experiments were performed to understand the UISS response to various forcings (Table 1). Firstly, we applied single forcings and then combinations of the single forcings and lastly, fluctuating forcings, both single and combined. The first set of experiments apply a linear forcing of sea level, air temperature and submarine melt to the model. Linear forcings are applied gradually after the 1000 year spin up and over 1000 years. This tests the sensitivity of the UISS to individual forcings and moreover, it tests whether the UISS responds in a non-linear fashion to a linearly forcing. Realistic magnitudes and rates of change since the LGM are difficult to define from the paleo record but modelling and observations of modern rates help indicate potentially realistic upper limits.

Table 3. Applied forcings used to reconstruct the retreat of the UISS. Experiment set 1 relates to single forcings that are applied individually in a stepped(s) and linear manner. Experiment set 2 includes a combination of forcings applied simultaneously and set 3 looks at the most realistic scenario of the retreat of the UISS. Note surface melt is only applied linearly.

Set	Sea Level (m)		Temperature (°C)		Submarine Melt Rate (m/yr^{-1})		Surface Melt Rate (m/yr^{-1})
1	SL-40 SL-20 SL0 SL10	SLs-40 SLs-20 SLs0 SLs10	T-25 T-20 T-15 T-10	Ts-25 Ts-20 Ts-15 Ts-10	SMR1 SMR10 SMR100 SMR500 SMR1000	SMRs1 SMR10 SMRs100 SMRs500 SMRs1000	C800 C1000 C1200 C1400
2	SL10_T-10 SL10_C1400 SL10_SMR1000 C1400_SMR1000 T-10_SMR1000 T-10_C1400 SL10_T-5_SMR1000_C1400 (Maximum scenario)						
3	GRIP SSLC GRIP_ELA GRIP_ELA_SSLC GRIP_SSLC_ELA_SMR1000 (realistice scenario)						

4.4.1. Single Linear forcings – Experiment 1

4.4.1.1. Sea Level

During the LGM relative sea level corrected for isostatic adjustment at the Central West GrIS continental shelf edge was predicted to be -60 m below present day levels (Simpson *et al.,* 2009). The sensitivity tests were run with sea level static at -60 m for the 1000 year spin up, and then increased linearly over 1000 years to -40 m, -20 m, 0 m and 10 (Fig. 29). In the stepped experiment, sea level was static at -60 m for the 1000 year spin up and then increased to -40 m, -20 m, 0 m and 10 m in year 1001.

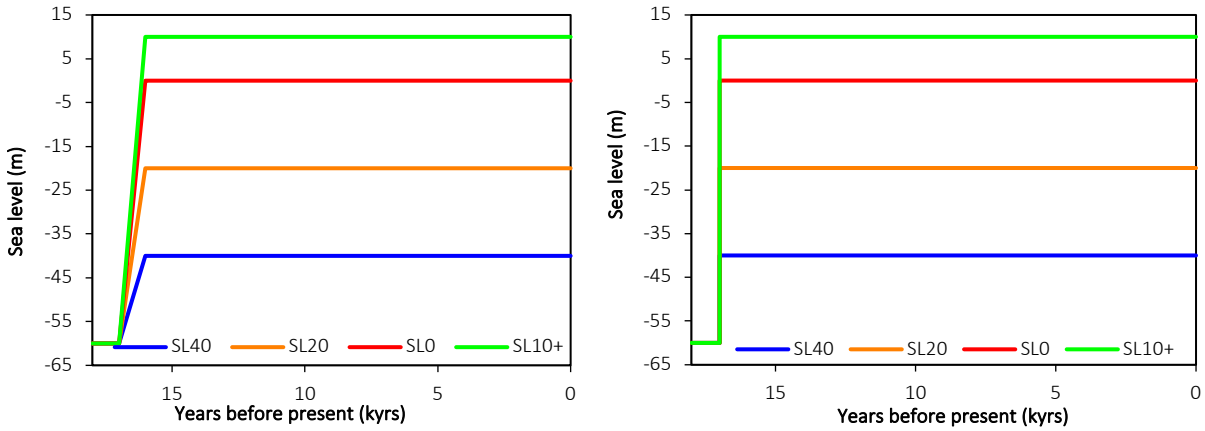

Figure 29. Applied sea level forcings for the left chart a Linear increase in sea level and the right chart, a stepped increase.

4.4.1.2. Ice Temperature

Since the model is isothermal, ice temperature changes are applied uniformly along the length of the ice stream and at all depths. Guided by glacial-interglacial temperature variations determined from the analysis of nearby cores, ice temperatures are varied by 15°C to represent the transition between the glacial and interglacial conditions for the realistic scenarios (Whitehouse *et al.,* 2017). The sensitivity tests were run with ice temperatures increasing linearly from -30°C after 1000 years to -25°C, -20°C, -15°C, -10°C over a period of 1000 years (Fig. 30). In a stepped scenario, ice temperatures increasing from -30°C after 1000 years to -25°C, -20°C, -15°C, -10°C in year 1001.

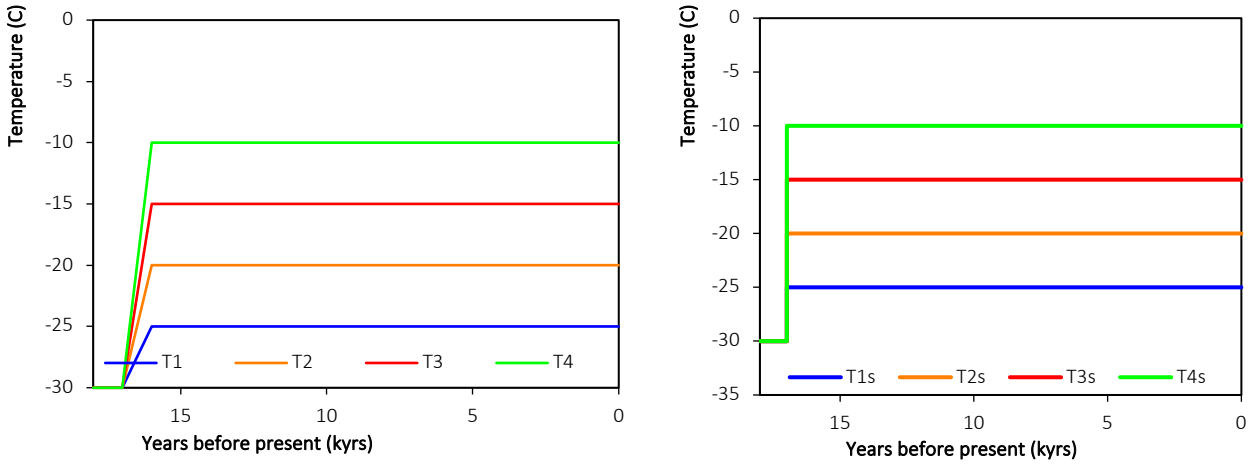

Figure 30. Linear and stepped increases in ice temperature. Scenarios relate to Table 2, T1 = T-25, T2 = T-20, T3= T-15, T4= T-10. T(s) refers to a stepped increase rather than a linear.

4.4.1.3. Ocean Melt

On rapidly retreating Greenland outlet glaciers, high submarine melt rates up to several hundreds of meters per year have been found as fresh, buoyant water exits from subglacial discharge at the base of the glacier and rises along the glacier front as buoyant plumes that drive convection (Jenkins,

2011). The plumes entrain the warm subsurface ocean water and enable exchange of heat between the ocean and ice (Stranaeo *et al.,* 2013). The plumes originate from submarine melt or from deep incised channels transporting subglacial melt water into the ocean. The rising of subsurface ocean layer also melts the ice mélange and thereby reduces the back stress.

Lower basal melt rates are assumed to have persisted during glacial periods due to the circulation of colder water beneath the ice shelf, but a lack of proxy data relating to palaeo-ocean temperatures in this region means that our sensitivity experiments are poorly constrained. Submarine melting during the LGM is set to -0.5 to represent glacial conditions. In the last cell of the ice stream, ocean melt rates, M, are applied using a parameterization that depends linearly on water depth. From a minimum rate of 0.1 m yr^{-1} the ocean surface, ocean melt increases to a maximum value, M_{max} at a depth of 1500 m, below which it is constant (Whitehouse *et al.,* 2017). The submarine melt rate (SMR) is limited to the final cell of the ice stream and therefore in this model experiment it is unlikely to play a substantial role in the retreat of the UISS system, thus limiting our ability to test the influence of melt rates on retreat of the UIS. However, by applying very high melt rates to the terminus cell this to some extent tests whether the terminus might respond to ocean forcing.

The maximum basal melt rate is varied between experiments depending on records of warm WGC from Jennings et al., (2017) and Sheldon et al., (2016), and this alters the rate at which basal melting increases with depth. After the 1000 year spin up, submarine melting is increased to 1, 2, 5, 10 m yr^{-1} over a 1000 year period at 17 ka BP (Fig. 31). In a stepped forcing scenarios the SMR is increased from -0.5 m /yr^{-1} to 1, 10, 100, 500, 1000 in year 1001.

A melt rate of 1000m/yr^{-1} (SMR1000) or 500 m/yr^{-1} (SMR500) is equivalent to a 10 cell ice shelf with a melt rate of 100 m /yr^{-1} or 50 m/yr^{-1} respectively (Fig. 31). Thus to replicate this effect a small ice shelf is imposed as there is little concrete evidence to suggest a large ice shelf was present (O'Cofaigh *et al.,* 2013b; Jennings *et al.,* 2017).

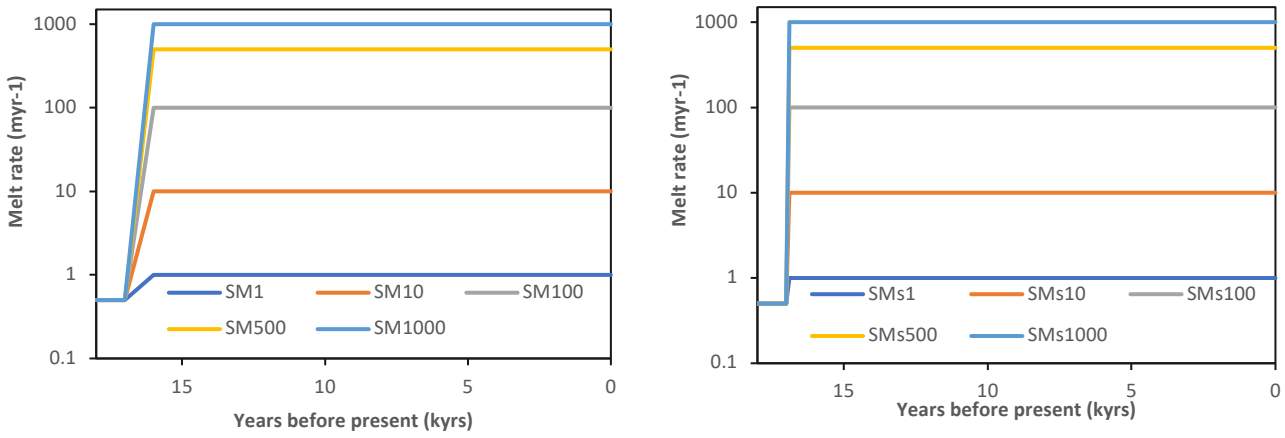

Figure 31. Linear and stepped increases in melt rate. Linear increases in the left chart and stepped increases on the right.

4.4.1.4. Surface melting

Surface melt was altered in the model in response to changes in accumulation and ablation. A prescribed ELA was used to force the model. In the linear forcing scenarios this was applied after the 1000 year spin up, increasing the ELA from 600 m asl to 800, 1000, 1200, 1400 m. In the stepped forcing scenarios the ELA was increased from 600 m asl after the 1000 year spin up to 800, 1000, 1200, 1400 m asl by year 1001 (Fig. 32).

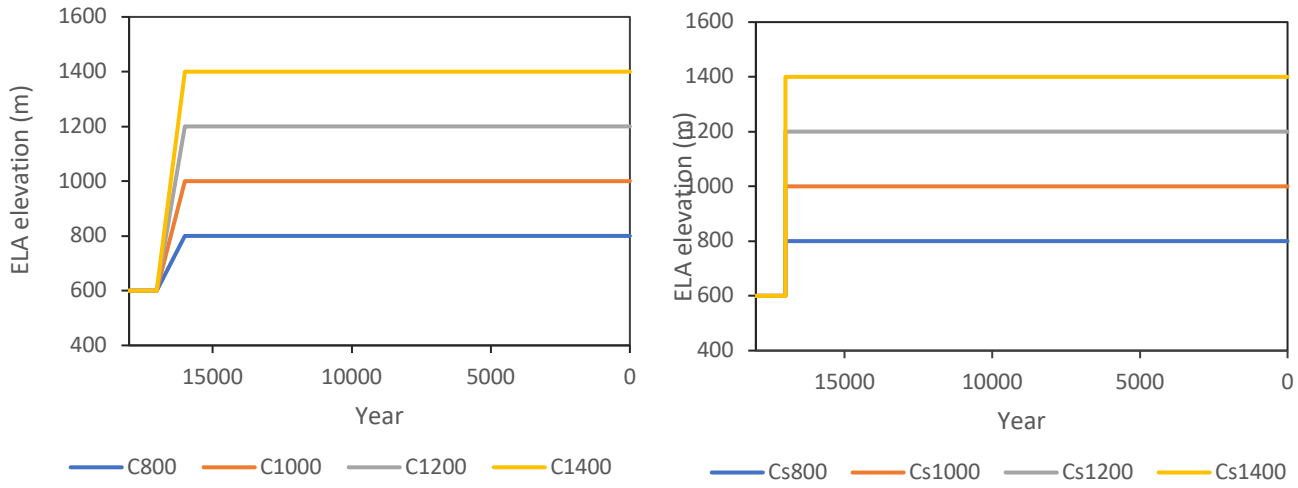

Figure 32. Linear and stepped increases in ELA elevation, linear increases on the left chart and stepped increases on the right.

4.4.2 Combined Linear forcings – Experiment 2

The second set of retreat experiments combined multiple linear forcings together. Two maximum single linear forcings for each variable, temperature, sea level, submarine melting and surface melting, were combined together to establish the impact of multiple forcings on retreat (Table 2).

4.4.3. Realistic forcings – Experiment 3

The third set of retreat experiments apply non-linear realistic forcings. In particular the GRIP record is used to control air temperature and ELA and Simpson *et al.,* 2009 model output (see section 4.3.2.2. below) are used to control sea level (Simpson sea level curve SSLC). The object of this set of retreat experiments is to test whether it is possible to achieve a retreat pattern similar to the one suggested by the landform record and the available radiocarbon dates from the UISS. These combined forcings used maximum values taken from the single forcing experiment and applied them in pairs. For example, an increase in temperature from -25°C to -10°C was applied, an increase in sea level from -60 m to 10 m, an increase in submarine melt rate from -0.5 to 1000 m/yr^{-1} and a rise in ELA from 600 m to 1400 m.

4.4.3.1. Temperature curve

For a more realistic simulation of the UISS, data from the Greenland ice core project (GRIP, 1992) is used to constrain the ice temperature of the model during the last 20,000 years. The original GRIP record is used as well as a shifted GRIP that is 11.86°C warmer to reflect conditions near the bedrock (Dahl-Jensen, 1998). A scaled GRIP is created by smoothing the temperatures as a running mean of 50 years, as Hubbard et al., (2009) suggest that ice streams do not respond to temperature fluctuations on an order of magnitude less than this. The temperature increase from average glacial to Holocene conditions was large, approximately 10°C.

An important question remains concerning how well this change of ice sheet surface temperature represents the change in atmospheric temperature though the troposphere above the ice sheet, given that the strength of near-surface temperature inversions may also have changed considerably. The record is fairly accurate from the last 20,000 years, however, results become increasingly speculative further back in time, due to masking of the surface temperature signal by the geothermal flux and uncertainties in the thickness history resulting from poor knowledge of rheological layering, deformation patterns deep in the ice sheet and ice sheet marginal position (Cuffey & Clow, 1997).

The GRIP ice core is favoured over the GISP2 because ice flow may have altered the chronological sequences of stratigraphy for the GISP2 core (Grootes *et al.,* 1993). The paleo-climate forcing was employed through a 20-year-bin mean of the GRIP $\delta^{18}0$ record (Andersen *et al.,* 2004). Because the ice stream will not respond immediately to changes in climate, the impact of changing climate is expected to be felt in a muted manner. Therefore, in order to avoid simulating an ice stream that is overly sensitive to small-scale high frequency climate variability, the 20 year mean record was smoothed using a 1000-year running mean to remove excessive noise (Fig. 33).

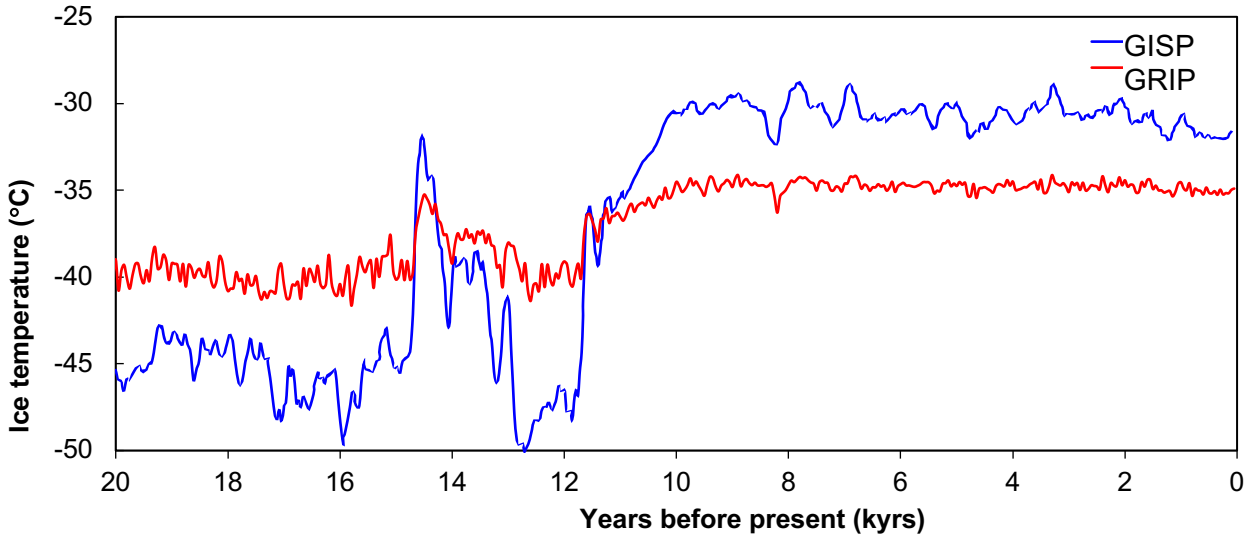

Figure 33. Comparison of the GRIP and GISP ice core profiles over the last 20,000 years.

4.4.3.2. Sea level curve

Changes to the mass and extent of the GrIS during the Last glacial cycle will have deformed the solid earth and altered the shape of the gravitation field such that water depth changes at the grounding line will not have tracked GMSL change (Farrell & Clark, 1976). It is beyond the scope of this study to self-consistently model the response of the solid Earth and the geoid to regional ice mass change. Instead, we use output derived from a glacial isostatic adjustment model (Simpson *et al.,* 2009) to estimate water depth changes near the edge of the continental shelf during the last glacial cycle. Following a 1000 year spin up, the model is forced with the Simpson *et al.,* (2009) relative sea level curve for the outer-shelf (Fig. 34).

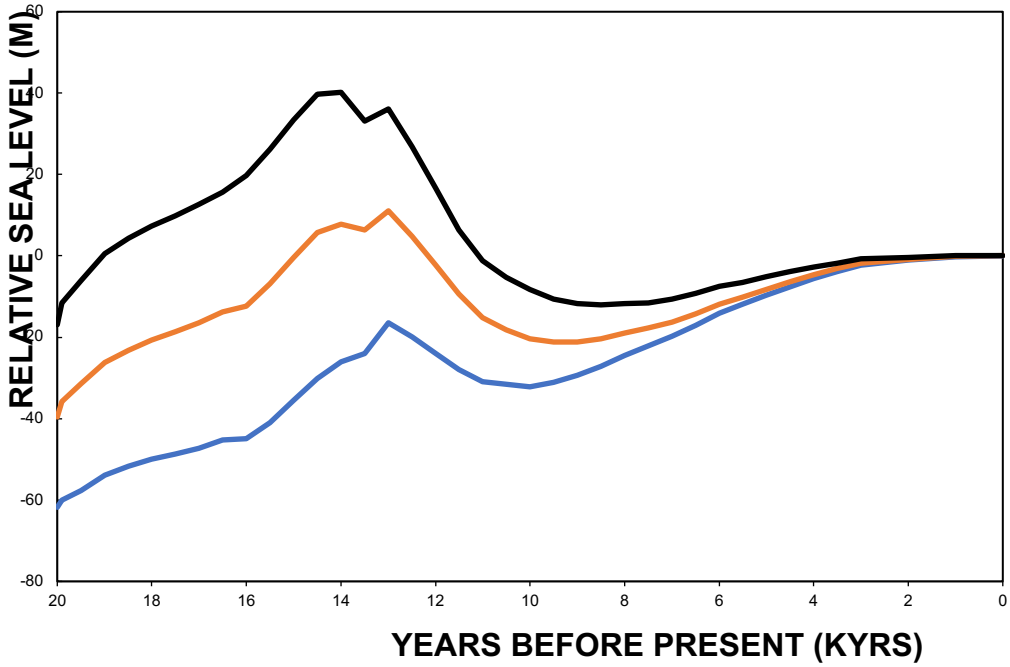

Figure 34. Simspon et al., 2009 sea level curve the outer (blue), mid (orange) and inner (black) regions of the central west Greenland shelf.

4.4.3.3. Fluctuating ELA

An ELA that responds to ice temperature was also applied to these realistic forcings to establish the impact of surface melting on the retreat of the UISS.

4.4.3.4. Maximum realistic forcing scenario

The final experiment applied used a fluctuating ELA (corresponding to the modified GRIP ice temperature curve), the SSLC from Simpson et al., (2009), the GRIP ice core curve and a fixed submarine melt rate of 1000 m/yr^{-1}.

5. Results

I present the results of each objective in turn, beginning with the generation of the LGM steady-state simulation and then perturbation experiments before finally introducing the more realistically forced simulations of the UISS.

5.1. LGM spin up results

5.1.1. Bed topography

The UISS LGM extent is very sensitive to bed depth below sea level. Bedmachine3 (Morlighem *et al.,* 2015) values are smoothed over a running mean of 10 cells so that the bed profile of the flowline is representative of topography across the width of the ice stream. This is demonstrated in figure 35 where the deeper bed topography leads to an unstable LGM configuration compared to an averaged bed topography that is required for stability at the outer shelf. Equally, the geomorphic constraints from field data fit better with an averaged bed topography whereby areas characterised by allochthonous blockfields and erratics denoted by Roberts *et al.,* (2013) to be ice free (red triangles – UBE 22) remain above the ice surface profile and features that were under the ice have post deglacial exposure (Lane *et al.,* 2015) remain below the ice surface (blue triangles).

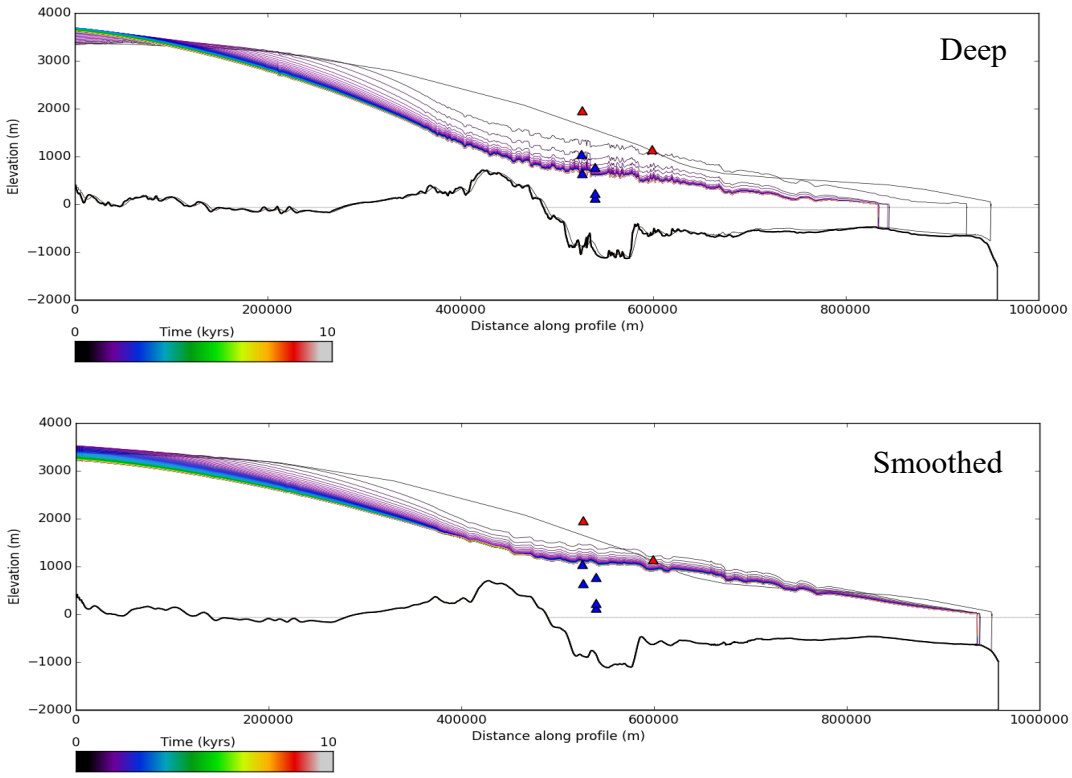

Figure 35. Original bed topography (top), and smoothed bed topography. Red triangles = regions that are ice free during the LGM and blue triangles = regions that were covered by ice during the LGM.

5.1.2. Lateral drag

Within the flowline model, resistance to flow is given by drag from the lateral margins of the glacier which contributes to the overall depth-averaged ice flow (eq. 7). As lateral resistance increases in a narrowing ice-stream, stabilization can even arise on a reversed bed (Jamieson *et al.,* 2012). Reducing the lateral drag (Fsoft >1) (eq. 8) decreases the magnitude of lateral resistance applied at the margins and mimics the development of a weak marginal shear zone allowing the ice surface to thin more readily and resulting in grounding line retreat (Fig. 36 – upper panel). A value of 1 indicates that basal and lateral stress factors are equal. Enhancing lateral drag (Fsoft <1) increases resistance and reduces fracture damage at the margins causing less retreat and thinning of the ice surface profile. Lateral drag, is important for ice streams that flow over weak beds with little resistance (Whillans & Van der Veen, 1997). The stability of the LGM configuration was determined by its ability for the grounding line to maintain a steady location (within a 10 km) range for over 50% of the model spin up. The LGM model was most stable when lateral drag was set to 1 suggesting a system with a strong shear margin and this seems logical for the UISS with topographically constrained walls providing ideal conditions for shear margins to develop. Additionally, geomorphic field data is better aligned to the scenario where the lateral drag is greater (Fig. 36).

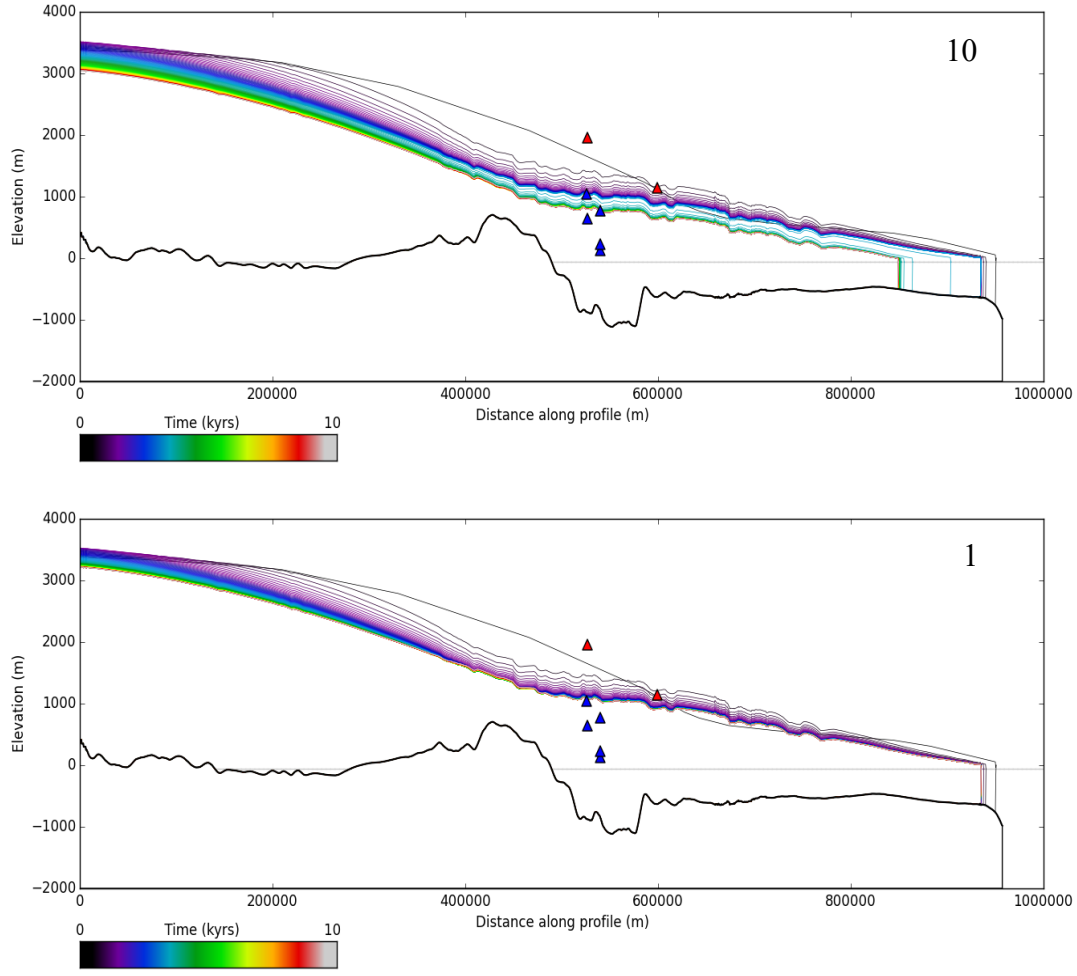

Figure 36. The difference in stability of the LGM configuration when Fsoft is 10 and 1. A higher Fsoft constraint results in staggered retreat from the continental shelf edge.

5.1.3. The importance of UISS tributaries

The UISS has a complex geometry with multiple glaciers feeding ice into the palaeo UISS at different locations along the central flow line. Therefore, this mass is added in the model based on summing the total accumulation over these smaller ice drainage basins. We carry out a sensitivity test that either includes or excludes the mass being injected from these tributaries (Fig. 37) and find that grounding line stability at the continental shelf edge is not possible without the ice from the adjacent tributaries. Therefore, although the Rinks-Karrat fjord is the largest outlet glacier in the Uummannaq region, accumulation solely from the Rinks-Karrat fjord does not provide enough ice to advance the grounding line to its outer shelf limit and ice discharge from tributary ice streams are crucial for LGM stability and extent.

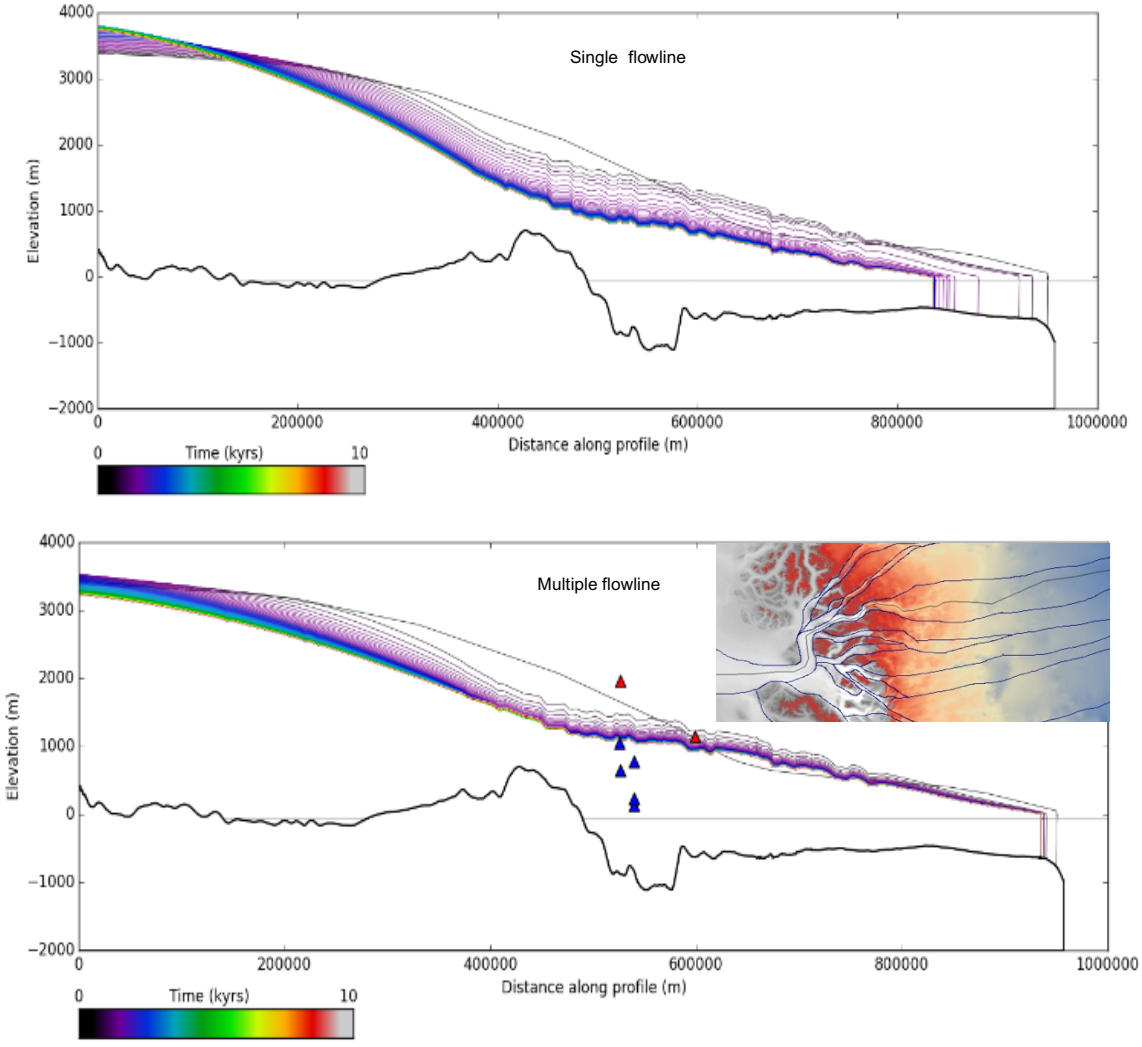

Figure 37. Model output showing the importance of accumulation from multiple tributaries vs the Rink-Karrat fjord, Injections of accumulation from outlet glaciers and neighbouring fjords. Red triangles = ice free regions during the LGM and blue triangles = covered by ice.

Overall Figure 38 is the best LGM simulation. The shape of ice surface profile of the LGM UISS configuration follows a smooth decline in the gradient of the ice stream from the ice divide (3 km asl) to the grounding line (0.1 km asl). The ice thickness in the interior of the ice sheet is approximately 3 km but around 400-500 km downstream it decreases to 700 m as the bed topography shallows around Rink-karrat fjord. Once the bed topography deepens again in Igdlorssuit Sund so does the ice thickness. The UISS is grounded on the continental shelf edge, 980 km from the ice divide and the water depth is around 800 m.

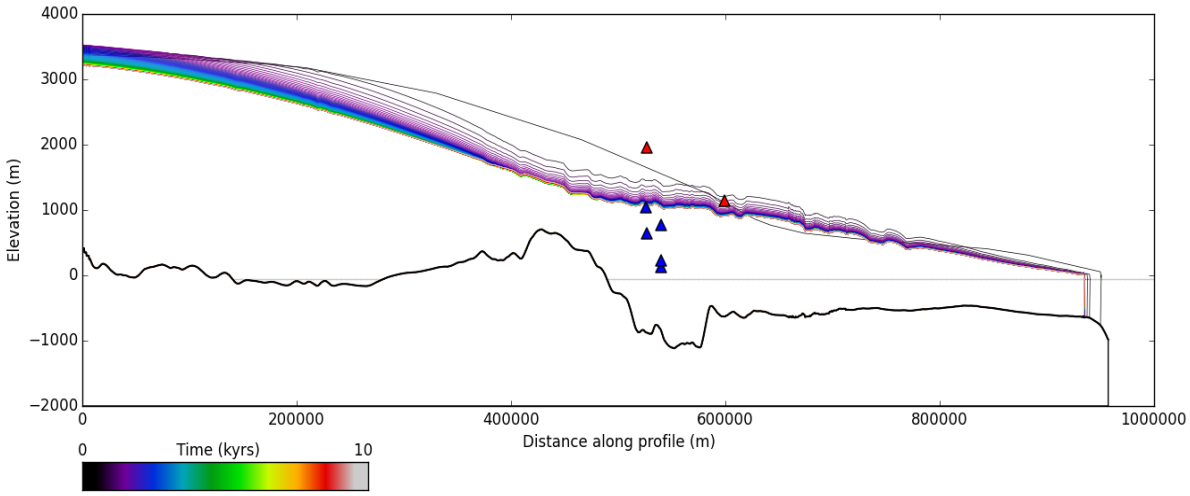

Figure 38. LGM best fit configuration of the UISS. The red triangles represent cosmogenic ages from areas that were ice free during the LGM and the blue triangles represent regions covered by ice.

5.2. Single Forcings Experiment 1 - Linear and stepped increases

The single forcing experiments are designed to test the sensitivity of the UISS to gradual and stepped changes to forcing. Below I introduce the outcomes of the individually forced sensitivity tests.

5.2.1. Relative sea level

The UISS seems relatively insensitive to a suite of sea level forcings: even the largest sea level rise scenario (SL+10) of 70 m is unable to cause retreat from the outer-shelf and past the outer grounding zone wedge. In the SL+10 there is only 4 km more retreat compared to -60 to -40 m (Fig. 39 SL-40) and thus confirming that the UISS is insensitive to changes in sea level. It is likely that the ice thickness of the ice stream between 1000-2000 m entering the deep trough (1000 m bsl) overrides the 70 m sea level perturbation which is insufficient to unground the ice. Nevertheless, a rise in sea level of over 40 m results in a deeper water column that increases ice velocity at the grounding line and enhances ice discharge (Fig. 40). The magnitude of retreat is identical whether the forcing is applied

in a linear or stepped fashion and again this is likely to be linked to the notion that the sea level perturbation is too small relative to ice thickness. However, the vertical thinning in a stepped scenario is greater in the SLs-40 than the SL-40 where the latter experiences periods of late Holocene thickening. Since there was little ice thinning and retreat it is difficult to match these sea level scenarios with the geomorphic data from Ubekendt and Karrat Ejland. In summary, the UISS was not able to reach the present day ice sheet configuration (in the fjord heads) in any of the sea level only scenarios and therefore, this would suggest that sea level was not a singular driving factor behind the retreat of the UISS.

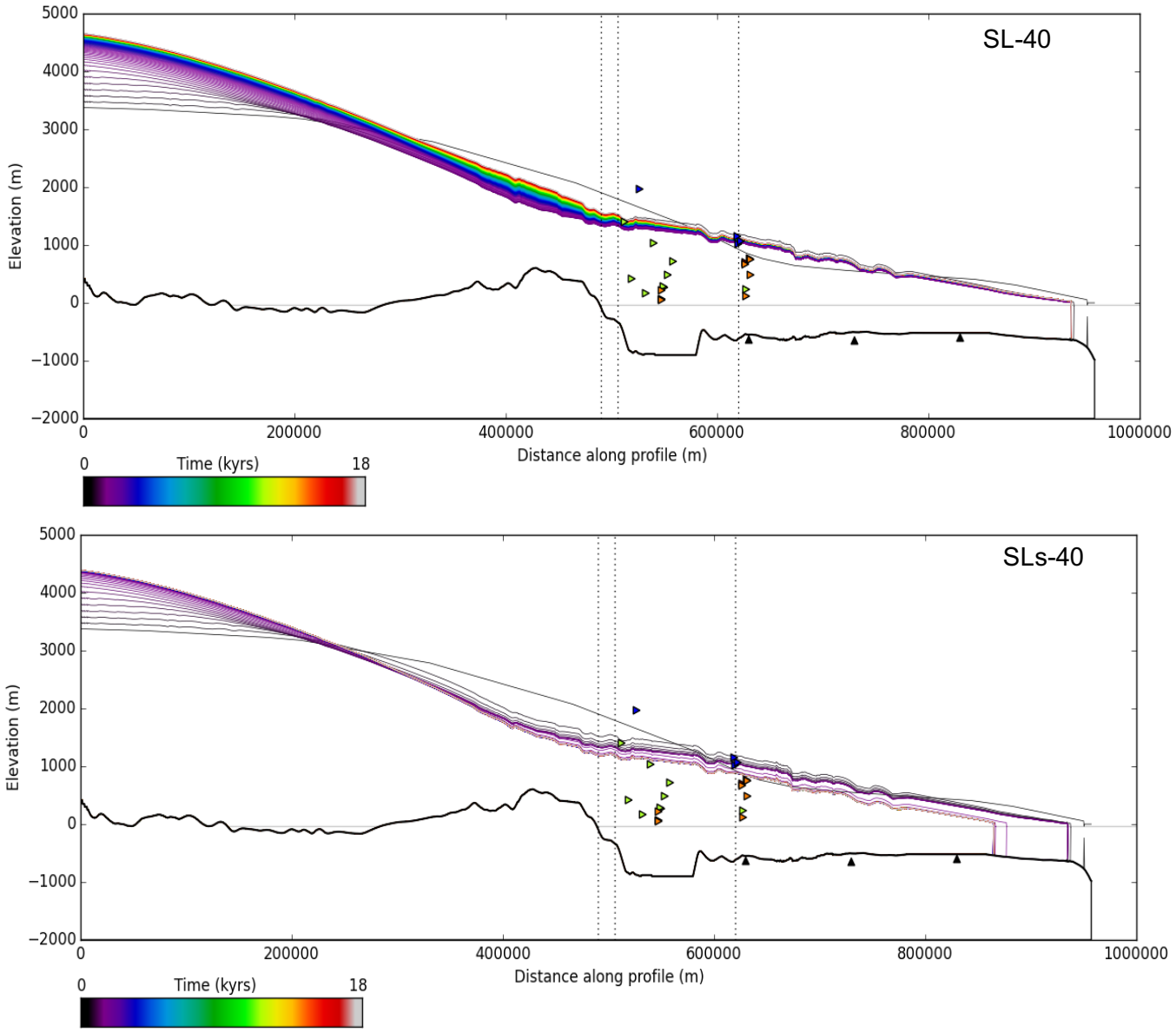

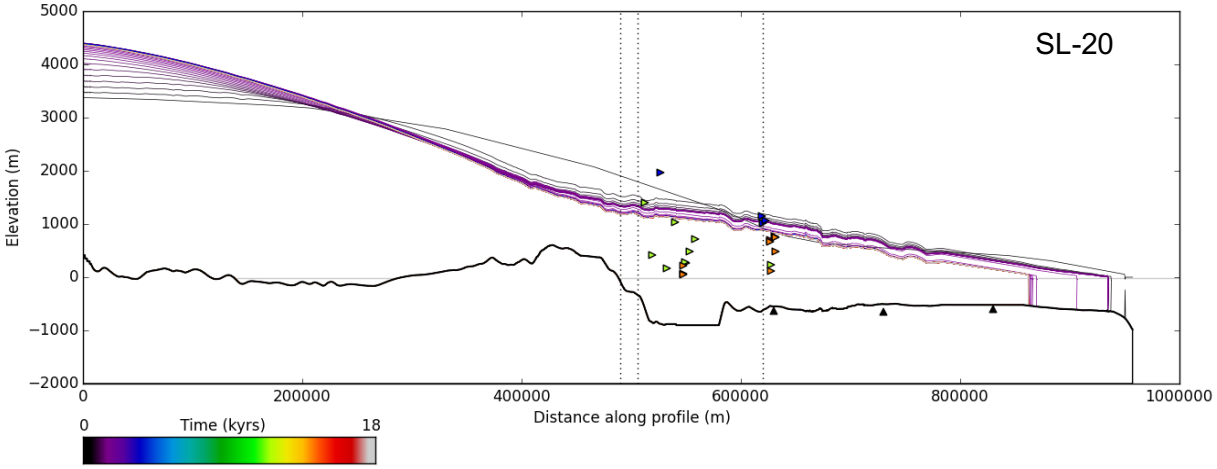
SL-20
Elevation (m)
5000
4000
3000
2000
1000
0
−1000
−2000
0
200000
400000
600000
800000
1000000
Distance along profile (m)
0
Time (kyrs)
18

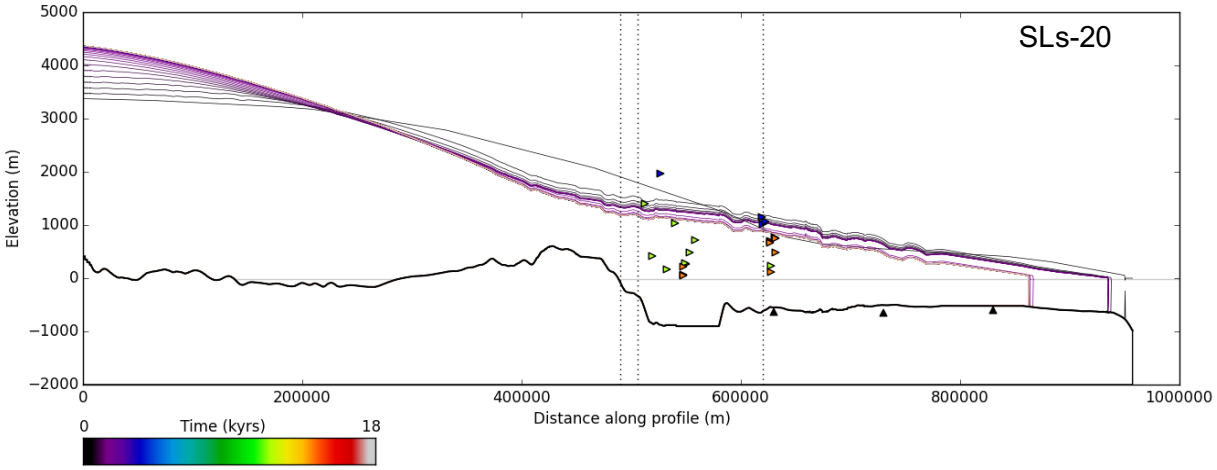
SLs-20
Elevation (m)
5000
4000
3000
2000
1000
0
−1000
−2000
0
200000
400000
600000
800000
1000000
Distance along profile (m)
0
Time (kyrs)
18

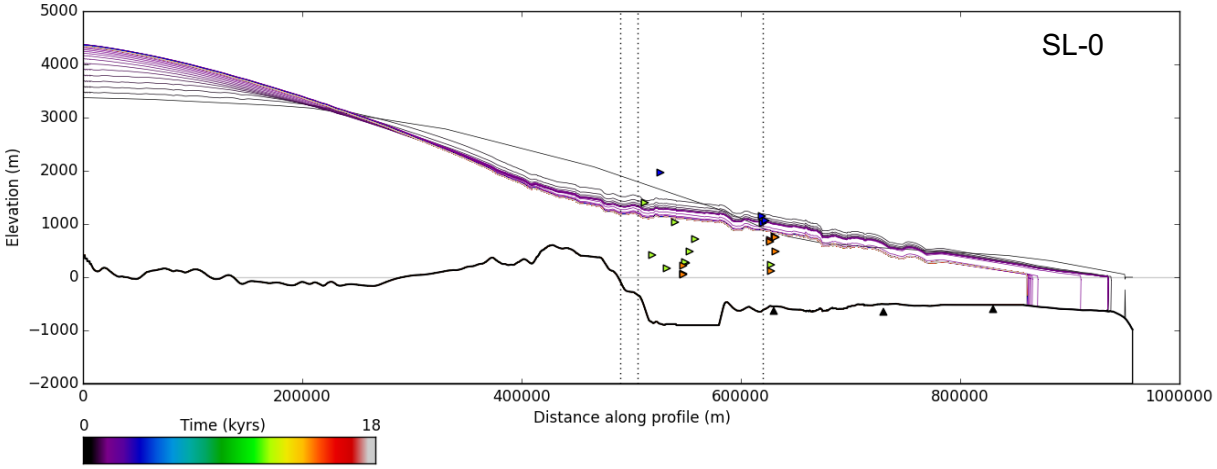
SL-0
Elevation (m)
5000
4000
3000
2000
1000
0
−1000
−2000
0
200000
400000
600000
800000
1000000
Distance along profile (m)
0
Time (kyrs)
18

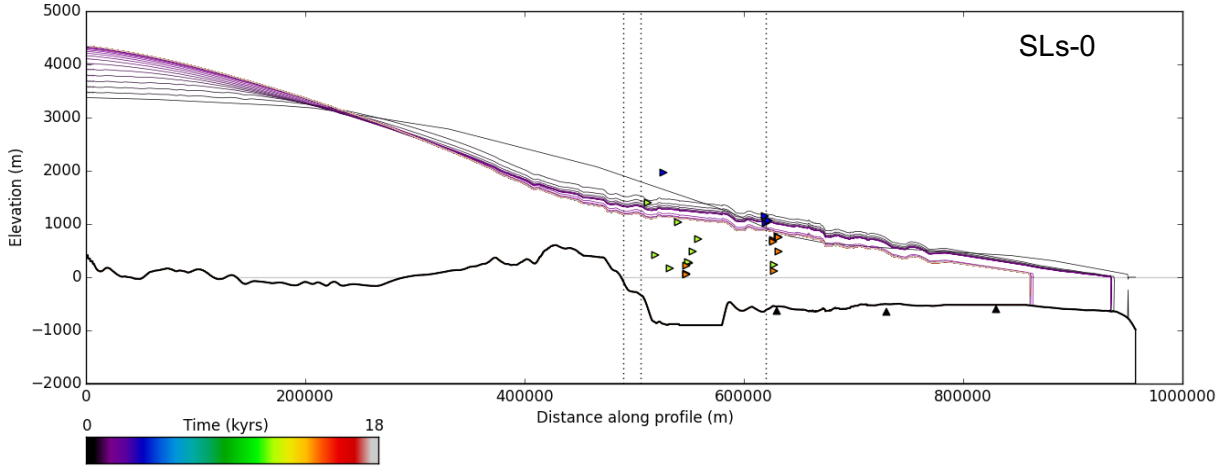
SLs-0
Elevation (m)
5000
4000
3000
2000
1000
0
−1000
−2000
0
200000
400000
600000
800000
1000000
Distance along profile (m)
0
Time (kyrs)
18

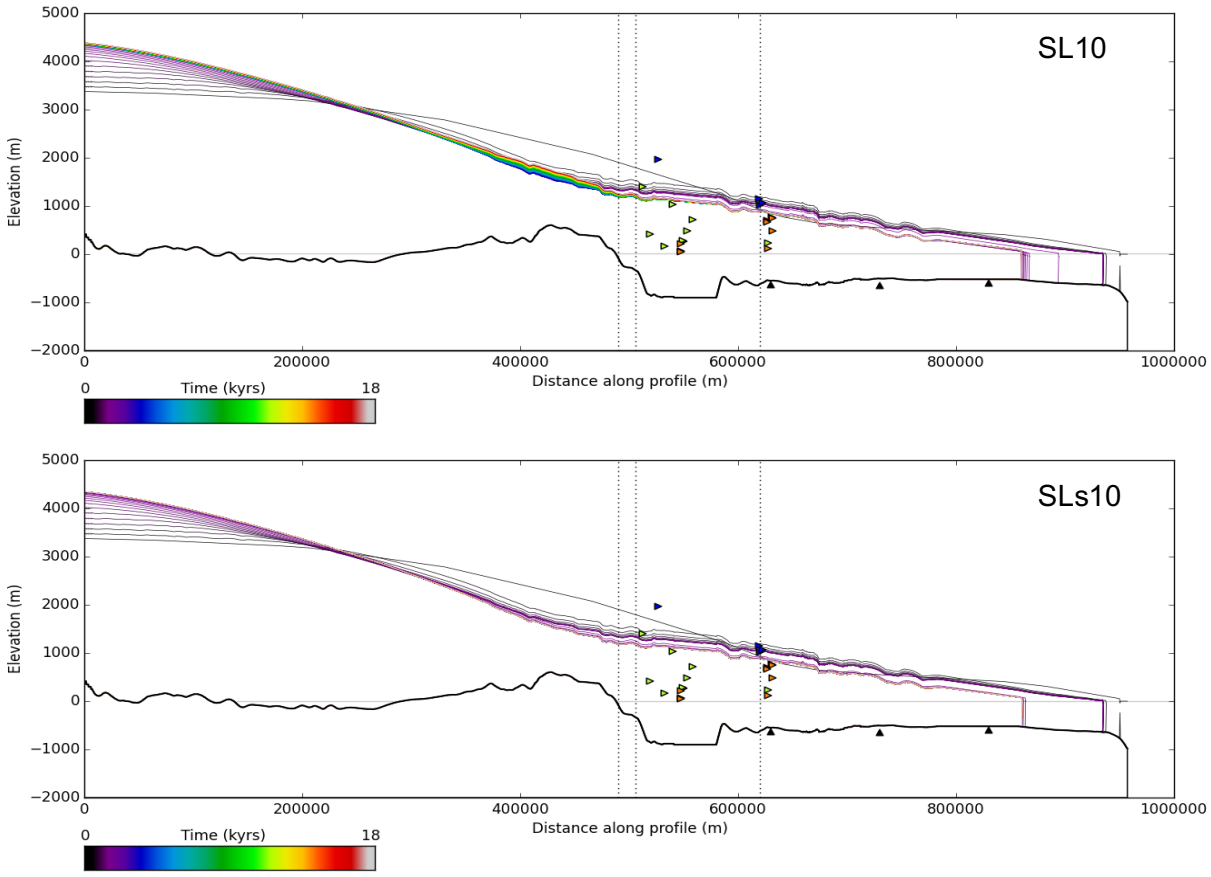

Figure 39. Sea level scenarios for a stepped and linear 20 m, 40 m, 60 m and 70 m increase in sea level from the LGM configuration of -60 m. All scenarios except SL-20 result in a small amount of retreat of the grounding line from the shelf edge.

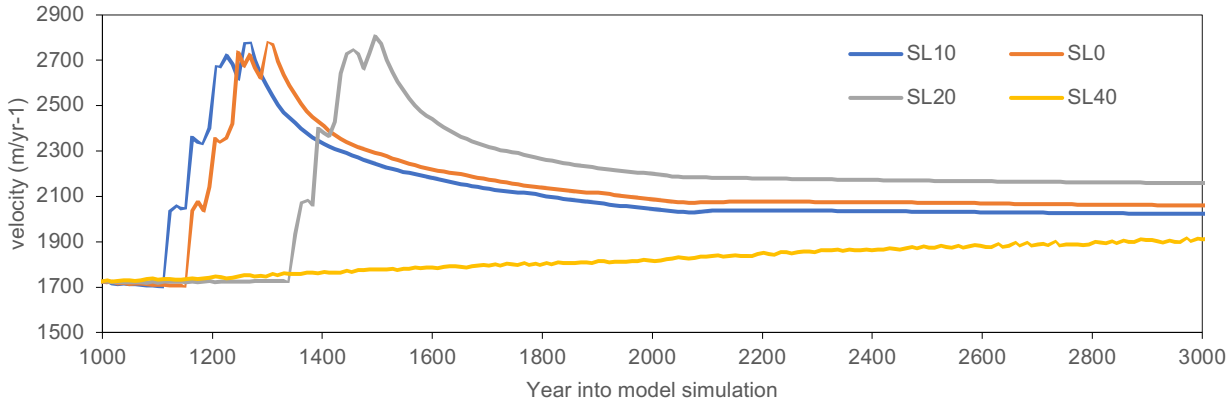

Figure 40. Ice velocity at the grounding line for sea level scenarios SL-40, SL-20, SL0, SL10. In models that show retreat an acceleration in ice flow at the grounding line is observed. As the grounding line retreats the grounding lines that are later in time and further inland have increased velocities in comparison to the LGM starting position.

5.2.2. Ice Temperature

The UISS is more sensitive to an increase in ice temperature than sea level, inducing over 100 km more retreat. The greatest increase in ice temperature (from -30ºC to -10ºC) results in the most retreat (210 km) and vertical thinning (T-10). The modern day ice surface profile is the lowest in the T-10 scenario, thinning from 4400 m at the ice divide to 3800 m. This is over six times greater than the thinning induced by the largest sea level forcing (SL10). The peak in velocities around 550 km downstream of the ice divide, from 200 m/yr^{-1} to 3000 m/yr^{-1}, occur in an area of deepening bed topography which would have enhanced ice retreat. Despite this, even a small (5ºC) increase in temperature (T-25) is able to induce 80 km of grounding line retreat and T-20 results in a further 100 km of retreat to the middle GZW. A small amount of systematic thinning can be seen (T-25) on Ubekendt as the grounding line jumps back exposing the upper section of the lateral moraine staircase (orange triangle). Although T-10 results in only 50 km more retreat than scenario T-25 the largest magnitude thinning occurs here. In a linear retreat (T-10) the grounding line stabilizes at the two outer GZWs allowing for the formation of the geomorphic landforms seen on Ubekendt (the lateral moraine staircase) and exposes samples sites on Karrat (Fig. 42).

There is no difference between grounding line retreat in a stepped and linear scenario, however the ice surface profile drops rapidly in the first stage of thinning following the stepped increase. This pattern is most evident with the greatest increase in temperature (Ts-10. Fig 41). During a stepped warming the grounding line retreats less gradually and in larger movements and spikes in the lateral shear stress follows this (Fig. 42). As the grounding line steps back lateral shear stress spikes as a result of an increase in ice thickness.

Retreat occurs in a nonlinear fashion in spite of the linear or instantaneous forcings applied. The retreat rates spike to values of up to 12,000 m/yr^{-1}, compared to the average rate of 0.4 m/yr^{-1} and the ice flux across the grounding line also spikes to 60 km^3/yr^{-1} as ice velocity increases (Fig. 43). The magnitude of retreat reflects the magnitude of retreat rates (Fig. 42). For example, the first step of grounding line retreat of 80 km occurring after 1,200 years results in an increase in retreat rates from 0.01 to 1000 m/yr^{-1}. The second step of retreat 3,500 years into the model simulation, results in 100 km of retreat and an increase in retreat rate from 0.2 m/yr^{-1} to 6,000 m/y^{-1}. The last step of grounding line retreat is a 115 km step, with retreat rates double than those previously seen (up to 12,000 m/yr^{-1}) and this coincides with where the trough width increases north east of Ubekendt in Igdlorssuit Sund (Fig. 50). Here, the lateral shear stresses are generally higher over a broad region of the inner shelf when the ice stream is larger and they decrease as the ice stream becomes smaller. Nevertheless, there are also sharp variations in lateral shear stress. The greatest spike in lateral shear stress (45 kPa – Fig. 42) occurs where the trough briefly narrows around Ubekendt Ejland: this is where retreat slows. Overall, the simulations clearly show that retreat rate is nonlinear regardless of whether forcing

is stepped or linear. Thus, one can see a disconnect between the retreat rate and the forcing pattern which in this case is likely to be significantly influenced by the variations in lateral shear stresses that result from differences in trough width along flow.

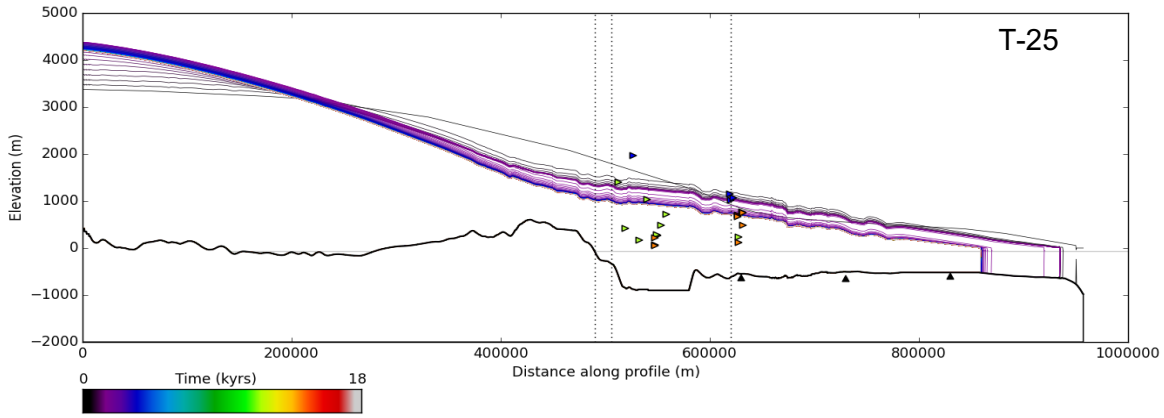

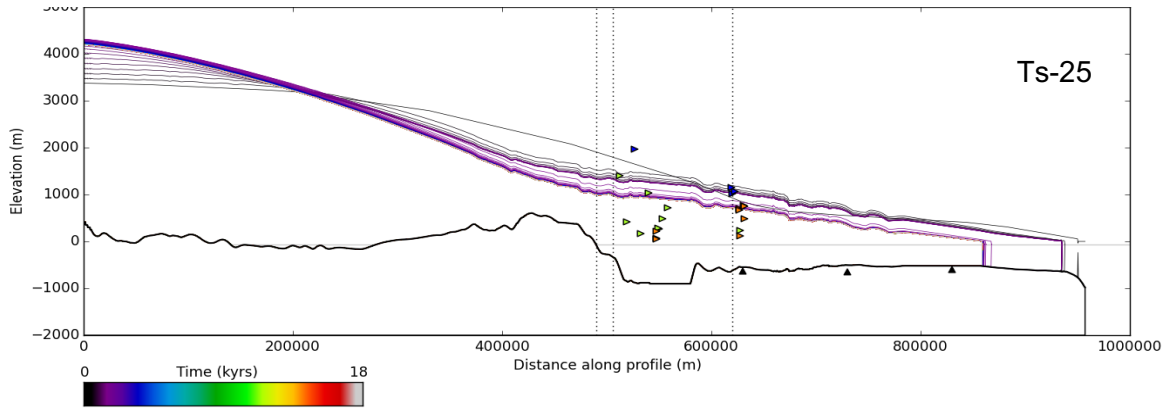

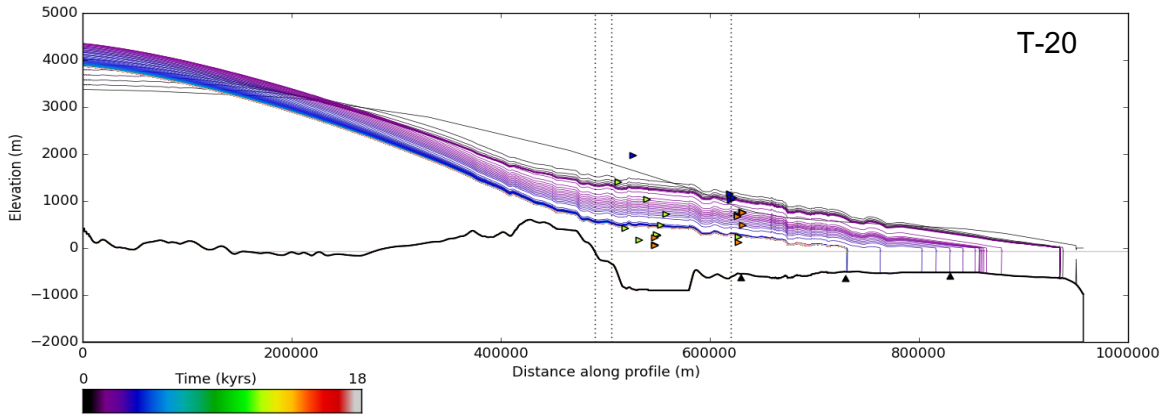

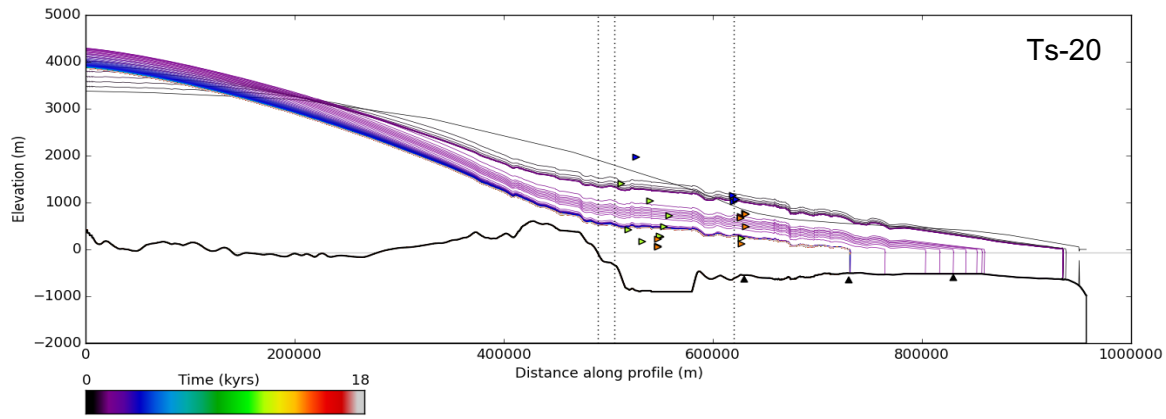

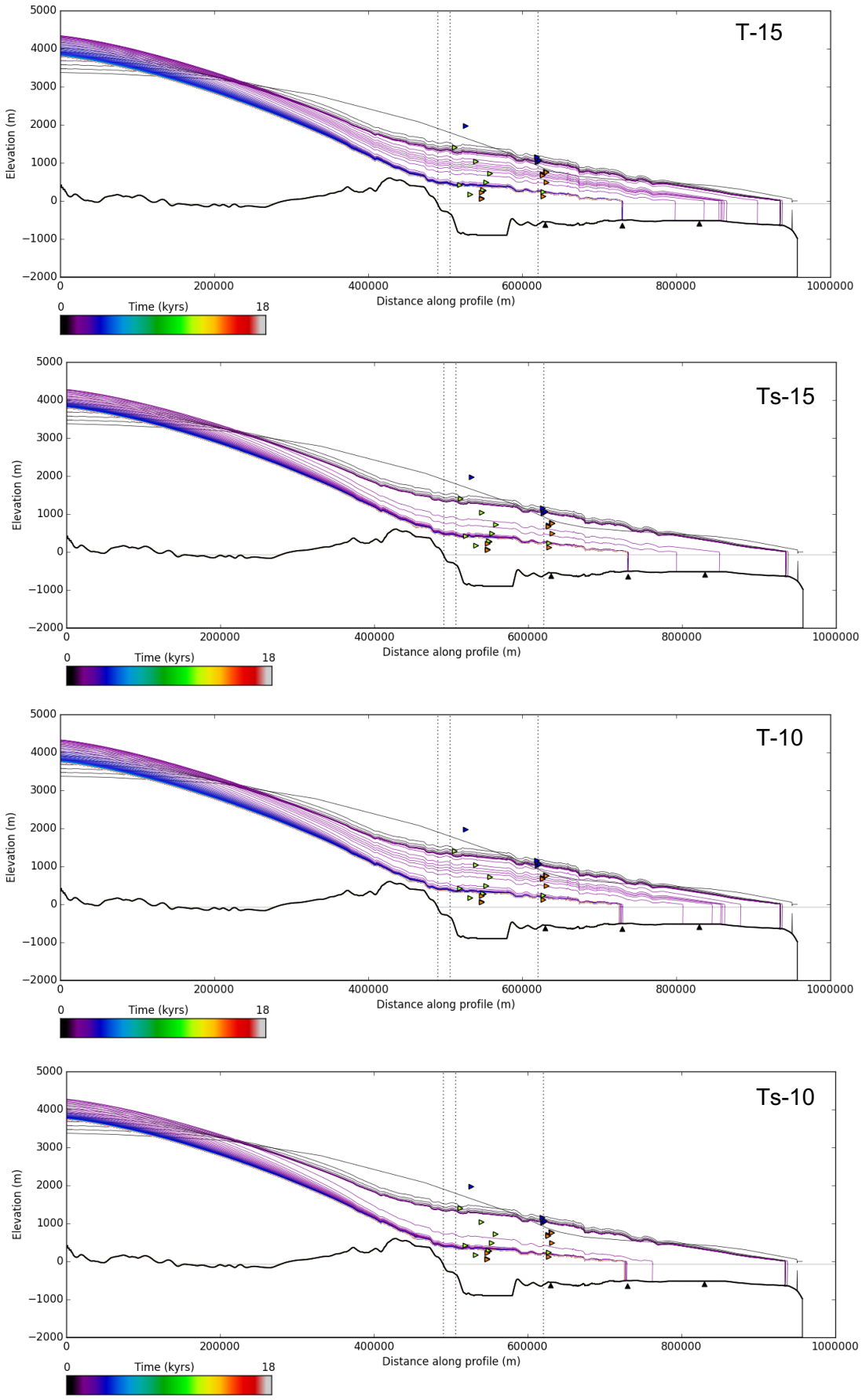

Figure 41. Model output for a stepped and linear increase in ice temperature of 5°C, 10°C, 15°C, 20°C. Retreat begins once the ice temperature is initially increased and is therefore seen in all outputs.

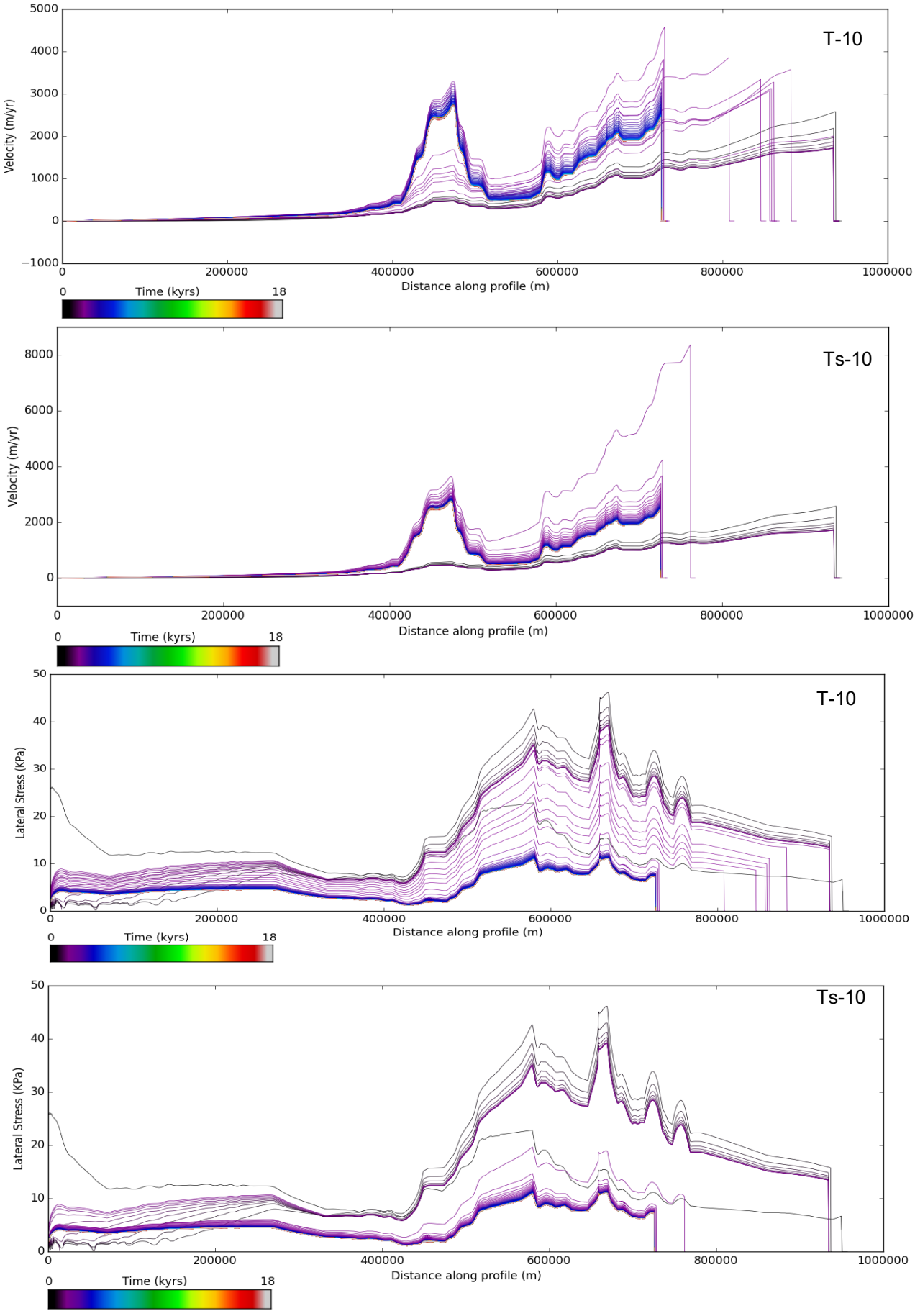

Figure 42. Ice velocity, lateral shear stress and basal shear stress for a linear and stepped ice temperature increase of 20°C. Lateral shear stress drops less gradually in the stepped temperature increase.

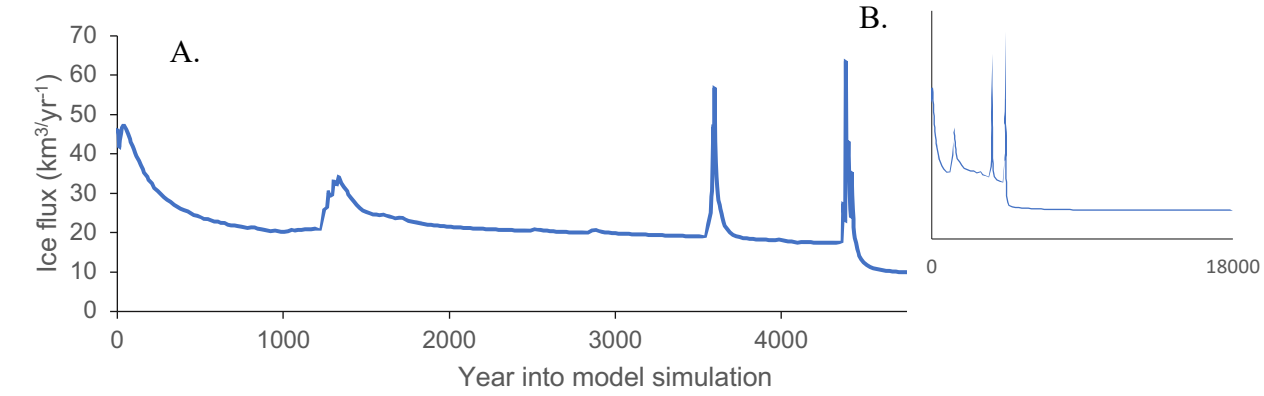

Figure 43. A) 6000 year simulation of the ice flux for a 20°C linear increase in ice temperature after the 1000 year spin up. B) 18,000 year simulation of ice flux for a 20°C linear increase in ice temperature after the 1000 year spin up period.

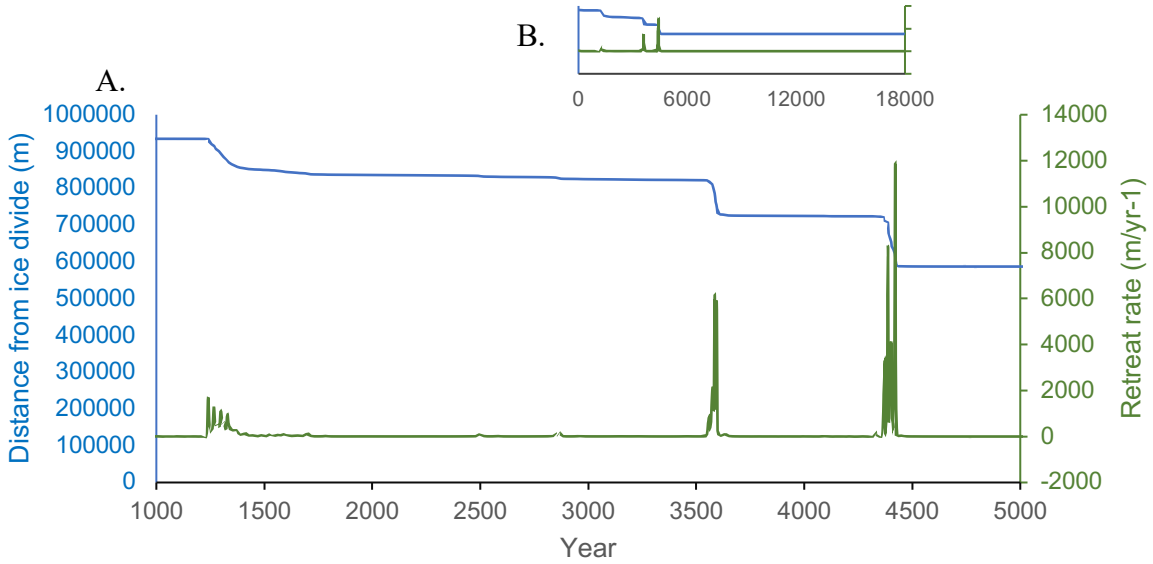

Figure 44. A) 4000 year simulation of the grounding line position and retreat rate in response to a linear T-10 forcing scenario (a temperature increase from 30°C to -10°C). B). The 18,000 year simulation of the distance from ice divide and retreat rate.

5.2.3. Submarine melting

Our results show that the UISS is relatively insensitive to submarine melting compared to ice temperature and the same behaviour is seen whether the forcing is applied in a stepped or linear fashion. The only visible difference between the stepped and linear forcings occurs in SMRs500 where the retreat happens in one movement rather than three (Fig. 45 - SMR500). This is likely to be because the model applies the submarine melt to the final cell of the ice stream and this surface area is not enough to induce significant melt. For this reason, the low melt rates were not felt by the system. Therefore, higher melt rates (500 m/yr^{-1} and 1000 m/yr^{-1}) were applied in order to more realistically replicate melting of the terminus where rapid mass loss from calving was suspected to occur (see section 2 – for iceberg ploughing). Only exceptionally high SMR (1000 m/yr^{-1}) are able to result in the retreat of the grounding line to the middle grounding zone wedge on the mid shelf. Furthermore, it is only in the SMR1000 scenario where the thinning begins to match the geomorphic evidence seen on Ubekendt and Karrat Ejland (section, 2). The other melt scenarios are not able to replicate the

magnitude of grounding line retreat and vertical thinning seen in the geomorphic evidence. However, similar to the sea level and ice temperature forcings, a pattern of nonlinear retreat behaviour is shown.

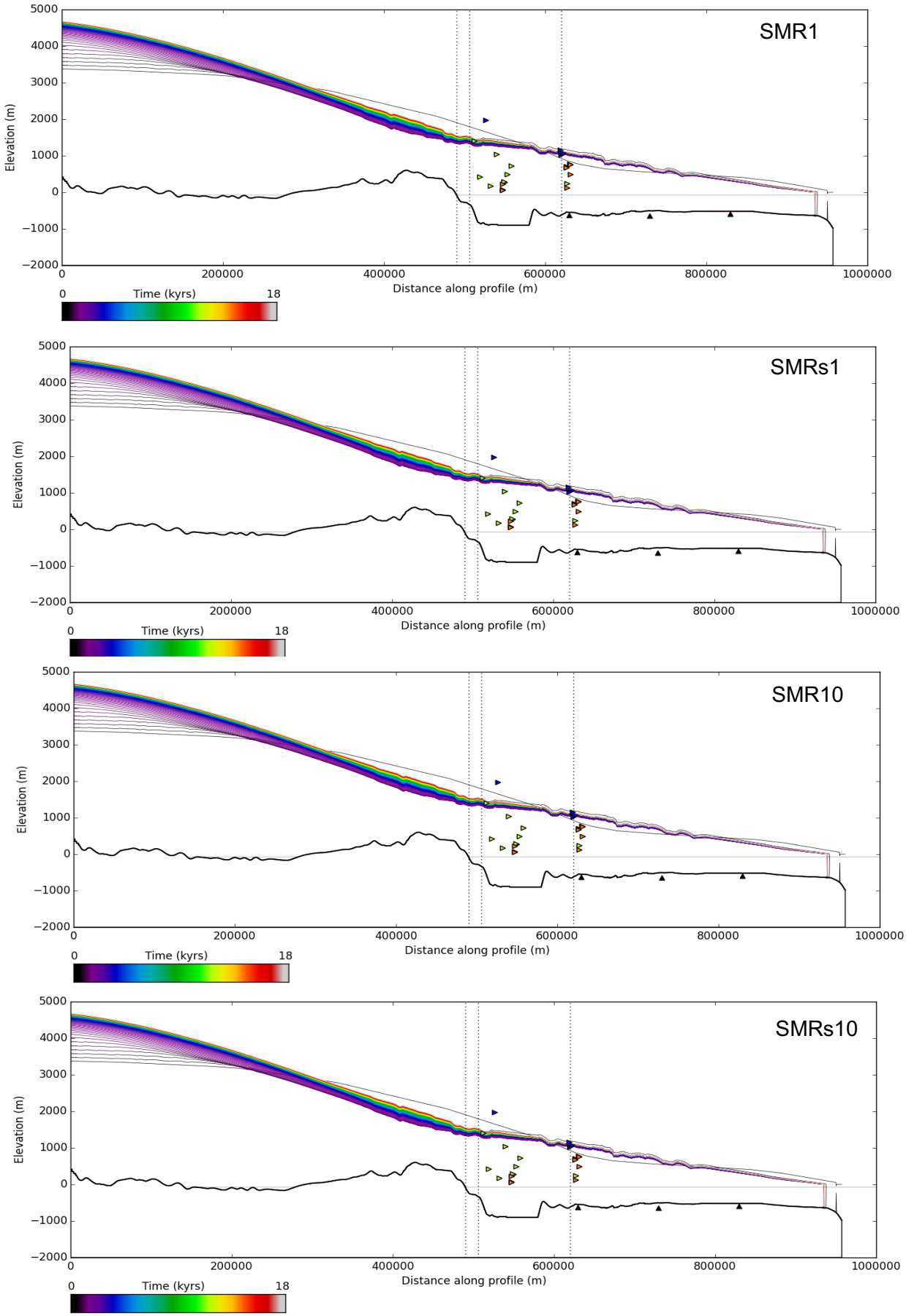

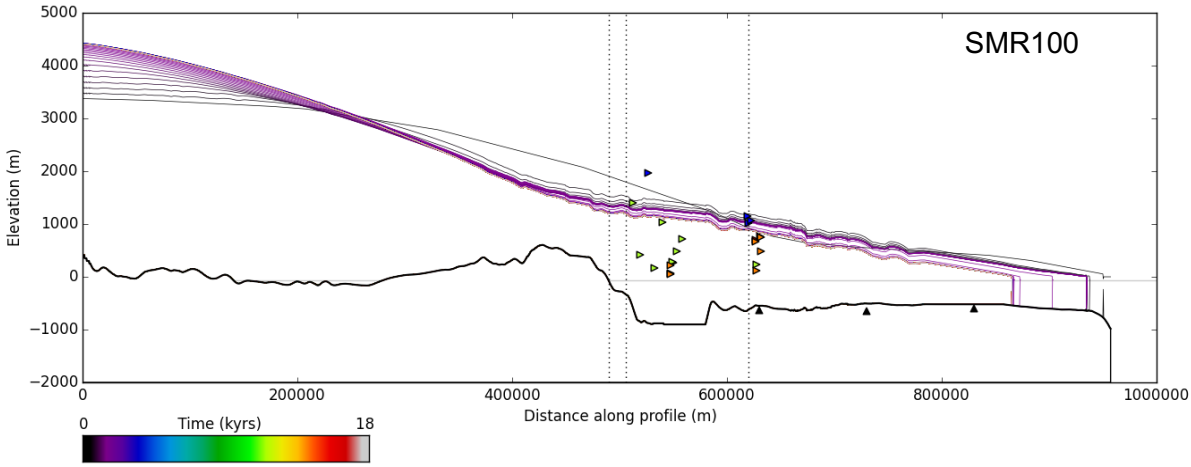
SMR100
Elevation (m)
5000
4000
3000
2000
1000
0
−1000
−2000
0
200000
400000
600000
800000
1000000
Distance along profile (m)
0
Time (kyrs)
18

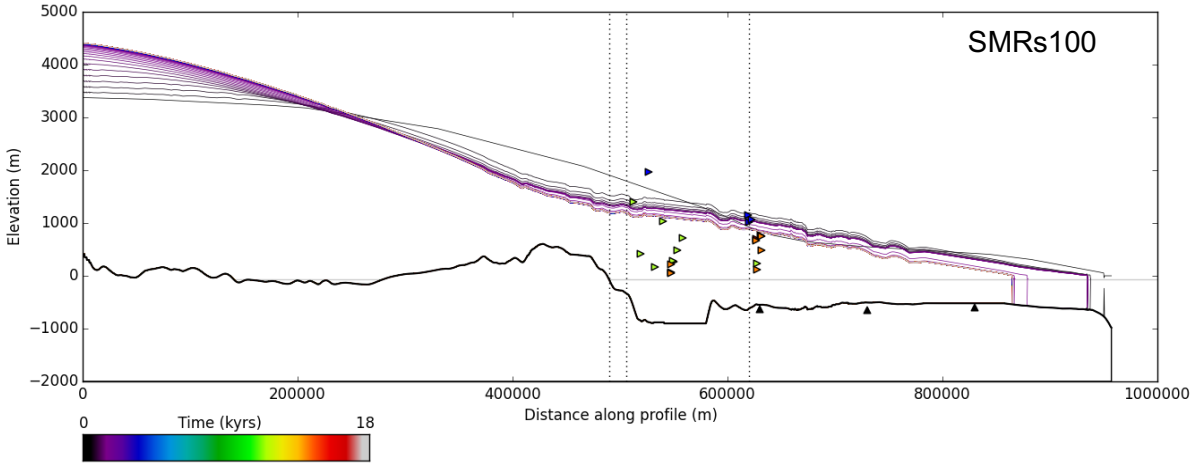
SMRs100
Elevation (m)
5000
4000
3000
2000
1000
0
−1000
−2000
0
200000
400000
600000
800000
1000000
Distance along profile (m)
0
Time (kyrs)
18

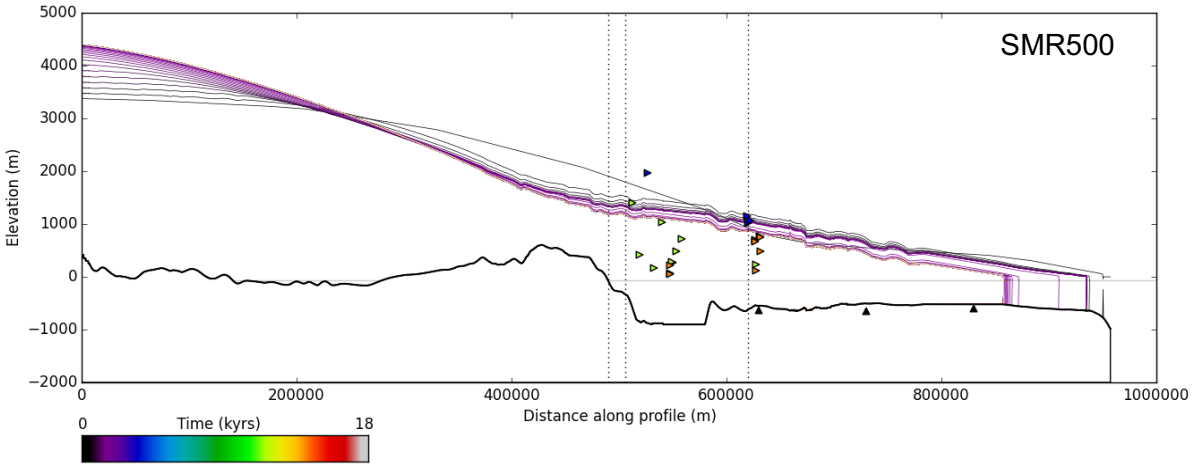
SMR500
Elevation (m)
5000
4000
3000
2000
1000
0
−1000
−2000
0
200000
400000
600000
800000
1000000
Distance along profile (m)
0
Time (kyrs)
18

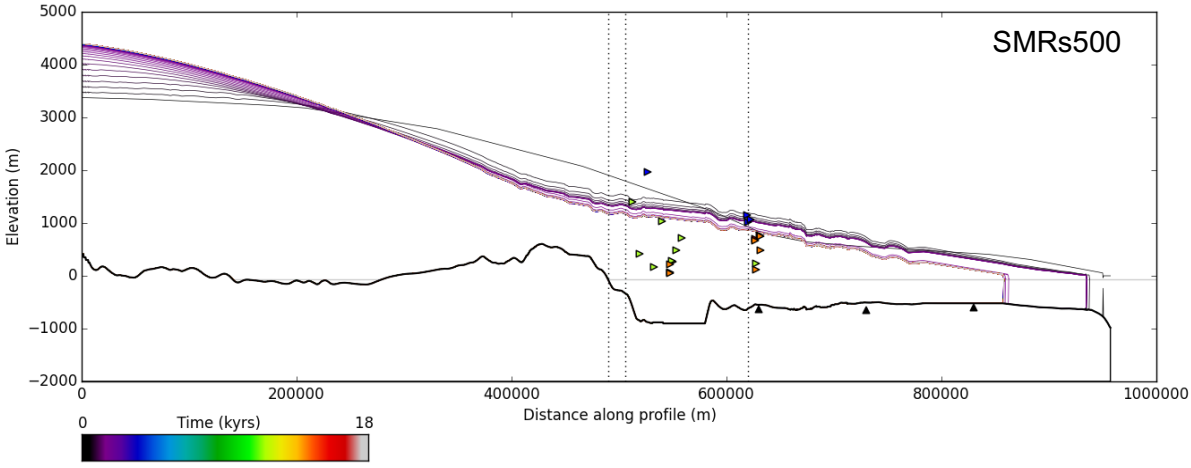
SMRs500
Elevation (m)
5000
4000
3000
2000
1000
0
−1000
−2000
0
200000
400000
600000
800000
1000000
Distance along profile (m)
0
Time (kyrs)
18

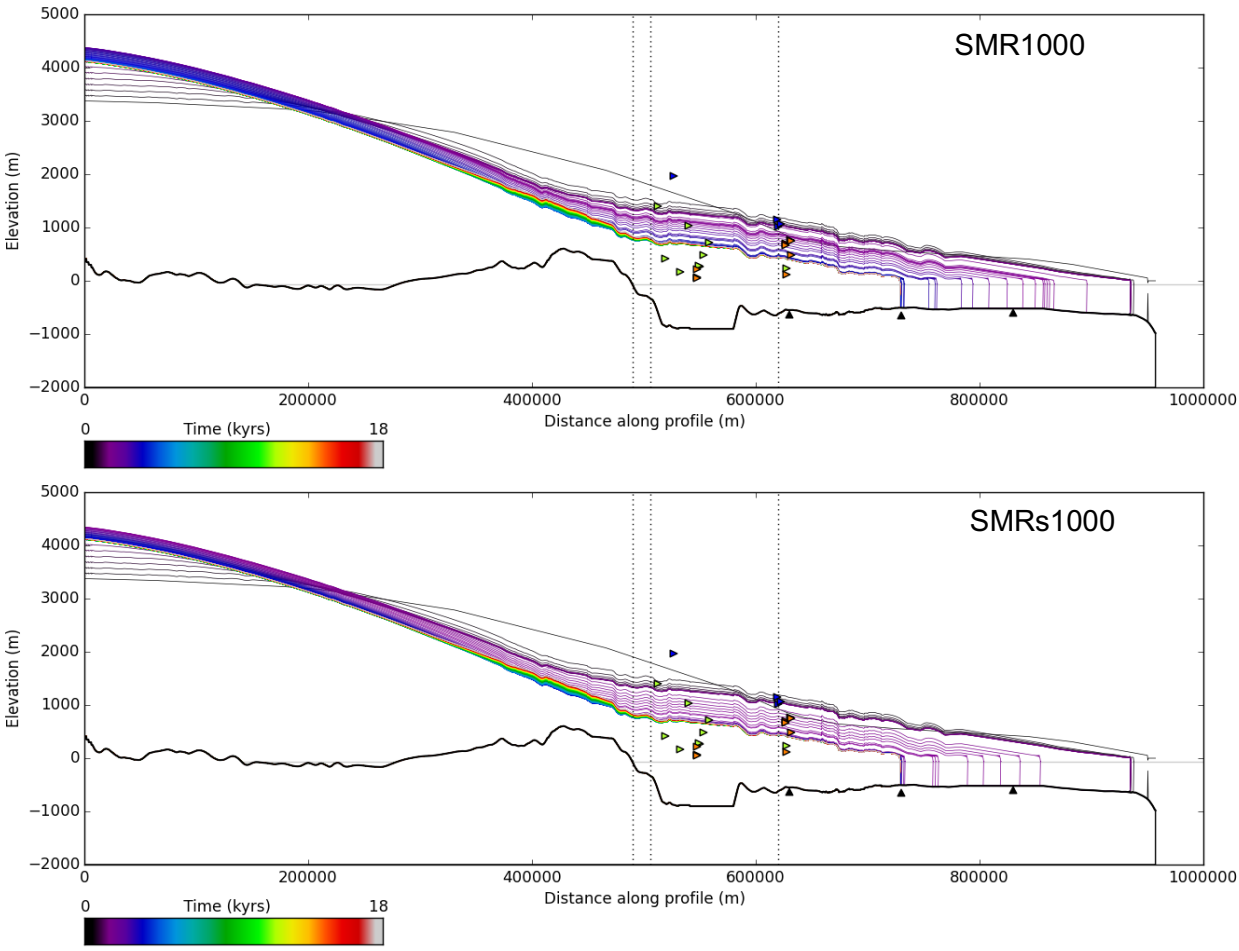

Figure 45. A stepped and linear increase in submarine melt rates of 1, 10, 100, 500, 1000 m/yr. Retreat begins to occur once the submarine melt rate exceeds 10 m/yr-1.

5.2.4. Surface melting

Experiments that apply a change in ELA equating to a lapse rate of 1.5/2°C change per 100 m and consequently, an increase in elevation of ELA from 500 m to 800 m (C800) and 1000 m (C1000) cause significant thickening in the ice stream interior upstream towards the ice divide as there isn't sufficient ablation to maintain the increased mass balance above the ELA (Fig. 46). This results in an ice surface over 1000 m higher than that predicted from modern day satellite altimetry (Thomas, 2006). In these two forcing scenarios the grounding line does not retreat from the outer grounding zone wedge, indicating the grounding line is insensitive to this magnitude of surface melt forcing.

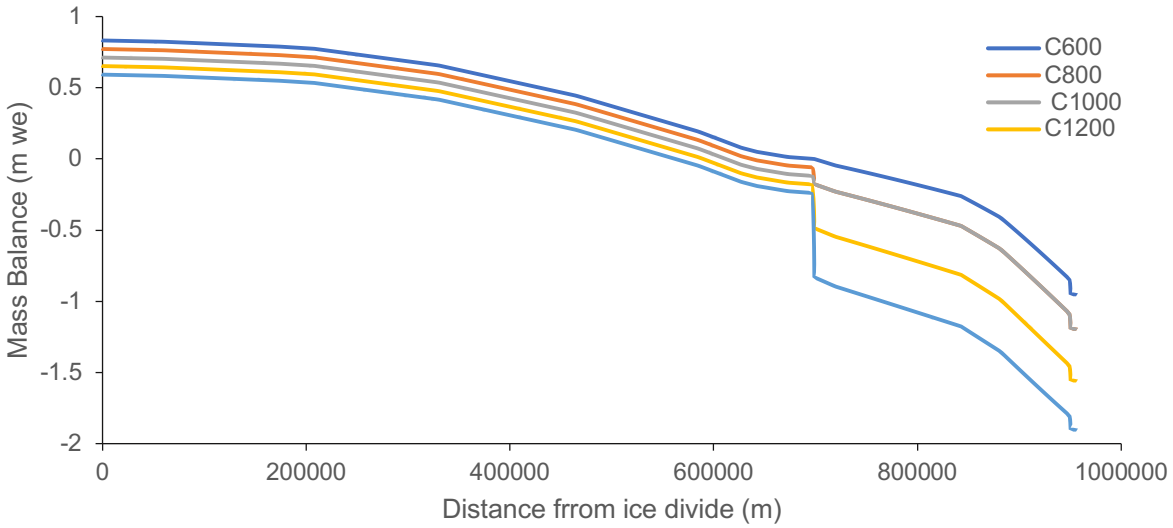

Figure 46. UISS mass balance for the five climate forcing scenarios dervived using the Poinar et al., 2015 equation for below the ELA.

Increasing the ELA elevation to 1200 m (C1200) doesn't change the magnitude of retreat seen in the previous two scenarios (Fig. 47), however, the ice surface profile no longer thickens in the interior and instead it is a more accurate representation of the modern day GrIS surface elevation. The C1200 scenario, is the first climate forcing where the model output begins to align with the geomorphic data. For example, the orange triangles on Ubekendt (Fig. 47) represent moraines and the thinning signal in C1200 whereby as the initial grounding line jumps back onto the topographic high, the ice surface drops down into a position that is very well aligned with the next Ubekendt sample site of the lateral moraine staircase. An increase from 600-1400 m (C1400) causes the greatest magnitude of grounding line retreat and thinning. The grounding line reaches the middle GZW and the thinning allows for the formation of more features on Karrat and Ubekendt. A key finding from this model simulation is that it infers that the lateral moraines were created on Ubekendt whilst the grounding line was still 200 km away and on the outer continental shelf. Thus we can use this model to begin linking specific offshore positions of the grounding line, as recorded by individual GZWs, with specific landforms on the islands that lie on the lateral margins of the UISS. Velocity at the grounding line is closely related to the grounding line retreat, suggesting that either velocity drives retreat or that grounding line retreat is accompanied by higher velocities (Fig. 49).

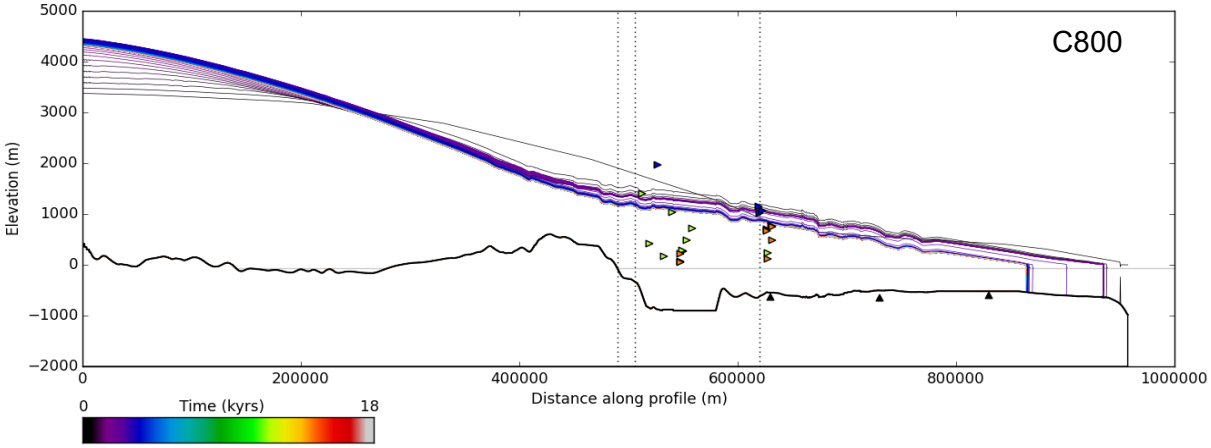
C800
Elevation (m)
5000
4000
3000
2000
1000
0
−1000
−2000
0
200000
400000
600000
800000
1000000
Distance along profile (m)
0
Time (kyrs)
18

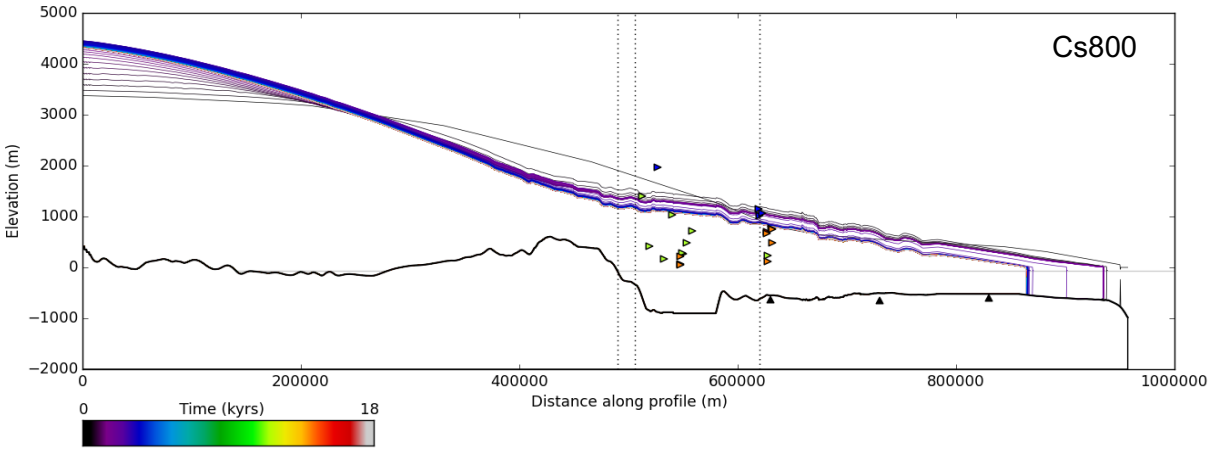
Cs800
Elevation (m)
5000
4000
3000
2000
1000
0
−1000
−2000
0
200000
400000
600000
800000
1000000
Distance along profile (m)
0
Time (kyrs)
18

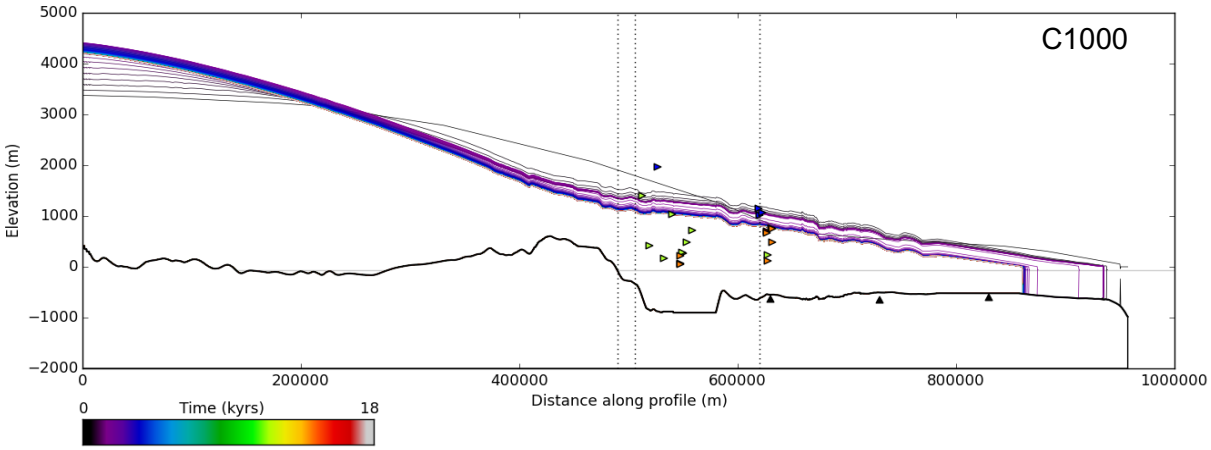
C1000
Elevation (m)
5000
4000
3000
2000
1000
0
−1000
−2000
0
200000
400000
600000
800000
1000000
Distance along profile (m)
0
Time (kyrs)
18

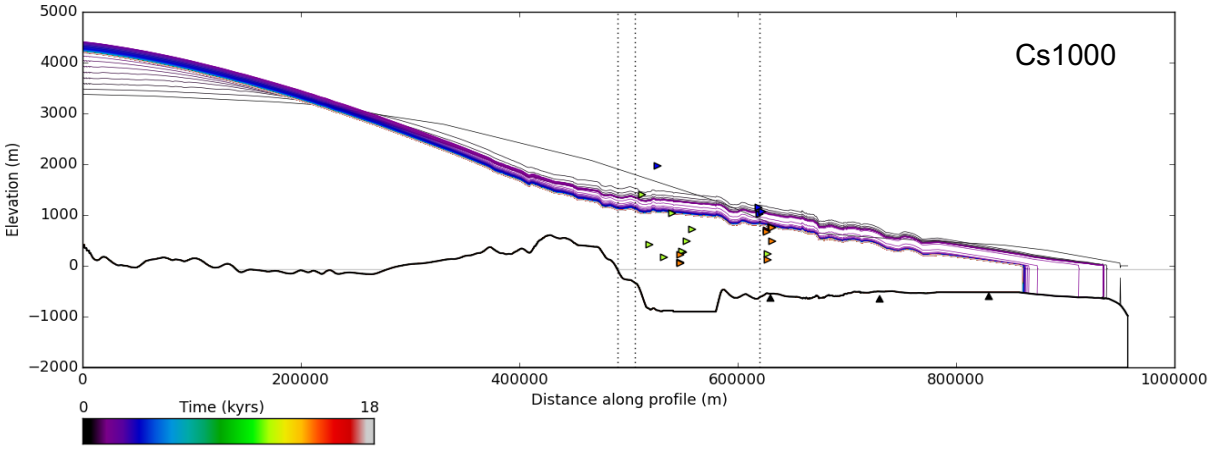
Cs1000
Elevation (m)
5000
4000
3000
2000
1000
0
−1000
−2000
0
200000
400000
600000
800000
1000000
Distance along profile (m)
0
Time (kyrs)
18

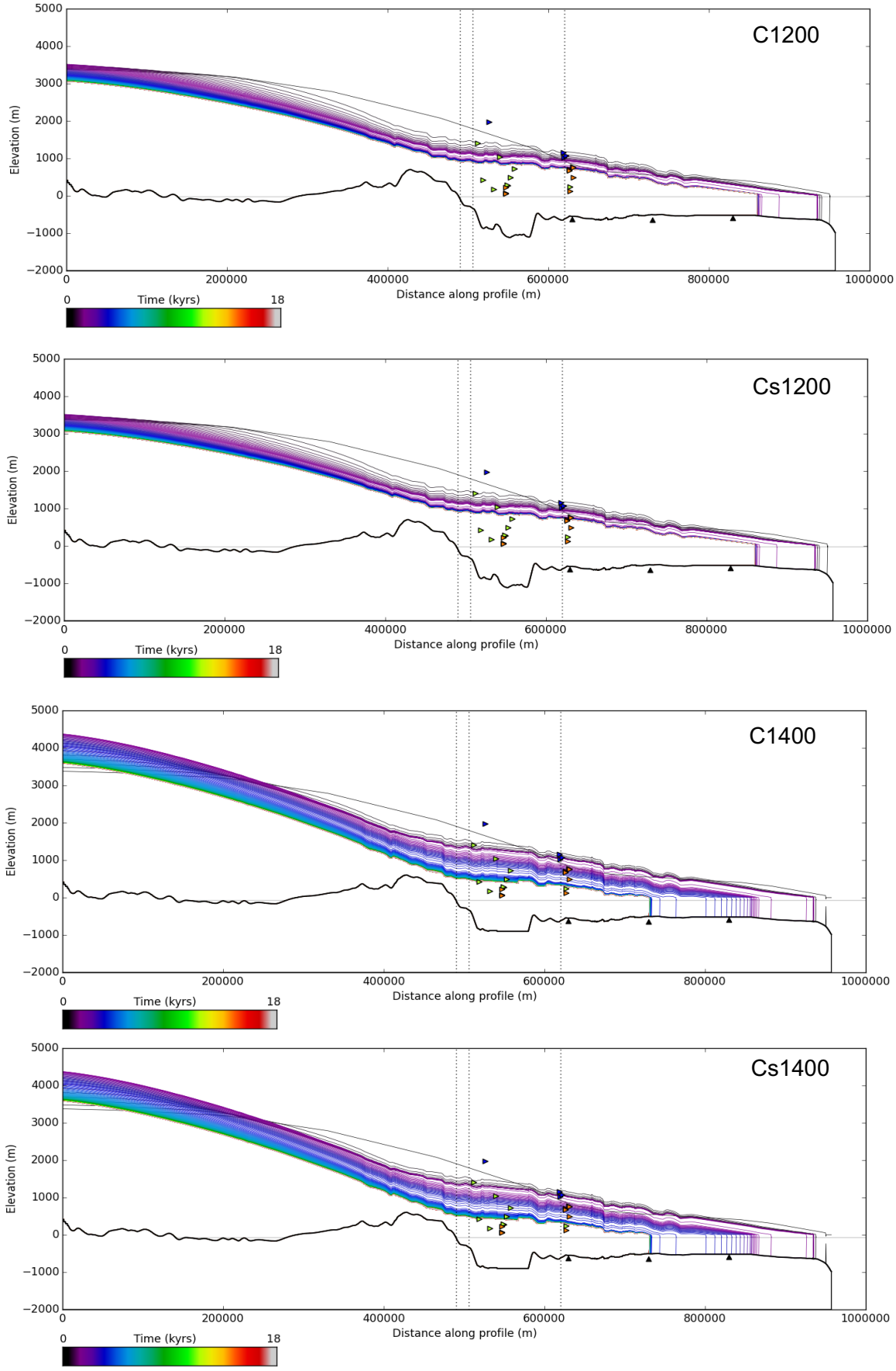

Figure 47. Climate forcing scenarios for an ELA elevation of 800 m, 1000 m, 1200 m, 1400 m. The largest increase in ELA elevation results in the largest increase in thinning and grounding line retreat.

The peak basal shear stress in the first 400 km of the UISS is 50kPA higher in the C1400 simulation compared to Ts10 and T-10 and this may be because the topographic high down stream which is stabilizing the grounding line is resulting in an increase in stress upstream (Fig. 48). As expected, the lateral stress is greatest near the area where the trough shallows and the width of the ice stream narrows (Fig. 47, Fig. 50).

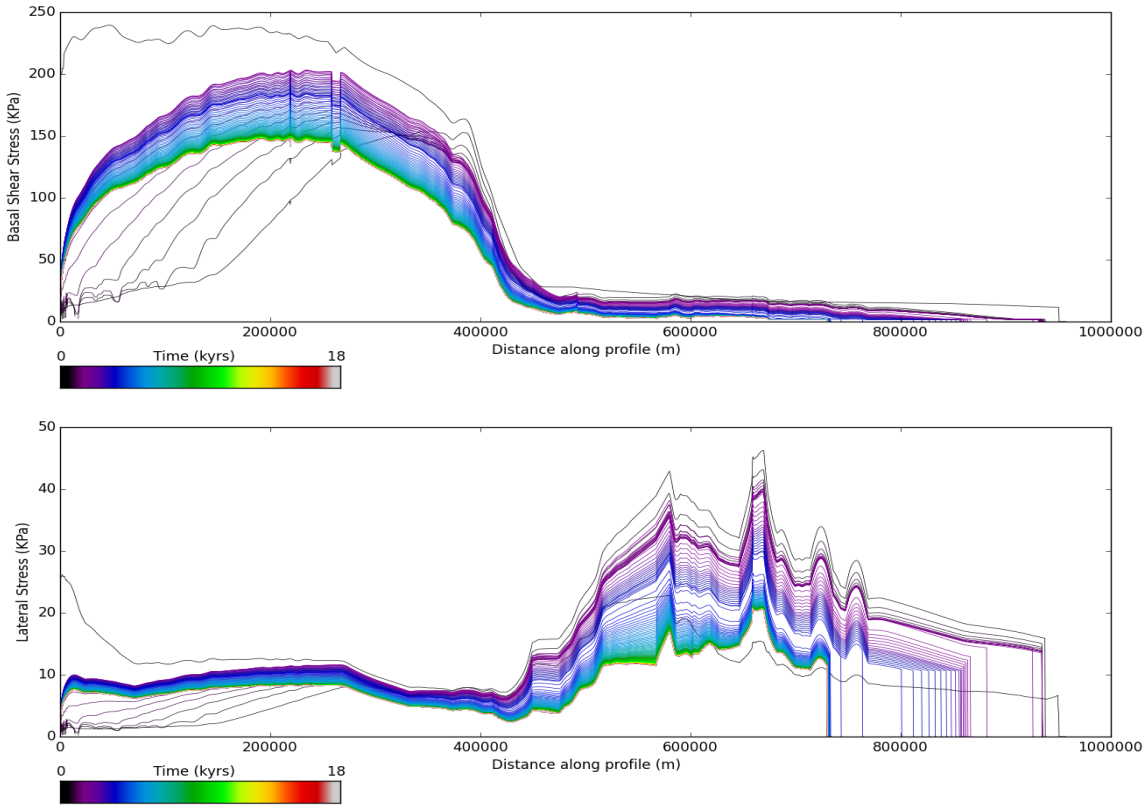

Figure 48. Model output for basal and lateral shear stress for the scenario C1400. Both lateral shear stress and basal shear stress continue to evolve up until 13,000 years into the model run.

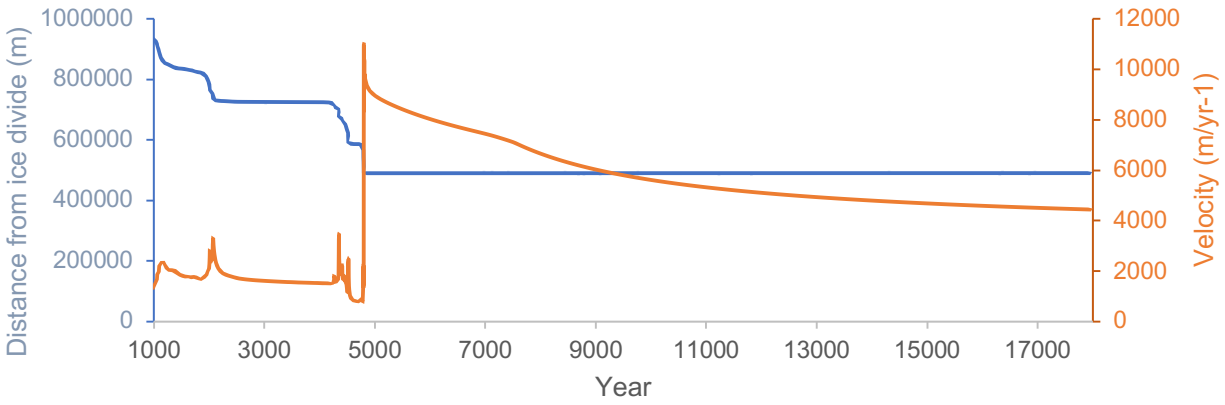

Figure 49. Grounding line position and ice stream velocity at the grounding line for the C1400 forcing scenario.

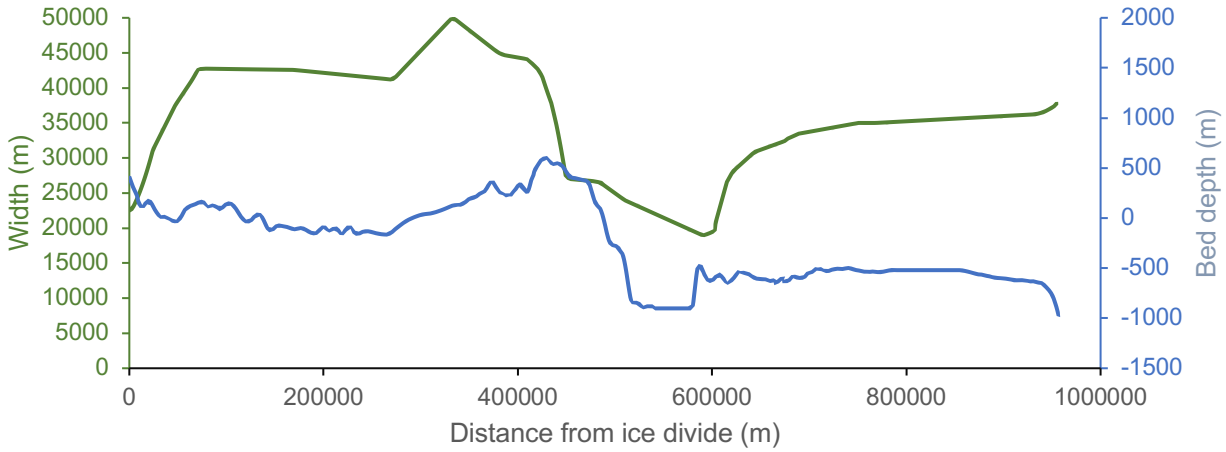

Figure 50. UISS channel width and bed depth from the ice divide in the interior of the GrIS to the grounding line on the continental shelf edge.

In scenarios with enough retreat we can start to see a relationship between the grounding line position and the thinning around Ubekendt and Karrat Ejlands. However, none of the single forcings are enough to cause retreat to the fjord heads and match the geological records. Instead, the grounding line remains on the outer to mid shelf for all of them, and none of them simulate grounding line positions that retreat to Ubekendt or Karrat, except T-10. Nevertheless, even when the grounding line is far from the islands, thinning is still reported upstream and into the island regions.

5.2. Linear combined forcings – Experiment 2

Combing two or more individual forcings allows the impact of multiple controls on the UISS to be investigated. In these simulations all increases are linear and over a 1000 year period. The maximum of each single forcing is applied; for sea level this was an increase from -60 m to +10 m, for temperature this was an increase from -30°C to -10°C, for melt rate this was an increase from -0.5 to 1000 m/yr^{-1}, for climate this was an increase in ELA elevation from 600 to 1400 m. The following scenarios were performed; SL10_T10 (maximum sea level and temperature), SL10_C1400 (maximum sea level and climate), C1400_SMR1000 (maximum climate and submarine melt), SL10_SM1000 (maximum sea level and submarine melt), T10_C1400 (maximum temperature and climate), T10_SMR1000 (maximum temperature and submarine melt).

5.2.1. Maximum sea level with maximum ice temperature increase

A maximum sea level and temperature increase (SL10_T-10) results in retreat to the fjord heads. The model recognizes the final grounding line to be in position '*A'* (Fig. 51), approximately 480 km from the ice divide, rather than grounding line B that has been pinned upstream of Ubekendt. Upstream of Karrat Ejland, sufficient thinning has caused the ice stream grounding line to retreat to position '*A'*, however, the model has developed a small ice shelf between A and B whose terminus grounds at be,

leaving a cavity beneath the floating ice (Fig. 51). The ice is pinned between A and B, and particularly at B, and this coincides with where the trough narrows and where a significant topographic pinning point exists on the bed, making the water depth significantly shallower at point B.

As the ice retreated through the trough, lateral shear stresses gradually reduced (Fig. 52). Peaks in lateral shear stress (25, 30, 40 kPa) relates to locations where the outer and central trough have topographic narrowings, but as the ice thinner and retreated the influence of these narrowings became reduced. By the time the retreat is complete, the point of highest shear stress remains at the location of the narrowing around Ubekendt Ejland and lateral shear stresses then gradually reduce along the remainder of the trough. Basal shear stress patterns are consistently low throughout the trough and throughout the period of retreat (20 kPa). These low values coincide with fast flow, thin, low gradient ice. Basal shear stress then ramps up significantly in the terrestrially grounded portion of the UISS in relation to the steepening of ice surface gradient and the significant increases in ice thickness (200 kPa). Variations in basal shear stress and lateral stress are confined to the first 3000 years of the simulation where the linear increases are applied (Fig. 52). After this time, the ice surface, grounding line position and basal shear stress do not evolve and the system appears to reach a steady state configuration.

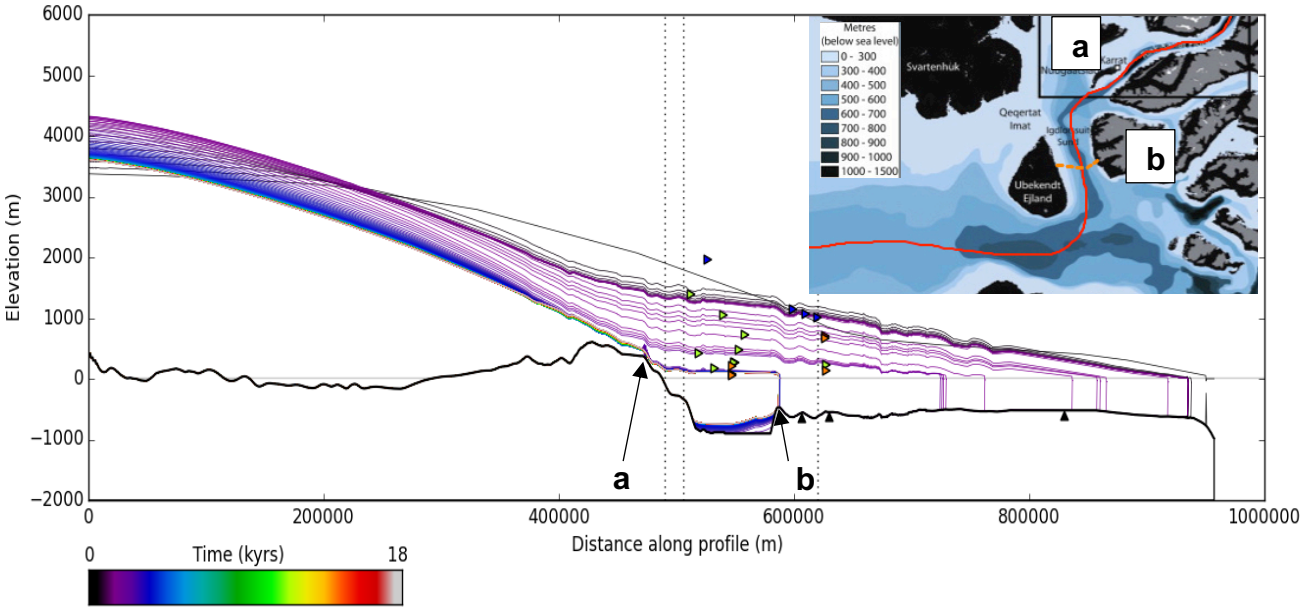

Figure 51. Ice surface profile for SL10_T-10. Black triangles = grounding zone wedges, orange triangles =lateral moraines, green triangles = cosmogenic ages. Blue triangles = ice free regions/or partially covered.

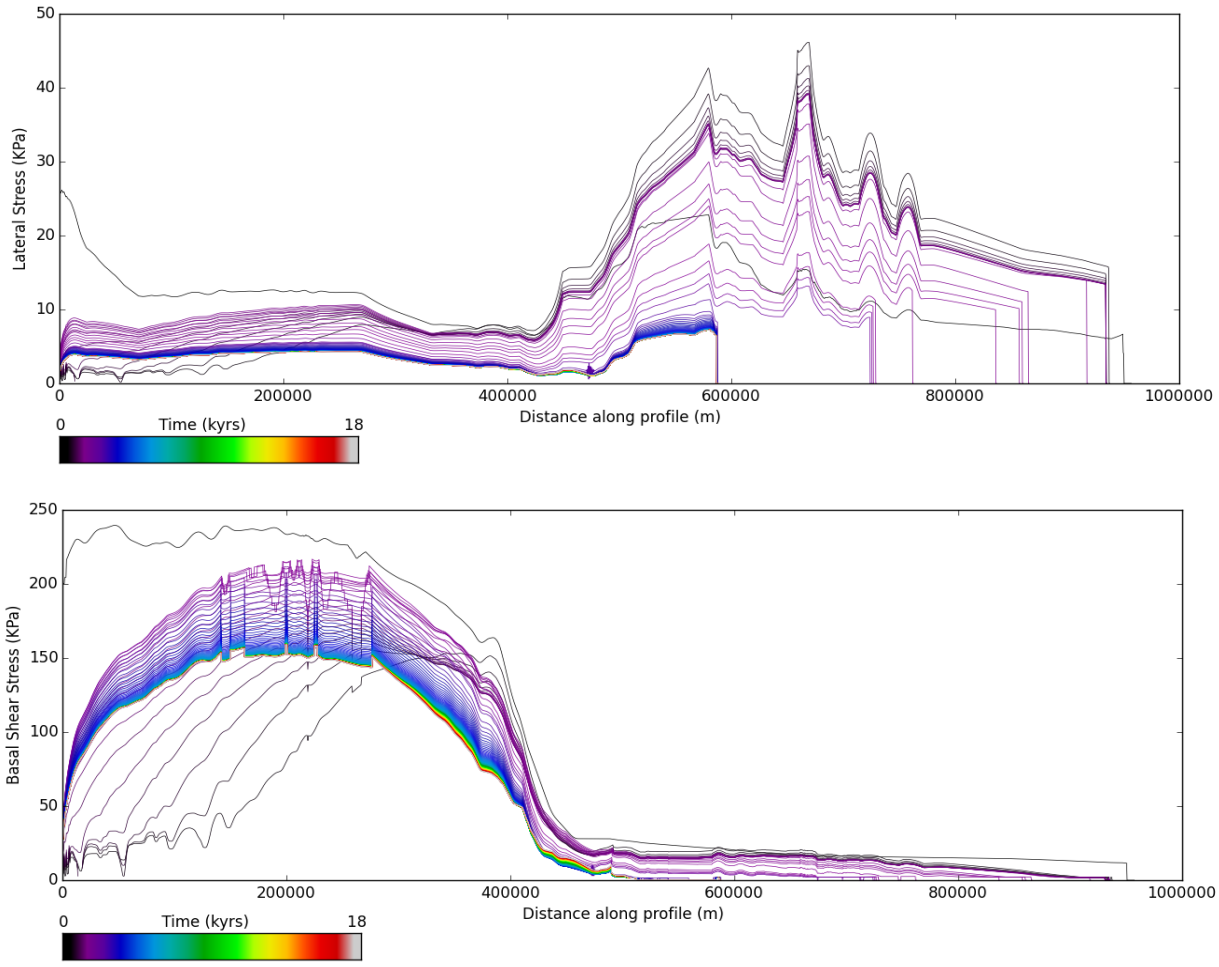

Figure 52. Lateral and basal shear stress gradually decrease during the simulation for SL10_T-10.

5.2.2. Maximum sea level and maximum ELA increase

A maximum increase in sea level and climate (SL10_C1400) are not sufficient to cause retreat to the fjord heads. However, it does cause more retreat than the majority of the single forcings. The ELA is providing the critical control on top down thinning in this scenario as it is a direct proxy for surface melting. When the grounding line jumps from its penultimate position to its final grounding position the ice surface profile simultaneously drops and this fits well with the cosmogenic data in Ubekendt and the formation of the lateral moraine (UBE 2 – upper limit of lateral moraine, UBE 14 – erratic on frost re-worked till, *Section 2.2.1*) (Fig. 53), equally, this same top down thinning effect is felt upstream at Karrat (K1 and K3 – the upper limit of a set of three moraines and the lower limit of a set of three moraines respectively, *Section 2.2.1*). Despite the climate causing the entire ice stream to thin, a dynamic change at the grounding line is responsible for triggering a rapid reaction in the ice surface that extends rapidly inland, particularly noticeable at Ubekendt but also visible at Karrat. The dynamic changes at the grounding line include dynamic thinning and grounding line retreat and there is a very strong causal relationship between retreat at the terminus and thinning inland (even up to 400 km away).

There is a noticeable difference in velocity patterns between scenarios SL10-T10 and SL10_C1400 (Fig. 53). In the former, the velocity increases, with some smaller scale fluctuation, towards the grounding line and peaks (8000 m/yr^{-1}) around the 500 km downstream of the ice divide where the grounding line becomes 'hooked' on the upward sloping bed. In comparison, in the SL10_C1400 the velocity displays a more gradual rise towards the grounding lien and peaks (2000 m/yr^{-1}) further downstream (where the final grounding line is positioned) at 730 km. Comparing these two experiments indicates that there is a clear relationship between final grounding line position and peak velocity (Fig. 53), with velocities increasing towards the grounding lines and with velocities increasing as retreat becomes more significant.

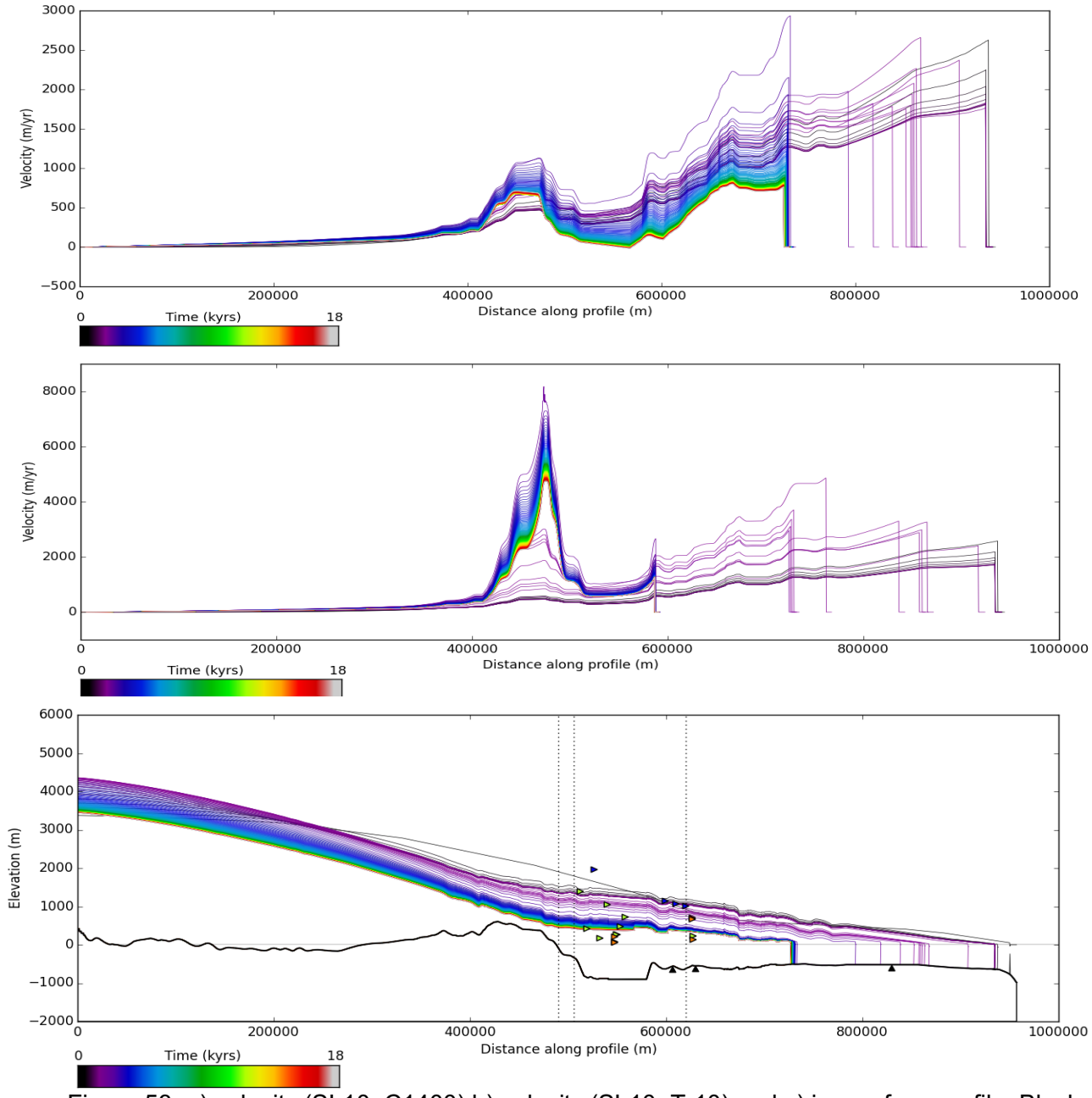

Figure 53. a) velocity (SL10_C1400) b) velocity (SL10_T-10) and c) ice surface profile. Black triangles = grounding zone wedges, orange triangles =lateral moraines, green triangles = cosmogenic ages. Blue triangles = ice free regions/or partially covered.

5.2.3. Maximum ELA and maximum submarine melt increase

The C1400_SMR1000 (a maximum increase in climate and melt rate) simulation had a similar outcome to the SL10_T-10 forcing. In both scenarios the ice stream retreated to the fjord head. However, in the C1400_SMR1000 the final stages of thinning occur between 3000-4000 years into the simulation, whereas in SL10_T-10 all thinning occurs within 1000-3000 years of the model run (Fig. 54). Thus the UISS responded much more rapidly to the experiment being forced by combined sea level and ice temperature than it did when being forced by changes in climate and submarine melt. Similar to the two previous experiments (Fig. 53), the peak velocity in the latter experiment occurs at the final grounding line position (Fig. 55) although it reaches a higher maximum value of ca. 10 km per year. The ice surface profile in this simulation produces a better fit with the geomorphology than the SL10_C1400 scenario.

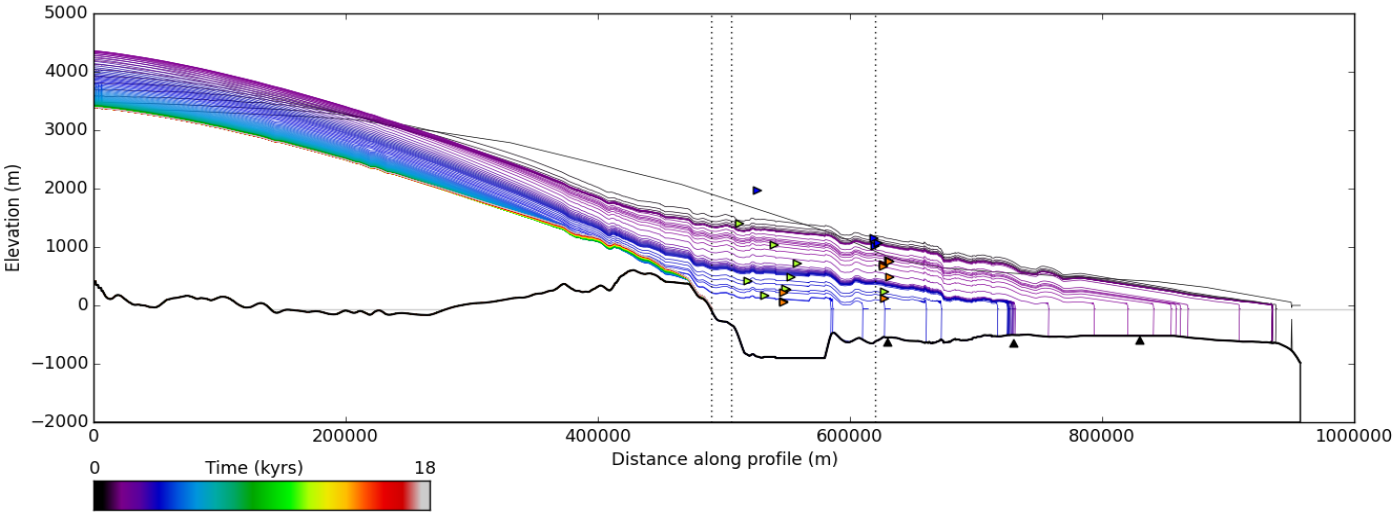

Figure 54. Ice surface profile for C1400_SMR1000 forcing scenario. Black triangles = grounding zone wedges, orange triangles =lateral moraines, green triangles = cosmogenic ages. Blue triangles = ice free regions/or partially covered.

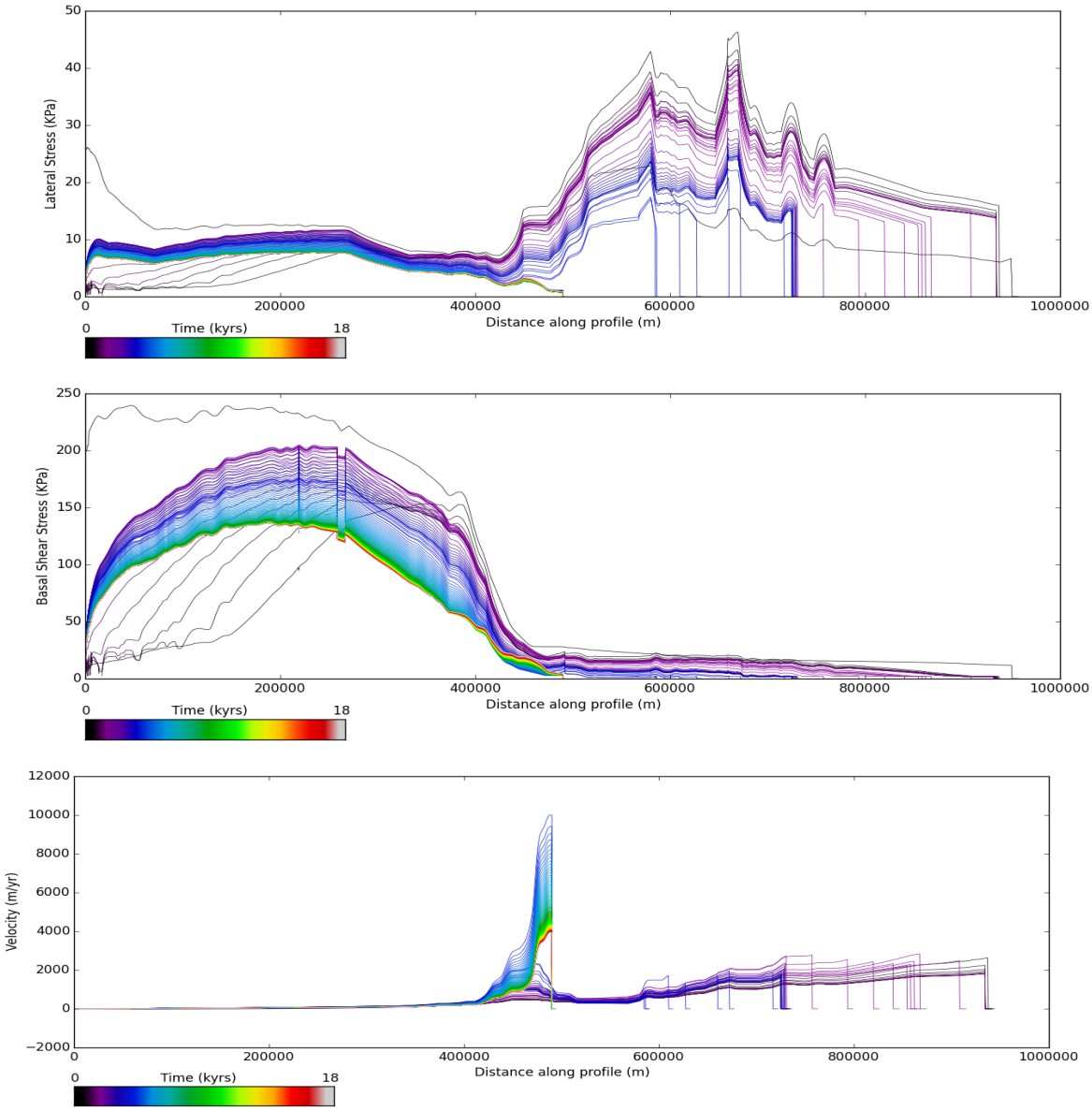

Figure 55. Lateral shear stress, basal shear stress and ice velocity for the C1400_SMR1000. The basal shear stress and velocity are constantly evolving in the model simulation up until the year 17,000.

5.2.4 Maximum sea level and maximum submarine melt increase

Maximum sea level and submarine melt rate increases (SL10_SMR1000) have the least effect on the grounding line position and this confirms the behaviours seen in their single forcing scenarios. Without the increase in ELA elevation the modern day ice surface profile is over 1000 m higher than the observed ice surface of the GrIS (Thomas, 2006) and there is not enough vertical thinning to allow for the formation of geomorphic landforms seen on both Ubekendt and Karrat Ejlands because most of these sites remain buried in this simulation. Peak velocity exceeds 3000 m/yr^{-1} and this is a commonality for simulations with SMR1000 (Fig. 56).

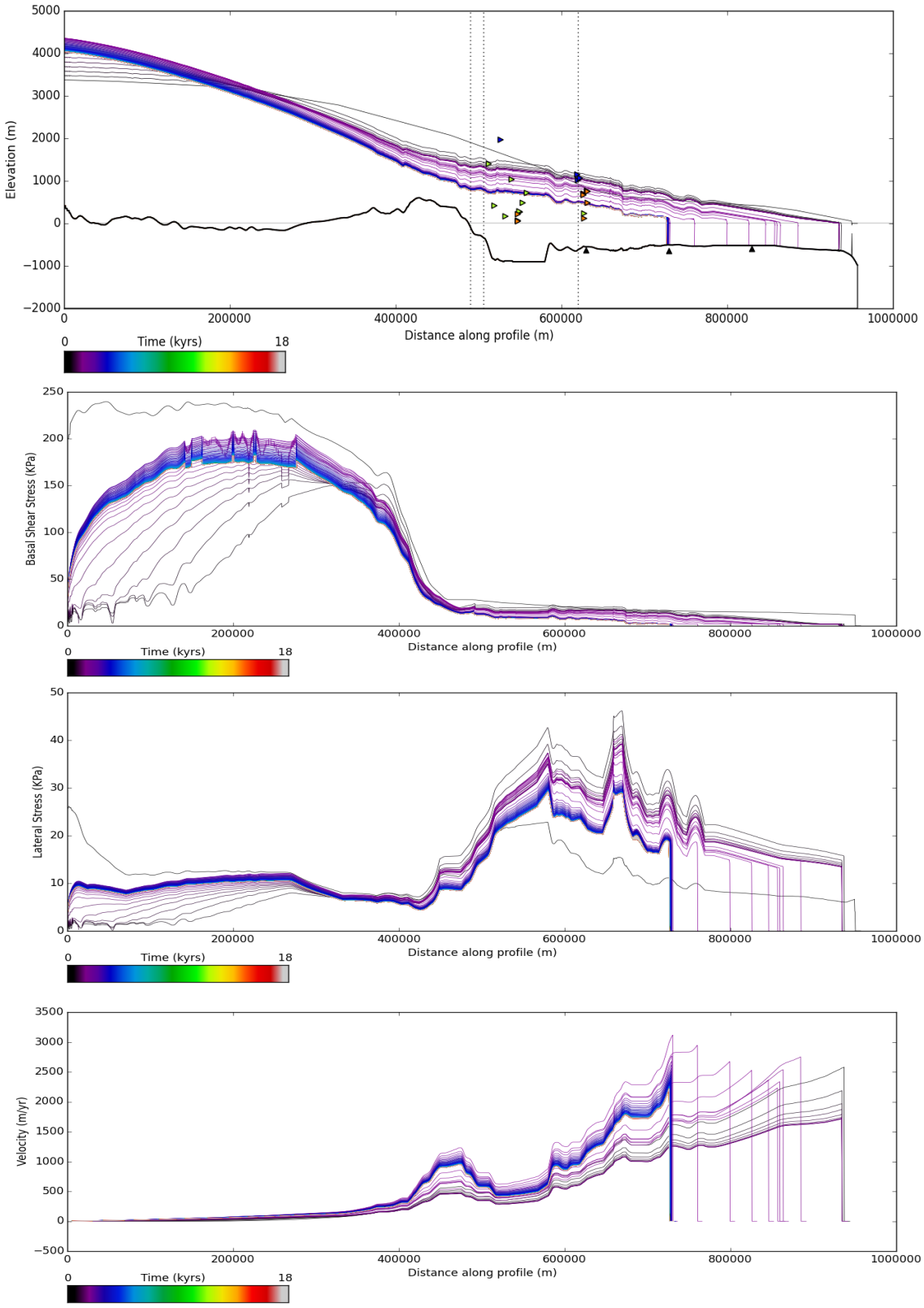

Figure 56. Ice surface profile: Black triangles = grounding zone wedges, orange triangles =lateral moraines, green triangles = cosmogenic ages. Blue triangles = ice free regions/or partially covered, basal shear stress, lateral shear stress and ice velocity for a SL10_SMR1000 forcing scenario. A sharp spike in lateral stress occurs at locations where the ice trough narrows. Overall, increased basal shear stress coincides with thicker ice and a steeper ice surface profile. Ice velocities increase as the grounding line retreats.

5.2.5. Maximum temperature and maximum ELA increase

A maximum temperature and climate forcing (Fig. 50, T-10_C1400) have a similar effect to sea level and temperature (SL10_T-10), however the climate component leads to more surface melting which causes enhanced vertical thinning in the UISS. This forcing fits better with the thinning and moraine formations on Ubekendt compared to SL10_T-10 as the jumps in ice surface match the vertical distances between consecutive landforms in the 'staircase' of moraine features on land. Again, the grounding line appears pinned behind Ubekendt on the bedrock high. Thinning is happening early and quickly over a 1000 years, and this matches the cosmogenic nuclide dates from Karrat (Roberts *et al.,* 2013) which show the thinning over a 1000 year window (contours are purple) and therefore it is thinning at an equally fast rate (thins between 12-11 kyrs from 1000-200 m from top of mountain that become ice free – Fig. 57). We note that the timing match is only relative as opposed to absolute because the forcings being used in these sensitivity experiments are being linearly applied and are not meant to reflect realistic patterns of forcing. Thus, the model thins earlier than the cosmogenic chronology would suggest (within the first 2000 years but this is because the forcing is applied linearly after 1000 years) but the overall time period is on the right scale. On Ubekendt there is a high elevation cosmogenic nuclide date and low elevation cosmogenic nuclide date that are both dated 12.3 ka BP and 12.5 respectively (Roberts *et al.,* 2013), and this suggests that ice down wastes almost instantaneously. We note that this is consistent with the jumping back of the grounding line from its position on the mid to outer trough, back into a location in the inner trough where there is a slight topographic high and a minor topographic narrowing. With each stage of stepped retreat when the grounding line moves inwards over the outer and mid trough, the velocity of the UISS systematically increases up to 4000 m/yr^{-1}, however, once the grounding line reaches the inner trough, the velocity increases significantly to 12,000 m/yr-1 at around 500 km downstream of the ice divide (Fig. 58) and this is where the grounding line reaches the fjord heads (inland of the present day ice stream today). This peak velocity is up to 4 times higher than the scenarios which include SMR1000 (Fig. 58).

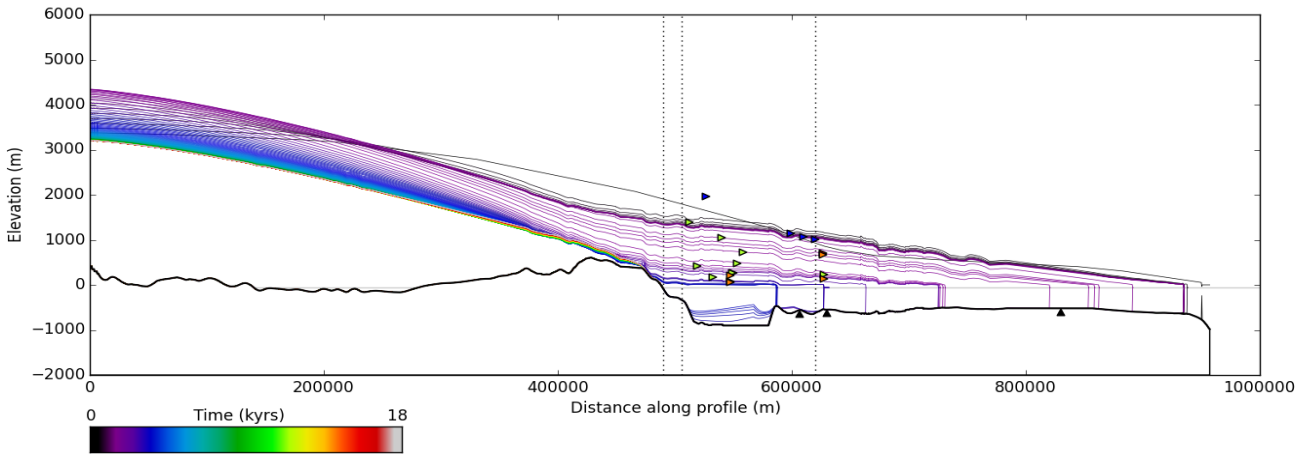

Figure 57. Ice surface profile for a T-10_C1400 scenario. Black triangles = grounding zone wedges, orange triangles =lateral moraines, green triangles = cosmogenic ages. Blue triangles = ice free regions.

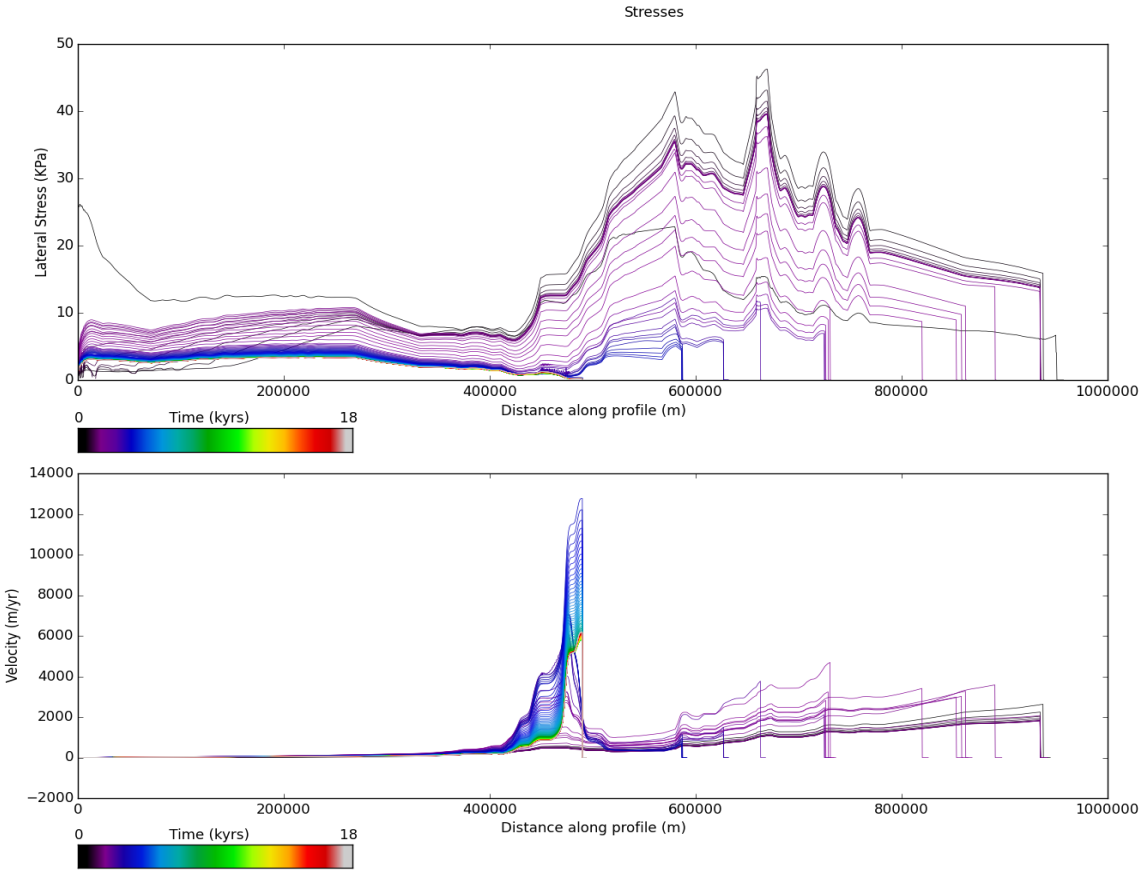

Figure 58. Lateral shear stress and ice velocity for T-10_C1400 forcing scenario. As the grounding line retreats, the velocities increase at the terminus, but then once the grounding line stabilizes in a particular location, velocities gradually reduce until the next step back in the retreat.

5.2.6. Maximum temperature and maximum submarine melt rate increase

Temperature increase and submarine melt rate increase (T-10_SMR1000) is not sufficient to cause retreat to the fjord heads, the grounding line retreat seems punctuated by three movements and it stays at around 750km for the last 15,000 years approximately (Fig. 59). However, some thinning around the fjord heads and Karrat occurs later at around 8,000 years ago. The peak velocity is the greatest in this forcing as it reaches up to 25000 m/yr^{-1} and this is likely to be because ice temperature warming and submarine melt rates have the greatest impact on ice stream velocity (Fig. 60). In this simulation ice thickness at the ice divide is a lot thicker than the historic thickness of ice in the interior of the ice sheet. Equally, ice thickness at the location of the known modern grounding line (around 470 km downstream of the ice divide) is very thin. Nevertheless, the vertical thinning history marked by the moraines and cosmogenic ages (orange and green triangles respectively) fits well with the ice surface profile even though the grounding line is grounded on a topographic high at 580 km.

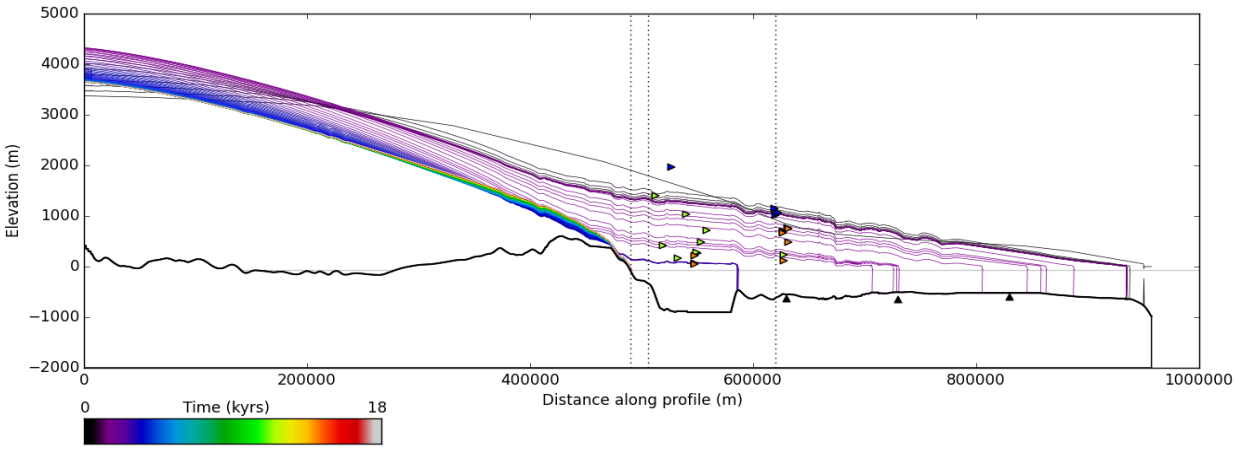

Figure 59. Ice surface profile for T-10_SMR1000 forcing scenario. Black triangles = grounding zone wedges, orange triangles =lateral moraines, green triangles = cosmogenic ages. Blue triangles = ice free regions/or partially covered.

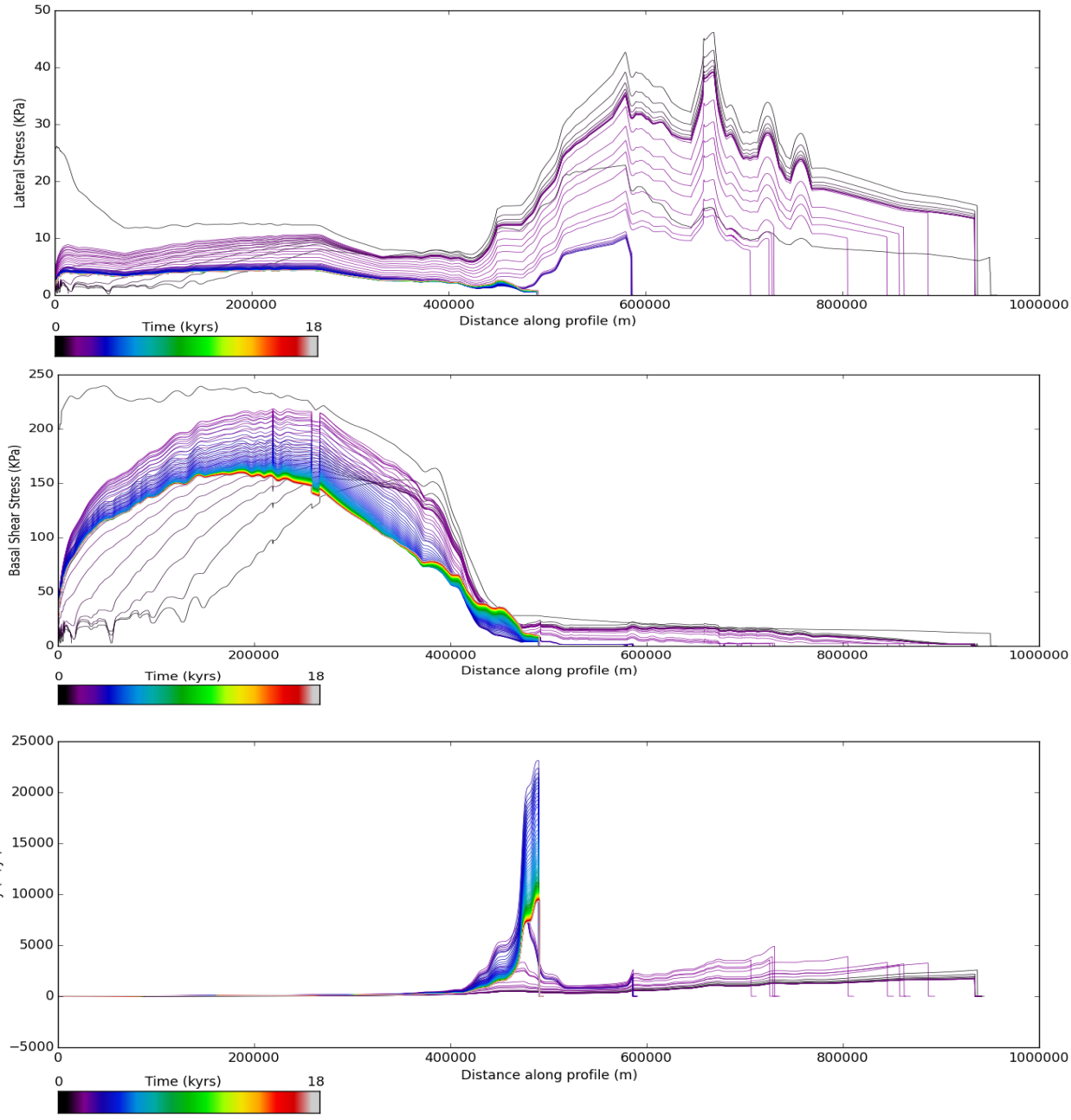

Figure 60. Lateral shear stress, basal shear stress and ice velocity for a T-10_SMR1000 forcing scenario.

5.2.7. Maximum sea level, ice temperature, ELA and submarine melt rate increase

A combination of all the maximum variations of the variables (SL10_T-10_C1400_SMR1000) unsurprisingly results in retreat to the fjord heads (Fig. 61). Inland thickening occurs early and rapidly in the simulation where the basal shear stresses in the inland region are high and restrict ice flow. During this time, the ice flux required to maintain a stable grounding line (Schoof, 2007) is higher than the actual ice flux being delivered because the high shear prevents the ice discharging into the ocean. As a consequence, the grounding line retreats. The ice surface profile does not fit with modern day observations as it is too high. The peak velocity is around 7000 m/yr^{-1}. After the first 2000 years there is little lateral shear stress in the UISS (Fig. 62).

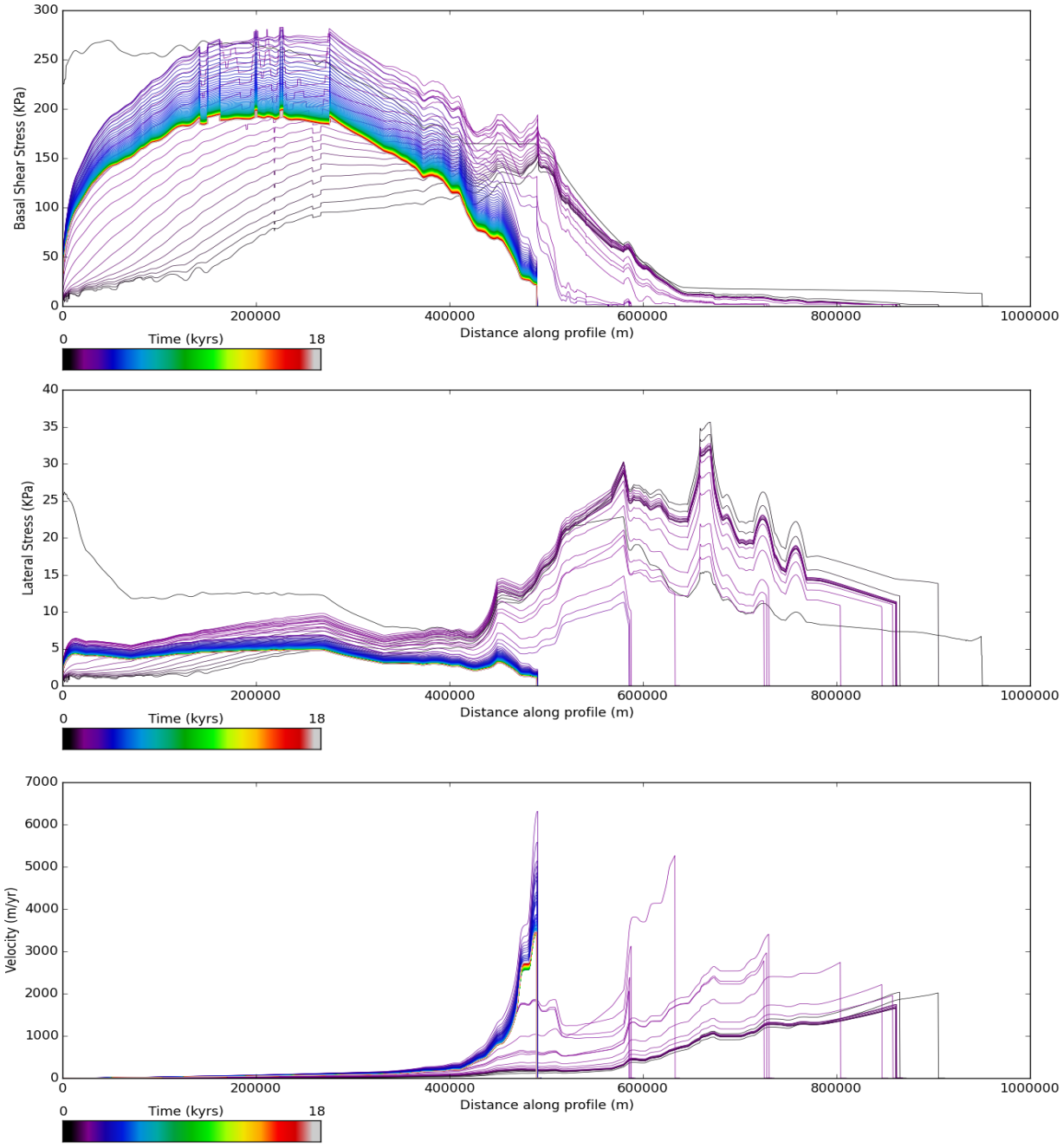

Figure 61. Basal shear stress, lateral shear stress and ice velocity for a maximum forcing scenario.

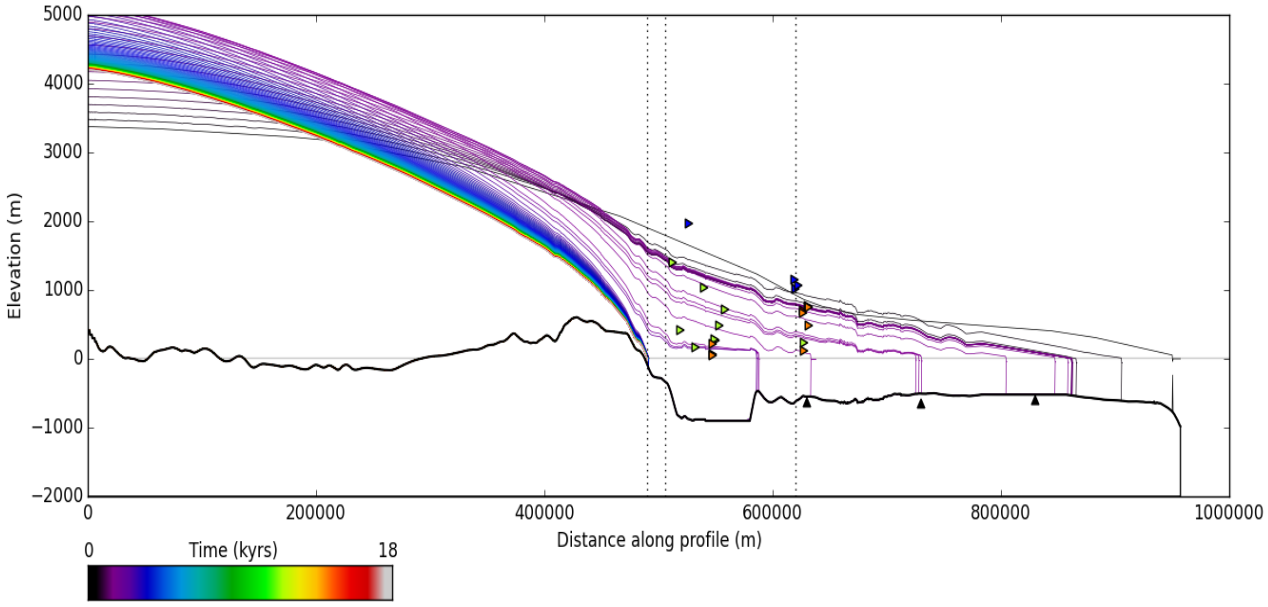

Figure 62. Ice surface profile for a maximum forcing scenario (SL10_T-10_C1400_SMR1000). Black triangles = grounding zone wedges, orange triangles =lateral moraines, green triangles = cosmogenic ages. Blue triangles = ice free regions/or partially covered.

5.2.8. Summary of combined forcings

In summary, ice temperature is the common denominator in reconstructing retreat to the present day margins and as proved earlier it is nearly capable of doing this as a single forcing. This is because warmer ice temperatures allow more internal deformation and thus enhanced basal lubrication and basal sliding. The ELA elevation is important for the vertical thinning of the ice stream as it determines the volume of surface melt. Whilst the UISS appears relatively insensitive to the single forcing sea level perturbations when applied in combination with another forcing more retreat occurs.

5.3. Realistic scenarios - Experiment 3

The previous experiments serve as an exploration of the potential sensitivity of the UISS to particular types of forcing in general. However, it is unlikely that the retreat of the UISS was triggered, and driven, by one single forcing over a 1000 year period We therefore applied some more realistic forcings in an attempt to simulate a response of the UISS that could be more closely considered a ‘reconstruction’. This was achieved using various combinations of the modified GRIP ice curve (described in section 4) to force variations in past ice temperature and ELA and a modelled sea level curve from Simpson et al., (2009). The experimental design was outlined in section 4 above, and the results of these simulations are detailed below.

5.3.1. Single forcings of the forcings presented in the literature

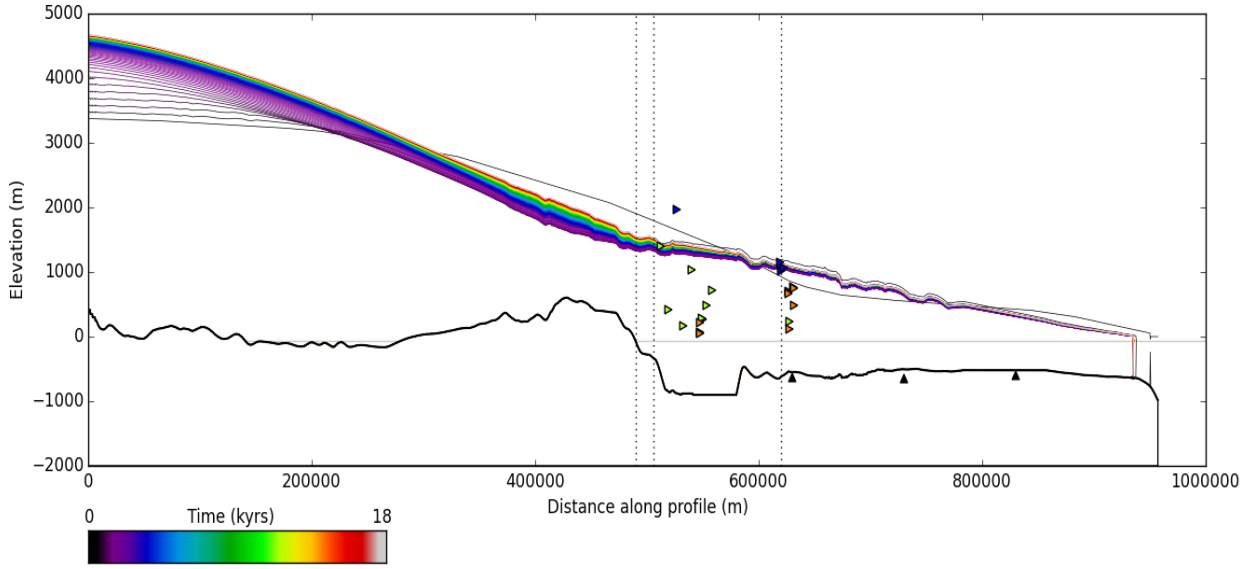

Figure 63. Ice surface profile for a single forcing GRIP experiment. Black triangles = grounding zone wedges, orange triangles =lateral moraines, green triangles = cosmogenic ages. Blue triangles = ice free regions/or partially covered.

5.3.1.1. GRIP forced ice temperature retreat scenario

The modified GRIP curve (see section 4) (Fig. 65) was used as a proxy for ice temperature over the 18,000 year simulation while sea level, submarine melt rates and climate were held constant at the LGM state (Fig. 63). This simulation (GRIP) is the first experiment that results in thickening of the ice stream around 400 km from the ice divide at approximately 12,000 years ago (6,000 years into the model simulation). Although no grounding line advance is observed during the same period, this thickening coincides with the cooler Younger Dryas. This differs from the constant retreat seen in the T-10 forcing (Fig. 41). This could be because a sustained warming signal in the GRIP profile doesn't occur until 12 ka BP (6,000 years into the model simulation). Alternatively, the UISS may not be able to respond to such rapid changes in ice temperature over short timescales. This is important because in the single forcing scenarios an increase in temperature from -30°C to -10°C was able to induce retreat of the UISS to the fjord heads, however in the GRIP forcing an increase to -10°C over a different time period was not able to reproduce the same magnitude of retreat (Fig. 65). Additionally, although the GRIP profile highlights the Holocene thermal maximum period and maintains the ice temperature within a 5°C range the grounding line appears to be insensitive to this (Fig. 63).

The GRIP forcing on its own is not enough to cause retreat of the UISS to the fjord heads, or even to the outer shelf GZW. In this scenario the UISS experiences little variations in lateral and basal shear stress and the velocity at the grounding line only increases marginally from 1700 m/yr^{-1} at the beginning of the simulation to 2100 m/yr^{-1} at the end of the 18,000 years (Fig. 64).

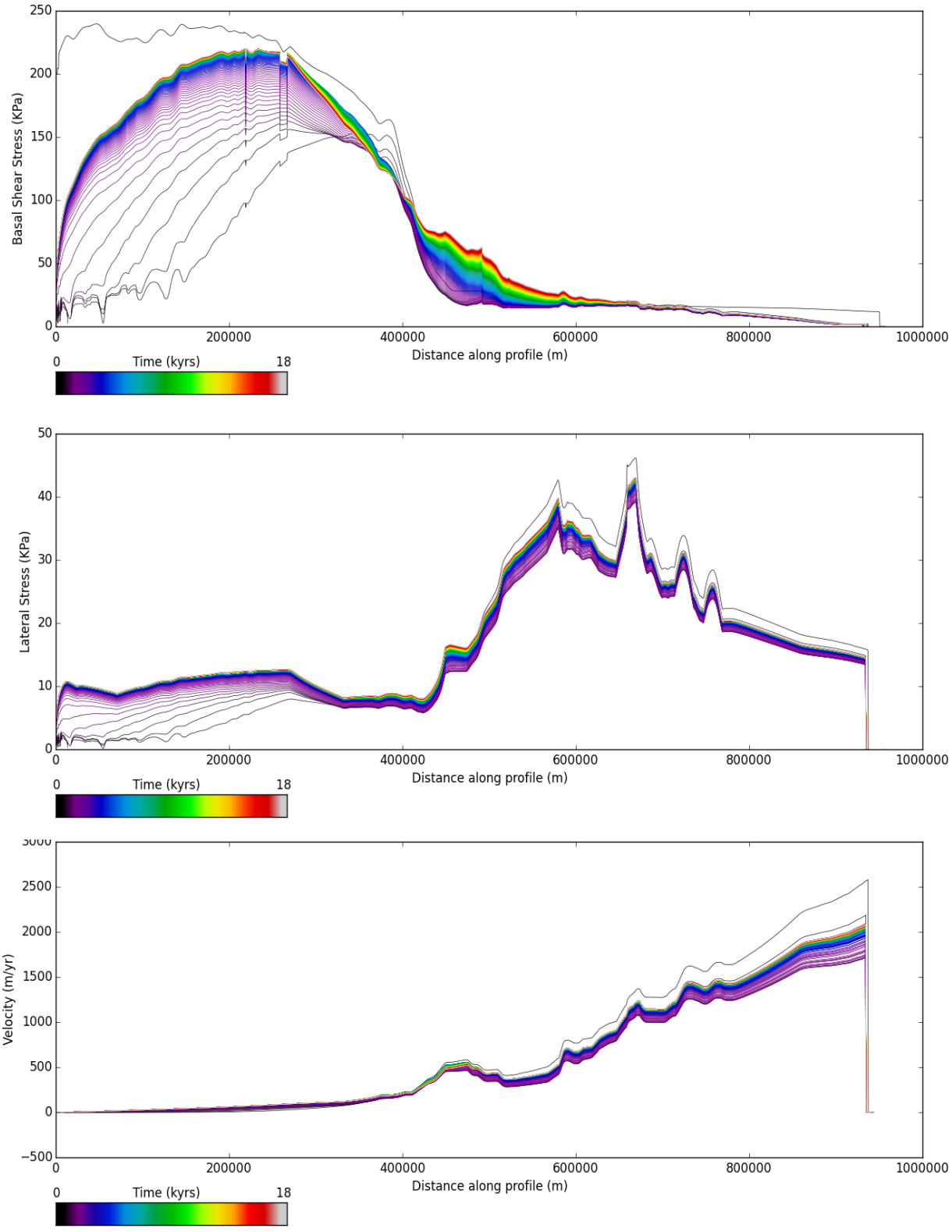

Figure 64. Basal shear stress, lateral shear stress and ice velocity for a GRIP forced ice temperature scenario.

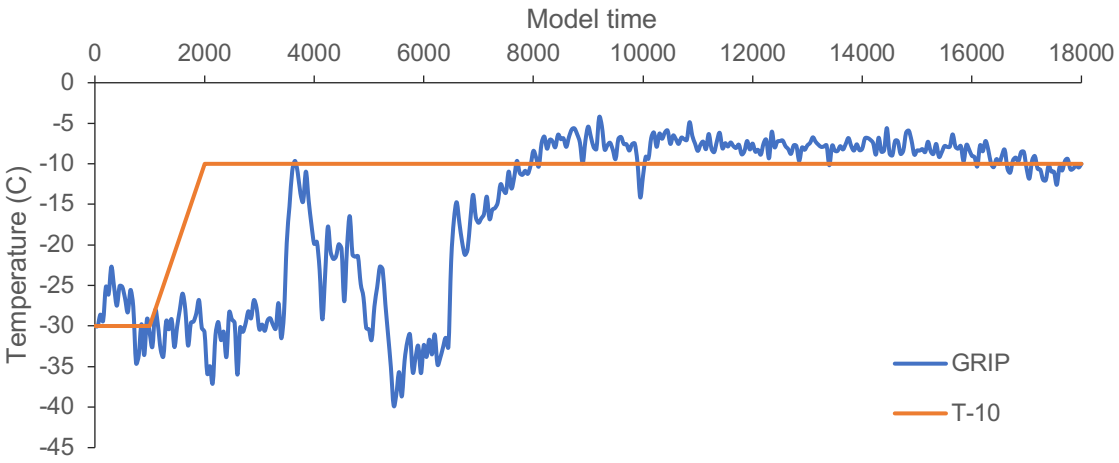

Figure 65. Ice temperature forcing for the GRIP profile and the linear forcing. 18,000 years into model time represent the year 2000.

5.3.1.2. Simpson sea level curve (SSLC)

Using the Simpson et al., (2009) curve for a realistic sea level forcing in the UISS trough illustrates up to 50 km more retreat from the shelf edge than when applying the GRIP forcing alone, however the grounding line is still unable to retreat past the outer GZW (Fig. 66) and the ice surface profile fails to thin to the modern day surface elevation.

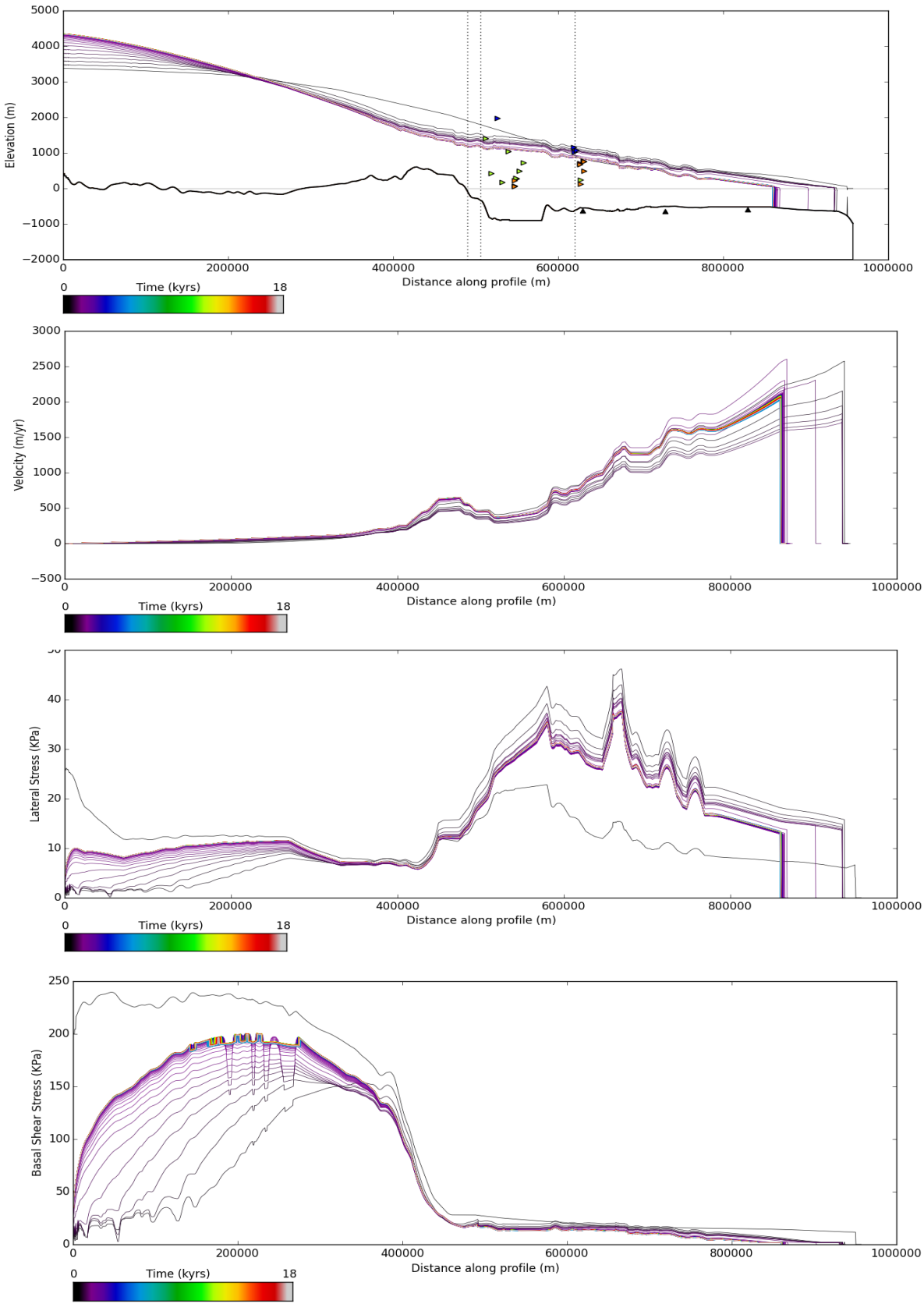

Figure 66. Ice surface profile, Black triangles = grounding zone wedges, orange triangles =lateral moraines, green triangles = cosmogenic ages. Blue triangles = ice free regions/or partially covered, lateral shear stress, ice velocity and basal shear stress.

5.3.1.3. GRIP forced ice temperature with corresponding ELA fluctuation

Applying a fluctuating ELA with the GRIP forcing (GRIP_ELA) demonstrates the controlling influence the ELA has on vertical ice thinning and ice stream retreat. Including the ELA fluctuation in this scenario induces retreat to the middle GZW (Fig. 67), compared to the GRIP simulation (Fig. 66) where the UISS remained on the shelf edge, a difference of 200 km in retreat. Consequently, using the GRIP curve to control ice temperature only makes a difference when combined with its use in simultaneously fluctuating ELA, thereby incorporating the evolution of surface melting. This scenario has the most thinning than compared to the combined simulations and the majority of this thinning occurs around 9,000 years ago during the HTM. The HTM is where ice temperatures are the highest, the ELA is the highest and the sea level is at the present day level. Ice thinning is recorded and jumps in ice surface lowering again occur as the grounding line retreats. This begins to support the formation of moraines on Ubekendt (UBE 2).

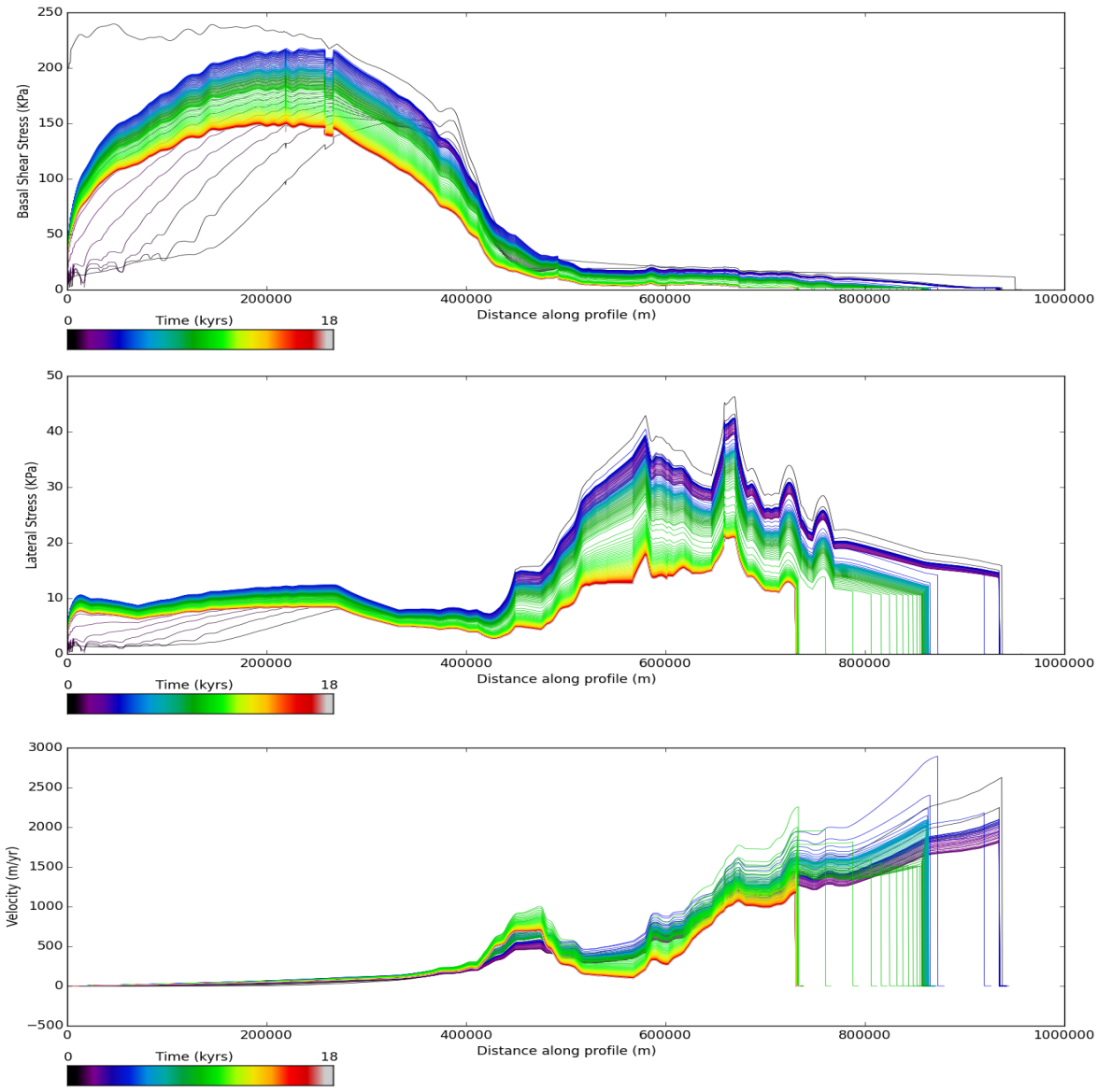

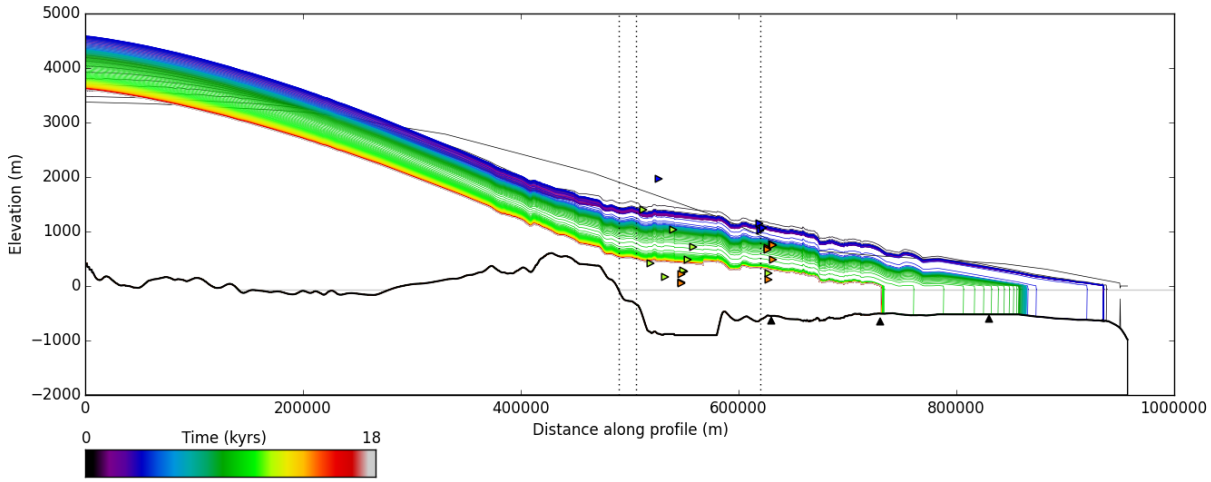

Figure 67. Ice surface profile, basal and lateral shear stress and ice velocity for the GRIP_ELA forcing scenario. Black triangles = grounding zone wedges, orange triangles =lateral moraines, green triangles = cosmogenic ages. Blue triangles = ice free regions/or partially covered.

5.3.1.4. GRIP_ELA_SSLC

Combining the GRIP curve, fluctuating ELA and Simpson sea level curve (SSLC) results in retreat to the inner GZW and ultimately to the fjord heads. The spatial pattern of grounding line position therefore fits very well with the positions of all GZWs mapped in the offshore region, and the ice retreats to a configuration that appears very similar to present day. Vertical thinning fits both the historic geomorphic data and the present day ice surface profile of the GrIS. For example, vertical thinning leading to the formation of moraines on Ubekendt and Karrat Ejland (UBE 2 and K1 and K3 respectively) fit the ice surface profile in the simulation (Fig. 68). The peak velocity (green) is 8000 m/yr^{-1} coincides with the grounding line retreat to the fjord head (Fig. 68), but towards the end of the experiment (red) velocity slows to a final velocity of 3000 m/yr^{-1}. This final velocity matches quite well with measured modern velocities in central west Greenland (Joughin *et al.,* 2010). Although in the single forcings sea level proved to be a relatively insignificant contributor to the retreat of the UISS, when combined with the GRIP forcing and the fluctuating ELA it makes a possible to reconstruct a retreat scenario that fits the present day UISS configuration and vertical thinning that fits with the geomorphic evidence. This simulation illustrates that a realistic full retreat reconstruction is possible with the above three forcings.

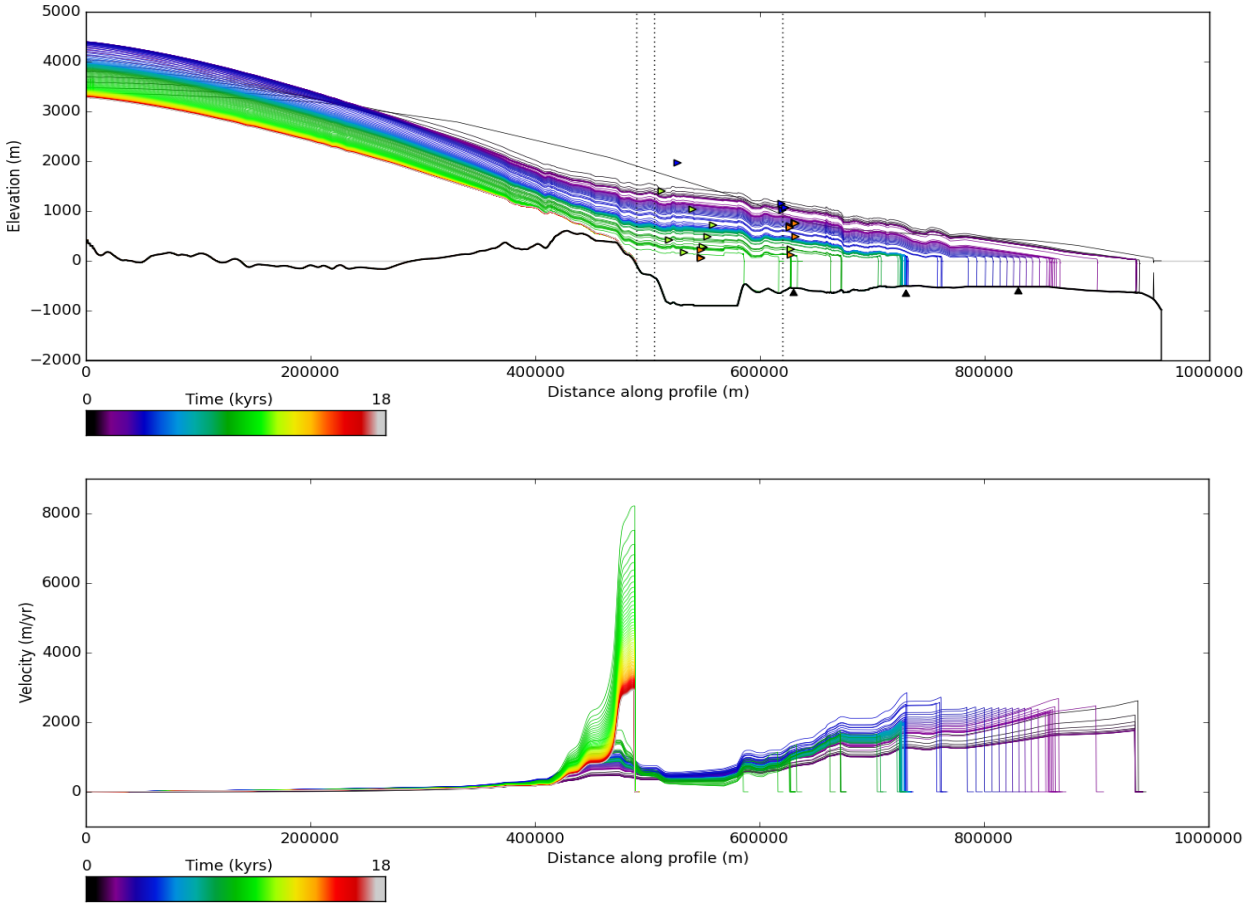

Figure 68. Ice surface profile and ice velocity for a GRIP_ELA_SSLC forcing scenario. Black triangles = grounding zone wedges, orange triangles =lateral moraines, green triangles = cosmogenic ages. Blue triangles = ice free regions/or partially covered.

5.3.1.5. A maximum scenario for realistic forcings

For the most realistic forcings the GRIP_ELA_SSLC simulation was repeated with a linear submarine melt applied (SMR1000) (Fig. 69). In the most realistic forcing scenario (GRIP_ELA_SSLC_SMR1000) the peak velocity was greater by 2000 m/yr^{-1} (Fig. 69) than the peak velocity in the GRIP_ELA_SSLC scenario. Therefore, the addition of the high submarine melting rate must have caused this. Nevertheless, in both scenarios the peak velocity occurred at the same time approximately 9000 years ago. The addition of the submarine melting results in a lower lateral shear stress around 9000 years ago (Fig. 69) and this is because the ice is thinner. Velocity is the lowest in the last 1000 years of the simulation and this may be because the UISS has reached and stabilised at its final grounding line position and stopped retreating (Fig. 70). This occurs because the water depth is negligible at this position so the velocity peaks and then declines rapidly as the ice surface draws down ice, resulting in the lowering of the ice surface profile gradient and thus reducing ice velocity and discharge.

The ELA forcing in the last two models results in the present day ice surface profiling fitting the final ice surface profile given by the model output. In addition, the grounding line pauses on each of the

bedrock highs in the outer system, and thinning fits with each exposure age identified. For example, thinning around the islands of Karrat and Ubekendt occur earlier in this simulation (3,000 years into the model simulation) than it does based on the cosmogenic nuclide evidence (UBE 2, KA 2 and KA9) that show they become exposed between 12.5 – 11.0 ka BP, however lower elevation features became exposed between 4,000-7000 years ago (K1-K3) and this fits with the model simulation. The grounding line remains on the outer-shelf for the first 2,500 years and then retreats to the mid shelf by year 5,000 and the inner shelf by year 6,000. The final jump to the inner fjords occurs 12,000 years into the model simulation. Basal shear stress inland of the fjord head, experiences shear stress levels between 200kPa in the first 1000 years and gradually decrease to half the amount (100 kPA) by the end of the 18,000 years (Fig. 70). Including SMR1000 results in retreat to the inner GZW earlier than when SMR1000 is not included (GRIP_ELA_SSLC).

Table 4. Cosmogenic nuclide exposure ages used in validating the model output.

No.	Model Yr age	Cosmogenic Age	Geomorphology	Comment	Reference
Ubekendt					
UBE2	5.5	12.4 (36Cl)	Upper limit of till and erratics	Constraint on deglacial thinning	Roberts et al., 2013
UBE1	0.8	17.2 (36Cl)	Base of lateral moraine	Elevation of features	Roberts et al., 2013
UBE14	5.7	12.3 (10Be)	Erratic on frost reworked till	Constraint on deglacial thinning	Roberts et al., 2013
UBE22	-68.9	86.9 (10Be)	Erratic on frost reworked till	Ice free during LGM	Roberts et al., 2013
UBE20	-50.8	68.8 (36Cl)	Erratic on frost reworked till	Ice free during LGM	Roberts et al., 2013
UBE10	-45.7	63.7 (36Cl)	Upper limit of lateral moraine	Elevation of features	Roberts et al., 2013
UBE13	-5.8	23.8	Quartzite boulder	Minimum LGM surface elevation	Roberts et al., 2013
Karrat					
KA2	6.4	11.6	Glacially abraded bedrock	LGM ice covered this point	Lane et al., 2014
KA9	5.86	12.14(10Be)	Glacially abraded bedrock	Constraint on deglacial chronology	Lane et al., 2014
Lake	6.6	11.4 (14C)	Glacially abraded bedrock lake	Constraint on deglacial chronology	Lane et al., 2014
KA24	-0.9	18.9 (10Be)	Partially abraded bedrock	LGM ice covered this point	Lane et al., 2014
K1	6.9	11.1(10Be)	Upper of set of 3 moraines	Constraint on retreat behaviour	Lane et al., 2014
K3	6.9	11.1(10Be)	Lowest of set of 3moraines	Constraint on retreat behaviour	Lane et al., 2014
Rink-Karrat spur					
KA3	-0.9	18.9	Bedrock	LGM ice covered this area	Lane et al., 2014
KA5	-74	92 (10Be)	Shattered bedrock	Ice free at all times	Lane et al., 2014
KA20	12.5	5.5 (10Be)	Glacially abraded bedrock	Constraint on deglacial chronology	Lane et al., 2014

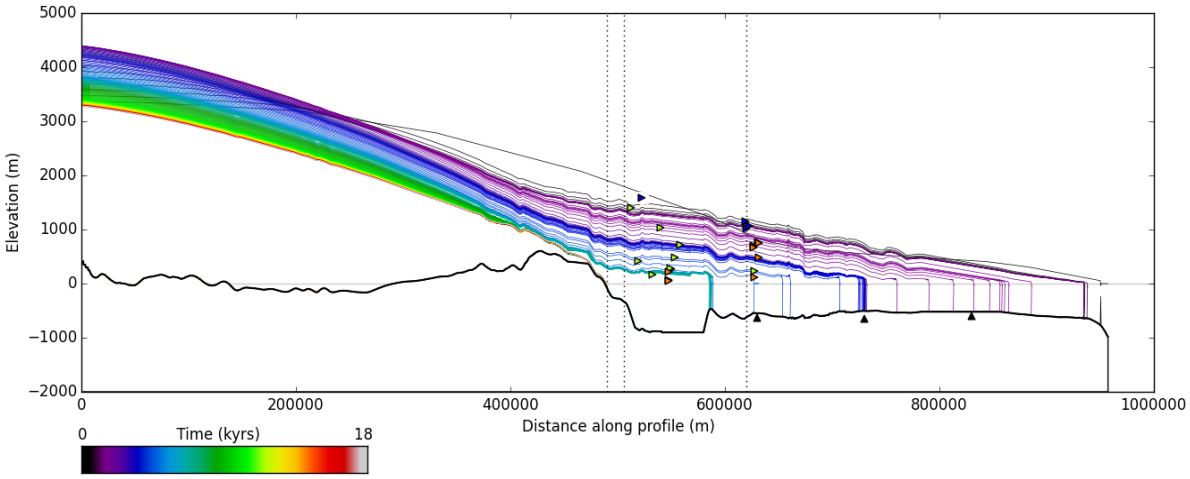

Figure 69. Ice surface profile for a realistic maximum forcing scenario, Black triangles = grounding zone wedges, orange triangles =lateral moraines, green triangles = cosmogenic ages. Blue triangles = ice free regions/or partially covered.

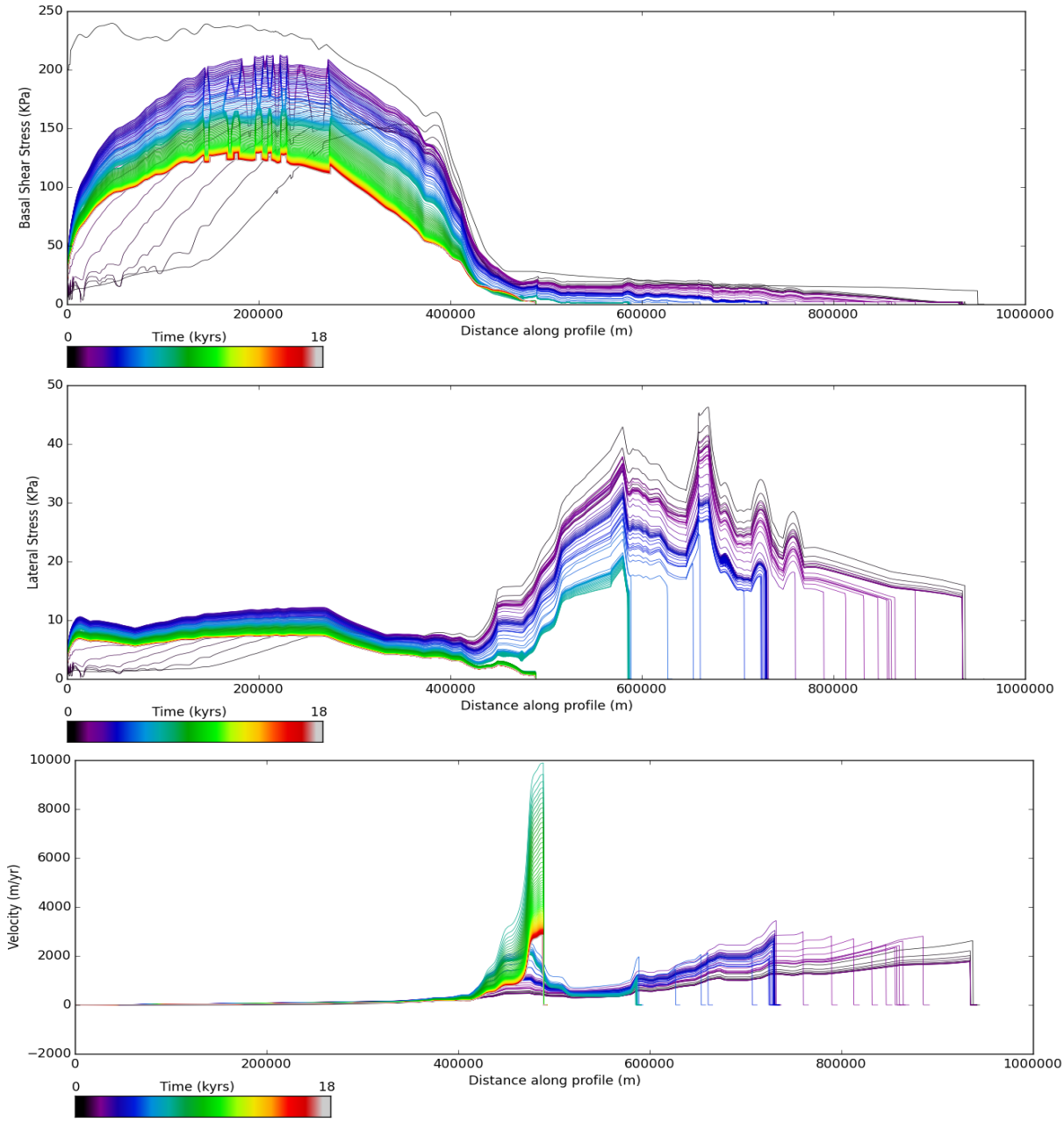

Figure 70. Basal shear stress, lateral shear stress and ice velocity for a realistic maximum forcing scenario.

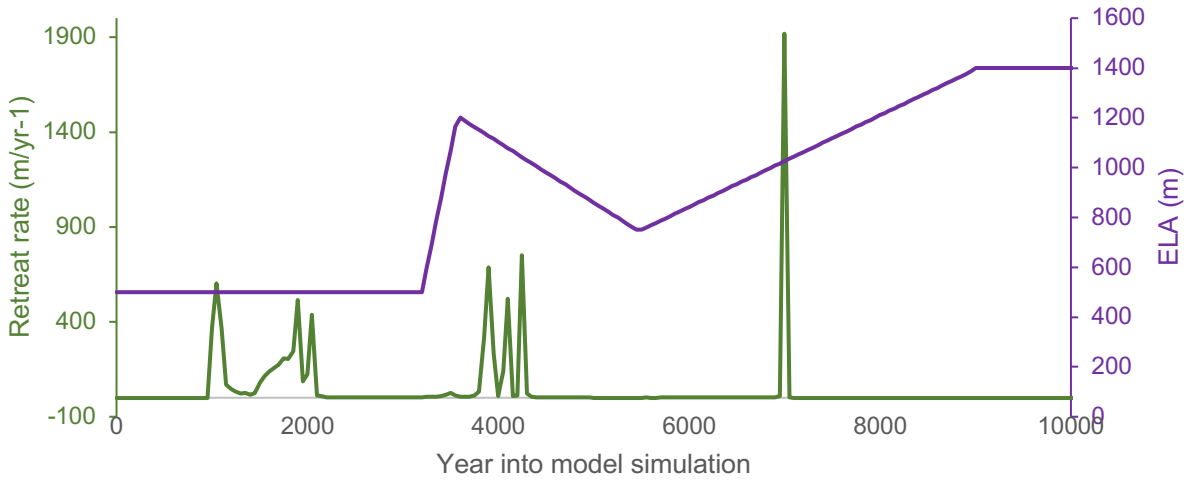

Figure 71. Relationship between retreat rate and ELA elevation for a realistic maximum forcing showing that although the ELA varies gradually, the retreat rates are nonlinear and highly variable through time.

5.4. Summary of results

Initial sensitivity tests showed the UISS was most responsive to ice temperature, however retreat couldn't be driven by a single forcing. Further sensitivity tests using a suite of maximum individual forcings combined enabled full retreat to occur. In particular, T-10_C1400 scenario enabled retreat to occur fully and the fit between the model and the geomorphology was good and allowed the grounding line position to be potentially matched to particular locations onshore in terms of ice surface thinning. Final experiments enabled a reconstruction of the UISS using 'realistic forcings' which required a fixed submarine melt factor, a GRIP temperature profile, a fluctuating ELA linked to the GRIP temperature profile and a sea level curve from Simpson et al., 2009. The outcome was a simulation that not only fitted well with the modern configuration of the UISS, but that fitted well with the onshore and offshore data in table 3.

6. Discussion and Interpretation

This section compares the model output of the 'realistic' scenario with knowledge of the LGM retreat and discusses the fit of the reconstruction with the geomorphic data, the overall retreat pattern and limitations of this study.

6.1. Model fit with field constraints

The grounding line in the model output of the 'realistic' scenario retreats from the outer shelf to the outer GZW in the first 2,500 years of the simulation (equivalent to 15.5 ka BP) (position 1 - Fig. 72). This supports evidence from core VC46 which suggests that retreat was underway by 17.1 ka BP (Jennings *et al.,* 2017), however, radiocarbon dating from VC45 yields a much later age of 14.8 ka BP (O'Cofaigh *et al.,* 2013). It is likely that the date from VC45 represents a minimum date on deglacial retreat from the outer shelf as the sample was taken from 5 cm above a basal till (VC45 - O'Cofaigh *et al.,* 2013).

Retreat from the outer GZW (position 1) to the middle GZW (position 2) occurs in the next 1,000 years (position 2 - Fig. 72 - equivalent to 15-14.0 ka BP). The grounding line reaches the inner GZW (position 3) in model year 5,000 (13 ka BP). This is supported by evidence from core MSM343520 which contains proximal glaciomarine sediment and provides a limiting constraining on LGM deglaciation (McCarthy, 2011). It suggests that retreat from the mid shelf was well underway before 10.8 ka BP (Roberts *et al.,* 2013).

Retreat of the grounding line from west of Ubekendt Ejland to west of Karrat Ejland occurs between 12.5 – 11.0 ka BP (position 3-4, Fig 72). However this does not agree with the YD readvance hypothesis proposed by Sheldon et al., (2016). The model fits well with patterns observed by Lane et al., (2014) and Philips et al., (2018) whereby the terminus retreated to the Rink-Karrat spur in the northern Uummannaq area by 11.6 ka BP - 11.0 ka BP. For example, radiocarbon dates from Marble lake lobe, Erratic lake, Bedrock lake and ^{10}Be dates around Semeg Avangardleq, central west Greenland (Fig. 74) suggest that the UISS reached its present day configuration by 10.5-11.8 ka BP (Philips *et al.,* 2018).

The final retreat of the grounding line to the inner fjords occurs 12,000 years into the model simulation (6 ka BP) and this fits with geomorphic evidence from glacially abraded bedrock and exposure ages from erratics (KA23, 110 m asl, KA27, 162 m asl, KA20, 400 m asl, KA21, 411 m asl, Roberts *et al.,* 2013; Lane *et al.,* 2014) suggesting that the Rink fjord outlet continued to retreat reaching 15 km from the present ice margin in the inner Rinks system by 5 ka BP (position 5 - Fig. 72). Equally, dated sediments from threshold lakes relying on the sharp transition between organic and inorganic

sediments constrain the duration of smaller-than-present ice (Briner *et al.,* 2005). The ages of 5.2 ka BP in mid-Kangilleq fjord (Fig. 72) constrain the ice retreat towards the present position of Rink Isbrae approximately 50 km east of Karrat.

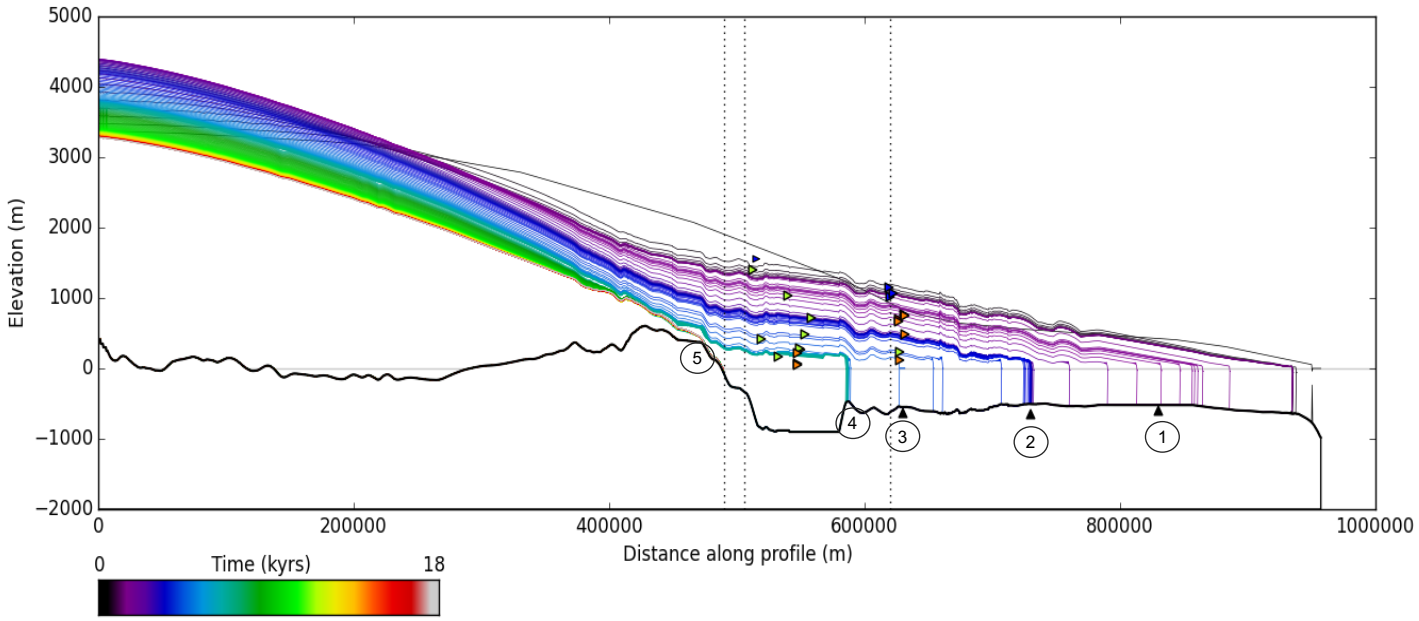

Figure 72. Ice surface profile for a realistic forcing scenario. From the right the vertical dotted lines indicate the position of Ubekendt Ejland, the entrance into the fjord head and the current grounding line position. Black triangles = GZWs, orange triangles = moraine, green triangles = cosmogenic exposure ages.

Thinning around the islands of Karrat and Ubekendt occur almost immediately in the model simulation (see purple and blue lines). High altitude cosmogenic nuclide dating evidence from Roberts *et al.,* (2013) on Ubekendt and Karrat document regions becoming ice free by 12.3 ka BP (UBE14, 770 m asl) and 11.6 ka BP (KA2, 720 m asl) respectively. However, the model output shows high altitude moraines on Ubekendt becoming ice free by 15 ka BP. It is likely that the high elevation regions on both islands became exposed between 12.5 – 11.0 ka BP and this is slightly later than what is seen in the model, although it is difficult to validate this given the exposure inheritance seen in the cosmogenic nucide ages from lateral moraines on Ubekendt Ejland (Table 3 – Roberts *et al.,* 2013). Nevertheless, at lower elevations, features on Karrat Ejland became exposed between 11 – 11.9 ka BP (K1, 210 m asl - K3, 49 m asl – KA6, 276 m asl – Lane *et al.,* 2014) and this fits with the model output (6,000 -7,000 years into the model simulation – equivalent to 11-12 ka BP).

6.2 What triggered the retreat of the UISS?

On the outer shelf, external forcings such as increases in ice temperature and air temperature drive the retreat of the UISS. Topography has little impact here as the bed is relatively low gradient and the

trough is at its widest (>30 km), thus lateral shear stress is at a minimum. Therefore, it is likely that retreat was underway by 17.1 ka BP (see evidence from VC45) following a period of increasing insolation (Huybers, 2006) causing rising ice temperatures, a rise in ELA and enhanced surface melt rate during the Bolling Allerod period (Lowe *et al.,* 2008 – Fig. 74). Consequently, in a scenario whereby the UISS is fronted by an ice shelf, it is likely that the retreat of the UISS occurred earlier (VC46 - 17.1 ka BP) in response to ocean warming that would have reached the bed of the UISS trough (Jennings *et al.,* 2017). This theory is supported by increased productivity in the sediment cores VC46 and 12PC (south UISS) prior to initial grounding line retreat which is consistent with moderate opening in sea-ice cover (Jennings *et al.,* 2017) and slightly lags Heinrich event 1 (16.8 ka BP) (Hemming, 2004). Subsequently, the retreat in West Greenland was actually closer in timing to that of ice retreat in East Greenland (18-17 ka BP) contrary to what was previously thought (Vaskogg *et al.,* 2015; O'Cofaigh *et al.,* 2013b, Jennings *et al.,* 2006; Evans *et al.,* 2002). Retreat would have been protected from accelerating mass loss (calving) by the buttressing ice shelf and by landward shallowing bathymetry on the outer shelf (Jennings *et al.,* 2017). Nevertheless, in the absence of an ice shelf it is not possible to test this theory.

6,000 years into the model the grounding line in the realistic scenario jumps from west of Ubekendt Ejland to west of Karrat Ejland during a period of a peak in sea-level rise, and rapidly increasing air temperatures (Fig. 74). Nick *et al.,* (2010) illustrates that this period coincides with increasing insolation, air temperatures and sea level rise that likely increased surface ablation and grounding line instabilities leading to accelerated calving (Nick *et al.,* 2010). These factors would have resulted in the collapse of the UISS, with over 100 km of retreat by 11.4-10.8 ka BP as seen by Roberts *et al.,* (2013).

Although the GRIP profile highlights the HTM and maintains ice temperature within a 5°C range, the grounding line appears to be insensitive to this because the ice thickens inland for a period before the large temperature warming. Therefore, there is a bigger store of ice and a steeper ice surface to deliver ice faster to the grounding line. As a consequence, the UISS doesn't respond in the same way to when the forcing was applied linearly in the warming sensitivity test. In addition, the warming does is not sustained like it is in the sensitivity experiment, therefore the previously experienced warming plays a role in sustaining the retreat of the UISS once the forcing is removed. Similarly, the model fails to show a grounding line advance that perhaps occurred during the Younger Dryas period as proposed by Sheldon et al., (2016). For example, south of the UISS in Disko Bay, Jakobshavn Isbrae experienced glacial advances between 12.9 -11.5 ka BP (Hogan, 2016). This is interesting because the water depth threshold for grounding line retreat is usually higher than the threshold for grounding line advance. This is because the gradient of the height above buoyancy on the land facing side is usually steeper than the gradient of the free water depth below the ice shelf at the seaward side (Huybrechts, 2012) and therefore we would expect to see these advances. Equally, it is difficult to get

well constrained geological records of a smaller than present GrIS because regrowth of the GrIS overran and destroyed any evidence on the landscape that would have helped delimit the configuration of a reduced GrIS.

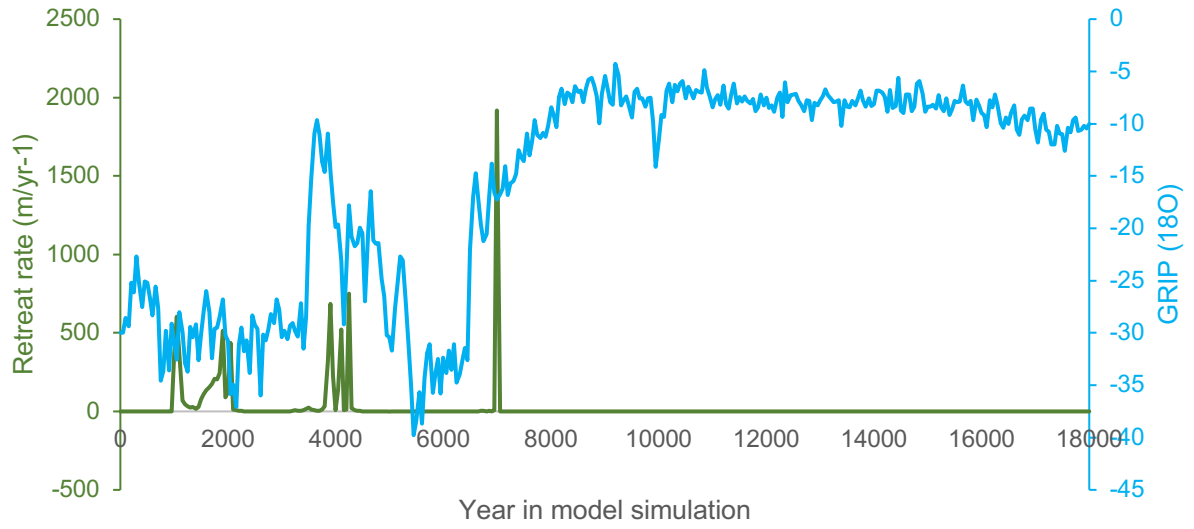

Figure 73. Retreat rate and GRIP forcing for the maximum realistic scenario showing that retreat rates spike in relation to changes in the air and ice temperature forcing but that retreat rates are also close to zero for the majority of model time.

The factors driving this final retreat from Karrat Ejland to the Rink Isbrae present margin around 6-5.0 ka BP to are unknown but are likely to be due to the persistence of warm air temperatures and the influx of the warm WGC into the Uummannaq region (McCarthy, 2011). Whilst the model doesn't fully account for ocean warming, it has been argued that the UISS is unlikely to have been driven from the shelf by increased ocean temperatures (*see section 3.2* - Sheldon *et al.,* 2016; Jennings *et al.,* 2017; Knutz *et al.,* 2011) as recent work constrains the arrival of warm the west Greenland current into this region around 8.4 ka BP (McCarthy, 2011). Nevertheless, ocean warming is likely to have played a role in the final retreat into the fjord heads around 6.0 ka BP.

The sea level perturbations alone were not enough to unground the ice and initiate retreat from the LGM maximum extent in the model output. This contrasts with contemporary ice sheet modelling whereby evidence of modern day grounding line retreat has been triggered by rising sea level (Clark, 2003: Gomez *et al.,* 2012), for example, Jennings et al., 2017 indicate that the GrIS began to retreat c17.1 ka BP in the Uummannaq Trough and at c.16.2 ka BP in the Disko Trough, coincident with gradual eustatic sea level rise associated with the main phase of deglaciation (Lambeck *et al.,* 2014). Equally, fast global sea level rise following melt water pulse 1B also supports the theory of continued grounding line retreat governed by sea level rise (Fairbanks, 1989). Around 5,000 years into our 'best fit' model simulation (12,000 years ago) relative sea level reached 10 m above the present day and during this period the grounding line was stable between Karrat and Ubekendt. Relative sea level (see SSLC- Section 3) gradually falls between 12 – 7.0 ka BP and during this period the ice had

retreated to Karrat by and then remained stable. Therefore, rising sea level does not appear to initiate retreat of the UISS or sustain retreat in the model output (Fig. 74).

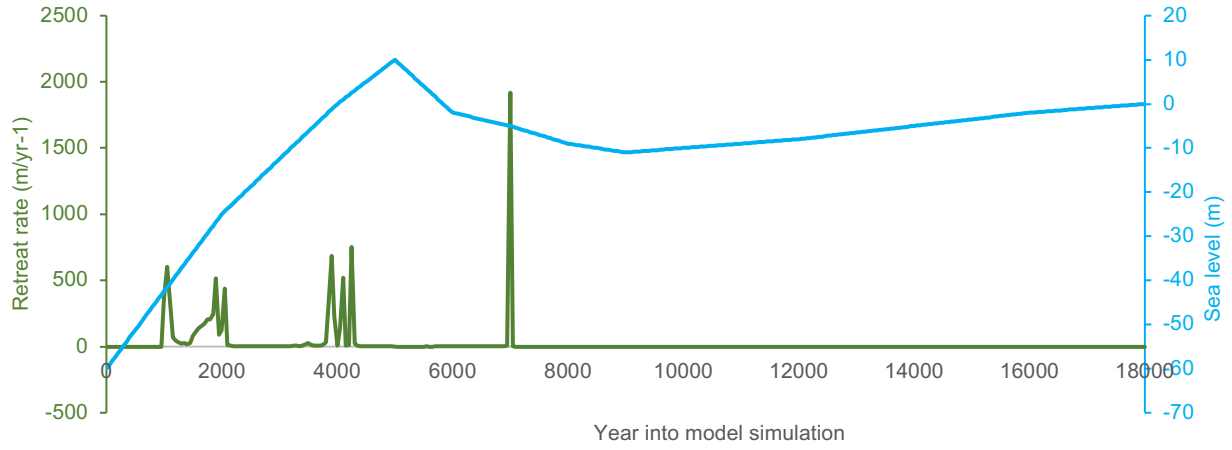

Figure 74. Relationship between retreat rate in the final model output and sea level for a maximum forcing scenario using the Simpson et al., 2009 sea level curve.

6.3. Importance of bed topography in modulating retreat rates

6.3.1. Retreat pattern is not linear

The retreat rates of the UISS illustrate that the retreat was rapid and non-linear. For the combined maximum scenario of maximum temperature, sea level and submarine melt rate increases, the retreat rates were clustered around 0.001 m/yr^{-1} and 0.1 m/yr^{-1}, whereas the more realistic scenario has retreat rates also grouped around 10 m/yr^{-1} and 100 m/yr^{-1} (Fig. 75). In the latter simulation, more retreat rates fell around 10 m/yr^{-1} than in the combined scenario and this is likely due to the non-linearity in the forcings applied. Equally, the spike in frequency of the smaller retreat rates (0.001 m/yr^{-1}) in the realistic scenario is explained by the slowdowns as the GRIP record cooled or sea level fell.

The 'realistic' scenario illustrates that although the initial retreat across the shelf was punctuated by three still stands, retreat between these GZWs was rapid and this was evident from the acoustically laminated and fine-grained sediments, derived predominately from turbid meltwater sources and by rain-out from icebergs (typical of overdeepened basins) (Dowdeswell *et al.,* 2016). However, the record of LGM and deglacial landforms is heavily reworked at water depths shallower than 450-500 m by the ploughing action of deep-keeled icebergs. This is typical of many high latitude shelves where high fluxes of large icebergs occurred during deglaciation. The retreat pattern seen in the model supports evidence by Dowdeswell *et al.,* (2008) who suggests that the presence of GZWs implies that retreat in Uummannaq Trough was episodic and punctuated by at least three stillstands, rather than a single catastrophic collapse.

Retreat from the shelf to the inner fjords occurred at a rate of 1900 m/yr^{-1} over a 20 year period, compared to Phillips et al., (2018) who suggested that the net retreat was between 300 -1100 m/yr^{-1} (Fig. 75). Therefore, it is likely that the model has simulated a system which collapses by rapid calving relating to the increasing water depth at the grounding line as it retreats. As this study only models the one flowline it is possible that this retreat didn't occur as fast as it may have during the LGM because of the high density of additional outlet glaciers that would have been feeding the same north-south trough. Relative to contemporary ice streams the collapse of the UISS was in line with modern day retreat rates seen in the North East Greenland Ice Stream which are around 1.2 km a^{-1} and are nearly half as slow ice streams in Antarctica such as ice streams in the Siple Coast and ice stream C (Kamb) which are retreating at velocities between 2.8 – 3.5 km/yr^{-1} (Rignot *et al.,* 2011).

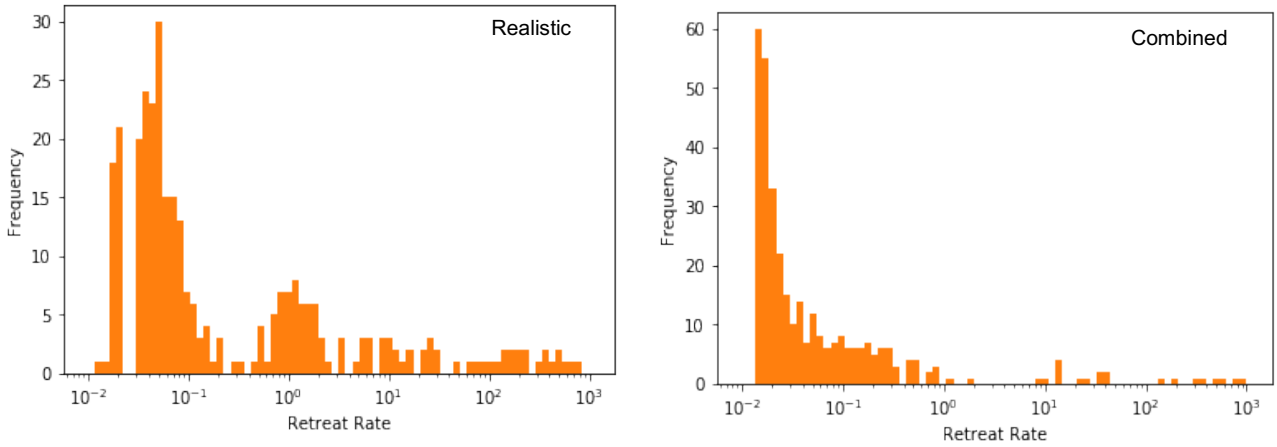

Figure 75. Frequency distribution of the retreat rates for the realistic forcing scenario (GRIP_ELA_SIMPSON_SMR1000) and the maximum combined forcing scenario (SL10_T-10_C1400_SMR1000).

6.3.2. Relationship between retreat rate and topography

The grounding line position of the UISS during the YD differs in the model to the field evidence. For example, the model depicts a period of rapid retreat (65 km in 0.7 ka) during the YD as the grounding line is exposed to a retrograde bed towards Karrat Ejland. This suggests that the bed topography was conducive for marine ice stream instability and overrode the climatic forcing. However, the grounding zone wedge west of Ubekendt (VC42) indicates that the UISS grounding line was present, and 'stable' in the mid trough during the YD for a period that was long enough to deliver large volumes of sediment (Sheldon *et al.,* 2016; Jennings *et al.,* 2017).

Once the grounding line of the UISS retreats past Ubekendt the bedrock is characterized by a topographic high, a narrowing of trough width which would have offset rapid retreat. Following this a brief deepening of the trough and a steep reverse bed slope occurs. Consequently, topography becomes more important as the ice stream moves between the islands and retreat between Ubekendt and Karrat was likely to be fast due to the deepening of the bed (Fig. 76).

Following this our model shows the UISS experienced ice marginal stabilization in Rink and Karrat fjord for up to 5000 years. During the HTM (9.0-5.0 ka BP) air temperatures across Greenland were marginally higher than those at present yet (Fig. 77- No. 3) the UISS remained stable at its grounding line position. This ice marginal stabilization was a function of topographic constriction as the trough narrows to approximately 5 km and rapid bathymetric shallowing to 400 m compared to the deeper topography to the east (>1000 m) and west (700 m). The shallowing of the bed would have reduced the relative magnitude of ice flux necessary to maintain a stable grounding line (Mercer, 1961; Schoof 2007; Jamieson *et al.,* 2012) and therefore retreat slowed significantly. Additionally, the narrowing of the channel would have reduced the flux required for stability via increased lateral resistance (Mercer, 1961; Whillans and Van Der Veen 1997) and up ice surface profile steepening (Jamieson *et al.,* 2012). These topographic effects appear to have been sufficient to result in reduce ice mass loss and subsequently reduced retreat rates. As a result, it appears likely that the topographic constriction and shallowing accentuated pinning of the ice margin during retreat (Lane *et al.,* 2014). Such topographically controlled retreat dynamics have been reported elsewhere in Greenland (Warren and Hulton, 1990) and modelled for ice streams in Antarctica (Jamieson *et al.,* 2012). For example, Enderlin *et al.,* (2013) illustrate the impact of deepened bed topography on the dynamic response of glaciers close to flotation across reverse bed slopes. Both the model output and geomorphic field data support the notion that the margin of the UISS remained stable during the Holocene thermal maximum period, even when neighbouring fjords (e.g. Ingia Fjord) continued to retreat (Lane *et al.,* 2014). Consequently, this demonstrates the potential importance of topographic control on grounding line stability, and its ability to override climatic forcing. After the still stand on Karrat Ejland, ice retreat resumed at 6.9 ka BP reaching the spur between Rink and Umiamako Fjords by 6.5 ka BP. Here, Rink and Umiamako Isbrae separated, their detachment evidenced by lateral moraines on the spur between the fjords.

This pattern of ice residing on Karrat 50 km beyond its present position during the middle Holocene is anomalous when compared to the deglaciation pattern within the Uummannaq fjord system and elsewhere on Greenland (Bennike, 2000; Funder *et al.,* 2011; Briner *et al.,* 2013; Roberts *et al.,* 2013). The asynchronicity between the deglaciation of the southern fjords compared to the north may relate to topographical/bathymetric controls and fjord geometry (Lane *et al.,* 2014). For example, the fjords are narrower to the north and south of Karrat than they are farther west and east. In addition, the fjord inland from Karrat not only widens but also deepens from 400-500 m to over 1000 m (Rignot *et al.,* 2016). Thus, once the ice retreated from Karrat, it probably would have receded quickly via rapidly calving through this major over-deepening until reaching shallower waters which exist near and behind the present position of Rink Isbrae (Morlighem *et al.,* 2014: Rignot *et al.,* 2015, 2016). The cause for this period of middle Holocene stability followed by 50 km of ice sheet recession may relate to the onset of oceanic warming which caused submarine melting of the ice front and destabilization

of the terminus, but our model is not capable of replicating this (Perner *et al.,* 2012; Briner *et al.,* 2014, 2016).

In conclusion, retreat does not always accelerate when the forcing is at its strongest therefore the bed topography is likely an influence; retreat consistently slows down in locations where the bed shallows, and width of the trough narrows.

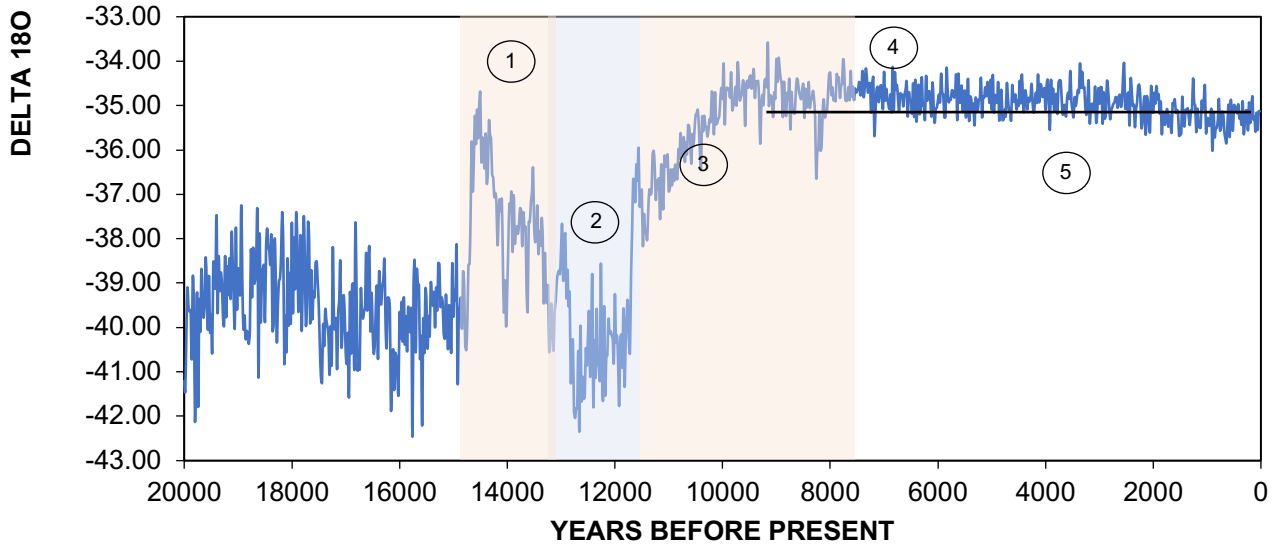

Figure 76. GRIP temperature record used in the model with warm periods (shaded red) and cooler periods (shaded blue). The numbers refer to the grounding-line locations in figure 77.

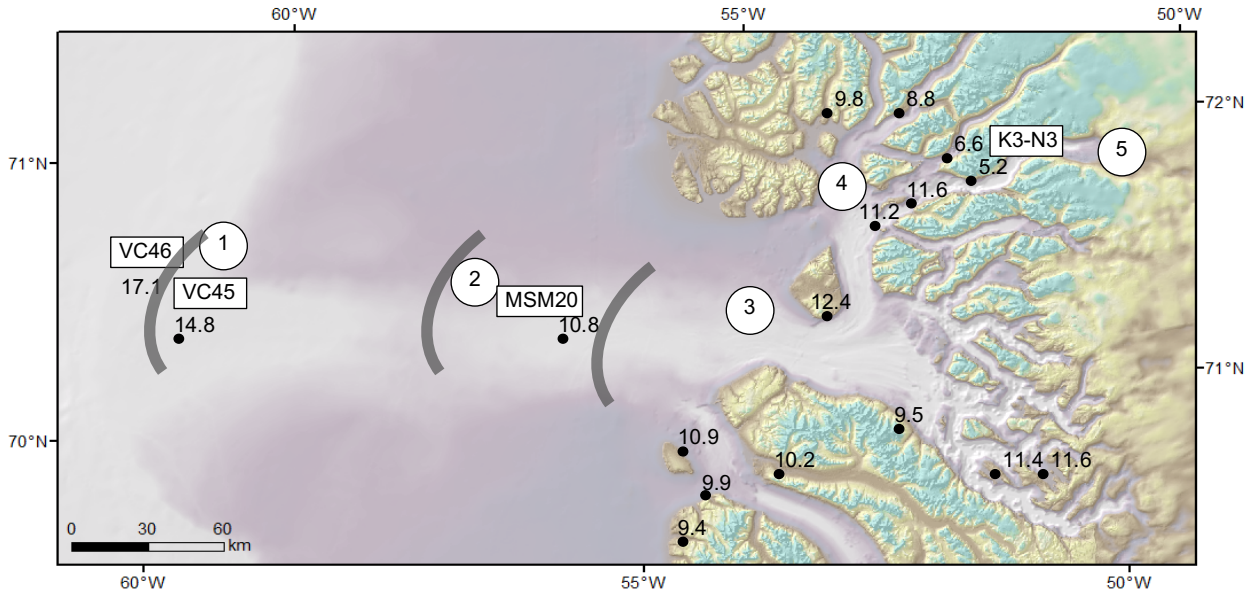

Figure 77. Uummannaq system and cosmo dates with the corresponding numbers from relating to the temporal position on the GRIP forcing (Fig. 76) during deglacial retreat. The grey lines represent the position of the GZWs.

6.4. How does the model improve our understanding of the geomorphology?

The model output allows links to be made between offshore grounding line positions and onshore ice surface profiles such that one can consistently make a connection between ice surface profile lowering that represents thinning whilst the grounding line is retreating.

6.4.1 Grounding line positions vs evidence for inland thinning

Across all the models there is a consistent relationship between grounding line retreat and vertical thinning. For example, when features such as dated moraines on Ubekendt (triangles sitting on purple lines - Fig. 78) the modelled grounding line was still on the outer shelf (Fig. 78 – position 1). This indicates thinning was occurring whilst the grounding line was on the outer shelf, producing a large GZW. Once the grounding line retreated back off the outer GZW, vertical thinning triggered the formation of the moraine staircase on Ubekendt (position 1-2, Fig. 79). The two youngest deglacial CRN ages on Ubekendt indicate ice margin thinning at ~ 12.4 ka BP (average of ages UBE 14 and UBE 2; 770 m asl and 122m asl) and this indicates rapid top down thinning, matching the model output (Fig. 79 - Position 1 and 2). This would suggest that the upper age at 700 m asl could still allow the YD limit to be west of Ubekendt and the lower age at 122 m asl would infer the YD limit is at Ubekendt. The lateral moraines on Ubekendt could relate to an early phase of UISS thinning in response to increasing mean summer (JJA) insolation followed by increased air temperatures between 16 and 14.5 ka BP in the run up to the Bolling Interstadial (cf. Roberts *et al.,* 2009; Van de Berg *et al.,* 2011). However, it is difficult to validate the chronologies of UBE1, UBE10 (*table 2 - section 5*) as their ages imply exposure inheritance. Therefore, chronologies at the outermost terrestrial site (Ubekendt) are slightly older than the grounding line position when it was just west of Ubekendt (MSM20) and this suggests that vertical thinning often occurs at a faster rate to grounding line retreat. Thus the further implications are that 1) care should be taken when interpreting marine chronologies separately from terrestrial ones because you need both to make inferences about the lateral and vertical deglacial pattern and 2) numerical models help 'join the dots' in terms of projecting an ice surface that indicates when marine vs terrestrial features were being produced – thus modelling is very informative in this situation.

Thinning around Karrat occurred even when the grounding line was on the mid to outer shelf (Fig. 78, position 2 -4). This is because were the gradient of the underlying bed slope steepens, the glacier responds by accelerating and becoming thinner (Cuffey and Clow, 1997).

The Rink margin stabilization fits with a dramatic decrease in retreat rate and temporary stagnation of the grounding line between 11.2 - 6.9 ka BP after the ice became pinned and this was when top down thinning occurred on Karrat (moraine formation K3- N3 – Fig 68, the orange triangles between the two dotted vertical lines would have formed when the grounding line retreated from position 4 to

position 5, between 6.9 and 5.0 ka BP). Overall the findings show that the Greenland ice sheet continually thinned and retreated during the deglacial transition and retreat unlike previous interpretations (Cuffey and Clow, 1997).

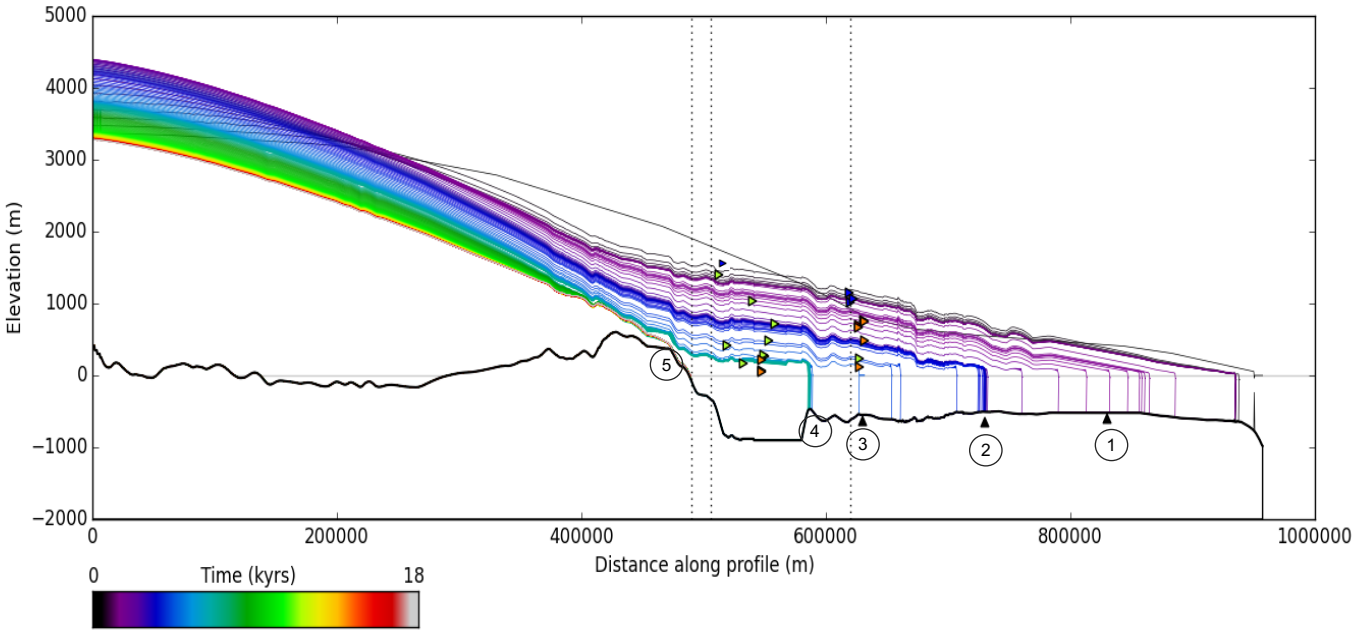

Figure 78. Ice surface profile for a realistic forcing scenario. From the right the vertical dotted lines indicate the position of Ubekendt Ejland, the entrance into the fjord head and the current grounding line position. Black triangles = GZWs, orange triangles = moraines, green triangles = cosmogenic nuclide dates.

7. Limitations

7.1. Constraining the timing of retreat

It is difficult to constrain the timing of retreat of the UISS as many of the smaller scale fluctuations in climate that could impact the grounding line position could not be reconstructed in the model. For example, submarine meltwater channels and a moraine ridge in Rink-Karrat fjord are interpreted to mark the ice stream advance during the LIA (Dowdeswell *et al.,* 1996) which occurred in west Greenland between 1500 and 1860 (Dahl Jensen et al., 1998; Fischer et al., 1998). Although the model doesn't show a LIA re-advance, based on LIA trimline zones it is likely that the ice margin advanced up to 300 m outboard of its present margin and this would explain why Marble Lake Lobe, Erratic Lake and Bedrock Lake are still presently proglacial lakes (Phillips *et al.,* 2018). Based on radiocarbon dated shells, Weidick (1972) constrained the timing of Fjord moraine deposition in Disko Bugt region to 9.2 and 8.2 ka BP with ^{10}Be exposure dating (Young et al., 2013a), suggesting a link to abrupt cooling events recorded in Greenland sediment cores and elsewhere (e.g., Alley et al., 1997; Rasmussen et al., 2007; Fleitmann et al., 2008). However, the model is not able to replicate any stabilisation or readvance during the 8.2 ka BP cooling event and consequently the Karrat-Nuugaatsiaq moraines preserved on the low-elevation eastern end of the island demarcate a palaeo-ice margin across central Karrat Ejland that dates to c.7–6 ka (Lane et al.2014).

7.2. Quality of data

7.2.1. Geomorphic data

Difficulty examining the GZW thickness from the bed topography data given the limited seismic data available could impact the accuracy of the bed topography smoothing (*section 5.1.1*) that aimed to make the GZWs more muted for the initial retreat experiments. Therefore, the GZWs may still have exerted a minor influence on the grounding line behaviour. However, in comparison to the magnitude of shallowing topography by 400 m around Karrat Ejland, the GZWs at less than 30 m in thickness are significantly smaller and would not strongly influence the retreat rate of the grounding line in this area.

Radiocarbon dated sediments from lakes constrain the timing of when the ice margin reached lakes during the Holocene Thermal Maximum. Ice over running mountainous terrain is thinner than ice thickness over valleys. Consequently, in the former, less erosion takes place resulting in the cosmogenic nuclide clock not resetting and therefore not resulting in minimum ages. For example, UBE10, UBE11 in table 1 illustrates exposure inheritance. Equally, ^{14}C dates are only minimum-limiting ages, which are often significantly younger than ^{10}Be ages of deglaciation in Greenland. As paired data has been collected at some sample sites in the UISS for ^{10}Be/^{26}Al bedrock and erratic

pairs this could be used with iceTEA (Jones et al., 2019) or probablistic modelling of the statistical distribution of exposure ages (Applegate et al., 2010) to better understand the cosmogenic ages and evaluate complex exposure histories, assess the reliability of exposure ages and explore potential age corrections would help better constrain the ages in the UISS and seek to resolve the long-term ice margin fluctuations of the UISS (Sinclair et al., 2016).

The surface of the low lying saddle across the centre of Ubekendt (200-350 m asl) is characterised by a distinct suite of depositional glacial landforms, for example fragmentary, lobate moraines composed of gravel and diamict with a smudged geomorphology suggesting that it have been overridden from an ice margin recession and re-advance/stillstand (Roberts *et al.,* 2013). The implication is that the ice was flowing not only in the trough to the South of Ubekendt, but was also split and flowed across the island. However, the 1D numerical flowline model does not account for more complex ice flow geometries like this although the impact of not incorporating this complexity is uncertain. Therefore, during the last glacial cycle, the role of topography would have been key in focusing ice flow through the UISS. Additionally, the drawdown of ice flow into the fjord heads would have increased ice flow velocities through strain heating, this would have generated a higher frictional heat flux triggering localised ice streaming and essentially increased melt-water generation at the bed. The basement bedrock has a low permeability thus further promoting sliding (Wellner *et al.,* 2001; Hall and Glassner 2003) and increasing ice flux. As ice temperature cannot vary throughout the ice column the model is not capable of replicating this.

7.2.2. Capturing the complexities of forcing data

There are challenges with developing forcing regimes for a model during periods when we do not have a clear understanding of the forcing that actually occurred. Therefore, the use of GRIP is a simplification for ice temperature. The prescribed climate forcing from GRIP only reflects temperature at a single point in the interior of the ice sheet and assumes the whole ice stream has a similar ice temperature at any given time, therefore it doesn't evolve across elevation and distance down stream. Equally, movement of the ELA is prescribed as a function of the GRIP ice core and therefore it does not account for accumulation changes influenced by precipitation. Consequently, strengthening of the west Greenland current throughout the early Holocene which could have decreased sea ice extent in Baffin Bay (Thomas *et al.,* 2006) and created a source of precipitation for the West Greenland ice sheet is not captured in this parameter. This increase in precipitation rate during summer months may have been able to offset ice margin retreat rate. Briner *et al.,* (2010) suggests that retreat between 6.8ka and 4.2 ka was relatively slow due to an increase in winter precipitation, however after 3.0 ka BP margins may have advanced to the present day position due to a decrease in winter precipitation and a cooling of summer temperatures from 3-2.0 ka BP. Nevertheless, despite some inland retreat of the west Greenland ice margin it has remained relatively stable and close to its current position

through the HTM. It is these reconstructions of a smaller than present GrIS that are most relevant for accurately predicting the dimensions of the GrIS and thus estimating its future contribution to GMSL.

7.3. Presence of an ice shelf

Evidence from Jennings et al., (2017) infers that the UISS grounding line was protected from accelerating mass loss (calving) by a buttressing ice shelf and by landward shallowing bathymetry on the outer shelf. It is therefore likely that this would have changed the way the ocean interacted with the ice front and the underside of the ice shelf to modify ocean melt and buttressing. The increase in IRD abundance (clasts greater than 2 mm) by 15.3 ka BP (Jennings *et al.,* 2017) is indicative of rapid calving and episodes of ice streaming in the UISS. This indicates the loss of the fringing ice shelf that was acting as a buttress allowing the calving debris laden icebergs (Jennings *et al.,* 2017). Therefore, in the presence of an ice shelf, buttressing could potentially prevent marine ice sheet instability on a retrograde bed and slow the retreat of the system (Gudmundsson *et al.,* 2012; Jamieson *et al.,* 2012). Whilst the issues with developing an ice shelf in this model were not resolvable, future experiments would benefit from the inclusion of an ice shelf if possible. Alternative factors that could influence retreat and may warrant further investigation include the role of ice mélange on buttressing ice shelves and cooling of the surrounding ocean and its influence on ocean circulation. The combination of icebergs and sea ice is called ice mélange and it behaves as a weak, granular ice shelf at the terminus of the glacier (Amundson *et al.,* 2010). Sea ice acts as a buttress to prevent icebergs from calving off. During summer, however, when icebergs are less bound by sea ice, calving rates increase significantly. Despite the issues above, our model results indicate that the deglacial retreat of the UISS and vertical thinning can be successfully reconstructed without the added buttressing of an ice shelf or ice melange. We also note that where the annual air temperatures were warmer than present day (as it was at a number of stages during our 18 ka simulations) it is unlikely that an ice shelf would have been sustained in these conditions. As Morris & Vaughan (2003) suggest, ice shelves begin to collapse in air temperatures warmer than -9°C. However, if an ice shelf was present for even part of the retreat, submarine melting would have played an important role on the retreat of the system by reducing buttressing and also by providing a large surface area of ice that contacts with the ocean, thus enabling enhanced mass loss.

A final note for future work is that it would be informative to apply the same experiments and forcings to a flowline in the south of the Uummannaq system because geochronological data demonstrates that the retreat rate of the northern and southern UISS became highly asynchronous during the early Holocene (Roberts et al. 2013) and therefore the pattern, rates and controls of grounding line retreat and thinning as the UISS separates into its different fjords after retreat past Ubekendt Ejland could have been different (Lane *et al.,* 2014).

8. Conclusion

Examining the LGM configuration and controls on the retreat of the UISS provides insight into the deglacial behaviours of outlet glaciers. The overall approach entailed modelling the post LGM retreat of the UISS and constrained this using a suite of geographical and geomorphic data. This section outlines the key findings of this work.

The UISS LGM reconstruction to a stable configuration required a 60 m drop in sea level from present day, a -20°C decrease in ice temperature, and an 800 m decrease in ELA elevation from present day. The sensitivity tests forced from the stable LGM configuration illustrated that no single forcing was able to induce sufficient retreat of the UISS to its present day position. However, when forced in combination sea level and temperature (SL10_T-10), sea level and climate (SL10_T-10) and climate and submarine melting (C1400_SMR1000) resulted in enough retreat to reach the inner shelf.

The realistic scenario was the best fit model of retreat and is most useful when identifying the timing and magnitude of the UISS's deglacial retreat, fitting well with both the geological and chronological evidence outlined above. Geomorphic evidence from Karrat Ejland and Ubekendt Ejland display a distinct relationship between the timing of vertical ice thinning and the formation of lateral moraines (for example, K1-K3). Furthermore, cosmogenic nuclide exposure ages point to a a signal in ice profile thinning and the deglacial retreat.

The first phase of retreat was controlled by climatic and oceanic forcings, enhanced by bathymetric depths. Based on onshore and offshore deglacial chronologies, once within the fjord confines, topographic constrictions became the dominant control upon individual outlet glacier dynamics overriding climatic forcings and causing early to mid Holocene ice marginal stabilization in Rink-Karrat fjord. Therefore, the final retreat of the GrIS after the LGM was asynchronous and thus was influenced by both topographic effects and local ice sheet dynamics (Jennings *et al.,* 2017).

The retreat patterns and rates of the UISS are always nonlinear regardless of the forcing and this is an indicator that the retreat of the UISS is strongly controlled by local topographic conditions, and in particular the depth and shape of the bed, and the width of the trough.

Using the model it is possible to 'join the dots' between offshore grounding line positions and onshore geomorphological evidence so that the understanding of the shape of the UISS is enhanced. We can use the model to say that when the grounding line is at a particular location, the ice surface will be thinning at another location further inland. This has implications for interpreting links between onshore and offshore chronologies and this learning should be transferred to other regions where extent and thinning histories are being developed.

Regardless of which forcing scenario was applied, we find that topography is a key modulator of retreat rate and lateral drag: the retreat of the UISS following the LGM was highly non-linear and was interrupted by stabilization on a reverse sloping bed where rapid unstable retreat is expected from theoretical considerations. These transient stabilizations were caused by enhanced lateral drag as the ice stream narrowed. Therefore, retreat is likely to be asynchronous to its forcing and this helps to explain temporal and regional variations in the rate of mass loss observed. Equally, it provides an explanation to why retreat patterns are not regionally synchronous (in the north and south) following the LGM or a particular forcing event such as the Younger Dryas period. The unstable retreat patterns reflects the peak in velocities as retreat occurs. The stepped pattern of retreat relates to the connection between the grounding line retreat offshore and the formation of onshore features, through vertical thinning, such as moraines on Ubekendt and Karrat Ejland.

Examining the retreat of the UISS in the context of future warming scenarios the period (7.8-1.2 ka BP) of high orbital precession index with summer temperatures within the projected warming for the end of this century (Larsen *et al.,* 2018; Kaufman *et al.,* 2004; Miller *et al.,* 2010b) the system can be viewed in a different light. Furthermore, whilst ice streams play a significant role in the mass of ice sheets over time their overall numbers decrease as they occupy a progressively smaller percentage of the ice sheet perimeter and their total discharge decreases (Stokes, 2016). Therefore, this should be considered when examining the future impact of ice stream instability. Nevertheless, the UISS displays a unique dynamic signal within Greenland and provides compelling evidence for a first order topographical control on ice margin stabilization in west Greenland. It also has major implications for our understanding and reconstructions of mid-Holocene ice sheet extent and Greenland ice sheet dynamics.

9. References

Alley, R.B., Mayewski, P.A., Sowers, T., Stuiver, M., Taylor, K.C., Clark, P.U., (1997). Holocene climatic instability: a prominent, widespread event 8200 yr ago. *Geology,* 25 (6), 483-486.

Andresen, C., Straneo, F., Ribergaard, M., Bjørk, A., Andersen, T., Kuijpers, A., Nørgaard-Pedersen, N., Kjær, K., Schjøth, F., Weckström, K. and Ahlstrøm, A. (2011). Rapid response of Helheim Glacier in Greenland to climate variability over the past century. *Nature Geoscience*, 5(1), pp.37-41

Applegate, P., Urban, N., Laabs, B., Keller, K. and Alley, R. (2010). Modeling the statistical distributions of cosmogenic exposure dates from moraines. *Geoscientific Model Development*, 3(1), pp.293-307.

Axford, Y., Losee, S., Briner, J. P., Francis, D. R., Langdon, P. G. & Walker, I. R. (2013) Holocene temperature history at the western Greenland Ice Sheet margin reconstructed from lake sediments. *Quaternary Science Reviews*, 59, 87-100.

Ballantyne, C.K. (1997) Periglacial trimlines in the Scottish Highlands. *Quaternary International,* 38-39, 18.

Bamber, J. L., Riva, R. E. M., Vermeersen, B. L. A., and Le- Brocq, A. M. (2009). Reassessment of the potential sea-level rise from a collapse of the West Antarctic ice sheet, *Science,* 324, 901–903,

Bamber, J., Alley, R. and Joughin, I. (2007). Rapid response of modern day ice sheets to external forcing. *Earth and Planetary Science Letters*, 257(1-2), 1-13.

Bassis, J.N and Walker, C. C. (2012) Upper and lower limits on the stability of calving glaciers from the yield strength envelope of ice, proceedings of the royal society, 468, 913-931.

Batchelor, C.L., Dowdeswell, J.A., (2015), Ice-sheet grounding- zone wedges (GZWs) on high-latitude continental margins, *Marine Geology* (1), 34-45

Benn, D. & Evans, D. J. A. (2010) *Glaciers and Glaciation.* pp. Hodder Education, London.

Bennett, M. (2003). Ice streams as the arteries of an ice sheet: their mechanics, stability and significance. *Earth-Science Reviews*, 61(3-4), 309-339.

Bennike, O. (2000). Palaeoecological studies of Holocene lake sediments from west Greenland. *Palaeogeography, Palaeoclimatology, Palaeoecology,* 155, 285-304.

Bindschadler, R. (2006). The environment and evolution of the West Antarctic ice sheet setting the stage, *Philosophical transactions of the royal society* (364). 1583-1605

Bjørk, A., Kjær, K., Korsgaard, N., Khan, S., Kjeldsen, K., Andresen, C., Box, J., Larsen, N. and Funder, S. (2012). An aerial view of 80 years of climate-related glacier fluctuations in southeast Greenland. *Nature Geoscience*, 5(6), 427-432

Box, J. (2006). Greenland Ice Sheet surface mass balance variability (1988-2004) from calibrated polar MM5 output. *Journal of Climatology*. 19, 2783-2800.

Briner, J. P., Miller, G. H., Davis, P. T. & Finkel, R. C. (2005) Cosmogenic exposure dating in arctic glacial landscapes: implications for the glacial history of northeastern Baffin Island, Arctic Canada. *Canadian Journal of Earth Sciences* 42, 67-84.

Briner, J. P., Stewart, H. A. M., Young, N. E., Phillips, W. & Losee, S. (2010). Using proglacial threshold lakes to constrain fluctuations of the Jakobshavn Isbræ ice margin, western Greenland, during the Holocene. *Quaternary Science Reviews*, 29, 3861-3874.

Briner, J.P., Håkansson, L., Bennike, O., (2013.) The deglaciation and neoglaciation of Upernavik Isstrøm, *Greenland. Quaternary Research,* 80, 459-467.

Buch, E (2000a) A Monograph on the Physical Oceanography of the Greenland Waters, Danish Meteorological Institute Scientific Report, 00-12

Buch, E (2000b) Air–sea–ice conditions off southwest Greenland, 1981–1997, *Journal Northwest Atlantic Fishery Science,* 26, 1-14

Chauché, N., A. Hubbard, J.-C. Gascard, J. E. Box, R. Bates, M. Koppes, A. Sole, P. Christoffersen, and H. Patton. (2014). Ice-ocean interaction and calving front morphology at two west Greenland tidewater outlet glaciers, *Cryosphere*, 8(4),1457–1468,

Christoffersen, P., R. I. Mugford, K. J. Heywood, I. Joughin, J. A. Dowdeswell, J. P. M. Syvitski, A. Luckman, and T. J. Benham, (2011) Warming of waters in an East Greenland fjord prior to glacier retreat: Mechanisms and connection to large-scale atmospheric conditions. *The Cryosphere*, 5, 701–714.

Clark, C. D (2003) Mega-scale glacial lineations and cross-cutting ice-flow landforms, *Earth surface processes and landforms,* 18 (1), 1-29.

Clark, P.U. and Walder, J.S. (1994) Subglacial drainage, eskers, and deformable beds beneath the laurentide and Eurasian ice sheets. *Geological society of America bulletin,* 106, 304-314.

Dahl-Jensen, D., Mosegaard, K., Gundestrup, N., Clow, G.D., Johnsen, S.J., Hansen, A.W., Balling, N., 1998. Past temperatures directly from the Greenland ice sheet. *Science* 282 (5387), 268–271.

Dowdeswell, J, Hagen, JM, Björnsson, H. (1997) The mass balance of circum-Arctic glaciers and recent climate change. *Quaternary Research* 48, 1–14.

Dowdeswell, J. A., C. L. Batchelor, K. A. Hogan, and H. W. Schenke. (2016). *Atlas of Submarine Glacial Landforms: Modern, Quaternary and Ancient,* vol. 46, chap. Nordvestfjord: a major East Greenland fjord system, pp. 43–44, Geological Society, London, Memoirs,

Dowdeswell, J. A., D. Ottesen, J. Evans, C. Ó Cofaigh, and J. B. Anderson (2008), Submarine glacial landforms and rates of ice-stream collapse, *Geology,* 36(10), 819–822.

Dowdeswell, J. A., K. A. Hogan, C. O'Cofaigh, E. M. G. Fugelli, J. Evans, and R. Noormets. (2014). Late Quaternary ice flow in a West Greenland fjord and cross- shelf trough system: submarine landforms from Rink Isbrae to Uummannaq shelf and slope, *Quaternary Science Review*, 92(SI), 292–309.

Dowdeswell, J., Kenyon, N., Elverhøi, A., Laberg, J., Hollender, F., Mienert, J. and Siegert, M. (1996). Large-scale sedimentation on the glacier-influenced polar North Atlantic Margins: Long-range side-scan sonar evidence. *Geophysical Research Letters*, 23(24), pp.3535-3538

Dowdeswell, J.A. and Fugelli, E.M.G. (2012) The seismic architecture and geometry of grounding-zone wedges formed at the marine margins of past ice sheets, *Geological Society American. Bulletin, 124,* 1750-1761

Dowdeswell, J.A., Jakobsson, M., Hogan, K.A., O'Regan, M., Backman, J., Evans, J., Hell, B., Löwemark, L., Marcussen, C., Noormets, R., Ó Cofaigh, C., Sellen, E., Sölvsten, M., (2010) High-resolution geophysical observations of the Yermak Plateau and northern Svalbard margin: implications for ice-sheet grounding and deep-keeled icebergs. *Quaternary Science Reviews* 29, 3518–3531.

Enderlin, E., Howat, I. and Vieli, A. (2013). The sensitivity of flowline models of tidewater glaciers to parameter uncertainty. *The Cryosphere Discussions*, 7(3), 2567-2593.

Ettema, J. et al. (2009). Higher surface mass balance of the Greenland Ice Sheet revealed by high-resolution climate modeling. *Geophysical Research Letters*, 36:1–5.

Evans, D. J. A. et al. (2002) "Geomorphology And Style Of Plateau Icefield Deglaciation In Fjord Terrains: The Example Of Troms-Finnmark, North Norway." *Journal of Quaternary Science* 17(3), 221-239.

Farrell, W. E. and Clarck, J.A. (1976) On postglacial sea level, *Geophysics journal Resaerch Astronomy Society*, 46, 647-667.

Fettweis, X., Mabille, G., Erpicum, M., Nicolay, S., and van den Broeke, M (2011a) The 1958–2009 Greenland ice sheet surface melt and the mid-tropospheric atmospheric circulation, *Climate Dynamics.* 36, 139–159.

Fleitmann, D., Mudelsee, M., Burns, S.J., Bradley, R.S., Kramers, J., Matter, A., (2008). Evidence for a widespread climatic anomaly at around 9.2 ka before present. *Paleoceanography*, 23 (1)

Funder, S. (1989). Quaternary geology of the ice free areas and adjacent sheles of Greenland. In R.J Fulton (ed.). Quaternary geology of Canada and Greenland. Geological Survey of Canada, *Geology of Canada* no.1. 743-792.

Funder, S. & Hansen, L. (1996). The Greenland ice sheet - a model for its culmination and decay during and after the last glacial maximum. *Bulletin of the Geological Society of Denmark*, 42, 137-152.

Funder, S. Kjledsen, K. Kjaer, K. & O'Cofaigh, C. (2011) . The Greenland Ice Sheet During the Past 300,000 Years: A Review. In: Ehlers, J. Gibbard, P.L & Hughes, P.D (eds) Quaternary Glaciations - Extent and Chronology: A Closer Look. Oxford: Elsevier

Gladish, C. V., D. M. Holland, A. Rosing-Asvid, J. Behrens, and J. Boje (2015), Ocean thermal forcing of Jakobshavn Glacier: Part I. Variability and renewal of Ilulissat icefjordwaters, 2001–2013, J. Phys. Oceanogr., 45(1), 3–32. Holland, Gudmundsson, G. H., Krug, J., Durand, G., Favier, L., and Gagliardini, O (2012)) The stability of grounding lines on retrograde slopes, *The Cryosphere*, 6, 1497-1505

Gudmundsson, G. H., Krug, J., Durand, G., Favier, L., and Gagliardini, O (2012)) The stability of grounding lines on retrograde slopes, *The Cryosphere*, 6, 1497-1505

Hakansson, L., Briner, J., Alexanderson, H., Aldahan, A. & Possnet, G. (2007a). Be-10 ages from central east Greenland constrain the extent of the Greenland ice sheet during the Last Glacial Maximum. *Quaternary Science Reviews,* 26, 2316-2321.

Hemming, S. R. (2004). Heinrich events: massive late Pleistocene detritus layers of the North Atlantic and their global climate imprint, *Reviews of Geophysics,* 42

Hill, E. A. Carr, J. R. Stokes, C. R and Gudmundsson, G. H. (2018). Dynamic changes in outlet glaciers in northern Greenland from 1948 to 2015. *The Cryosphere,* 12, 3243-3263.

Hogan, K.A. Dix, J.K. Lloyd, J.M. Long, A.J. Cotterill, C.J. (2011) Seismic stratigraphy records the deglacial history of Jakobshavn Isbræ, West Greenland, *Journal of Quaternary Science* 26, 757-766

Hogan, K.A. Ó Cofaigh, C. Jennings, A.E. Dowdeswell, J.A. Hiemstra, J.F. (2016) Deglaciation of a major palaeo-ice stream in Disko Trough, West Greenland, *Quaternary Science Reviews*

Holland, D., Thomas, R., de Young, B., Ribergaard, M. and Lyberth, B. (2008). Acceleration of Jakobshavn Isbræ triggered by warm subsurface ocean waters. *Nature Geoscience*, 1(10),.659-664.

Howat IM, Joughin I, Fahnestock M, Smith BE and Scambos T (2008) Synchronous retreat and acceleration of southeast Greenland outlet glaciers 2000–2006: ice dynamics and coup- ling to climate. *Journal of Glaciology* 54(187), 646–660

Hughes, T, and Nakagawa, M. (1989), Bending Shear: The Rate-Controlling Mechanism for Calving Ice Walls: *Journal of Glaciology*, v. 35, 260-266.

Huybers, P.(2006). Early Pleistocene Glacial Cycles and the Integrated Summer Insolation Forcing. *Science,* 313, 508-511.

Jamieson et al., (2012) Ice-stream stability on a reverse bed slope. *Nature Geosci.*, **5**(11), 799–802.

Jenkins, A. (2011) Convection-Driven Melting near the Grounding Lines of Ice Shelves and Tidewater Glaciers, American Meterological Society,

Jennings, A. E., M. Hald, and M. Smith (2006), Freshwater forcing from the Greenland Ice Sheet during the Younger Dryas: Evidence from southeastern Greenland shelf cores, *Quat. Sci. Rev.,* 25, 282–298.

Jennings, A.E. and Andrews, J.T. and O Cofaigh, C. and St Onge, G. and Sheldon, C. and Belt, S.T. and Cabedo-Sanz, P. and Hillaire-Marcel, C. (2017) 'Ocean forcing of Ice Sheet retreat in central west Greenland from LGM to the early Holocene.', *Earth and planetary science letters.*, 472 1-13.

Jennings, A.E. Walton, M.E. Ó. Cofaigh, C. Kilfeather, A. Andrews, J.T. Ortiz, J.D. *et al.* (2014) Paleoenvironments during Younger Dryas–early Holocene retreat of the Greenland ice sheet from outer Disko Trough, central west Greenland, *Journal of Quaternary Science*, 29 (1) 27-40

Jones, R., Small, D., Cahill, N., Bentley, M. and Whitehouse, P. (2019). iceTEA: Tools for plotting and analysing cosmogenic-nuclide surface-exposure data from former ice margins. *Quaternary Geochronology*, 51, 72-86.

Joughin I, Smith B, Howat IM, Scambos T and Moon T (2010a) *MEaSUREs Greenland ice sheet velocity map from InSAR data.* NASA Distributed Active Archive Center/National Snow and Ice Data Center, Boulder, CO. Digital media: http://nsidc.org/data/ docs/measures/nsidc0478_joughin

Joughin I, Smith BE, Howat IM, Scambos T and Moon T (2010b) Greenland flow variability from ice-sheet-wide velocity mapping. *Journal of Glaciology* 56(197), 415–430.

Joughin, I. and Alley, R. (2011). Stability of the West Antarctic ice sheet in a warming world. *Nature Geoscience*, 4(8), 506-513.

Joughin, I. Smith, B. E., Howat, I. M., Scambos S, T. & Moon, T. (2010). Greenland flow variability from ice-sheet-wide velocity mapping. *Journal of Glaciology*, 56, 415-430.

Joughin, I., B. Smith, I. Howat, and T. Scambos. 2015, updated 2017. *MEaSUREs Greenland Ice Sheet Velocity Map from InSAR Data, Version 2*. [Indicate subset used]. Boulder, Colorado USA. NASA National Snow and Ice Data Center Distributed Active Archive Center.

Kelly, S. Briner, J. Young, N. (2013) Rapid ice retreat in Disko Bugt supported by 10Be dating of the last recession of the western Greenland Ice Sheet, *Quaternary Science Review.,* 82, pp. 13-22,

Kelly, M. (1985). A review of the Quaternary geology of western Greenland. In: ANDREWS, J. T. (ed.) Quaternary Environments in Eastern Canadian Arctic, Baffin Bay and Western Greenland. Boston: Allen and Unwin.

Khan, S. A., Wahr, J., Bevis, M., Velicogna, I. & Kendrick, E. (2010). Spread of ice mass loss into northwest Greenland observed by GRACE and GPS. *Geophysical Research Letters,* 37, L06501.

Kleman, J., Hattestrand, C. & Borgstrom, I. (1997) Fennoscandian palaeoglaciology reconstructed using a glacial geological inversion model. *Journal of Glaciology* 43.

Knutz, P.C. Sicre, M.A. Ebbesen, H. Christiansen, S. Kuijpers, A. (2011) Multiple-stage deglacial retreat of the southern Greenland Ice Sheet linked with Irminger Current warm water transport, *Paleoceanography,* 26

Krabill, W. (2000). Greenland Ice Sheet: High-Elevation Balance and Peripheral Thinning. *Science*, 289(5478), 428-430.

Lambeck, K. Rouby, H. Purcell, A, Sun, Y, Sambridge, M. (2014) Sea level and global ice volumes from the Last Glacial Maximum to the Holocene, *Proceedings of the National Academy of Science USA*, 111, 15296-15303

Lane, T. P., Roberts, D. H., Rea, B. R., Ó Cofaigh, C., Vieli, A. & Rodés, A. (2014). Controls upon the Last Glacial Maximum deglaciation of the northern Uummannaq Ice Stream System, West Greenland. *Quaternary Science Reviews,* 92, 324–344.

Lane, T.P. and Roberts, D.H. and O'Cofaigh, C. and Rea, B.R. and Vieli, A. (2016) 'Glacial landscape evolution in the Uummannaq region, West Greenland.', *Boreas.,* 45 (2). 220-234.

Larsen, N., Levy, L., Carlson, A., Buizert, C., Olsen, J., Strunk, A., Bjørk, A. and Skov, D. (2018). Instability of the Northeast Greenland Ice Stream over the last 45,000 years. *Nature Communications*, 9(1).

Lloyd J. M., Park, L. A., Kuijpers, A. & Moros, M. (2005). Early Holocene palaeoceanography and deglacial chronology of Disko Bugt, West Greenland. *Quaternary Science Reviews*, 24, 1741-1755.

Long, A. J. & Roberts, D. H. (2002). A revised chronology for the 'Fjord Stade' moraine in Disko Bugt, west Greenland. *Journal of Quaternary Science,* 17, 561-579.

Long, A. J., Roberts, D. H. & Wright, M. R. (1999). Isolation basin stratigraphy and Holocene relative sea-level change on Arveprinsen Ejland, Disko Bugt, West Greenland. *Journal of Quaternary Science*, 14, 323-345.

Lowe, A. L. & Anderson, J. (2002) Reconstruction of the West Antarctic ice sheet in Pine Island Bay during the Last Glacial Maximum and its subsequent retreat history. *Quaternary Science Reviews 21*, 1879-1897.

Lowe, J. J., Rasmussen, S. O., Bjorck, S., Hoek, W. Z., Stefensen, J. P., Walker, M. J. C. & Yu, Z. C. (2008). Synchronisation of palaeoenvironmental events in the North Atlantic region during the Last Termination: a revised protocol recommended by the INTIMATE group. *Quaternary Science Reviews*, 27, 6- 17.

McCarthy, D. J. (2011). Late Quaternary ice-ocean interactions in central West Greenland. PhD, Durham University.

Mercer, J. H. (1961). The Response of Fjord Glaciers to changes in the Firn Limit. Journal of *Glaciology,* 3, 850-858.

Moon, T. & Joughin, I. (2008). Changes in ice front position on Greenland's outlet glaciers from 1992 to 2007. *Journal of Geophysical Research Letters* 113, F02022.

Morlighem et al. (2017). BedMachine v3: Complete bed topography and ocean bathymetry mapping of Greenland from multi-beam echo sounding combined with mass conservation, *Geophysical Research Letters,* 44.

Morlighem, M, E. Rignot, J Mouginot, H. Seroussi, and E. Larour. (2015). High-resolution ice thickness mapping in South Greenland. *Annals of Glaciology*, 55(67), 1–7.

Morlighem, M., E. Rignot, J. Mouginot, H. Seroussi and E. Larour. (2014). Deeply incised submarine glacial valleys beneath the Greenland Ice Sheet, *Nature Geoscience*, 7, 418-422.

Morris, E. and Vaughan, D. (2003). *Spatial and temporal variation of surface temperature on the Antarctic Peninsula and the limit of viability of ice shelves*.

Mosola, A. and Anderson, J. (2006). Expansion and rapid retreat of the West Antarctic Ice Sheet in eastern Ross Sea: possible consequence of over-extended ice streams? *Quaternary Science Reviews*, 25(17-18), 2177-2196.

Mote, T. L.(2007) Estimation of runoff rates, mass balance, and elevation changes on the Greenland ice sheet from passive microwave observations, *Journal for Geophysical Research* (108), 4056,

Mouginot, J., E. Rignot, B. Scheuchl, and R. Millan. (2017). Comprehensive Annual Ice Sheet Velocity Mapping Using Landsat-8, Sentinel-1, and RADARSAT-2 Data, *Remote Sensing,* 9(4),

Nick, F. M. Vieli, A. Howat, I.M. Joughin.I (2009) Large-scale changes in Greenland outlet glacier dynamics triggered at the terminus, *Nature Geoscience,* 394, 110-11.

Nick, F. M., A. Vieli, M. L. Andersen, I. Joughin, A. Payne, T. L. Edwards, F. Pattyn, and R. S. W. van de Wal (2013), Future sea-level rise from Greenland's main outlet glaciers in a warming climate, *Nature,* 497

Nick, F. M., C. J. Van der Veen, A. Vieli, and D. I. Benn (2010), A physically based calving model applied to marine outlet glaciers and implications for the glacier dynamics, *Journal of glaciology,* (56) 781-794

Ó Cofaigh, C., Dowdeswell, J. A., Jennings, A. E., Hogan, K. A., Kilfeather, A., Hiemstra, J. F., Noormets, R., Evans, J., McCarthy, D. J., Andrews, J. T., Lloyd, J. M. & Moros, M. (2013a).

An extensive and dynamic ice sheet on the West Greenland shelf during the last glacial cycle. *Geology* 41, 219–222.

Ó Cofaigh, C., Dowdeswell, J., Evans, J., Kenyon, N. H., Taylor, J., Mienert, J. & Wilken, M. (2004). Timing and significance of glacially influenced mass- wasting in the submarine channels of the Greenland Basin. *Marine Geology,* 207, 39-54.

Ó Cofaigh, C., Andrews, J.T., Jennings, A.E., Dowdeswell, J.A., Hogan, K.A., Kilfeather, A.A. & Sheldon, C. (2013b) Glacimarine lithofacies, provenance and depositional processes on a West Greenland trough-mouth fan. *Journal of Quaternary Science*. (28), 13-26.

Oerlemans, J. (1992) Climate sensitivity of glaciers in Southern Norway: application of an energy balance model to Nidgardsbreen, Hellestugubreen and Olfotbreen, *Journal of Glaciology* 38 (129) pp. 223-232

Ottesen, D. Dowdeswell, J. Rise, L. (2005) Submarine landforms and the reconstruction of fast-flowing ice streams within a large Quaternary ice sheet: the 2500-km-long Norwegian-Svalbard margin (57°–80° N) *Geological Society of American Bulletin* 117, 1033-1050,

Ottesen, D., Rise, L., Andersen, E.S., Bugge, T., Eidvin, T., (2009) Geological evolution of the Norwegian continental shelf between 61°N and 68°N during the last 3 million years. Norwegian, *Journal of Geology,* 89, 251–265.

Paterson, W. S. B. (1994) *The Physics of Glaciers*. pp. Pergamon, Oxford.

Pattyn, F., Schoof, C., Perichon, L., Hindmarsh, R. C. A., Bueler, E., de Fleurian, B., Durand, G., Gagliardini, O., Gladstone, R., Goldberg, D., Gudmundsson, G. H., Huybrechts, P., Lee, V., Nick, F. M., Payne, A. J., Pollard, D., Rybak, O., Saito, F., and Vieli, A.: Results of the Marine Ice Sheet Model Intercomparison Project, MISMIP, *The Cryosphere,* 6, 573–588,

Pedersen, G. K. & Pulvertaft, T. C. R. (1992). The nonmarine Cretaceous of the West Greenland Basin, onshore West Greenland. *Cretaceous Research,* 13, 263-272

Philipps, W., Briner, J., Bennike, O., Schweinsberg, A., Beel, C. and Lifton, N. (2018). Earliest Holocene deglaciation of the central Uummannaq Fjord system, West Greenland. *Boreas*, 47(1), 311-325.

Pritchard, H., Arthern, R. J., Vaughan, D. G. & Edwards, L. A. (2009). Extensive dynamic thinning on the margins of the Greenland and Antarctic ice sheets. *Nature,* 461, 5.

Rasch, M. (2000) Holocene relative sea-level changes in Disko Bugt, West Greenland, *Journal of Coastal Research*, 16, pp. 306-315.

Rasmussen, S.O., Vinther, B.M., Clausen, H.B., Andersen, K.K., (2007). Early Holocene climate oscillations recorded in three Greenland ice cores. *Quaternary Science Reviews*, 26 (15), 1907-1914.

Reeh, N. (1985). Was the Greenland ice sheet thinner in the late Wisconsinan than now? *Nature,* 317, 797-799.

Ribergaard, M.H., Olsen, S.M., Mortensen, J., (2008). Oceanographic Investigations off West Greenland 2007. NAFO SCR Doc. 08/3, Scientific Council Meeting, June 2008.

Rignot, E. (2006). Changes in the Velocity Structure of the Greenland Ice Sheet. *Science*, 311(5763), 986-990.

Rignot, E. Mouginot, J. Scheuchl, B. (2011) Ice flow of the Antarctic Ice Sheet, *Science,* 333 (6048) pp. 1427-1430

Rignot, E., I. Fenty, Y. Xu, C. Cai, and C. Kemp. (2015). Undercutting of marine-terminating glaciers in West Greenland, *Geophysical Research Letters,* 42(14), 5909–5917.

Rignot, E., I. Fenty, Y. Xu, C. Cai, I. Velicogna, C. O'Cofaigh, J. A. Dowdeswell, W. Weinrebe, G. Catania, and D. Duncan. (2016). Bathymetry data reveal glaciers vulnerable to ice-ocean interaction in Uummannaq and Vaigat glacial fjords, west Greenland, *Geophysical Research Letters*, 43(6), 2667–2674.

Roberts, D. H., A. J. Long, B. Davies, and C. Schnabel (2010), Ice stream influence on west Greenland Ice Sheet dynamics during the Last Glacial Maximum, *Journal of Quaternary Science*, 25, 850–864.

Roberts, D. H., A. J. Long, C. Schnabel, M. Simpson, and B. Davies (2009), Ice sheet extent and deglacial history of the central western sector of the Greenland Ice sheet, Quat. Sci. Rev., 28, 2760–2773.

Roberts, D. H., and A. J. Long (2005), Streamlined bedrock terrain and fast ice flow, Jakobshavns Isbrae, West Greenland: Implications for ice stream and ice sheet dynamics, Boreas, 34,25–42.

Roberts, D., Rea, B., Lane, T., Schnabel, C. and Rodés, A. (2013). New constraints on Greenland ice sheet dynamics during the last glacial cycle: Evidence from the Uummannaq ice stream system. *Journal of Geophysical Research: Earth Surface*, 118(2), pp.519-541

Schoof, C.(2007a) Ice sheet grounding line dynamics: steady states, stability, and hysteresis, *Journal of Geophysical Research Letters,* 112, F03S28,

Shepherd, A. et al. (2012) A reconciled estimate of Ice-Sheet Mass Balance, *Science,* 338 (6111), 1183-1189

Siegert, M.J., Marsiat, I., ((2001). Numerical reconstructions of LGM climate across the Eurasian High Arctic. *Quaternary Science Reviews* 20 (15), 1595–1605.

Simpson, M. J. R., Milne, G. A., Huybrechts, P. & Long, A. J. (2009). Calibrating a glaciological model of the Greenland ice sheet from the Last Glacial Maximum to present-day using field observations of relative sea level and ice extent. *Quaternary Science Reviews*, 28, 1631-1657.

Sinclair, G., Carlson, A., Mix, A., Lecavalier, B., Milne, G., Mathias, A., Buizert, C. and DeConto, R. (2016). Diachronous retreat of the Greenland ice sheet during the last deglaciation. *Quaternary Science Reviews,* 145(1), 243–258.

Stokes, C. R. & Clark, C. D. (2001) Palaeo-ice streams. *Quaternary Science Reviews* 20, 1437–1457.

Straneo, F., and P. Heimbach (2013), North Atlantic warming and the retreat of Greenland's outlet glaciers, *Nature,* 504, 36–43.

Straneo, F., D. A. Sutherland, D. Holland, C. Gladish, G. S. Hamilton, H. L. Johnson, E. Rignot, Y. Xu, and M. Koppes. (2012). Characteristics of ocean waters reaching Greenland's glaciers, *Annals of Glaciology,* 53(60, 2), 02–210.

Straneo, F., Hamilton, G., Sutherland, D., Stearns, L., Davidson, F., Hammill, M., Stenson, G. and Rosing-Asvid, A. (2010). Rapid circulation of warm subtropical waters in a major glacial fjord in East Greenland. *Nature Geoscience*, 3(3), 182-186

Streuff, K., Ó Cofaigh, C., Hogan, K., Jennings, A., Lloyd, J., Noormets, R., Nielsen, T., et al. (2017). Seafloor geomorphology and glacimarine sedimentation associated with fast-flowing ice sheet outlet glaciers in Disko Bay, West Greenland. *Quaternary Science Reviews,* 169, 206-230

Swift, D. A., C. Persano, F.M. Stuart, K. Gallagher, and A. Whitham (2008), A reassessment of the role of ice sheet glaciation in the long-term evolution of the East Greenland fjord region, *Geomorphology*, 94,109–125.

Syvitski, J.P.M., Stein, A.B., Andrews, J.T., Milliman, J.D., (2001) Icebergs and the sea floor of the East Greenland (Kangerlussuaq) continental margin. *Arctic, Antarctic, and Alpine Research* 33, 52–61.

Thomas, R., Frederick, E., Krabill, W., Manizade, S. and Martin, C. (2006). Progressive increase in ice loss from Greenland. *Geophysical Research Letters,* 33(10),

Velicogna, I. (2009). Increasing rates of ice mass loss from the Greenland and Antarctic ice sheets revealed by GRACE. *Geophysical Research Letters*, 36,

Velicogna, I. and Wahr, J. (2006). Acceleration of Greenland ice mass loss in spring 2004. *Nature*, 443(7109), 329-331

Vieli, A. and Payne, A. J. (2005). Assessing the ability of numerical ice sheet models to simulate grounding line migration, *Journal of Geophysical Research,* 110, F01003.

Vieli, A., and F. M. Nick, (2011) Understanding and modelling rapid dynamical changes of tidewater outlet glaciers: Issues and implications. *Surv. Geophys.,* 32, 437–458,

Vorren, T. (1998). Trough mouth fans — palaeoclimate and ice-sheet monitors. *Quaternary Science Reviews*, 16(8), 865-881

Weertman, J .(1974) Stability of the junction of an ice sheet and ice shelf, *Journal of glaciology,* 13, 3–11, 1974.

Weidick, A., (1972). *Holocene Shorelines and Glacial Stages in Greenland: an Attempt at Correlation.* Copehagen, Grønlands Geologiske Undersøgelse, Grønlands Geologiske Undersøgelse, p. 39.

Weidick, A. (1996). Neoglacial changes of ice cover and sea level in Greenland - a classical enigma. In: Gronnow, B. (ed.) The Paleo-Eskimo Cultures of Greenland. Copenhagen: Danish Polar Centre.

Weidick, A. & Bennike, O. (2007). Quaternary glaciation history and glaciology of Jakobshavn Isbrae and the Disko Bugt region, West Greenland: A review. *Geological Survey of Denmark and Greenland Bulletin,* 14, 1-78.

Wellner, J., Lowe, A., Shipp, S. and Anderson, J. (2001). Distribution of glacial geomorphic features on the Antarctic continental shelf and correlation with substrate: implications for ice behavior. *Journal of Glaciology*, 47(158), 397-411.

Whillans, I. M., and C. J. van der Veen (1997), The role of lateral drag in the dynamics of Ice Stream B, Antarctica, *Journal of Glaciology,* 43(144), 231–237.

Whitehouse, P. L., M. J. Bentley, A. Vieli, S. S. R. Jamieson, A. S. Hein, and D. E. Sugden (2017), Controls on Last Glacial Maximum ice extent in the Weddell Sea embayment, Antarctica, *Journal of Geophysical Research Earth Surface,(*122), 371–397.

Young, N.E., Schaefer, J.M., Briner, J.P., Goehring, B.M., (2013b). A ^{10}Be production-rate calibration for the Arctic. *Journal of Quaternary Science,* 28 (5), 515-526.